MIRU

Design of an Air Safety Investigation UAV
Final Report

Delft University of Technology

TU Delft

Final Report

by

T.J. Asijee	4293037
C.A. Blauw	4290771
M. Desmedt	4221095
J. Driezen	4285395
B. von den Hoff	4278755
C.C. Petersen	4293657
F.S. Straver	4281314
N.D.K. Sutopo	4227069
D.C. Wijnker	4280598
R.A.A. Willemsen	4290674

Supervisors

Tutor	Dr. C.D. Rans
Coaches	Ir. M.J. Schuurman
	Ir. B.D.W. Remes

TU Delft

Preface

This report was written for the Design Synthesis Exercise (DSE) of Aerospace Engineering at the Delft University of Technology. A group of ten soon-to-be engineers were assigned to come up with a conceptual design of an airborne platform to assist in securing, observing and documenting an air accident site in tandem with an investigation team. This is an upcoming application for investigations, however there is no UAV especially designed for this purpose, so we designed MIRU. MIRU is an abbreviation of Multipurpose Imagine and Research UAS.

The report describes in detail the outcome of the past eleven weeks. An example of an air safety investigation is set out to show what problems the UAV should overcome. From requirements, trade-offs and real life investigation experience, a choice was made for the most suitable UAV. Not only the UAV, but the whole system is described, including the groundstation. Besides the technical aspects such as its functions, operations and budgets, also some business related subjects are considered, such as feasibility, risk and the market analysis. As the DSE has come to an end, the future and realisation of the concept was analysed.

We would like to express our sincere gratitude to our tutor, Dr. Calvin Rans, and our coaches, Ir. Michiel Schuurman and Ir. Bart Remes, for the open attitude towards the team, their willingness to help and answer our questions and the generosity in sharing their time, knowledge and material. Furthermore, the effort they put into realising the air safety investigation experience is greatly appreciated.

Also, we are grateful to the Faculty of Aerospace Engineering of Delft University of Technology for providing a working place and providing us with office supplies which helped a lot organising the project efficiently. The TAs Derek Beeftink, Alper Kenger and David Jimenez-Lluva did a great job in answering our questions and providing us with the necessary study material.

June 28, 2016

Tom, Alexander,
Michiel, Jorne,
Bieke, Co,
Floris, Kinan,
Dirk and Roger

[0]Image Cover page, `https://www.pexels.com/photo/flight-plane-accident-crash-3803/`

Contents

List of Figures

List of Tables

List of Symbols

Greek symbols

α Angle of attack (°)

δ_e Elevon deflection (°)

λ Eigenvalues (s^{-1})

Ω Rotational speed (rps)

ϕ Roll angle (°)

θ Pitch angle (°)

Roman symbols

A Aspect ratio (–)

b Wing span (–)

C Charge capacity (Ah)

c Chord (m)

C_r C-rating (C)

C_D Drag coefficient (–)

C_L Lift coefficient (–)

C_{m_α} Moment coefficient derivative with respect to α (–)

C_m Moment coefficient (–)

C_{N_α} Normal coefficient derivative with respect to α (–)

C_P Propeller power coefficient (–)

C_T Propeller thrust coefficient (–)

D Drag (N)

d Diameter (m)

E Energy capacity (Wh)

e Oswald efficiency factor (–)

I Current (A)

J Propeller velocity coefficient (–)

l Length (m)

P Power (W)

p Roll rate (° s^{-1})

q Pitch rate (° s^{-1})

r Yaw rate (° s^{-1})

T Thrust (N)

U Voltage (V)

u Deviation in horizontal airspeed (ms^{-1})

V Velocity (ms^{-1})

W Weight (N)

w Deviation in vertical airspeed (ms^{-1})

List of Abbreviations

ADC	Analog to Digital Converter
ATC	Air Traffic Control
COM	Communication
CTR	Control
DSE	Design Synthesis Exercise
ELT	Emergency Locator Transmitter
ESC	Electronic Speed Controller
FBS	Functional Breakdown Structure
FFD	Functional Flow Diagram
GNC	Guidance, Navigation and Control
GNSS	Global Navigation Satellite Sytem
GPS	Global Positioning System
I2C	Inter-integrated Circuit
IMC	Instrument Meteorological Conditions
IMU	Inertial Measurement Unit
INS	Inertial Navigation System
IR	Infrared
LIDAR	Light Detection And Ranging
LIPO	Lithium Polymer
LLT	Lifting Line Theory
MIRU	Multipurpose Imaging and Research UAS
MP	Mega Pixel
MTOW	Maximum Take-Off Weight
NTSB	National Transport Safety Board
PCB	Printed Circuit Board
PD&D	Project Design and Development
PID	Photo-Ionisation Detector
PID	Proportional-Integral-Derivative
PLB	Personal Locator Beacon
PWM	Pulse Width Modulation
RAMS	Reliability, Availability, Maintainability, and Safety
RGB	Red Green Blue
RHCP	Right Hand Circular Polarised
RPM	revolutions per minute
RPS	rotations per second
SAR	Search And Rescue
SFY	Safety
SHF	Super High Frequency
SPI	Serial Peripheral Interface
STR	Structure
SUR	Surveying
SWOT	Strengths, Weaknesses, Opportunities, Threats
SYS	System Requirement
UART	Universal Asynchronous Receiver/Transmitter
UAS	Unmanned Aerial System
UAV	Unmanned Aerial Vehicle
UHF	Ultra High Frequency
USB	Universal Serial Bus
VLM	Vortex Lattice Method
VTOL	Vertical Take-Off and Landing

Abstract

Air safety investigations have a primary goal to find the reason that an aerial vehicle crashed, in order to prevent it from happening again. This means the investigators have to document every single piece of information, from the way parts are deformed to the place it was found on the accident site. Not only do they work on the ground, but they also use aerial photography to get a complete overview from another perspective.

In an air safety investigation, geological factors such as mountains or political factors such as conflicts are often delaying and obstructing the investigators from reaching the accident site. A UAV has the potential to extend possibilities for gathering information. Currently, investigators are limited to ground based investigation tools or single purpose aerial solutions, which are both very costly and time consuming. A multipurpose aerial solution would be a great aid to overcome those problems.

For this reason, to aid air safety investigators, the Multipurpose Imaging and Research UAS – MIRU – is designed. It exists out of one modular UAV and a groundstation. The UAV has three different configurations, which all have their mission specific benefits. First of all, the tailsitter configuration can do both forward flight and hovering and is the UAV in its most complete form. It can perform vertical take-off and landing, from where it can transition to forward flight. The flying wing has a better forward flying performance due to the smaller attached fins, but cannot hover and needs a larger clearing to take-off. The last configuration is the quadcopter. It has better hover performance than the tailsitter due to the fact that the wings are taken of, but is therefore limited in forward flight performance. The UAS can perform the four functions for which it is needed: coarse mapping and detailed mapping of the accident site, functioning as a communication relay between the investigators of the ground and detecting the possible toxins at the crash site.

The feasibility of the UAV was tested by means of aerodynamic, structural and performance analyses, which showed that MIRU is feasible. Also, a market analysis showed that the current market of air safety investigations has promising potential for MIRU. Other potential markets include mapping of land registry and tracking in the event of disasters, where MIRU distinguishes itself through its flexibility in deployment.

Because of the modularity of the UAV, its feasibility and a good market perspective MIRU is a great solution for the problems that many investigators face during their work. It will make an investigation shorter and cheaper without adding an excessive amount of extra operations for the investigators.

1 Introduction

The past few years, UAVs became more and more common for a range of purposes. Especially for mapping, it is a huge improvement as it bridges the gap between satellites, aircraft or helicopters and making images from the ground. This is mainly due to the lower cost and shorter time frame, the possibility to generate a large overview, which is hard to do from the ground, and its possibility to map details, which is hard to do with a satellite or aircraft. Here the opportunity was identified to design a UAV to aid air safety investigators with their investigation.

This report analyses the feasibility of a design of MIRU. MIRU is a Multipurpose Imaging and Research UAS with the main mission objective to locate and map an air accident site. When an accident site is not easily accessible, investigators can deploy MIRU on a search and mapping mission. This UAV is able to locate a wreckage in remote areas and coarse map these during daytime, in the absence of sunlight, and even when the wreckage is camouflaged in its surroundings. After this, a detailed map is generated by MIRU when the investigators have arrived on site. Also, when there is a risk of leaked toxic or explosive gases, MIRU can inspect whether these gases are present, before the investigators arrive on site.

In order to analyse the advantages and feasibility of MIRU, first a case study is illustrated that shows how MIRU significantly increases the efficiency of an air accident investigation. MIRU is able to do this due to its modularity and compactness. The UAV is a tailsitter which performs both horizontal and vertical flight. This tailsitter can be configured in a flying wing configuration when a longer horizontal flight endurance is desired. However, when a longer vertical flight endurance is desired for a specific mission, the tailsitter can be transformed to a quadcopter that has a higher vertical flight endurance. The operationality of MIRU are carried out in Chapters 4, 5 and 6, respectively.

In order to fulfil the mission objectives, MIRU is built up of several subsystems, designed specifically for its missions. This is treated in Chapter 8. MIRU carries a payload with three different cameras, a visible light camera, an IR camera, and a multispectral camera, which is explained in Section 8.1. Furthermore, the structure is very lightweight (max. 2.44 kg) and the parts are detachable making it very modular, such that it fits inside a backpack. This means that the investigators can easily carry it to the accident site. The materials used in this UAV are analysed in Section 8.7. In order to correctly use MIRU, the user has to perform certain operations. In order to communicate with the UAV at all times, the UAV is equipped with long range (for the remote mission) and short range (for the on-site mission) communication devices, and so is the groundstation. This is further elaborated upon in Section 8.2. The groundstations main functions are to facilitate the operations of the mission, and to present the data the UAV has sent. The details of the groundstation are analysed in Section 8.3. In order for the UAV to fly autonomously and actually perform its mission, a guidance navigation and control unit is present on board the UAV which is explained in Section 8.4. Control surfaces are installed on board the UAV to ensure the vehicle remains airborne and performs the actions as instructed by the GNC module, this is treated in Chapter 8.6. The structure of the UAV - which must be lightweight, strong, and durable - is analysed in Chapter 8.7. In order to propel the vehicle, a propulsion system is needed, this is designed in Chapter 8.8. To integrate all these subsystems, an electrical system is needed that connects all these components, which is analysed in Chapter 8.9. After all these systems were designed, analysed and discussed, the feasibility of the design was analysed to know if the design is able to meet all the requirements and can be implemented in the market. This is treated in Chapter 9. After it was proven that the design is feasible to put on the market, the market itself is analysed to confirm that a large enough offset is possible to make the system feasible in economic sense, which is carried out in Chapter 11. After it can be confirmed that the design is feasible in sense of design risk and economics, the further course of the design is determined, which is treated in Chapter 12.

2
Case study: Agusta A-109E helicopter terrain impact

In this section, a case study is presented that is presented to justify the capabilities of MIRU to highlight the importance of certain design aspects to the mission. Section 2.2 describes the common investigation procedures applied to the case, to analyse what aspects can be improved upon.

2.1. Case description

The case study is used to present the capabilities of MIRU, and is a helicopter crash that occurred on June 9, 2009 in the United States. The Agusta A-109E helicopter departed from a remote location, in a mountainous area near Santa Fe, New Mexico, where it crashed shortly after take off. The probable cause of the accident was stated as “the pilot’s decision to take off from a remote, mountainous landing site in dark (moonless) night, windy, instrument meteorological conditions (IMC)” [35, p. vii, 65].
The wreckage of the helicopter was eventually found at an altitude of about 3.5 km. The closest possible location to reach by car was a ski resort, located 6.2 km away from the accident site. At the beginning of this ski area, the basecamp was set up (referred to in the investigation report as the Incident Base). The shortest ground route from this basecamp to the accident site was 8.9 km, which would result in a 1.5 h walk for the investigators and SAR team. To avoid this, a helicopter was used to transfer the teams to the accident site. Two helicopters were also used to search the area and locate the main wreckage, which was however very difficult as the grey coloured wreckage was camouflaged between the rocks.
Moreover, the SAR team described the environment of the accident site as “ dangerously steep, rocky, and covered with snow and ice” [35, p. 8], thus being very inaccessible.
Because the wreckage was camouflaged in the environment and the accident site was so inaccessible, the search and documentation of the accident site was clearly hampered. Only the search phase, so locating the main wreckage, took up 8.5 hours, with the last known point of radar contact only 0.5 km away. As two helicopters were used to search the area, this was clearly a costly operation as well -chartering a helicopter would cost an average of €3000,- per hour [1].

Based on the environmental conditions and location of the accident site, the conclusion was made that any additional aid in locating the wreckage would have been of crucial importance for a faster search and rescue operation, as well as a more efficient and lower cost air safety investigation. As a summary, the most important wreckage location information is gathered in Table 2.1.

[1] URL:`http://www.aircharterguide.com/AircraftSearch.aspx?AircraftCategory=Helicopter&pageNum=1` [cited 25 June 2016]

Table 2.1: Case study wreckage location information, based on the investigation report [35]

Description	Value
Altitude location (km)	3.5
Distance to basecamp by ground (km)	8.9
Distance to basecamp by air (km)	6.5
Distance to closest airport (km)	40
Approximate debris field size (m)	150 x 300
Distance between last point of radar contact and main wreckage (km)	0.5

2.2. Major phases in an investigation procedure

In this section, a brief overview of a normal air accident investigation is laid out, to establish the fundament for the application of MIRU to an investigation as is described in detail in the next Section 2.3. The phases of the investigation defined here are the prelaunch phase, the search phase and the documentation phase. These phases are deduced from the NTSB Aviation Investigation Manual [34].

2.2.1. Prelaunch phase

In the initial set-up of the investigation, the prelaunch phase, available information on the accident is gathered, and the logistic planning is made. Also, any initial administrative actions are performed in this stage.The time span of this phase ranges from just after the notification of the accident, upon arrival at the accident location.

In the last part of this phase, the basecamp is set up at an accessible location, as close as possible to the accident location. After this, an on site briefing is performed, to communicate the planning. It was deduced that the time needed for set up at the accident site or basecamp was about an hour for the case study, excluding the travel time. In the case study described in Section 2.1, the complete prelaunch phase happened mostly overnight and in the early morning.

2.2.2. Search phase

After the prelaunch, the search and rescue phase is initiated. The goal during this phase is to locate the main wreckage and rescue potential survivors. Main focus of the investigators is on the search aspect of the wreckage, in parallel with the SAR team, who focus on the rescue of survivors and therefore start this phase as early as possible. Upon locating the main wreckage, the smaller wreckage pieces, such as a horizontal stabilizer, have to be located as well. At the same time, documentation of the main wreckage can start. The search phase for the Agusta A109E helicopter accident took in total 8.5 hours.

2.2.3. Documentation phase

Documentation of the crash site is done by identifying the damage that occurred to the wreckage parts, and checking the surrounding environment of the wreckage for any impact damage due to the accident. All parts and sub-components need to be located and the state of each of these parts is determined. An overview is currently hand-drawn in an accident field sketch. In general, this phase consists of gathering as much relevant factual information about the air accident as possible, where the relevance is of course assessed by the investigator.

All in all, the prelaunch phase consists of various small tasks in order to set up the investigation, as well as travelling to the accident site. However, the search and documentation phases are most time intensive, especially for remote accident locations.

2.3. Investigation procedures with MIRU

In this section, the benefits of MIRU to an investigation are presented. This is applied to the mission case which was defined earlier in Section 2.1. The most important differences during an investigation with and without MIRU are presented in Table 2.2.

2.3.1. Prelaunch phase

In the prelaunch phase, the investigator in charge has to make sure that MIRU is taken together with the basic equipment to the accident location. Since the system can be stored in its casings in a backpack, the system is always ready to be taken to an investigation, meaning it is just a matter of a couple of minutes in extra preparation time. In the worst case, the system still has to be prepared for transportation because for instance maintenance was performed. However, preparing the system for transportation is also only a matter of a couple of minutes. Especially when it is compared to the total length of the prelaunch phase, the extra time needed for preparation is negligible. In the case study, the total time of the prelaunch phase was approximately 13 h, and therefore no effects can be seen in this phase when taking MIRU to an investigation.

2.3.2. Search phase

The search phase of an investigation can be considerably shortened when using MIRU. Even if the deployment of the system is taken into account in this phase, the search time can be decreased a lot. Given a deployment time of 30 min, and the fact that the UAV has to travel from the basecamp to the accident site and back, the expected time to locate is likely within 3 h for the case study. This 3 h search time is based on the last known radar locations, which served as the starting point for the search mission. In the case study, MIRU would need 10 min to fly to the accident site when starting out from the basecamp. Within the 70 min flight time that is left, the UAV is able to map an area of 2 x 2 km. The distance between the last known point of radar contact and the main wreckage location was 0.5 km, and therefore mapping the largest possible area, MIRU is likely able to locate the wreckage in one flight. This results in a total time for the search in less than 3 h, excluding any small administrative actions that need to be done in the search phase. The wreckage was largely camouflaged between the rocks, so it was very difficult to locate the wreckage using helicopter by eye [35]. Therefore, MIRU is in that case deployed with its multispectral camera, in flying wing configuration, to easily distinguish the wreckage from its surroundings.

If no space is available to perform a hand-launched take-off, MIRU can also be deployed in the tailsitter configuration, which decreases the search area mapped in one flight, but increases versatility as vertical take off and landing VTOL is possible. Deploying the UAV also enables easy transitioning to the documentation phase, as the UAV can directly make detailed images after locating the wreckage. Thus, using the tailsitter naturally links the search and documentation phases together. Extra benefit is that the UAV is then taken to the accident site by itself where it can easily perform a vertical landing.

Of course there is the probability that the wreckage was not found within one flight, which would require changing the batteries at the basecamp and setting out another flight, which would take an additional two hours. Even in that case, the main wreckage would have been found earlier than the actual time that was needed for the search phase (8.5 h). Also, the wreckage can be found earlier by deploying MIRU already during the prelaunch phase, while setting up the basecamp and performing the briefings.

2.3.3. Documentation phase

MIRU's aid in the documentation phase is done by deploying the system on site. The system is used in its quadcopter configuration, which enables it to make detailed images of the wreckage parts. The system is easily transportable in a backpack, which means the investigators could take MIRU with them during their helicopter flight to the accident site, which remains the easiest way of transportation to the accident site. It is expected that a helicopter is still needed in the described case study, but the time a helicopter is needed is tremendously decreased. A helicopter needs to be deployed for transportation to and from the accident site only, instead of using two helicopters for a full day for the search (2 x 8 h). This would result in the fact that chartering a helicopter for only 3 h in total would be sufficient (or 1.5 h per day), and is even optional as walking to the accident site is also possible. Walking to the accident site is however time consuming.

The operational cost of MIRU is by all means a lot lower, only €60,- per hour, which greatly reduces the total equipment operational cost, as seen in Table 2.2. In the operational cost with aid of MIRU, a helicopter is chartered for 3 h, to transport the investigators. For the normal procedure, it was assumed two helicopters were chartered for 8 h plus and additional 2 h to transport the investigators. Operational cost of the basic equipment is not included in this comparison, as these remain the same.

The documentation is sped up by making detailed images of the parts, and less walking back and forth is

needed as the locations of all wreckage parts are known and visible via the tablet. The actual accident site of the Agusta A-109E helicopter was 150 x 300 m, as seen in Table 2.1, which means that MIRU can detail map this site in 20 min, while in the mean time replacing the batteries once. The usual administrative actions still take up some of the time, and therefore the conservative estimation was made that the full documentation phase still takes up half a day, in the mean time, MIRU can map other areas that might be of interest as well, just outside the debris field.
Not only for remote areas, but also at airports MIRU is able to greatly reduce the time for the documentation phase. This results directly in less loss of turnover at airports, as the close down time of the runway is shortened a lot.
Given the mission case, the expectation was made that MIRU is able to speed up the documentation phase by at least a factor two, as debris fields at airports are often relatively small.

Concluding the case study
To conclude an investigation with MIRU, it is clear that search and documentation time during an investigation is greatly reduced. Also, the equipment operational cost is decreased. Without MIRU, locating a remote accident site is very time consuming, meaning important information might get lost and the chance of rescuing survivors is decreased. Documenting is done faster as well, as less walking back and forth is needed because of the high detail map made by MIRU. For airports, the main benefit is in the documentation phase, as locating the wreckage is often less of an issue. Furthermore, documenting the accident site in half the usual time has a great benefit for the airport as the business can continue sooner, resulting in less loss of profit.

Table 2.2: Comparison table, effectiveness of an investigation with and without MIRU for the Agusta A-109E accident

Phase	**Performance measure**	**Normal procedure**	**With aid of MIRU**
Search	Time to locate main wreckage (h)	8.5	< 3.0
Documentation	Time to document accident site (day)	1	< 0.5
Search+documentation	Equipment operational cost (€)	54,000.-	9,400.-

3

Mission definition

The main mission objective of MIRU is to locate and map an air accident site. MIRU is designed to aid air accident investigators by facilitating a faster and lower cost investigation. MIRU locates air accident sites and maps these. By using MIRU, a coarse map of the wreckage can be made without having entered the accident site. After the coarse map is delivered and the investigators have arrived on site, a detailed map is generated by MIRU. MIRU also aids air accident investigators when the accident site is directly accessible. In that case, MIRU delivers a coarse map first, after which it will generate a detailed map of the site. MIRU can operate in horizontal flight (flight with wings) and vertical flight (hovering flight). Next to this, MIRU also has the capability to detect the presence of toxins, in order to know whether it is safe for the investigators to perform an investigation on site. Before the UAS can be designed, the different mission objectives must be analysed. There are four mission types possible with MIRU as explained below.

1. **Remote mission: coarse mapping**
   The remote mission is carried out when the crash site is not directly accessible for the investigators. It is then desirable to have a coarse map of the crash site in order to estimate the severity of the crash and have a first overview of the crash site. If the location of the wreckage is not yet exactly known, the UAV must first perform a search mission, after which coarse mapping is performed. If the endurance and range still permit, the coarse mapping is done directly after locating the crash site, without returning to basecamp first. In this mission, the UAV mainly operates in horizontal flight.

2. **Remote mission: coarse mapping and toxins detection**
   In this mission profile the UAV does not only make a coarse map, but it also performs toxin detection. This implies the detection of toxic gases and of explosive gases. Usually it is known beforehand, from the cargo list of the aircraft, whether there were toxins in the cargo and which these were, such that a specific detection can be performed. It is important to know whether it is safe for investigators to enter the accident site to perform an investigation. The UAV operates in horizontal flight whilst generating the coarse map, and it operates in vertical flight whilst investigating the presence of toxins.

3. **On-site mission: coarse mapping and detailed mapping**
   In case of the on-site mission, the crash site has generally been mapped during the remote mission. The detailed mapping is performed afterwards, which requires a higher ground resolution. In case of detailed mapping, the UAV operates in vertical flight. It can also occur that the crash site was accessible without need of a remote mission. If this is the case, a coarse map has not been made yet, thus the UAV must deliver a coarse map first, to get an impression of the crash site from an aerial view, before the detailed mapping can commence. In this case the UAV operates in horizontal flight.

4. **On-site mission: communication relay**
   In case the accident site is situated in a remote area where no communication infrastructure is present, the investigators still need to have a possibility to communicate with each other to aid in the investigation. This is also applicable if an existing communication infrastructure is not functioning. Thus the UAV must be able to perform missions as a communication relay, facilitating communication between investigators when they are in the vicinity of the UAV. The configuration used for this is the flying wing, since it has the best endurance.

4

System description

MIRU performs the missions that are defined in Chapter 3 by operating in different configurations that are optimal for those missions. These are the tailsitter, the flying wing and the quadcopter configurations. In Section 4.1 these configurations are treated and their respective mass, power and cost budgets will be given. Following this, the layout of the payload is treated in Section 4.2. The layout of the payload is treated separate from the layout of the other subsystems within the system, since the payload is leading in the design of the rest of the system. In Section 4.3 the internal layout of MIRU is treated, in which focus is put on the rest of the subsystems. In Section 4.4 the operational limits, determined by the subsystems, are given, to show the driving factors for the UAV. Finally a breakdown of the mass, power and cost budget of the system are given in Section 4.5, to give an overview of the budget for each subsystem.

4.1. Planform

The three configurations in which MIRU performs its missions are given in Figure 4.1. More detailed, technical drawing can be found in Appendix A. The tailsitter configuration, depicted in Figure 4.1a, is used for the remote mission when MIRU has to generate a coarse map and perform toxin detection, as described in Chapter 3. The flying wing configuration is used in the remote mission when solely coarse mapping (and possible locating of) the accident site has to be performed. In this configuration MIRU is able to obtain a much longer endurance in horizontal flight. The UAV is used as a communication relay in both the tailsitter configuration and the flying wing configuration. In the quadcopter configuration (see Figure 4.1c), the UAV can obtain low speeds by means of vertical flight and this configuration will be used for detailed mapping during the on-site mission.

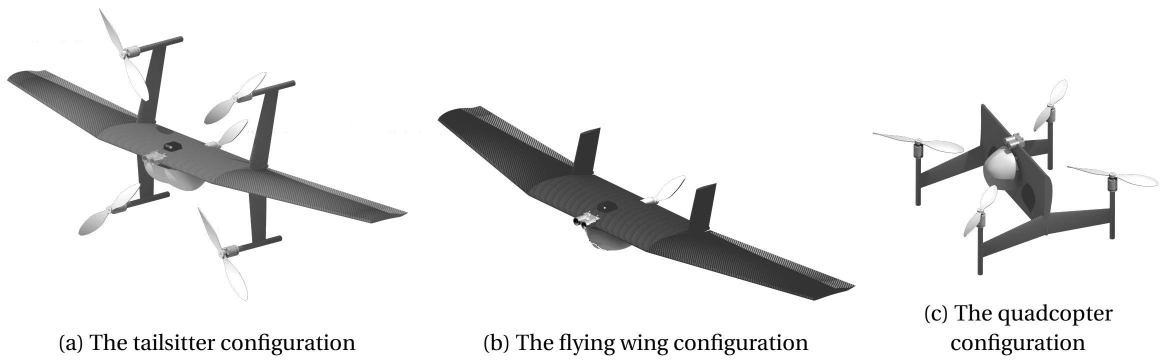

(a) The tailsitter configuration (b) The flying wing configuration (c) The quadcopter configuration

Figure 4.1: The three configurations in which MIRU will perform its missions

The tailsitter configuration

MIRU is in its heaviest configuration when operating as a tailsitter. In this configuration the platform consists of a body, two wings, two fins , four vertical flight motors and one horizontal flight motor. The tailsitter is able to perform both vertical and horizontal flight.

In case the tailsitter configuration is used because it needs to perform toxin detection (vertical flight) and coarse mapping (horizontal flight), the payload will always carry a mapping device and the toxin detection sensor, making it the heaviest payload configuration. The payload fairing and the devices are mounted such

that the mapping device is pointing towards the Earth during horizontal flight. The toxin detection sensor is positioned in the most compact way in the payload bay (the orientation towards the Earth or parallel to the Earth of this sensor results in the same performance). The payload components selection and working principle are further explained in Section 8.1.
In case the exact location of the accident site is unknown and when there is a high priority of toxin detection, a search mission needs to be performed with the tailsitter. The tailsitter then first locates the accident site, after which it performs toxin detection. If there is still sufficient power left, the UAV coarse maps the accident site as well. If not, the UAV returns to basecamp first.
The tailsitter is also used when only coarse mapping needs to be performed when the accident site is in remote areas and when there is not enough space for a bungee launch (see Section 8.8.3). In this case the UAV must perform a vertical take-off and landing, thus a tailsitter is necessary. In this case, only a mapping device is placed inside the payload bay and thus a flying wing payload fairing could be used.
The tailsitter can also function solely as a communication relay, however, the flying wing is preferred since it has a higher endurance.

Flying wing configuration
When MIRU operates as a flying wing, it is in its lightest configuration and it has the longest endurance (122 min, see Section 8.8.2). In this configuration the UAV consists of the body, two wings, two small fins and one horizontal flight propeller. The flying wing performs a bungee assisted take-off (see Section 8.8.3) and a belly landing.
With this configuration, MIRU has the same mapping capabilities as the tailsitter configuration, but it has a higher range and endurance. When the location of the accident site is not yet exactly known, the flying wing firstly executes a search mission. If still sufficient power is available after the search mission, MIRU also coarse maps the accident site. The payload fairing of the flying wing always covers only one mapping device, thus the fairing is more compact than the payload fairing of the tailsitter. In this configuration, the payload bay is designed such that the mapping devices are always directed to the Earth's surface when the UAV is operating in horizontal flight.
Furthermore the flying wing is also solely used as a communication relay. In this case there is no payload fairing mounted to the UAV, resulting in a lower weight, and thus higher endurance.

The quadcopter configuration
MIRU operates in the quadcopter configuration during the on-site mission. The platform consists of the body, two fins and four vertical flight propellers. This configuration is necessary for detailed mapping as lower flight speed is required, which cannot be obtained using the configurations with the wings. The quadcopter carries a payload bay in which only one mapping device is present, since no toxin detection needs to be performed by the UAV, when the investigators are allowed on site. In this configuration, the payload fairing is mounted such that the mapping devices are directed to the Earth's surface during vertical flight. This means that in this case the cameras are mounted parallel to the body.

4.2. Payload layout
MIRU carries a swappable payload which contains either a mapping device, or a mapping device in tandem with a toxin detection sensor. In order to fulfill the mission objectives as set in Chapter 3, the payload contains a visible light camera to map during daytime, an IR camera to map in the absence of sunlight, and a multispectral camera to map a camouflaged wreckage. The cameras that are installed on the UAV are the Mapir Survey 2 (RGB), the FLIR Vue Pro R (IR), and the Tetracam ADC Snap (multispectral). The toxin sensor used is the MicroRAE. The specific device selection analysis is carried out in Section 8.1. These devices are grouped in different configurations, belonging to different mission objectives, which are treated in Section 8.1.2.
There are three payload fairings, one for each configuration of the platform (see Section 8.7.4). Within these fairings, the different payload configuration are installed. The mass and cost budgets of these payload configurations are given in Table 4.1.

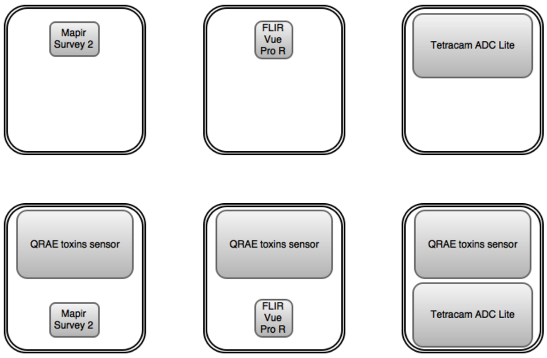

Figure 4.2: Payload layouts for the different mission scenarios.

Table 4.1: Mass budgets and costs for each payload configuration

Configuration	**Mass** (g)	**Cost (€)**
Visible light camera	47	345
Infrared camera	100	3,499
Multispectral camera	90	3,495
Visible light camera + toxin sensor	227	1,136
Infrared camera + toxin sensor	280	4,290
Multispectral camera + toxin sensor	270	4,286

4.3. System layout analysis

To gain insight in how MIRU fulfils the mission objectives, the system layout must be analysed. In order to do this the subsystems have been identified and the layout is discussed. Since the design of MIRU is dependent on the design of its payload, the payload was discussed previously. The functions needed from the subsystems are described with flow diagrams in Appendix B.

4.3.1. Identifying the subsystems

MIRU consists of several subsystems, which are needed to perform its missions. Each subsystem fulfils a certain function within the system and has interaction with other subsystems. To design MIRU efficiently, the subsystems need to be designed in parallel. Thus it is important to identify the functions and interactions of each subsystem. The following subsystems were identified: payload, communication, groundstation, guidance, navigation and control, airframe, control surfaces, propulsion and electrical system.

To gather certain data important for the investigation, payload is needed on the UAV. This data can be mapping data or toxin detection data. The payload was sized before the rest of the subsystems were designed, as the payload requirements and thus the dimensions and weight were driving for the design of the other subsystems.

To transfer this payload data to the investigators, the communication subsystem is needed. The communication system provides the user feedback on the gathered data and the UAV's status. This allows the user to change the mission parameters, based on the feedback. The communication also contains a communication relay, which enables communication between different groundstations. This is used when multiple users on the accident site need to communicate to each other over a large distance.

The groundstation consists of all the necessary operational items to facilitate the investigation. It consists of a communication system, control and visualisation devices and data processing devices. The data sent by the communication system on-board the UAV is received and displayed to the user on the control and visualisation device. This device also enables the user to send new area of interest input commands to the UAV, when the user observes something interesting that the UAV should examine. After the UAV has performed its mission, data processing devices are used to process the data gathered.

Now that the UAV can gather data and send this to the groundstation, the UAV needs a system to guide and control it into the air, in flight and back to the ground. The guidance, navigation and control are the brains

of the UAV that takes care of this. The UAV needs to be autonomous such that the investigators can focus on performing the investigation, rather than losing time operating the vehicle. When in flight, the UAV can encounter obstacles or environments it needs to avoid, and for this the hardware and software of this unit work closely together to ensure a safe and efficient flight.
The subsystem performing the actions as instructed by the GNC unit is the control and stability subsystem. This system on the UAV is of great importance, since the flight and manoeuvres that the UAV performs need to happen in a controlled fashion. Therefore control surfaces are used together with actuators, which are triggered by the GNC.
In order to get the UAV into the air and to operate, the propulsion system is needed. This consists out of vertical flight propulsion and horizontal flight propulsion, such that both types of propulsion can be performed most optimal.
Now that all the subsystems are identified, there is some source needed to power the subsystems. This is the electrical subsystem, which delivers and distributes the power needed. Next to that, it also connects all the subsystems to ensure mutual communication, so information can be exchanged from one subsystem to another.

4.3.2. Layout of subsystems within the UAV

In order to make the UAV as compact and efficient as possible, the subsystems were positioned and integrated carefully. The position of the subsystems discussed in 4.3.1 is depicted in Figure 4.3 .

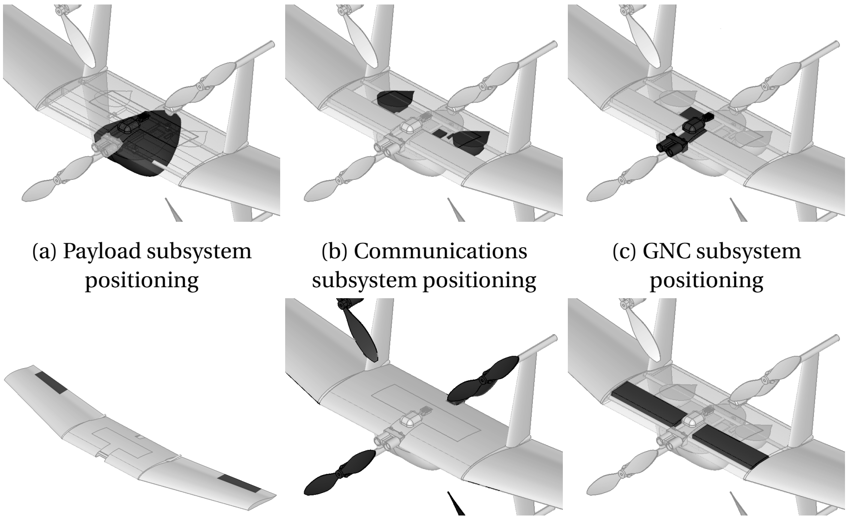

(a) Payload subsystem positioning
(b) Communications subsystem positioning
(c) GNC subsystem positioning
(d) Location of the control surfaces
(e) Propulsion subsystem positioning
(f) Electrical subsystem positioning

Figure 4.3: Subsystems layout inside the body of the UAV and outside the body

Since the payload unit is switchable and needs to be easily accessible for a good operationality, the payload is attached on the bottom, outside of the body (see Figure 4.3a). In this way the payload can easily be switched, without needing to disturb other subsystems.
The communication subsystems is divided over the UAV and the groundstation. It contains hardware on the outside bottom of the UAV, for optimum receiving and transmitting performance. Hardware that does not transmit to or receive from the groundstation is positioned inside the body of the UAV, as can be seen in Figure 4.3b.
The GNC consists of hardware and software, and the hardware is distributed inside the main body and on the top outside the body (see Figure 4.3c). The autopilot is positioned central in the body, such that the hardware that feed back data to the autopilot are all positioned optimally around it. The hardware that obtain inertial measurements of the UAV are positioned inside the body and the hardware that obtain data about the environment are positioned outside the body. However, the sensing apparatus that senses objects on the UAV's flight path is positioned in the nose, on the inside of the UAV such that it is always pointing in the direction of flight and the apparatus is protected from the environment.
The control surfaces that ensure stability and control of the UAV consist of elevons on the wings, as depicted

in Figure 4.3d. These are controlled by servos which lie inside the wing, and are connected to the autopilot.
In order to propel the UAV four vertical flight propellers are installed on the tips of the fins, and one horizontal flight propeller is installed on the back of the body, see Figure 4.3e. In order to perform the most optimal vertical flight at all attitudes, several sets of four propellers can be installed on the UAV, see Section 8.8, meaning that these propellers are easily switched.
Lastly the electrical unit distribution is shown, as this is dependent on the positioning of the other subsystems. The batteries needs to be replaced regularly, so they were positioned conveniently such that they could be pulled out at the tips of the body, near the leading edge. One battery was placed on the left of the center and one on the right, see Figure 4.3f, to allow for symmetric loading. The wiring through the body was optimally placed such that as little wiring as possible was used. However, it was still constrained by the manufacturability of the internal structure of the UAV.

4.4. Operational limits

The operational limits are highly dependent on the subsystems. From the subsystems certain environmental conditions were identified in which MIRU can and cannot operate. First there is a altitude range, which is determined by the propulsion system. MIRU can operate between sea level and 4500 m. Above this altitude the propulsion system does not provide enough thrust anymore for the UAV to hover.
There is also a minimum temperature of -20 $°C$ and a maximum temperature of 45 $°C$. The minimum temperature was determined by the batteries, since at lower temperatures the battery life and capacity decrease to unacceptable levels. The maximum temperature was determined by the propulsion system, since the motors produce heat. Temperatures above 70 $°C$ cause permanent damage to the motors, this does not happen under a temperature of 45 $°C$.
Lastly MIRU cannot operate near the sea, since the structure and electrical components cannot withstand salty conditions. Furthermore MIRU cannot operate during severe storms, because the UAV is only splash waterproof, so the heavy rainfall can damage electrical components inside the UAV. Furthermore it is uncertain if the UAV can withstand high gusts, since this could not be determined by the models used, as described in Section 8.8.4.

4.5. System budgets

The driving budgets for MIRU are the mass and power. Table 4.2 shows an overview of each of these budgets for all three configurations. Next a brief discussion is given for each individual budget to highlight the important aspect regarding the design.

Table 4.2: Mass and power budgets of the three configurations

Configuration	**Mass** (kg)	**Power** (W)
Tailsitter	2.21 - 2.44	5.74
Flying wing	1.20 - 1.73	5.74
Quadcopter	1.99 - 2.04	5.76

4.5.1. Mass budget

As the MIRU has three different configurations, with different payload options, there is not one single value for the mass of the UAV. Table 4.3 shows the masses for the three configurations for each different payload option as described in Section 8.1.2. From Table 4.3 it is clear that the worst case mass of MIRU is 2.44 kg, which is driving for the design. The quadcopter configuration does not include the Tetracam Snap for any mission. Another important note is that in the tailsitter configuration also the toxin detector is built in.

Table 4.3: Mass of the three configurations with the respective payload

Payload	**Tailsitter** (kg)	**Flying wing** (kg)	**Quadcopter** (kg)
Mapir Survey 2	2.39	1.68	1.99
FLIR Vue Pro R	2.44	1.73	2.04
Tetracam Snap	2.43	1.72	2.03

In order to create a broader overview of how much the different subsystems contribute to the total mass, the pie chart from Figure 4.4 was created. The electrical system and performance and propulsion have by far the greatest impact on the design, as they together hold 70% of the mass. The electrical system includes the battery and wires, together good for 1.54 kg. The motors have the greatest influence in the performance and propulsion subsystem, as they are 78 g per motor. The details of all the subsystems are elaborated on in the sections of Chapter 8.

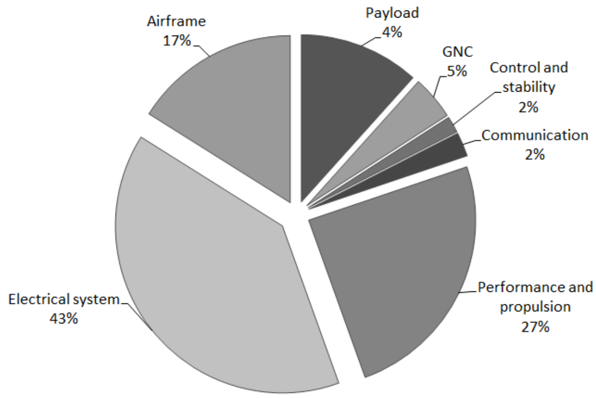

Figure 4.4: Mass breakdown of the UAV

Another mass breakdown was performed for the remote and on-site mission. Those are shown in Figures 4.5 and 4.6 respectively. Their masses are 64 kg for all the basecamp equipment and 6.1 kg for the weight of the on-site equipment, both excluding the UAV. The on-site mission groundstation holds the same components as is brought in the backpack elaborated upon in Section 6.3.2.

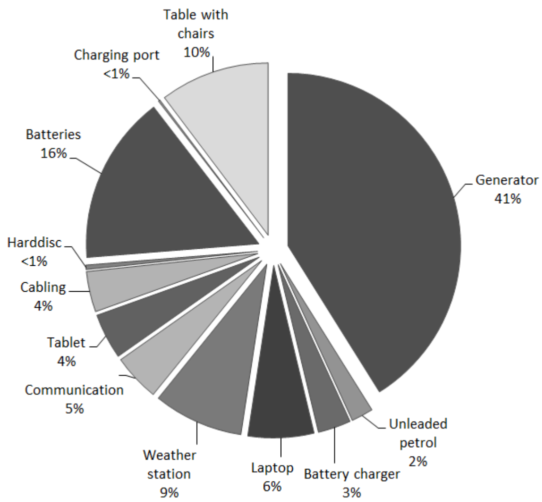

Figure 4.5: Mass breakdown of the groundstation for the remote mission

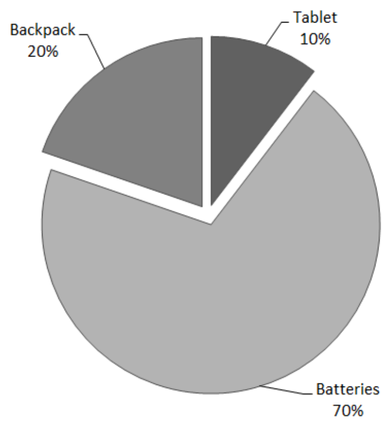

Figure 4.6: Mass breakdown of the groundstation for the on-site mission

4.5.2. Power budget

As more energy is required during a mission, more battery capacity is needed on-board of the UAV. In order to keep the UAV as light as possible, this power required was minimised as much as possible. An overview of the peak power and average power consumption of all the electrical components can be seen in Table C.2 from Appendix C. In order to calculate the average power required, the endurance of a nominal mission is considered to be about 100 min, as this is the endurance of a mission in hybrid configuration, as described in Section 8.8.2, which is demanding the most power. In order to get an overview of the average power required, the pie charts in Figures 4.7 and 4.8 were created.

In Appendix C in Table C.2, it can be seen that the peak power consumption is about 9.39 W. This power has to be converted from battery voltage -14.8 V nominal- to 5 V for the electrical subsystem, as described in Section 8.9. This means a peak current of about 1.98 A wil occur, which is a stringent requirement for choosing the appropriate power converter and wiring in Section 8.9.
Also the extra battery capacity needed for the electrical components should be considered, as this increases the total capacity of the battery, and thus the weight. In Appendix C in Table C.2, it can be seen that the average power consumption is about 5.88 W, which, after a nominal mission of 100 min, adds up to a required energy capacity of about 10.61 Wh. This means the battery on the UAV needs to be able to deliver this amount of energy, which will be further discussed in Section 8.9.3.
From Figure 4.7, it can be seen that the GNC subsystem and the payload have the highest peak power. However, considering the time they are on, only the GNC subsystem consumes the most power on average, illustrated in Figure 4.7, as it is operating continuously during the mission. The most power demanding component is the GNSS receiver, which will be discussed in Section 8.4.1 consuming 1.16 W continuously. This means the GNSS receiver was driving for the sizing of the electrical part of the battery, using 20% of the average power, illustrated in Figure 4.8.

Next to the GNC subsystem, the communication and control subsystems are the subsystems consuming the highest average power, as seen in Figure 4.7. This is due to the transmitter and receiver modules, which have a relatively high power demand, continuously, as seen in Figure 4.8, and the servos, which have a power demand of 1 W combined. The electrical subsystem only uses about 4% of the total average power consumption, due to passive and low-power electronic components.

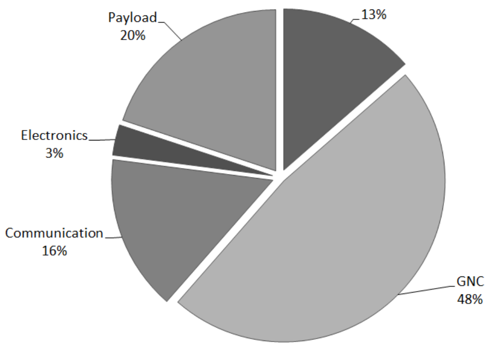

Figure 4.7: Subsystem power budget breakdown

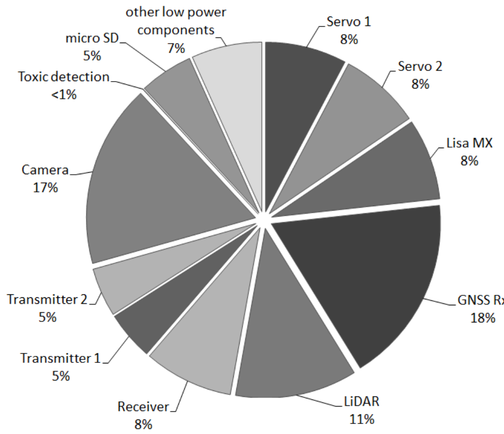

Figure 4.8: Component power budget breakdown

It should be noted that the power required for the propulsion subsystem is not included in the power budget, as the power consumption by this subsystem is large compared to the power required for all the other subsystems combined. Adding the power required for the propulsion subsystem here would give a distorted view on the budgets. However, the power required for the propulsion subsystem is described in Section 8.8.

4.5.3. Cost budget

The total component cost of MIRU is €23,500,-, of which €2,900,- is the cost of the platform, €9,900,- the payload and €10,700,- the groundstation. The complete breakdown of the cost is presented in Appendix D. The costs are not expected to rise much, as most of the components are off-the-shelf products. Still, a contingency of 20% has been included as MIRU is still a concept design. The cost has been split up for two different situations. There is a cost breakdown for the whole system, shown in Figure 4.9, and one for the UAV only, as can be seen in Figure 4.10.

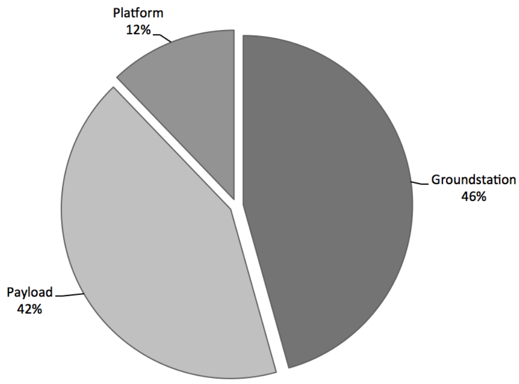

Figure 4.9: Total cost breakdown of MIRU

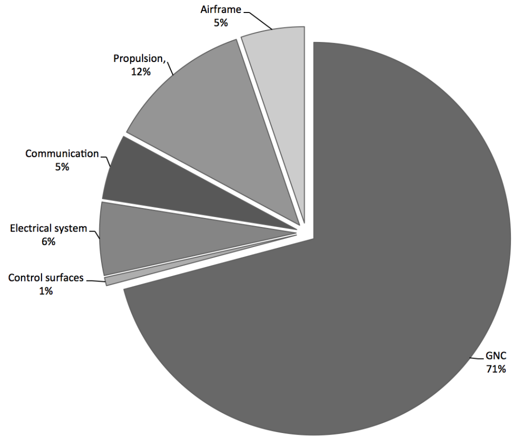

Figure 4.10: Cost breakdown of the UAV.

Getting into more detail, it is the GNC that uses 71% of the costs for the platform. This is due to one expensive component, the GNSS receiver, with a cost of €1,200,-. This GNSS receiver however is needed to guarantee accurate positioning in as many areas as possible. The payload and groundstation are more expensive then the platform due to the rather expensive payload, €3,499.- for the IR camera and €3,495,- for the multispectral camera, and expensive equipment placed at the groundstation (€3,750,- for the weatherstation, €1,050,- for four tablets including short range communication and €1250,- for a laptop). The acquisition costs can be found in Section 12.3.

5
Mission profiles

To properly assess the performance of the UAV mission profiles were made for the different missions in different configurations. This is done to combine the performance from the flight modes, since a mission does not consist of a single flight mode. Several possible mission profiles are considered for certain configurations and payloads to give the most complete overview.

With the analysis it was found that the payloads with IR camera significantly reduce the area that can be mapped. This is because the maximum velocity for the IR camera is much lower than the optimal speed for range. Furthermore it was found that the percentage energy needed for the manoeuvre to perform toxin detection was relatively small. However, the added weight of the toxin detector has a significant negative impact on the area that can be mapped. All results from the analysis can be found in Table 5.5.

5.1. Mission profile analysis method

It would be irrelevant for the report to assess all mission profiles for all configurations at all the operating conditions. Thus, only a few specific mission profiles were selected, which give the best understanding of the performance of the UAV.

For the remote mapping mission, the flying wing and tailsitter configuration were analysed. The flying wing gives the longest range, but the take-off of a flying wing might not always be possible. Thus for the remote mapping mission the tailsitter configuration was also analysed. A tailsitter provides vertical take-off and landing, in this case. For the remote mapping mission with toxin detection, the tailsitter configuration was analysed since this is the only configuration that is able to perform this mission. For the on-site mapping mission, the quadcopter configuration was analysed, since this configuration provides the low velocities needed for detailed mapping. The communication mission and on-site mapping mission with the tailsitter or flying wing configuration are not discussed, because these missions are very similar to the remote mapping mission and require less performance than the remote mapping mission.

The mission profiles were analysed by calculating the energy needed to perform a certain part of the mission profile, based on the performance calculations, described in Section 8.8. This is done for different altitudes and payloads to give a performance range. The mission profiles were assessed at the altitudes 0 and 4500 m, since these give the minimum and maximum performance. Only the payloads including a multispectral camera, so payload configurations 3 and 6 (from Section 4.2), were not analysed, since these give almost the same performance as the corresponding payload with the visible light camera. These payloads are used at approximately the same altitude and velocities and the impact of the mass difference between the cameras is negligible on performance. Thus payloads 1 and 2 were analysed for the remote mapping mission with flying wing and tailsitter. Payload configurations 3 and 5 for the remote mapping and toxin detection mission with tailsitter, and payload 7 and 8 for the on-site mapping mission with quadcopter. For each mission profile an energy breakdown was made, since these are straightforward to compare, so factors that decrease performance are clear to identify. The energy was calculated by multiplying the power calculated for a certain flight mode and the expected time needed for a certain flight mode. These values are increased by 10% to account for gusts and small corrective manoeuvres.

5.2. Remote mapping mission in flying wing configuration

The remote mapping with flying wing mission profile can be seen in Figure 5.1. In Table 5.1 the description of the ID's can be found.

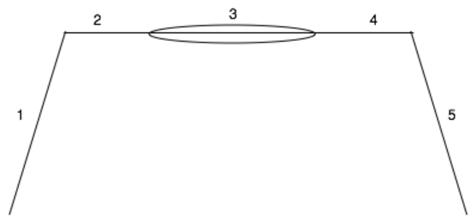

Figure 5.1: Remote mapping mission profile in flying wing configuration

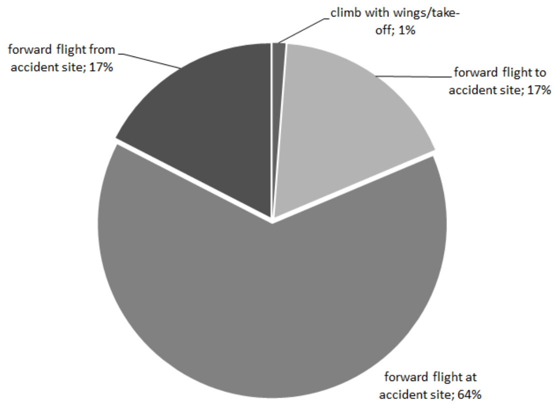

Figure 5.2: Energy breakdown for the remote mapping mission profile in flying wing configuration

Table 5.1: Remote mapping mission profile ID's in flying wing configuration

ID in profile	**Flight mode**
1	Bungee launch/climb with wings
2	Forward flight to accident site
3	Forward flight at accident site (mapping)
4	Forward flight from accident site
5	Descend with wings/belly landing

This mission profile starts with a take-off with the bungee launcher. Since most of the energy at take-off is given by the bungee chord and the take-off is relatively short, it was assumed that the energy needed for take-off is included in the climb energy. The take-off is followed by climb with wings with a climb rate of 3 ms^{-1}. Once arrived at the cruise height of 75 or 150 m the UAV flies with a velocity between 15 and 20 ms^{-1}, depending on the height and payload, to the accident site. These velocities are optimal velocities for range, determined in Section 8.8.2.

When arrived at the accident site the UAV starts mapping. This is also done at the optimal velocity. However for payload configuration 2, this is not possible, since the maximum velocity for this payload is lower than the optimal velocity. This gives a lower performance for payload configuration 2. When the UAV is done mapping it flies back to the basecamp. This is again done at an optimal cruise velocity. When the UAV is back at the basecamp it descends and lands. Descend is done with a descent rate at 3 ms^{-1}, which uses no power so that more energy can be used for cruise flight. Landing is done by giving reverse thrust and making a belly landing. Since low power was calculated for the reverse thrust and the time is expected to be very short, it was assumed that the energy needed for landing is included in the contingency factor.

In Figure 5.2 the energy breakdown for this mission can be seen. Most of the energy is needed to fly to and from the accident scene and for mapping flight. 72% of the energy is used for mapping flight. This gives a mapping time between 48 and 55 min, for payload configuration 1. This allows the UAV to map 9.5 to 10.5 km^2. For payload configuration 2 the mapping time is between 55 to 63 min, which allows the UAV to map 1.5 to 1.7 km^2. The difference between the mapping areas for different payloads is caused by the velocity restriction for payload configuration 2 (IR camera). This forces the UAV to fly at a less optimal speed for range, which decreases the range greatly and thus decreases the mapping area. This phenomenon applies to all payloads with an IR camera (payload configurations 2, 5 and 8).

5.3. Remote mapping mission in tailsitter configuration

For the remote mapping mission, bungee launch is not possible when there is not enough space available. Then the remote mapping mission can be performed by the tailsitter configuration, which provides vertical take-off and landing. The mission profile for this mission can be seen in Figure 5.3. The ID descriptions can be found in Table 5.2.

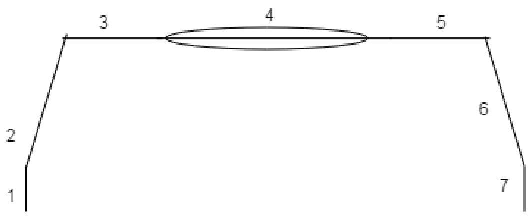

Figure 5.3: Remote mapping mission profile in tailsitter configuration

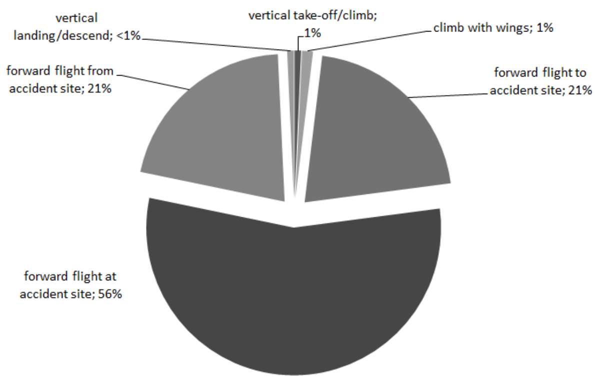

Figure 5.4: Energy breakdown for the remote mapping mission profile in tailsitter configuration

Table 5.2: Remote mapping mission profile ID's in tailsitter configuration

ID in profile	Flight mode
1	Vertical take-off/climb
2	Climb with wings
3	Forward flight to accident site
4	Forward flight at accident site (mapping)
5	Forward flight from accident site
6	Descend with wings
7	Vertical landing/descend

As can be seen the mission profile is roughly the same as for the remote mapping mission with flying wing. They differ in take-off, climb, descend and landing. Take-off is done using vertical take-off. After that the UAV climbs vertically to 15 m where it performs transition. It was not possible to unambiguously determine power or time for transition (see Section 8.8.2). For this analysis it is assumed that the energy for transition is included in the 10% contingency for extra manoeuvring. After transition the UAV performs a climb with wings, just like the flying wing, to a mission altitude between the 75 to 120 m. The UAV descends with wings just like the flying wing does. However at 15 m height, it performs transition again and descends the remaining 15 m vertically.

Again an energy breakdown was made, which is shown in Figure 5.4. Here less than 2% is used for the vertical take-off and landing. Compared to the flying wing more energy is used to fly to and from the accident site, because of the higher mass. This leaves 56% of the energy to be used for mapping flight. This allows the UAV to map 7.1 to 7.3 km^2 with payload configuration 1 and 0.7 and 1.3 km^2 with payload configuration 2.

5.4. Remote mapping and toxin detection mission in tailsitter configuration

For the remote mapping with toxin detection both a long range and hovering capability are needed. This is given by the tailsitter configuration. The mission profile for this mission can be seen in Figure 5.5. The ID descriptions can be found in Table 5.3.

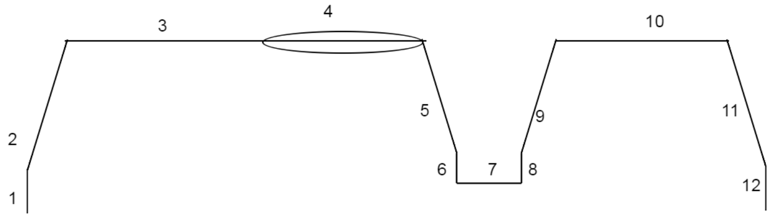

Figure 5.5: Remote mapping and toxin detection mission profile in tailsitter configuration

Table 5.3: Remote mapping and toxin detection mission profile ID's in tailsitter configuration

ID in profile	Flight mode
1	Vertical take-off/climb
2	Climb with wings
3	Forward flight to accident site
4	Forward flight at accident site (mapping)
5	Descend with wings
6	Vertical descend
7	Hover
8	Vertical climb
9	Climb with wings
10	Forward flight from accident site
11	Descend with wings
12	Vertical landing/descend

This mission profile is similar to the remote mapping mission with tailsitter. However this mission also performs a toxin detection. To do this the UAV has to descend with wings at the accident site. It descends to a height of 15 m. After that, transition is performed and the UAV descends further vertically. Then the UAV hovers for 5 s while the toxin sensors make measurements. After that the UAV climbs vertically back to 15 m and performs transition. After that the UAV climbs back to the mission height of 75 to 120 m and continues its mapping mission.

The energy breakdown for the remote mapping mission with toxin detection can be found in Figure 5.6. It can be seen here that the energy needed for forward flight to and from the accident site is significantly larger compared to the tailsitter for the remote mapping mission, seen in Figure 5.4, which is caused by the increase in payload mass. Thus the heavier tailsitter has to fly at a less optimal angle of attack than the lighter tailsitter. Also almost 4% of energy is used to do the toxin detection. This leaves less energy for mapping and with the decreased efficiency, less time for mapping. This results in an area of 5.5 to 5.7 km^2 that can be mapped with payload configuration 4 and 0.5 to 1.0 km^2 with payload configuration 5.

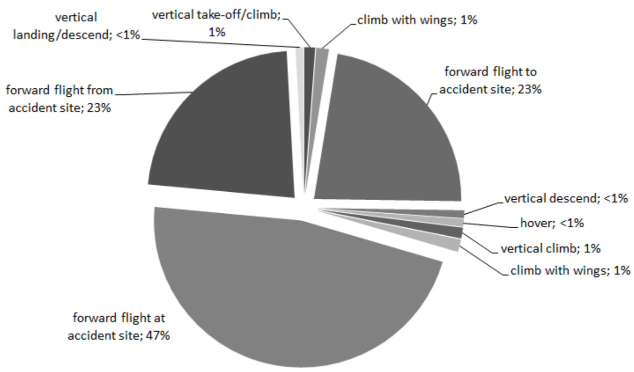

Figure 5.6: Energy breakdown for the remote mapping and toxin detection mission profile in tailsitter configuration with payload configuration 5

5.5. On-site mapping mission in quadcopter configuration

The mission profile of the on-site mission performed by the quadcopter configuration is shown in Figure 5.7. A description of the ID's used can be found in Table 5.4.

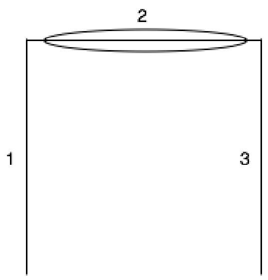

Figure 5.7: On-site mapping mission profile in quadcopter configuration

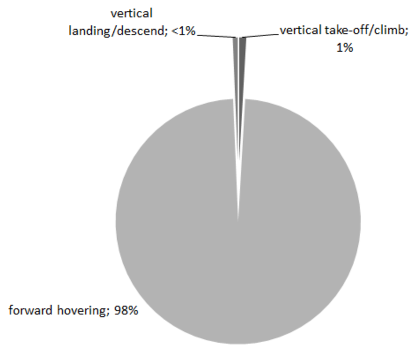

Figure 5.8: Energy breakdown for the on-site mapping mission profile in quadcopter configuration

Table 5.4: On-site mapping mission profile in quadcopter configuration

ID in profile	Flight mode
1	Vertical take-off/climb
2	Forward hovering (mapping)
3	Vertical landing/descend

The on-site mapping mission with quadcopter consists of a vertical take-off which continues in a vertical climb to 15 m. The climb is done with a velocity of 3 ms^{-1}, acceleration and deceleration are taken into account by the 10% contingency factor. Once arrived at 15 m height the UAV stops climbing and performs forward hovering flight. Forward hovering flight is done at a forward velocity of 3.7 ms^{-1} for payload configuration 7 and at a forward velocity of 1.0 ms^{-1} for configuration 8. Forward flight is used by the UAV to get to an area of interest or to map an area of interest, for this analysis it was assumed that the UAV uses all its time in forward flight for mapping. After mapping the UAV descends 15 m to the ground with a descent rate of 3 ms^{-1}. For the power used during this flight mode the same power as for hovering was assumed, since the thrust provided was estimated to be only a little lower than that for hovering.

The energy breakdown for detailed mapping for this mission was determined, which is shown in Figure 5.8. It can be seen that almost all energy is used for forward hovering flight. With payload configuration 7 an area between 2.00 ha and 3.37 ha can be mapped depending on altitude. And with payload configuration 8 an area between 0.15 ha and 0.25 ha can be mapped. This area is much lower compared to payload configuration 7, because the velocity is lower. This is explained in further detail in Section 8.8.4.

Concluding the mission profiles

The final results of the mission profile analysis can be found in Table 5.5. Here it can be seen that the IR camera does not influence the endurance significantly. However due to the decrease in possible velocity because of the IR camera, the area that can be mapped is much smaller compared to that of the visible light camera. It can be seen that the maximum mapping area is for the flying wing configuration with payload 1. 10.5 km^2 can be mapped in 48 min, this is at an altitude of 4500 m. With the quadcopter the maximum mapping area is 3.4 ha, which takes 15 min. This is at sea level. To give a better understanding of the numbers presented, a typical air accident site is not larger than 1 km^2 and a soccer field is 0.75 ha.

Table 5.5: The results of the analysed mission profiles

Mission	**Configuration**	**Payload** configuration	**Mapping time** (min)	**Mapping area** (km^2)
Remote mapping	Flying wing	1	48 - 55	9.5 - 10.5
Remote mapping	Flying wing	2	55 - 62	1.5 - 1.7
Remote mapping	Tailsitter	1	33 - 40	7.1 - 7.3
Remote mapping	Tailsitter	2	24 - 46	0.7 - 1.3
Remote mapping and toxin detection	Tailsitter	4	25 - 30	5.5 - 5.7
Remote mapping and toxin detection	Tailsitter	5	20 - 35	0.5 - 0.9
On-site mapping	Quadcopter	7	9 - 15	2.0 - 3.4 (ha)
On-site mapping	Quadcopter	8	10 - 16	0.1 - 0.2 (ha)

6

Operations and logistics description

In order to correctly use MIRU, the user has to perform certain operations. The operations need to be identified and structured, in order to guarantee easy and quick deployment for the user and to assess possible difficult operations which have to be performed by the user. This is elaborated upon in Section 6.1. Here the operations are analysed to find any actions that is expected to take the user too long, or is too hard for the user to perform. Thus a user friendly system can be guaranteed. From the operational flow diagrams, it turned out that maintenance and inspection are very important factors to have successful operations. Inspection can only be performed well if the inspector, in this case the user, knows what to inspect and what he should recognise as damage and this also has to be a simple and user friendly process.
With the operational procedures known, one might wonder how MIRU is brought to the accident site. This is covered by the logistics of MIRU. As rapid deployment and easy transportation of MIRU are key assets of the design, the logistics have to be known for the users. To have easy transportation, all UAS components fit in three transportation boxes which can be transported in a truck to the basecamp. From there, all components necessary for the on-site mission fit in one backpack.
It was found that the operations are kept as simple as possible. The actions that can be done by the system itself do not have to be done by the user. Also the operations make sure that the UAV functions properly during flight and that defects are detected timely. The operation that can still be improved is the assembly of the UAV. The process of assembly is expected to take longer than necessary, since bolts are used to secure different components. To decrease time simpler connections can be used.

6.1. Operations

The user has to be familiar with the operations of MIRU in order to correctly use MIRU and to get the most out of the UAS. To do so, the operations are identified and structured in a logical order of which operations have to be performed. The whole operation has been split into four stages: pre-flight, during flight, relaunch and post-flight operations. The four stages were examined by determining the flow of the operations. The operations are to be performed at the groundstation. At the groundstation, tablets are placed to receive data from the UAV and laptops to process data gathered by the UAV. For an elaborate description of the groundstation, see Section 8.3. An important operation is the assembly of the UAS, which includes the assembly of the UAV and setting up the groundstation. Without these operations, no flight would be possible.

6.1.1. Main flow of operations

The pre-flight operations are needed to set-up the supporting systems for the UAV and to make the UAV ready for flight. The operations during flight give the user the ability to monitor and somewhat control the UAV. The relaunch operations are needed to get the UAV back in the air after it has finished a mission. Finally post-flight operations are necessary to disassemble the UAV and to get it ready for transport and storage.

Pre-flight operations

An overview of the pre-flight operations can be found in Figure 6.1. The pre-flight operations start with the transportation of all the components of MIRU to the basecamp, which is elaborated further upon in Section 6.3. The components are packed in several cases, out of which the groundstation at the basecamp can be set up. Now that the basecamp groundstation is set up, a map should be loaded on the microSD card using Google

Earth[1]. At least a map of an area of 50 x 50 km around the basecamp should be loaded as to ensure that the autopilot receives enough geographical data of the environment to provide more efficient routes towards the area of interest.

Once at the basecamp, the user can decide to either perform the remote or on-site mission. If an on-site mission has to be performed while the accident site is not accessible by truck or car, meaning the basecamp is not stationed at the accident site. Not the whole UAS is necessary for the on-site mission and thus not all components have to be transported to the accident site by backpack. The next process starts by selecting the components that are expected to be needed at the accident site. This includes the configuration of the UAV, the number of portable groundstations, the number of batteries and the payload necessary to perform the mission. The components that are selected are inspected to identify any damage that needs to be replaced or repaired. After the inspection, the components can be packed in a backpack and transported to the accident site.

Once arrived at the accident site, the best UAV configuration to perform a certain mission can be chosen. If the accident site is close to the basecamp or if a remote missions is being performed, the UAV configuration can be chosen at the basecamp. Again, an inspection has to be performed on the chosen components and if necessary, they have to be replaced or repaired. The inspection and replacement methods are further discussed in Section 6.2.

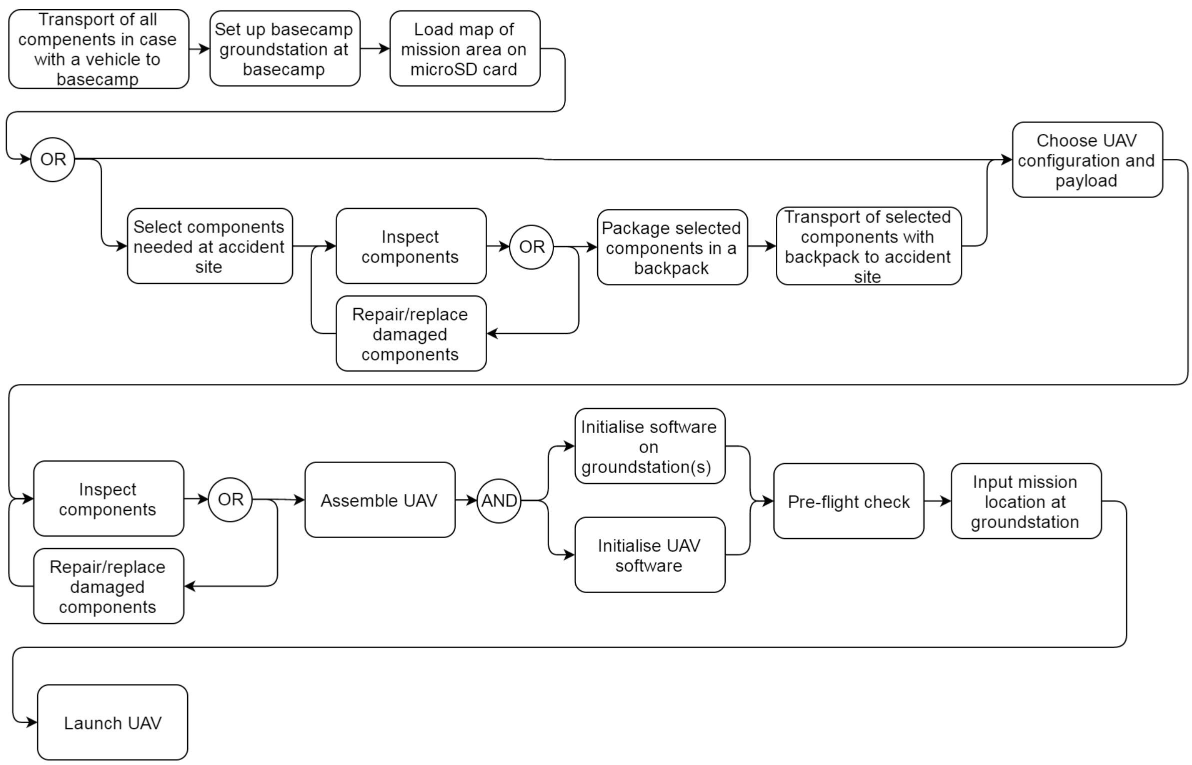

Figure 6.1: Pre-flight operations

Finally the UAV can be assembled by connecting the components necessary. The details of the assembly are presented in Section 6.1.2. When the UAV is assembled, the software on the UAV and groundstation(s) can be initialised. After this a pre-flight check is done to check if the software is working correctly and if all components are working correctly. The pre-flight check is further discussed in Section 6.2. After the pre-flight check the weather sensors on the UAV are calibrated, however this requires no user input as the laptop and tablet are connected through Bluetooth and the tablet sends data to the UAV.

[1] URL:`https://www.google.com/earth/explore/products/desktop.html` [cited 17 June 2016]

Finally the mission location can be defined on either the basecamp groundstation or on one of the portable groundstations, by letting the user give area of interest inputs on the groundstation. After that, the UAV can be launched. If the tailsitter or quadcopter configuration is chosen the UAV performs vertical take-off. If the flying wing configuration is chosen, the UAV needs to be launched using the bungee launcher.

Operations during flight

During flight the user can give and receive certain feedback to the UAV. An overview of these operations can be found in Figure 6.2. The user can check the status of the UAV and receive data from the payload. Based on this, new areas of interest input can be added or edited. Finally there are emergency operations which are present to account for safety. These operations allow the user to give commands for immediate landing or return before the mission has been finished. These operations could be used when the user notices something that compromises the UAV. This can be either a malfunction of the UAV or dangerous environmental conditions which could harm the UAV.

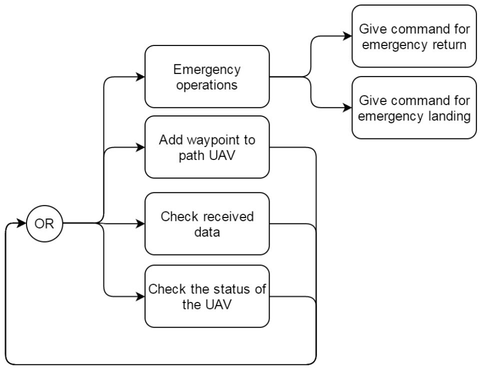

Figure 6.2: Operations during flight

Relaunch operations

After one flight the user can decide to make another flight to increase the effective time of use of the UAV. To accommodate this, the relaunch operations were examined. An overview of the relaunch operations can be found in Figure 6.3. It is very important that relaunching should take a limited amount of time and should be able to be performed easily by the user.

The UAV lands autonomously, or the user can send a command to the UAV to land. After that the wings or the wing caps need to be detached. This allows for inspection of the components used in flight and the components needed for the next flight. With the wings or wing caps detached the batteries can be changed. Also the microSD card can be switched for another one, so processing can be done in between flights. For the next flight the user can choose to change the payload or the configuration of the UAV. With the new configuration set, all UAV components needs to be assembled again.

Next the software on the UAV needs to be initialised and the pre-flight check is done. On either the basecamp or portable groundstation the area of interest is inputted. Then the UAV is ready for take-off. For the flying wing configuration the UAV will take off using the bungee launch.

The batteries can be charged at the basecamp groundstation and the microSD card can be inserted in the laptop, to analyse the collected data. These actions can be performed for the remote mission as well as for the on-site mission if the basecamp is nearby the accident site. If, for the on-site mission, the basecamp is relatively far from the accident site, the batteries and microSD card could still be carried back to the groundstation by the user to be charged and analysed at the basecamp. Finally the unused components are stored in the backpack or case to prevent any damage.

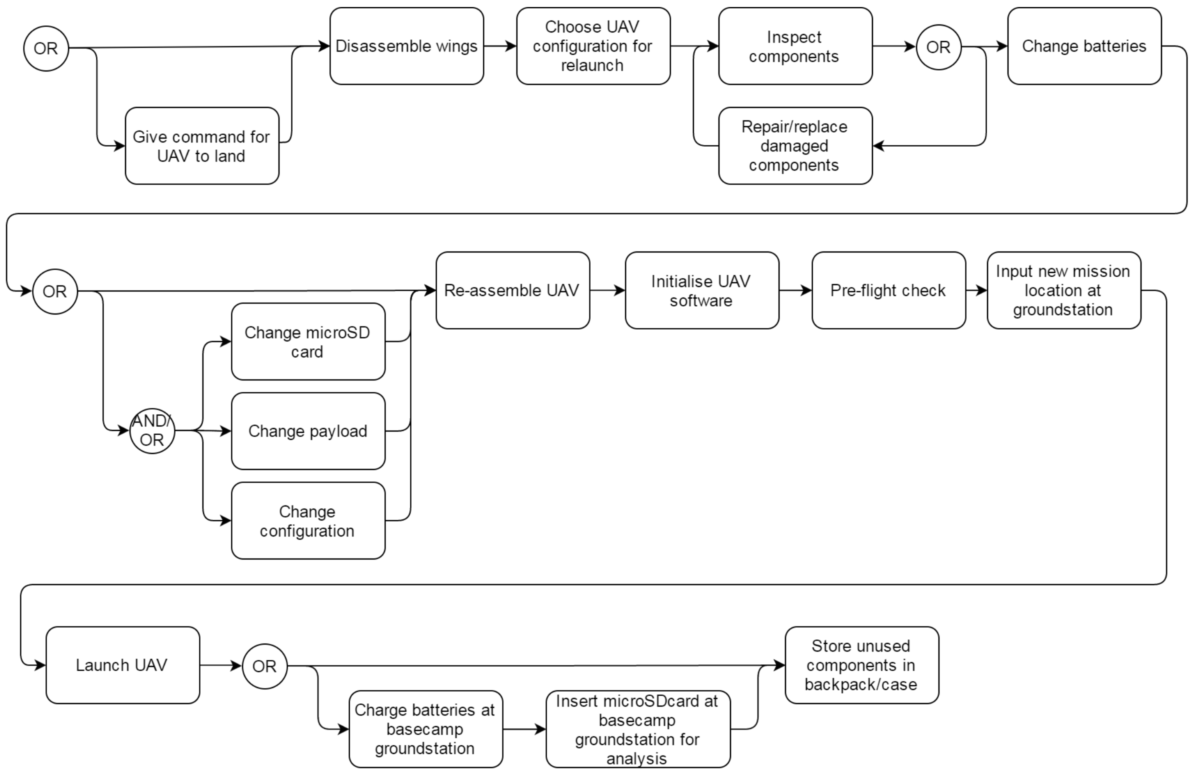

Figure 6.3: Relaunch operations

Post-flight oprations
After the UAV has performed its final flight of the day or mission, the post-flight operations are initiated. An overview can be found in Figure 6.4. The UAV can autonomously decide to land or the user can send a command to the UAV to land. Then the UAV has to be disassembled into its different components, after which the user is allowed to remove the microSD card from the body of the UAV. After disassembly, each component is thoroughly inspected.

The UAV components can be stored in a backpack if the components need to be transported from the accident site to the basecamp. When the UAV is already at the basecamp or when the user arrives at the basecamp, the UAV components can be stored in a case. The microSD card is inserted in the laptop at the basecamp groundstation, so the collected data can be analysed. When the analysis is done the basecamp groundstation can be disassembled and stored in a case. When the whole system is stored in the transportation boxes, the system is ready to be transported back to the aviation safety board.

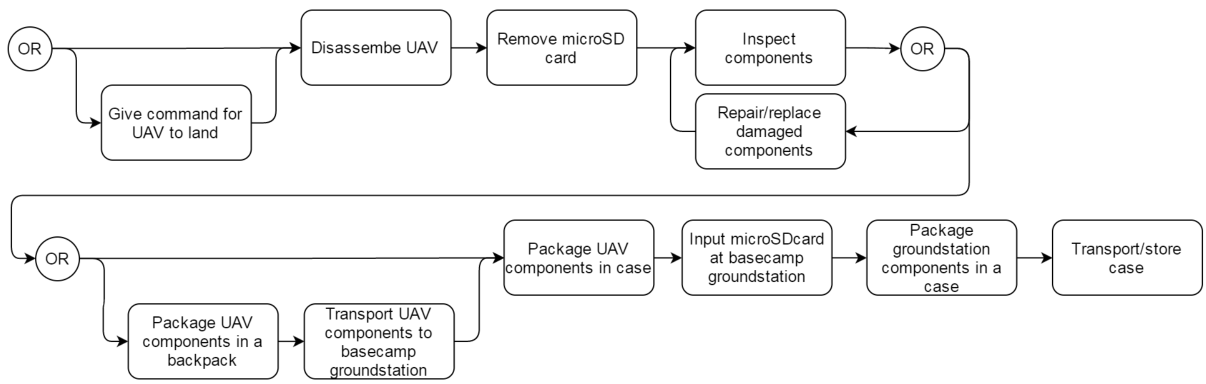

Figure 6.4: Post-flight operations

6.1.2. Assembly

In order to make the UAV ready for flight, the constituent parts need to be assembled first. The joints where the parts are connected are analysed in Section 8.7.2 and are not discussed here. In order to make sure that the right parts are connected to each other, the connecting areas are indicated with the same symbol. First of all the top lid of the main body is removable by four bolts. To make sure that this lid is placed back in the right manner, the front of the lid is indicated with an arrow to the front. Now the different configurations can be assembled. In Figure 6.7 the sequence of the tailsitter and flying wing assembly is organised. In Figure 6.8 the sequence of the quadcopter assembly is depicted.

Assembling the tailsitter

The left wing and the side of the body to which it must be connected contain both a square on the side, on the male and female parts. This can also be seen in Figure 6.5. The right wing and the side of the body to which that wing must be connected both contain a star on the side. The wings are then secured to the body using two bolts for each connector from the bottom of the body. Therefore each wing is secured using a total of four bolts. The fins both contain a triangle, as well as on the top of the location of the body where these fins must be connected. Since these fins are symmetrical, both fins carry the same figure. The fins are secured using a single bolt, which is screwed in the internal thread at the back of the male connector. This bolt therefore prevents the fin from sliding backwards. Furthermore, there are three sets of four vertical flight propellers available, which can be seen in Figure 6.6. The propellers designated with "I" are to be installed for flight between 0 - 2500 m altitude from sea level, for flight from 2500 - 3500 m from sea level the propellers with "II" have to be installed, and for 3500 - 4500 m from sea level the propellers depicted with "III" have to be installed. Furthermore, the clockwise rotating and counterclockwise rotating propellers have colors corresponding to the motor it has to be attached to. Also the horizontal flight propeller has to be attached to the aft of the body, the connecting location on the body and the propeller are indicated with a droplet sign. For the tailsitter the payload fairing designated with "I" or "II" on the connecting surface must be installed, depending on the mission.

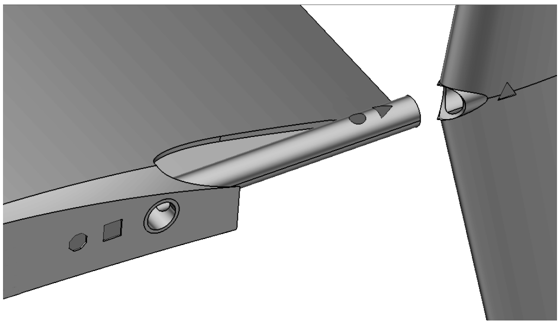

Figure 6.5: Vertical stabilizer joint with matching symbols to simplify the assembly

Figure 6.6: The different propellers with different marks

Assembling the flying wing

The wings are installed in the same manner as for the tailsitter. However, for this configuration the small fins are attached to the body. These are indicated with the circle, and must be connected to the wing where the circles are indicated, which corresponds to the location for the large fins. These small fins function as vertical stabilizers and do not carry propellers. The forward flight propeller is the same as for the tailsitter, which was indicated with a droplet. The payload fairing to be attached on the flying wing is indicated with "II".

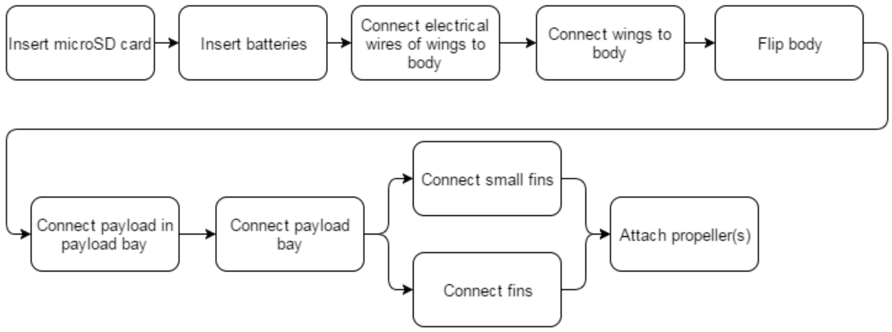

Figure 6.7: Tailsitter and flying wing assembly

Assembling the quadcopter
Instead of the wings, two caps are attached to both sides of the body. The left cap and the side of the body to which this cap is attached are indicated with a hexagon. For the right cap and the other side this is indicated with a plus sign. The caps are secured using the same bolts as for the wing attachment. The fins are attached to the body the same way as for the tailsitter, and the propellers for the designated altitude as well. Furthermore the payload fairing to be installed on the quadcopter is designated with "III".

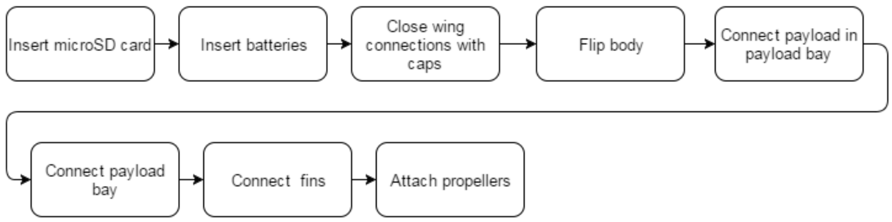

Figure 6.8: Quadcopter assembly

6.1.3. Setting up the basecamp groundstation

To setup the basecamp groundstation, a couple of necessary actions have to be taken. The actions are depicted in Figure 6.9. A manual-like instruction has been made as to improve the user friendliness of the system. This instruction can be found below.

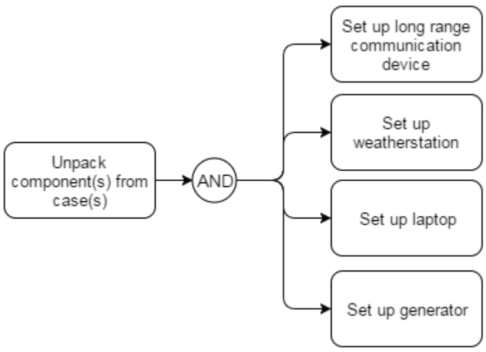

Figure 6.9: Setting up the groundstation

Setting up the long range communications
Set up the tripod on waist height and stabilize the tripod using tent pegs. If the tent pegs cannot be used due to the surface (sand/rock), a stabilization weight should be hung in the designated hook. Mount the backside of the plate on the tripod head using the designated mounting (clicking system). Insert the coax cable in the back of the plate next to the tripod mounting and insert the other end in the tablet. Point the tripod towards the UAV. The direction of the UAV can be estimated using the indicated direction of the UAV, presented on the tablet.

Setting up the weatherstation
Set up the tripod on waist height. Stabilise the tripod using tent pegs. If the tent pegs cannot be used due to the surface (sand/rock), a stabilization weight should be hung in the designated hook. Mount the weatherstation on the top of the tripod by sliding the mounting of the weatherstation over the tripod. Properly secure the mounting by tightening the designated handle. Plug the power cable into the power generator. Plug the USB cable in the laptop.

Setting up the laptop
Start up the laptop. If necessary, plug the laptop charger in the generator. Connect the hard disk to the laptop. Start the MetPak RG weatherstation software. Calibrate weather sensors. Start the Pix4D software. Process images taken by the UAV.

Setting up the generator
Insert 0.4 L of the fue into the generator fuel tank, so the g fuel tank is full. Start up the generator. Now the generator is ready to be used.

6.2. Maintenance

Maintenance is needed to guarantee the systems availability. Maintenance is split into two categories: maintenance that is performed by the user and that is performed by a specialist.

The maintenance performed by the user is done before each flight by inspection and a pre-flight check, as described in Section 6.1. The primary maintenance exists of changing the batteries, the microSD card, payload and choosing the configuration of the UAV. The batteries are located on both sides of the main body in order to allow easy replacement. Also the microSD card is located on the outside of the main body for the same reason. In order to set up another configuration, the vertical fins can easily be removed or added by only attaching or detaching one bolt per fin. For the quadcopter configuration, wing caps are placed on the wing-body connection to keep the batteries fixed in place and to protect the components inside the main body from the environment.
The secondary maintenance that has to be performed by specialists consists of two categories: inspection and repair. Pre-flight inspection is done by the investigators themselves, but regular inspections need to be done by specialists as they have more knowledge about specific systems. These inspections have to take place periodically, and if necessary, a repair is conducted. Inspections by specialists are performed while the UAS is in storage.

User performed maintenance
The users of the UAV have to perform a standard set of checks before and after each flight to make sure the UAV is operable. This can be divided in inspection and a pre-flight check. Inspection consists of visual inspection where the user can detect flaws that are directly visible. During the pre-flight check, the UAV checks some components using software, while the user has to check the components that cannot be checked with software. The user has to check if the servos for the control surfaces work, if the payload is not hindered from making clear pictures and if everything is assembled well together. The servos for the control surfaces are checked by deflecting the control surfaces, which the user has to provide feedback on. For the payload check, a test picture is made which is analysed by the user. The software checks are implemented in the software on the tablets and UAV. The software tests if the batteries, electrical system, microSD card, antennas, GNC sensors and motors are working correctly by means of feedback from the components. If no feedback is received from a component, this component is broken or the wiring to this component is broken, and a warning is shown on the tablet.

Some of the defects that can be detected with inspection and the pre-flight check can be fixed by replacing the component or changing the UAV configuration. Some components however cannot be fixed by the user, these have to be repaired by a specialist.

Specialist performed maintenance
Both before and after each flight the UAV is inspected to find any damaged or malfunctioning components. The pre- and post-flight inspection do often not detect discrete flaws, such as defects in the carbon fibre skin.

This means that the UAV also must be checked regularly while in storage and after longer period of operation by specialists. Furthermore specialists are needed to repair components that were found to be broken by the user.

Maintenance overview
In Table 6.1 the components of the UAV are shown. It can be seen what damage is expected for each component and how this is detected. Also the repair actions are shown. The components which are not designed to be repaired by the user are the motors, servos, wiring, electrical connections, structural connections, UAV structure, GNC components and antennas. Those components are mostly off-the-shelf products and need to be sent back to the manufacturer in order to analyse and repair the component or a new component is purchased. For the batteries, the depth of discharge is a concern as it increases over time and usage. Thus it should be taken into account and when the depth of discharge is too high, the batteries need to be replaced, this can be seen on the user interface.

Table 6.1: Overview of the maintenance of different components

Component	Possible damage	Inspected by	Repaired by
Propeller	Broken/cracks	Inspection	Replace with a new propeller
Battery	Broken	Pre-flight check	Replace with a new battery
Motor	Broken	Pre-flight check/inspection	Replace fin/repair by specialist
Servo	Broken	Pre-flight check	Repair by specialist
Wiring	Broken	Pre-flight check	Repair by specialist
Payload bay	Scratches	Pre-flight check/inspection	Replace protective film
Payload	Broken	Pre-flight check/inspection	Replace payload
Electrical connection	Dirty	Pre-flight check/inspection	Clean connection
	Broken	Pre-flight check/inspection	Repair by specialist
Structural connection	Broken/cracks	Inspection	Repair by specialist
UAV structure	Broken/cracks	Inspection	Repair by specialist
Carbon fiber skin	Misalignment/gaps	Specialist inspection	Repair by specialist /replacement
GNC sensor	Broken	Pre-flight check	Repair by specialist
microSD card	Broken	Pre-flight check/inspection	Replace microSD card
Communication antenna	Broken	Pre-flight check	Repair by specialist
Tablet/laptop	Broken	Inspection	Replace with a new tablet/laptop

Lastly, there are the defects that can neither be detected nor repaired by the user. This damage must be repaired before it grows and creates an incident for the UAV. This applies for the carbon fiber skin, which can include misalignment and gaps. The carbon fiber is analysed in-between operations while in storage by non-destructive testing to check the status of the skin. It should be repaired by a specialist or a complete new wing/body should be purchased as the skin is not detachable from the foam. When a crack or any damage is visible during the operations, the component has to be replaced to ensure that no other component is damaged.

6.3. Logistics

The transportation of the whole UAS to the basecamp is done by truck as the basecamp is set-up at a location as close as possible to the accident site which is accessible by decent means of transportation. From there, all components of the UAS necessary to facilitate the on-site mission are brought to the accident site by the investigators in backpacks.

6.3.1. Transportation to the basecamp

All components of the UAS are stored in three large boxes for transportation: one holding the UAV payload, batteries and laptop, one holding the groundstation components and one holding the generator and propellant. The dimensions and mass of the boxes are tabulated in Table 6.2. The dimensions have been determined such that all components – including their casing – fit in the box. The boxes are equipped with optional wheels, such that they can be easily transported once at the basecamp. The dimensions and the mass of the components including casing are tabulated in Table E.1 in Appendix E.

Table 6.2: Box dimension and mass for transportation by truck

Box	**Size** ($lxwxh$ **in** mm)	**Mass** (kg)
UAV incl. batteries and laptop	560 x 350 x 280	19.4
Groundstation	970 x 450 x 345	24.3
Generator	510 x 475 x 375	24.6

Several cases store multiple components. The grouping was determined depending on their use and expected mission in which they are used. A more elaborate description of the groundstation components can be found in Section 8.3.

The whole UAV is cased in three different casings. One holding the main wings and small fins, one holding the fins including motor mounts and wing caps and one holding the body. Next to that, a payload fairing is necessary to prevent damage to the payload in flight. The fairings are coupled with the payload anticipated to their mission. Thus the flying wing fairing is cased together with the multispectral camera, the quadcopter fairing is cased together with the IR and visible light camera, and the tailsitter fairing is cased together with the toxin detector.
The tablets are cased per one as to improve flexibility in the number of tablets used as a groundstation. The UAV battery is packed in packages consisting of four missions, so in total eight smaller batteries. They are coupled together in one package. The UAV battery charger is cased separately as the ratio between battery packs and charger is not one-to-one.
The two long-range antennas and the communication module are pre-mounted on a plastic plate with hinges. The plate can be folded at the hinges to minimize the length of the component. The plate and the necessary coax cable are placed together in one casing. Next to this casing, a separate casing is used for the tripod as it has a very distinctive shape.
The weatherstation is brought in a casing provided by the producer. The casing is made such that all components fit in the case. Again, a separate casing is used for the tripod as it has a very distinctive shape. The laptop casing includes space for a hard disk, internal storage of the UAV and laptop charger.
The electricity generator is the heaviest component of the total UAS.

6.3.2. Transportation from the basecamp to the accident site

When travelling from the basecamp to the accident site, the necessary components are transported in a backpack. As reference, a 60 L backpack with approximately rectangular dimensions has been chosen[2]. The components necessary to perform the on-site mission are the UAV, UAV batteries, one tablet, payload including payload fairings and internal storage.
To minimise the burden of carrying different bags and cases to the accident site, all the components necessary for the on-site mission fit in one backpack. It is not anticipated that investigators should investigate alone, but this allows for other investigators to bring other necessities. Most importantly for the investigation, the investigator has to bring compulsory investigation items set up by the NTSB such as a cell phone including a set of spare batteries, a laptop and at least 50 business cards [34]. Although not all safety boards use the standards of the NTSB, the necessities set by the NTSB can be set as guideline due to the major role of the NTSB in large air accidents. Next to these items, food and drinks have to be brought to the accident site to make sure that the investigators can perform their job. Table E.1 in Appendix E gives an overview of all components of the UAS which have to fit in the backpack for an on-site mission during the day, or during night indicated by check marks.

[2] URL:https://www.thenorthface.com/shop/equipment-technical-packs/cobra-60?variationId=AGH [cited 17 June 2016]

Only the quadcopter payload fairing is brought as the UAS has already performed the remote mission including detecting the accident site and the toxin detection. Thus the gas detector and the multispectral camera do not have to brought along. The UAV's wings also have to be brought along to provide the communication relay, since this occurs with the UAV in flying wing configuration without a payload bay to ensure maximum endurance. The relay becomes import when other investigators also arrive at the accident scene. Two battery packages are brought along to provide sufficient flight time, amounting to seven times in the quadcopter configuration and once in the flying wing configuration.
As can be seen in Figure 6.10, all components of the UAS fit readily into the backpack and the total mass of the backpack can be easily carried around for a longer period of time with a total mass of 10.5 kg without the necessities of the investigator.

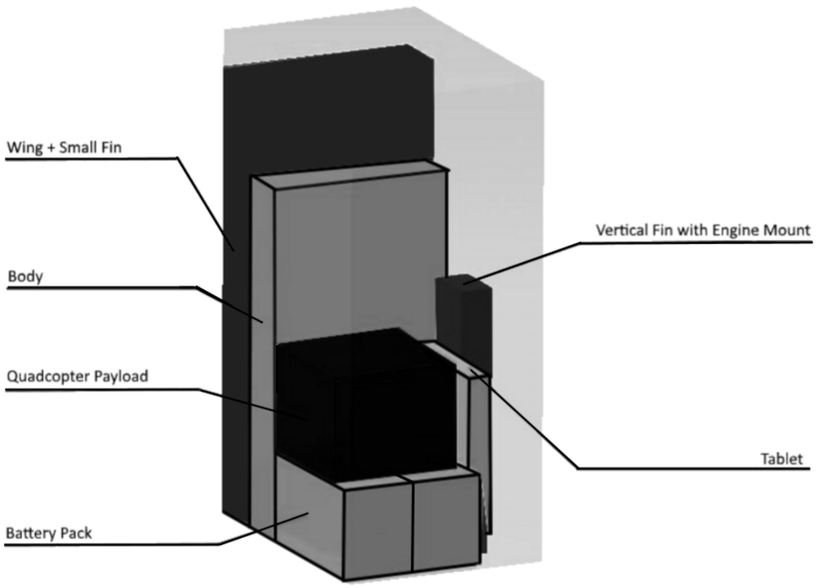

Figure 6.10: On-site mission backpack layout

Concluding the operations and logistics
Concluding, the operations necessary to correctly use MIRU were analysed step-by-step. While doing so, important steps to be taken were identified such as easy assembly and maintenance, and easy transportation of the UAS.
The user is always presented with instructions while operating MIRU, which makes is user-friendly. The components to be assembled have been labeled with small figures at the connection points, in order for the users to easily identify the components that have to be connected and where they have to be connected. Next to that, each propeller set has their individual markings as to omit the possibility of mounting two different sets of propellers. Also all components of the groundstations have been included with a manual as to how to set-up the system.
For the maintenance, the inspections and repairs which can be performed by the users were identified. The actions to be taken vary from rebooting the software to replacing the certain components.
MIRU is brought to the accident site in three transportation boxes, of which one weighs 19.4 kg and the other two weigh less than 25 kg. The boxes are rather small, so they are easy to transport. From the basecamp, all components necessary to perform the on-site mission fit in one backpack. Including the weight of the backpack, excluding the investigators necessity, the total mass is 12.4 kg, so the on-site mission can be performed by one investigator.

7 Conceptual design

MIRU consists of a tailsitter UAV which can be reconfigured to a flying wing or quadcopter. This choice was made in the conceptual design phase so that all missions can be performed by a single system, which is easier for the operator and cheaper. This chapter summarizes the decisions made on the concept choice.

7.1. Trade-off summary

For the UAV platform several concepts were considered, which are: a fixed wing with tail, flying wing, closed wing, multirotor, coaxial rotor, helicopter, tailsitter, tilt rotor, tilt wing and transforming tricopter. These concepts were all evaluated on several criteria. A first value or estimate was found for each criteria based on reference UAVs or quick calculations. The relative results of this process can be found in Table 7.1. In this table the lightest grey indicates good performance for a certain criteria. Dark grey indicates average performance and black indicates bad performance. However, the concepts were hard to compare as there are basically two different missions, on-site and remote. Therefore for each mission the optimal configuration was picked. This was done by using the same criteria, but with different weight factors.

Due to the importance of range and endurance it was concluded that a flying wing or fixed-wing with tail was the best option for the remote mission, since flying with a wing is the most efficient for range and endurance. The advantage above the other configurations is also that there is no need for transforming, like with the tilt wing or tilt rotor, which adds weight and thus decreases performance. Therefore, these would be the most optimal designs. A multirotor was the best option for the on-site mission as it is able to hover and fly at low velocities, which allows for very high quality images. Moreover, it has a lower weight than the others as it does not need to carry its wings along, resulting in a longer endurance. It also has a high manoeuvrability as it can control the rotors separately and if it has an even number of rotors, but favourable four, it is very stable. Also, it does not have to tilt the wings or body before it can start the hovering mission and therefore is more efficient for this maneuver than the other configurations.

7.2. Final concept decision

It was found that UAVs in these configurations are already commercially available and can easily meet the requirements. However, the user has to familiarise themselves with two different +s and has to bring two UAVs to the mission site if it is not known what type of mission has to be performed. Moreover, the toxin detection system requires hovering flight to make its measurements. Toxin detection can be needed for a remote mission and the flying wing cannot provide hovering flight, while the multirotor cannot provide the range required. Based on these findings it was decided to choose a hybrid platform, which can perform all missions.

The final platform chosen is a UAV that can be configured to a tailsitter, quadcopter or flying wing. This platform was chosen because it can perform the required missions. The missions can be separated into two categories: an on-site mission and a remote mission. For the on-site mission low speeds and high manoeuvrability were identified as important mission characteristics. These are obtained by a quadcopter configuration. For the remote mission long endurance and long range were identified as important mission parameters. For this type of mission a flying wing gives the required characteristics. However a special remote mission was also identified. This mission is used for gas detection and it requires the UAV to have a long range and to have hovering capability. This is achieved by the tailsitter configuration, which can switch between horizontal flight, flight with wings, and vertical flight, hovering flight. Furthermore it was identified that a reconfigurable UAV is easier in use, since the user only has to familiarise with one system and only one system has to be brought to the mission site. The choice for this platform was identified as the best option by means of a trade-off process.

Table 7.1: Trade summary of the UAV concepts

	Mass	Range	Endurance	Manoeuvrability	Size	Complexity	Certainty
Fixed wing with tail	0	+	+	0	-	+	+
Flying wing	0	+	0	0	0	+	+
Closed wing	+	+	+	0	-	+	-
Multirotor	+	-	-	0	+	0	+
Coaxial rotor	+	-	-	0	+	-	0
Helicopter	-	0	0	0	0	0	0
Tailsitter	-	+	0	+	0	0	0
Tiltrotor	-	0	0	+	0	-	0
Tiltwing	-	0	0	+	0	-	-
Transforming tricopter	+	-	-	+	+	0	-

+	Better
0	Average
-	Worse

8
System characteristics

To fulfill the missions and functions set out in the preceding chapters, the system has been broken down into various subsystems. Each subsystem performs specific tasks in order to achieve successful operation of the missions. In the following sections, the design of each of the subsystems is presented and justified. The complete system characteristics are clarified as the technical details are presented in their appropriate section.

Firstly, the payload is discussed in Section 8.1. This subsystem performs the main goal of the mission. Then the communication subsystem is discussed in Section 8.2 which sends the payload data and telemetry to the user. This data is received and displayed to the user by the groundstation, discussed in Section 8.3. On the UAV guidance, navigation and control is needed to let the UAV navigate. This is discussed in Section 8.4. After that the aerodynamics design is discussed in Section 8.5. This leads to stability and controllability in Section 8.6, which is highly dependent on the aerodynamic form. Then the structural characteristics are discussed in Section 8.7, which is needed to maintain the aerodynamic form and carry the loads on the UAV. Finally propulsion and performance are discussed in Section 8.8, which enables the UAV to fly. The last subsystem is the electrical subsystem, discussed in Section 8.9, which is needed to provide power and communication to all subsystems.

8.1. Payload

In Chapter 3 the mission profiles have been explained. The payload needs to contain devices that are able to map the air accident site for the different mission profiles. For these different mission profiles, different specific payload configurations are needed. The payload contains a visible light camera, an IR camera and a multispectral camera. Using this payload, MIRU is able to locate and map an air accident site during daytime, in the absence of sunlight and when the wreckage is camouflaged by its surroundings. These cameras must be able to obtain images with sufficient resolution for identification and recognition. The UAV also carries a toxins sensor in order to perform toxin detection.

8.1.1. Payload components analysis

This section analyses the payload components. Following Chapter 3, three mission profiles are distinguished. However, these do not apply specifically to the missions of the payload. The specific systems chosen for the UAV are now analysed further.

Visible light camera: Mapir Survey 2

The visible light camera is used in both the on-site and the remote mission. The camera selected is the Mapir Survey 2 which is available at a cost of €355,- [1]. The camera characteristics and the obtainable ground resolution at a height of 100 m with this camera can be seen in Table F.1 in Appendix F. At a height of 100 m the obtainable ground resolution is 20 pxm^{-1}, and at 10 m this is at least 200 pxm^{-1}. The dimensions of this camera are 59 x 41 x 30 mm, the mass is 47 g and it consumes 1 W. This camera is chosen for the very high resolution in combination with its robustness, low weight and low price.

IR camera: FLIR Vue Pro R

[1] URL:`http://www.mapir.camera/collections/cameras/products/survey2-camera-visible-light-rgb` [cited 31 May 2016]

The IR camera is used for locating the wreckage and for the coarse mapping and locating the air accident site in the absence of sunlight. The camera chosen for this UAV is the FLIR Vue pro R which is available at a cost of €3499,- [2]. The camera specifications and the obtainable resolution are given in Table F.1 in Appendix F. Here it can be seen that with a 19 mm lens this camera is able to obtain a resolution of 11 pxm^{-1} at a height of 100 m. At a height of 50 m, the ground resolution increases to 22 pxm^{-1} and at 10 m height the ground resolution is 110 pxm^{-1}. The spectral band which this camera can detect is 7.5 μm to 13.5 μm, which is in the near infrared spectrum. The dimensions of this camera are 45 x 45 x 45 mm for the body, with an additional 20 mm in depth which accounts for the 19 mm lens. The mass is 100 g and its maximum power consumption is 1.2 W. IR cameras are generally very bulky and do not obtain very high resolution images. Even though the cost is rather high, this camera was chosen for its compactness and low weight, in combination with a relatively high resolution.

Multispectral camera: Tetracam ADC Snap
The multispectral camera is used for locating the wreckage when the wreckage is camouflaged within its surroundings. This camera is used solely to detect a wreckage when it is camouflaged and when it is found it will generate images of it where it can be seen in what environment it is situated. The chosen multispectral camera is the Tetracam ADC Snap which is available at a cost of €3495,-[3]. The camera specifications and ground resolution are given in Table F.1 in Appendix F. Here it can be seen that this camera is able to obtain a ground resolution of 20 pxm^{-1} at 100 m height. The dimensions of this camera are 75 x 59 x 33 mm and its mass and power consumption are 90 g and 2 W respectively. The spectral band of this camera ranges from 520 nm up to 920 nm, with which it can distinguish aluminum from vegetation. Since the spectral band of this camera is so narrow, the images delivered do not show a wide variety of the materials on the ground. The map generated by this camera is not used for analysis, but solely to map where the parts of the wreckage are located as not all different materials can be distinguished but mainly aluminm from vegetation.

Toxin detection sensor: MicroRAE
The investigation of toxic gases is carried out using electronic sensors. The existing solution suited for this UAV's mission is the MicroRAE toxin sensor which costs €791,-. This gas detection system on the UAV is 76 x 117 x 24 mm and its mass is approximately 0.18 kg, the power usage is at most 0.6 W [4]. For different cases, different sensors are applicable. When there is a risk of an explosion, the gas detection sensor is either an IR sensor or a catalytic bead sensor to detect the volatile gases that can cause explosions. The other case is the detection of toxic gases. This is done through the use of electrochemical sensors or PID sensors, to detect the wide variety of gases toxic to humans. The use of the gas detection is primarily to determine whether the accident site is safe to enter, since the dangerous goods can already be dispersed in the air. The explanations of the different sensors are given in Appendix F.

Ground resolution analysis
In order to prove that the selected cameras are the best fit, research was done where it was investigated which ground resolution can be obtained with variable pixel format and height. The setup of this research is explained in Appendix F. It was analysed which ground resolution is required for recognition and identification, which holds for coarse mapping and detailed mapping respectively. Coarse mapping is performed at a height of approximately 100 m, and detailed mapping at 15 m. The precise mapping heights are determined in Subsection 8.1.3. Following the results of this research, the requirements for the imaging cameras were set. At a height of 100 m, the camera must obtain images with a ground resolution of at least 17 pxm^{-1} and at a height of 15 m for recognition, the ground resolution must be at least 70 pxm^{-1} for identification. Now that the resolution requirements have been set for the imaging cameras, the systems selected are verified.

Visible light camera: Mapir Survey 2
This camera obtains a ground resolution of 20 pxm^{-1} at 100 m height, and at a height of 15 m this is at least 200 pxm^{-1}. According to the requirements set, these are sufficient resolutions for recognition and identification respectively for the visible light camera.

[2] URL:http://www.flir.com/suas/content/?id=75250 [cited 31 May 2016]
[3] URL:http://www.tetracam.com/Products-ADC_Snap.htm [cited 1 June 2016]
[4] URL:http://www.raesystems.com/products/microrae-multi-gas-detector [cited 9 May 2016]

IR camera: FLIR Vue Pro R
This IR camera obtains a ground resolution of 12 pxm^{-1} and 75 pxm^{-1} at a height of 100 m and 10 m respectively, with a 19 mm lens. This meets the requirement for detailed mapping, but not the requirement for coarse mapping. However, when the height is decreased to 75 m, this camera obtains a ground resolution of 17 pxm^{-1}. This height is still sufficiently high for coarse mapping, thus this camera also meets the resolution requirements for coarse mapping, but at a lower height.

Multispectral camera: Tetracam ADC Snap
This camera is able to obtain a ground resolution of 20 pxm^{-1} at a height of 100 m, meeting the recognition requirements. The reason an IR camera does not suit for detecting wreckages when they are camouflaged, is because the spectral band starts at 7.5 μm, whereas the wavelengths emitted by aluminum and snow for example start at 0.2 μm and 0.5 μm respectively. These wavelengths must be detected as well in order to distinguish the wreckage from its surroundings. The multispectral camera will not be analysed for detailed mapping, since it is not be used for detailed mapping.

8.1.2. Payload configurations

The three mission types set in Chapter 3 are performed under several environmental conditions, see also Chapter 4. The different payload configuration per mission type and for each environmental condition are given in Table 8.1. These configurations are inserted into the swappable payload bay which is mounted on the UAV. The most used configurations are the ones containing the Mapir Survey 2. The configurations containing the IR and multispectral camera are used only occasionally, when it is really necessary. Since most of the time the visible light camera will suffice for the mission of MIRU, the Tetracam ADC Snap and the FLIR Vue Pro R are optional for the user to purchase, reducing the base price of the payload unit significantly.
The configuration of the payload during the remote mission and the on-site mission during daytime are the same, as well as the configuration for mapping these missions in the absence of sunlight. The configurations containing the multispectral camera are only applied for the remote mission, where the main purpose is to locate the air accident site and make a coarse map of the locations of the debris. Toxin detection is solely carried out by the UAV during the remote mission, since it should be known whether it is safe for the investigators to perform the investigation before they arrive on site. It may occur that toxins still leak when arrived on site, while the toxins have not been detected during the remote mission, or when there was no initial remote mission needed, but the risk of leaking toxins is still present. If toxins detection must be performed on site, this will be done manually by investigators on the ground. It is then not necessary to carry the sensors on board the UAV.

Table 8.1: Payload configurations per mission objective including mass and cost budgets

Mission objective	Configuration	Mass (g)	Cost (€)
1.Remote mission: coarse mapping and/or locating during daytime	Mapir Survey 2	47	345
2. Remote mission: coarse mapping and/or locating in the absence of sunlight	FLIR Vue Pro R	100	3,499
3. Remote mission: coarse mapping and/or locating of camouflaged wreckage	Tetracam ADC Snap	90	3,495
4. Remote mission: toxin detection, coarse mapping and/or locating during daytime	MicroRAE + Mapir Survey 2	227	1,136
5. Remote mission: toxin detection, coarse mapping and/or locating during nighttime	MicroRAE + FLIR Vue Pro R	280	4,290
6. Remote mission: toxin detection, coarse mapping and/or locating of camouflaged wreckage	MicroRAE + Tetracam ADC Snap	270	4,286
7. On-site mission: detailed mapping and potentially coarse mapping during daytime	Mapir Survey 2	47	345
8. On-site mission: coarse mapping during nighttime	FLIR Vue Pro R	100	3,499

8.1.3. Mapping heights and speeds

After the configurations for the different missions of MIRU were determined, the heights and mapping speeds at which the mapping devices operate have been determined. These include the maximum and operational mapping speeds and heights.

Maximum mapping heights and speeds

With the obtainable ground resolutions of the cameras the maximum heights for identification and recognition are set. For identification these are 30 m for the Mapir Survey 2, 17 m for the FLIR Vue Pro R and 28 m for the Tetracam ADC Snap. For recognition the heights are 120 m, 75 m and 115 m respectively. At these heights, the ground resolution of all the cameras is the minimum required of 70 pxm^{-1}. In order to obtain clear images at these heights, the UAV is limited in its cruise speed when generating the detailed map or coarse map. These speeds are dependent on the shutter speed of the specific camera used, the obtainable resolution, the overlap percentage of the images and the capture speed. The capture speed is dependent on the writing speed of the memory card. The memory card installed in the UAV is the LEXAR1000r 128GB, resulting in a capture speed of 2 s [5]. The maximum velocities are related to the maximum heights at which the UAV can operate for identification and recognition as well, so the values given in Table 8.2 are the maximum velocities at the given heights as given for those cameras. The overlap percentage for the coarse map is set to 30 % which is the minimum set requirement for sufficient stitching results and the overlap percentage for the detailed map is set to 70 % such that using software a 3D map can be generated during post processing.

Operational mapping heights and corresponding mapping velocities

The maximum heights and velocities are not the values at which the UAV operates. In order to be most efficient, the UAV coarse maps at the maximum heights for the respective camera, but with the optimum cruise speeds for each configuration at that height. As an indication, the range of the optimum speeds at sea level and at an altitude of 4500 m are given for the flying wing and the tailsitter in Table 8.2. These optimum speeds follow from Section 8.8.2. However since the maximum speed at which the IR can map is 15.1 ms^{-1} the UAV maps at this lower speed when mapping with the IR camera. For detailed mapping, the height for all cameras is set to 15 m, such that the UAV can increase height but remain mapping, when it for example has to fly over obstacles. At these heights the maximum velocities are calculated, which are 3.7 ms^{-1} and 0.95 ms^{-1} for the visible light camera and IR camera respectively. Since the multispectral camera is not used for detailed mapping, there is no need to set a detailed mapping height, ground resolution and speed for this device. An overview of the operational heights, operational ground resolutions and operational velocities are given in Table 8.2. Note that the operational mapping heights presented in this section are the heights from the ground and not from sea level.

Table 8.2: Maximum and operational mapping heights and corresponding maximum velocities.

Camera	**Mapir Survey 2**	**FLIR Vue Pro R**	**Tetracam ADC Snap**
Maximum height for identification (m)	30	17	28
Maximum velocity for identification (ms^{-1})	9.9	1.5	2.8
Maximum height for recognition (m)	120	75	115
Maximum velocity for recognition (ms^{-1})	92.6	15.1	26.7
Operational height for identification (m)	15	15	-
Operational ground resolution for identification (pxm^{-1})	140	80	-
Operational velocity for identification for quadcopter (ms^{-1})	3.7	1.0	-
Operational height for recognition (m)	120	75	115
Operational ground resolution for recognition (pxm^{-1})	17.5	16	17
Operational velocity for recognition at 0 m and 4500 m from sealevel for tailsitter (ms^{-1})	16.1 - 20.2	15.1	16.1 - 20.2
Operational velocity for recognition at 0 m and 4500 m from sealevel for flying wing (ms^{-1})	15.6 - 19.6	15.1	15.6 - 19.6

[5] URL:`http://www.dataio.nl/lexar-128gb-micro-sd-1000x-uhs-ii-u3-usb-reader-150mbs/` [cited 13 June 2016]

Concluding the payload
In order to perform the mission objectives in the broad range of environmental conditions, the payload contains either the visible light camera, Mapir Survey 2, the IR camera, the FLIR Vue Pro R, or the multispectral camera, the Tetracam ADC Snap. These cameras are chosen for their high ground resolution performances and compactness. These cameras can be carried on board in tandem with the MicroRAE toxins sensor, in case MIRU has to perform a toxins detection. Detailed mapping is always performed at a height of 15 m from the ground, with 3.7 ms^{-1} and 1.0 ms^{-1} for the visible light camera and the IR camera respectively. At these heights, the visible light camera obtains a resolution of 140 pxm^{-1} and the IR camera obtains 80 pxm^{-1}, which is sufficient for recognition. Coarse mapping is performed at the maximum height at which the designated camera can obtain sufficient resolution for recognition, which are 120 m, 75 m, and 115 m from the ground, for the visible light camera, the IR camera and the multispectral camera respectively. At these heights the UAV maps the area at the optimum cruise speeds given for that altitude.

8.2. Communication

To send real time imaging taken by the payload (Section 8.1) and to make this available to the investigation team while the UAV is performing its mission, communication is necessary. With real time imaging, the accident site can already be identified before the UAV has returned and the investigators can anticipate on the findings and the external conditions seen on the imaging. To have this communication link between the ground and the UAV, a communication system has to be established which can cover the 15 km distance at which the UAV performs its remote mission. For the on-site mission, it is advantageous to all investigators to be able to communicate with each other, while being independent of the communication infrastructure present at the accident site as this quality might not be sufficient or the network not reliable or available. So it is beneficial to the investigation to have an independent communication relay system which the investigators can access when they are in the vicinity of the UAV.

8.2.1. Characteristics of the communication system

The communication system is characterised by the frequency of radiation and the polarisation and direction of the antennas. After an extensive trade-off of the characteristics it was determined to use UHF or SHF for the frequency. The main argument for this decision is that for higher frequency, smaller antennas can be used. In the indicated range, possible frequencies were 900 MHz, 1.3 GHz, 2.4 GHz and 5.8 GHz. The higher the frequency, the higher the chance that the signal is not able to penetrate through obstacles such as trees and walls. But a higher frequency results in smaller antennas. Thus it was determined to use a 2.4 GHz frequency to be less sensitive to objects, while still maintaining small sizes of antennas. For both the remote and on-site mission, the polarisation of the antennas of the groundstation and UAV are right hand circular polarised (RHCP) due to the larger availability of RHCP antennas. It has been determined to use omnidirectional and directional antennas on the groundstation. This is to ensure that the groundstation can make contact with the UAV when it is both near and far away from the groundstation. On the UAV, only omnidirectional antennas are mounted as to prevent the use of a heavy antenna tracker module. It was also determined to use only one data link, which both processes the telemetry and the data link as the telemetry link uses minimal data compared to the data link.
With the characteristics, the receivers, transmitters and antennas have been sized. Transceivers have not been considered as their main advantage over separate transmitters and receivers are the reduction in cost. The disadvantages is that only half-duplex transmission mode is possible, thus the antenna can either receive, or transmit data. This is not favourable when the communication relay is used. Each antenna thus has one receiver or one transmitter attached to it.

8.2.2. Performance of the communication subsystem

The performance of the system is determined by the link budget. The data rate is a function of the signal-to-noise ratio and the bandwidth [3]. The data over the data link consists of telemetry, data gathered by the UAV and the communication relay. The noise consists of the thermal noise and the signal depends on the receiver sensitivity. Over the remote mission distance, a data rate of 13.5 $Mbps$ can be achieved. Over this data rate 1 $Mbps$ has been reserved for the communication relay.

Every two seconds, a 16 MP image is sent from the UAV to the groundstation. Over the relay, investigators are able to communicate with each other using the means of speech and instant messaging, including images. At

one time, up to 10 investigators can make use of the communication relay as speech requires 96 $kbits^{-1}$ and messaging 15 $kbits^{-1}$ [3]. Images taken by the investigators are scaled and compressed before they are sent to the UAV to make it possible to allow speech and instant messaging at the same time.
Over all the data sent by the communication link, an encryption algorithm ensures that the data is protected.

However, when there is no line-of-sight due to obstacles like mountains, trees and walls in between the base-camp and the area of interest, there is no connection possible with the UAV from the groundstation.
A solution using other technology is satellite communications, however with current technology, the antenna module for satellite communication is heavy, expensive and it consumes a lot of power [4]. This makes satellite communications not a solution for small UAVs.
The only consequence of no line-of-sight for the UAS is that the UAV does not send any data to the groundstation and the user has to wait until the UAV is back at the basecamp to read the data from the internal storage. If it is crucial for the remote mission to receive data from the UAV while it is in flight, the UAV can fly back to the location just before the connection signal was lost. This allows for the transfer of data gathered by the UAV when it was out of line-of-sight. As the UAV is completely autonomous in flight, and thus not dependent on communication, and since all the data gathered by the UAV is stored on an internal memory, this does not impact the operations and thus does not further impact the UAS.

8.2.3. Communication system design

The communication system can be sized using many different sorts of combinations of antennas, receivers and transmitters. So first the constraints were analysed. For this, the link budget was used.
In the link budget, the power received is usually negative and needs to be larger (less negative) than the receiver sensitivity. This sensitivity varies with the receiver, but most of the receivers available today have a sensitivity of -90 dBm. The losses are the sum of all losses encountered in between the transmitter and receiver. These losses are the transmitter, receiver and path losses. For the transmitter and receiver loss, a value of 3 dB has been taken into account. As the Times Microwave Systems data sheet [46] advices, a coax cable loss of 0.02 dBm^{-1} is reasonable. Thus the 3 dB value leaves a margin in the link budget. To account for any other losses, a miscellaneous loss of another 3 dB is taken into account.
For the remote mission, the UAV operates outside physical line-of-sight, making communication essential for this mission. Thus it was determined that there must be a communication link possible at a maximum distance of 20 km which is a data link range redundancy of 33%. For the on-site mission there is no redundancy in range as the UAV stays in the physical line-of-sight of the investigators. Thus the communication link will be the maximum distance of the user away from the UAV when it is in a grid of 1 x 1 km, or 1.5 km radius.
The free-space loss was determined using a function of the distance of the communication link, the frequency and the speed of light[3]. This results in a maximum free-space loss of 126.1 dB for the remote mission and 103.6 dB for the on-site mission. Other considerations which influenced the link budget are the interference of the transmitted power with other subsystem and payload.
The antennas to be mounted on the UAV have to be small and lightweight. On the groundstation, larger antennas could be placed, but they should be easy to install and robust as non-specialists (investigators) use them. The groundstation and the UAV have the same omnidirectional antenna for simplicity. Because of this constraint, first the short range communication system has been sized.

Short range (1.5 km) communication system

For the on-site mission, both the groundstation and the UAV use the same transmitter and receiver. There is one receiving antenna and one transmitting antenna on both the groundstation and the UAV. The omnidirectional antenna must have a gain of approximately 3 dB to still have circular radiation.
Using the link budget and using antennas with a gain of less than or equal to 3 dB, the following combination of transmitter and antenna is necessary (Table 8.3):

Table 8.3: Possible short range communication transmitter-antenna combination

Transmitter gain (dB)	**Transmitted power** (mW)
0	200
1	126
2	79
3	50

As it is preferred to have a low transmitted power on the UAV, a 3 dB omnidirectional antenna is used. The Boscam 2.4 GHz RHCP [6] is used for the design because of its low weight of 10 g.

Long range (20 km) communication system
For the long range communication mission it is possible to have a high power transmitter at the groundstation, as the transmitting antenna can be placed apart from the other systems. To prevent overheating of the transmitter, the transmitted power must not be more than necessary.
The groundstation and the UAV make use of different antennas. First the link from the groundstation to the UAV was analysed.As the omnidirectional antenna was sized for the on-site mission, it has a gain of 3 dB. Table 8.4 indicates the possible combinations for the groundstation antenna gain and the transmitter power.

Table 8.4: Possible groundstation to UAV long range communication transmitter-antenna combination

Transmitter gain (dB)	**Transmitted power** (mW)
10	1600
11	1300
12	1000
13	800

Transmitter gain (dB)	**Transmitted power** (mW)
14	630
15	500
18	250
23	100

From Table 8.4 it is determined to use a 1000 mW transmitter on the groundstation. The rather high transmitter power does not harm other systems on the groundstation as the antenna can be placed on a different place away from the other systems.
Next was the choice of antenna. The mass, size and beam width are the most important parameters when deciding on the antenna. The beam width determines the necessary pointing accuracy of the antenna to make contact with the UAV. It is determined to use a small patch antenna, which is the ImmersionRC SpiroNET 2.4GHz Patch Antenna[7]. It has a 35° beam width in both horizontal and vertical direction, thus the groundstation requires a tripod to mount and point the antenna. This is further elaborated upon in Section 8.3.

Due to the limiting beam width, the groundstation cannot make contact with the UAV when it is near or above the groundstation. In order to make contact, the groundstation has to make use of the antennas chosen for the short range communication system. Thus the groundstation used for the remote mission should always be equipped with both types of antennas to function properly.

The final step was to check whether the UAV can also transmit data to the groundstation using its omnidirectional antennas.
With the 50 mW transmitted power on the UAV and using the 3 dB gain antenna, to achieve a communication link with the groundstation, the antenna gain on the groundstation has to be at least 25 dB. Since not many antennas with this much gain are available, one can either increase the transmitted power on the UAV, or add another omnidirectional antenna with larger gain on the UAV. An increased transmitter power was preferred as an additional antenna has larger consequences to the UAS, i.e. more drag, more weight and higher complexity. The necessary transmitted power and the antenna gain are presented upon in Table 8.5.

[6] URL:http://www.tecnic.co.uk/Boscam-Dual-Band-5.8Ghz-and-2.4Ghz-RHCP-FPV-Antenna-SMA.html [cited 17 June 2016]
[7] URL:http://www.immersionrc.com/fpv-products/spironet2g4patch/ [cited 17 June 2016]

Table 8.5: Possible UAV to groundstation long range communication receiver-antenna combination

Receiver gain (dB)	**Transmitted power** (mW)
22	100
18	250
15	500
14	750
12	1000

When using the same type of receiver on the groundstation as the transmitter, the antenna has a gain of 13 dB. This requires a transmitter power of 1000 mW. This is rather large and causes trouble with interference with the other subsystems and payload on board the UAV. Thus a third antenna and an extra transmitter has to be placed on the UAV.
Using the same 50 mW transmitter on the UAV and the 13 dB receiver on the groundstation, the UAV requires an antenna with at least a gain of 15 dB. There are not many high gain omnidirectional antennas. But there is one 16 dB omnidirectional antenna, the DJI 2.4 High Gain Rx RHCP[8]. It is compact (R = 35 mm, h = 35 mm) and lightweight (15 g).

The transmitter and receiver are placed close to the antenna, so there is minimal wiring. As established in Section 8.9, the electrical wiring density is 50 gm^{-1}. A rough estimate to take into account wiring is 10 cm per antenna.

Concluding communications
To conclude the communications subsystem, a summary of the performance is given. On the UAV, there are three antennas placed: two for short range communications and one for long range transmission. They are all omnidirectional as to omit the use of a heavy antenna tracker. On the ground, the groundstation is equipped with four antennas of which two are used for short range communications and two for long range communications. The long range communication system is directional and thus has to be pointed towards the UAV.
With this system, there is communication possible with the UAV over a distance of at least 15 km to cover the range necessary for the remote mission. Over this communication link, the UAV continuously sends telemetry and a 16 MP image every two seconds to the groundstation. The interval time is limited by the payload writing speed. The communication relay can be both used for speech and instant messaging including images and does not affect the telemetry and the images sent to the groundstation. Investigators within a radius of 1.5 km can make use of the communication relay. A maximum of up to 10 investigators can use the relay for speech.
However, when there is no line-of-sight due to objects between the basecamp and the area of interest, there is no connection possible with the UAV from the groundstation. The only consequence for the UAS is that the UAV does not send any data to the groundstation when it is out of line-of-sight and the user has to wait until the UAV is back at the basecamp. However, as the UAV is completely autonomous in flight and since all the data gathered by the UAV are stored on the internal memory, this does not limit the operations.

8.3. Groundstation

The groundstation's main function is to facilitate the operations of the mission, which has been covered in Section 6.1, and to present the data the UAV has sent. At the groundstation all components have to be available to successfully perform the mission. This includes a broad range of components; from tablets to present the data received by the UAV to a weatherstation to calibrate the weather sensors on board the UAV. With the different missions, different components of the groundstation are necessary. To make life easier for the investigators, an indication has been given as to what components of the groundstation are necessary for a particular mission.
The user and UAV are connected through the interface of a tablet. The software on the tablets is initialised using an application. Through the application, the user is guided through checklists, making use of a neat interface while the UAV is performing its mission and can communicate with other investigators using the communication link.

[8]URL:https://www.amazon.com/16dbi-Leaves-Cloverleaf-Omnidirectional-Antenna/dp/B00NIRY55I [cited 17 June 2016]

8.3.1. Identification of the groundstation components

To identify and size the components of the groundstation, first the necessary components and its capabilities were determined. As essential groundstation components for UAS operation a visual display/system, communication system and a weatherstation were identified. For post processing, a data processor and visual display is needed.

Visualisation display/system

The visual display is used to let investigators indicate their areas of interest and to receive data from the UAV. Since safety investigators control the UAV, the control inputs are limited to giving flight path directions by marking the areas of interest on the visual display. Next to that, the telemetry and the received images that the UAV collects, are shown on the display device.
It was decided to use an 8" tablet, as it fits nicely into the hand and can be easily carried around. It is important that either it has a removable battery or a long lasting battery. Also, it should have a replaceable internal storage to transfer data to other groundstations or the data processor.
It was determined to use a Lenovo Yoga Tab 3[9] as it has a tested battery life of over 15 h and can hold a microSD memory card. Another advantageous aspect is that the tablet is rather cheap, being €170.

Communication system

An elaborated sizing of the communication system was performed in Section 8.2. But next to the antennas, the mounting locations of the antenna on the groundstation had to be determined.
It was determined to mount the short range communication antennas on the back of the tablet as it makes the groundstation portable. The antennas need to be spaced at least half a wave length away from each other. This resulted in a separation of 6.25 cm. The transmitter and receiver are connected to the microUSB port of the tablet to receive power and they are directly connected to the processor of the tablet. The communication module uses an extra 0.9 W of power. With the 6200 mAh two cell battery of the tablet, the battery should last for approximately $11h$ in full use. The antennas are covered by a protective cover to make it more robust. It has an ergonomic shape so the tablet still fits nicely into the hand. With the integration of the communication systems, the tablet has a dimension of 210 x 226 x 7-25 mm and weighs 520 g.
For the long range communication system, the separation is again 6.25 cm. It is placed on a tripod to ensure that the antennas are continuously pointed in the same and right direction. No antenna tracker is used as it is sensitive to failure and this makes the investigators unnecessary dependent on technology. The antennas are mounted on a flat plate which can be clicked onto the tripod. A coax cable runs in between the antennas and the tablet to ensure long range communication. From analysis, it was found that the ratio between the maximum and folded length of a tripod is around 3. To store the antenna and tripod together in one case, the tripod has the same length as the width of two antennas and the separation (465 mm). Thus the unfolded length is 1.4 m. The weight is approximately 1.5 kg. To stabilise the tripod, tent pegs are used to secure the tripod legs to the ground. If no tent pegs can be used, a stabilising weight can be hooked on the tripod.

Weatherstation

The weatherstation is used to calibrate the weather sensors on board of the UAV. More elaboration on the weather sensors mounted on the UAV can be found in Section 8.4. The weatherstation has to be compact, light weight and accurate.
It was determined to use the MetPak RG weatherstation [43], as it satisfies all these criteria. There are weatherstations which are lighter and smaller, but the accuracy is often a tenth less accurate. The weatherstation is placed on a pole, as high as possible to allow for the sensors to measure without disturbance. Instead of a pole, a similar tripod as the communication tripod is used which reaches a height of 2 m. The folded length is 667 mm and weighs approximately 2 kg.

Data processing and visual display

After the UAV has returned to the basecamp, all the data gathered by the UAV is processed. A laptop works best as processing device as it is portable, rechargeable and a lot of data can be stored using external hard drives. It has to be able to stitch the images taken by the UAV together to make a large map of the accident site, identify possible wreckage on the coarse map and be able to render 3D images out of several images of

[9] URL:`http://shop.lenovo.com/us/en/tablets/lenovo/yoga-tablet-series/yoga-tab-3-8/` [cited 17 June 2016]

the same object using the program Pix4Dmapper.[10] Thus a very powerful processor is necessary so an Intel i7 or another processor with similar performance is used. As reference, the HP EliteBook 8570W[16] is used.
To be able to read of the data measured by the weatherstation, the laptop first has to be installed with the weatherstation software. When the software is installed and when the weatherstation is connected to the laptop, the data is shown on the laptop in the producers' user interface. In order to convert the detailed images to a 3D model, the aforementioned Pix4D software is used. This software takes the images from the UAVs SD card as input and outputs a 3D point cloud, true orthomosaic and a 3D textured model. This software was chosen for its compatibility with every camera and the good quality in image processing. From these 3D models, the investigators are able to take measurements from the accident site.

8.3.2. Groundstation design

For the remote and on-site mission, different groundstation components are necessary. It has to be noted that if both the remote and on-site mission are performed, the groundstation components of both mission should first be brought to the basecamp. An elaborate explanation on all the logistics of the groundstation is given in Section 6.3.

Remote mission

For the remote mission, the groundstation is set-up at the basecamp, thus the configuration of the necessary items for this mission is called basecamp groundstation. At the basecamp, the tablets used for the on-site mission can be charged. Next to that the laptops have to be powered, thus an electricity generator needs to be present. To generate the power, a fossil fuel powered generator was chosen as alternative energy sources, as wind or solar energy, can not guarantee continues power supply.

For the remote mission, the following groundstation components are necessary:

- UAV battery
- UAV battery charger
- Tablet including short range communication
- Tablet charger
- Long range communication
- Weatherstation
- Laptop including charger
- Internal storage (for inside UAV)
- External hard disk
- Bungee cord
- Foldable table and chair
- Generator including propellant

The number of UAV batteries which have to be brought to the basecamp has to be sufficient to provide the communication relay over a sufficient amount of time to assist the investigators on site. The configuration of the UAV with the largest endurance is the flying wing with 122 min of endurance. But as the investigators also have to use the UAV to perform the detailed mapping in hovering configuration, there should be sufficient batteries available to perform this mission. It is thus determined to bring batteries worth of 12 operations to the basecamp: 3 to be used for the communication relay, and 9 to be used for the on-site mission. Of course, depending on the circumstances, the distribution of batteries can be varied and more (or less) batteries can be brought to the basecamp.
One LiPo charger[11] is used to charge the batteries as they require a rather large amount of power (538 W for a charger with a 4C discharge rate). This large power consumption is compensated by the time needed to recharge one battery (15 min). But as high C-rate generates more heat, which increases the risk of failure of the charger, it was determined to use a C-rate of one. Using a parallel charging board, four batteries can be charged in one go consuming the same amount of power. The charging times is 1 h for eight batteries.
At the basecamp, four tablets are placed. However, for the remote mission only one is necessary. As the battery of the tablet is long lasting, only two chargers consuming 40 W are provided. The long range communication system is connected to the tablet using a coax cable plug. The long range antenna is connected to the tablet using coax cables. LMR-Lite 400 coax cables were used as they have a low cable loss of 0.02 dB^{-1} [46]. Five meters of coax cables weigh 1.1 kg and is enough to connect the tripod with the tablet.
Next to the long range antennas, the weatherstation is placed. The measured data of the weatherstation needs to be displayed on the laptop. No extra wires and cables are necessary as the weatherstation comes with all the necessities to attach the weatherstation to a laptop using the USB port.

[10] URL: `https://pix4d.com/product/pix4dmapper-pro` [cited 16 June 2016]
[11] URL: `http://www.hobbyking.com/hobbyking/store/__82840__Turnigy_Reaktor_QuadKore_1200W_80A_4_X_300W_20A_DC_Synchronous_Balance_Charger_Discharger.html` [cited 16 June 2016]

At least one laptop is necessary to read out the weather sensor data and to post-process the images taken by the UAV.
The UAV is equipped with a 128 GB internal storage, in the sense of a microSD card. To make sure that there is enough internal storage available during the on-site mission, four extra internal storages are brought to the basecamp. This also makes it possible to send the UAV on to a next mission, while the data gathered on the previous mission is processed and analysed at the basecamp. Next to internal storage, also a 4 TB hard disk [30] is present with all programs and documents for the investigator necessary for the investigation. Next to that, the investigator can make a back-up of the files processed by the Pix4D software.

Continuing with the components not related to electronics, a bungee cord including a tent peg to fix the cord is necessary to provide launch for the flying wing and a foldable table and chair [12] is required to make proper use of the laptop on the groundstation.
Finally, a generator was chosen. To choose a proper generator, first the power budget of the groundstation was determined. This is done in Table 8.6.Analysing the power budget of the groundstation, the groundstation uses a maximum of 743 W when the UAV batteries, tablet and laptop are charged together with the use of the long range communication.

Table 8.6: Basecamp groundstation power budget

Component	Power (W)
UAV battery charger	538
Tablet charger	80
Long range communication	5.1
Laptop and charger	120
Total	743.1

Important considerations when choosing a generator were the size, mass, operating time and the noise generated. It was determined to use the Yamaha EF2000iS [48]. It has a running power output of 1600 W and has a running time of 8 h when running at half of its maximum output. The weight of the generator is rather light (20 kg) and is one of the most compact in his class (49 x 28 x 45.5 cm). The fuel used is unleaded petrol and the capacity is 0.4 L. It produces 61 dB when running on full power, which is as quiet as an refrigerator or a running air-condition nearby.
A diesel powered generator was preferred as the truck driving to the basecamp is often powered by diesel. However, there is no diesel generator with a mass, dimensions and running hours near the chosen generator.

On-site mission
All groundstation components necessary for the on-site mission need to be able to be brought to the accident site in a backpack. Thus this groundstation is referred to as the portable groundstation.

The following components were identified as necessary for the on-site mission:

- Tablet including short range communication
- UAV battery
- Internal storage (for inside UAV)
- Bungee cord

Three tablets are brought to the on-site mission to facilitate communication between the investigators using the communication relay. Additionally, the bungee cord including tent peg and additional internal storage is also brought along. The number of batteries brought to the accident site varies with each mission. If the images of the coarse map acquired by the remote mission show a lot of larger pieces of wreckage over a small debris field, less batteries may be required then a very large debris field with a lot of smaller wreckage. Also if there is an opportunity to recharge the batteries during the on-site mission, less batteries may be necessary to be brought along. If it is known beforehand that several groups of investigators depart from the basecamp to the accident site, the number of batteries can be split between the groups. When one group of investigators

[12] URL:`http://www.higear.uk.com/hi-gear-elite-set-p324074` [cited 16 June 2016]

returns from the accident site to the basecamp, they can bring used batteries to the basecamp for recharging.

With the identification of all the component of the groundstation for each mission, the interrelation between the components have been established using a communication and data handling diagram, Figure 8.1. Several operations are included such as the calibration of the weather sensors and the processing of the high resolution images taken by the UAV in flight.

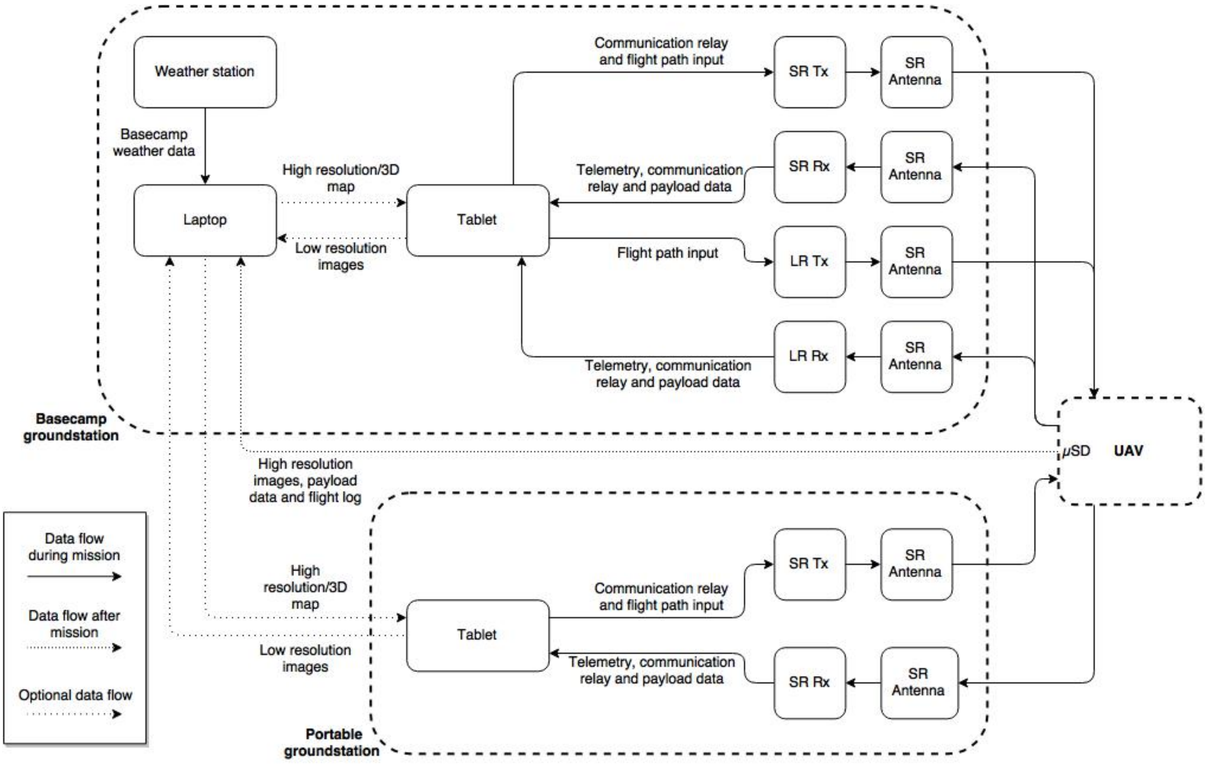

Figure 8.1: Communication and data handling diagram

8.3.3. Groundstation user interface

The groundstation user interface is accessed from an application which is specifically designed for MIRU and its groundstation. It is advised to download data or load data from Google Maps[13] before the start of the mission, as it gives geographic information of the surrounding area. This could give investigators a first hint or clue for the investigation. The UAV is loaded with data from Google Earth as to determine an efficient flight path to fly to the area of interest.

In Figure 8.2a, the software initialisation screen is depicted. First a configuration and then a mission is chosen by the user. A warning screen pops up if a strange combination of configuration and mission is chosen i.e. the quadcopter and the communication relay. Also, the UAV recognises what payload is mounted. If the wrong payload is mounted for a specific mission, again a warning shows up.

For the remote mission: before flight, the user has to indicate the area of interest on a map generated by Google Maps. In this example interface, the map corresponds to the accident case introduced in Chapter 2 and is depicted in Figure 8.2b. If an area has been indicated, the user gets feedback on the flight time, the time to map a 1 x 1 km grid and the flight time left. Also as the UAV in this particular mission operates in a mountainous area, a warning pops up indicating that the communication may be lost during flight as the line-of-sight might be broken due to the mountains. After indicating the area of interest, the user is guided through a pre-flight checklist. Next the UAV does an automated pre-flight check to confirm whether all components are connected correctly to the UAV. If not, a warning pops up.

When the UAV is in-flight, the interface changes slightly compared to the interface before flight, as depicted in Figure 8.2c. Now the user has the time, orientation (compass), battery status, signal strength and its current

[13]URL:`http://maps.google.com/maps` [cited 17 June 2016]

configuration and its mission at its disposal in one glance. Next to that the travel time remaining, airspeed and the altitude above sea level is indicated. At the bottom of the screen there are five buttons. The cloudy-sun button indicates the important atmospheric conditions at the UAV, such as the pressure, humidity and temperature. The 'start mapping' and 'add new area of interest' button do exactly what the buttons says. If the investigator wants to have a visual of the path taken by the UAV as the wreckage has not yet been found, they could start mapping while the UAV is underway. If due to some new insights another area of interest was located, the user can send commands to the UAV. A map button has been faded as there is no data yet of anything mapped by the UAV. There are two buttons incorporated for safety: the 'return to base' button and the 'emergency' button. The return to base button makes sure that the UAV flies back to the basecamp, which might be necessary due to changing weather. The emergency button ensures that the UAV makes a safe emergency landing as soon as possible. This button should especially be used when the UAV is endangering nearby users due to malfunction. The last button is not expected to be used, but as always: better safe than sorry.

(a) Software initialisation (b) Remote mission: before flight (c) Remote mission: during flight

Figure 8.2: User interface 1/2

When the UAV has arrived at the area of interest, images are sent to the groundstation as depicted in Figure 8.3a. Compared to Figure 8.2c, two buttons are added: the map and 'quit mapping' button. The map button presents all the mapped area and the remaining area to be mapped. The 'quit mapping' button does exactly what the button says: quit mapping and continue with mapping of the next area of interest. The UAV is programmed such that it can map until a certain percentage of the battery has been used, depending on the mission, so that the battery capacity used the moment is lands is 80%. Then it automatically returns to the basecamp.

The on-site mission makes use of the coarse map on which the user can identify his areas of interest, as depicted in Figure 8.3b. Only one commander tablet can give those inputs to prevent the UAV from flying everywhere. Users can indicate the object of which they would like to have a detailed image of. When detailed mapping is underway, the user interface changes to Figure 8.3c (unedited image courtesy of International Business Times[14]). Most of the buttons are again the same as for the remote mission, except for the message button. This button indicates the availability of the communication relay. The relay has a similar interface as the established instant messaging applications.

[14] URL: `http://www.ibtimes.co.uk` [cited 17 June 2016]

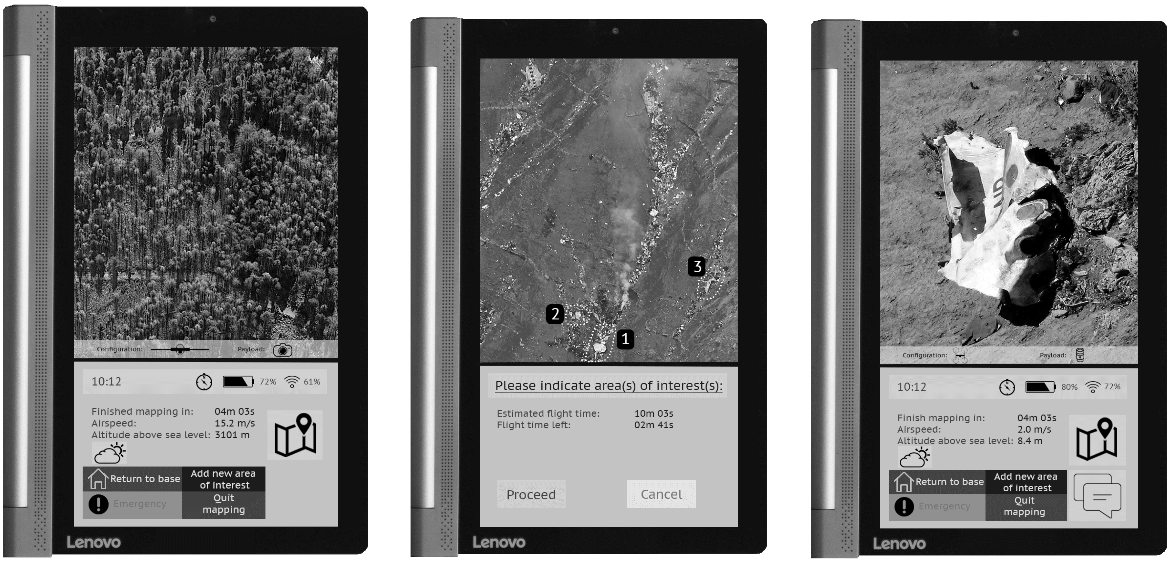

(a) Remote mission: at site

(b) Remote mission: before flight

(c) On-site mission: at site

Figure 8.3: User interface 2/2

Next to the interfaces presented here, the user interface guides the user through a pre-flight check list and a step-by-step instruction on how to visually inspect the UAV components pre-flight. Possible damage is highlighted using example images. Next to these safety features, many pop-ups shows up as to ensure that all precautionary inspections and actions have been been performed before the UAV is sent on its mission. This may become annoying, but this reminds the user of certain actions which have to be performed in order to successfully operate MIRU.

Concluding groundstation

To conclude the groundstation design, the groundstation consists of all components necessary to perform the missions. All data sent by the UAV is received and presented on a tablet. There are two types of groundstations: one portable and one fixed at the basecamp. The difference between the two is that the tablet at the basecamp groundstation is connected to the long- and short range communication system while the portable groundstation consist of a tablet with short range communication. Using the tablet, the investigator can make use of the communication relay. There is one commander tablet which can send area of interest inputs to the UAV. The hardware of the portable, basecamp and commander tablet is exactly the same and they are thus interchangeable. A division is made between groundstation components necessary when the UAV is in the air performing its mission and the components necessary to process and analyse the data gathered by the UAV. The components are selected such that they are compact and light weight to allow easy transportation. The tablets make use of user friendly interfaces, which were especially designed for each mission. The interface can be accessed using an app. The software on the app makes sure that there are enough pop-ups showing up on the tablet to ensure that the user is reminded of all pre-flight, during, relaunch and post flight operations which have to be performed.

8.4. Guidance, navigation and control

Since the UAV is not remotely controlled by an operator, it needs to be able to take-off, fly, perform its mission and land autonomously. The guidance, navigation and control (GNC) unit takes care of this by initiating commands to perform manoeuvres and setting waypoints for the flight path. The sole input from the operator is the area of interests or deviations from the waypoints set by the GNC, when an alternative route is preferred by the operator. In order for the UAV to be able to do this, an autopilot system is needed, which incorporates the hardware and software systems. The autopilot uses on-board sensors (hardware) to estimate its position and orientation, and performs flight control by translating flight commands into actuator commands (software). It also translates commands to the payload and performs payload control if necessary.

8.4.1. GNC hardware: autopilot and GNC sensors

The GNC module contains the Lisa/MX which is the autopilot, the Aspirin v2.1, which is the IMU unit, a GNSS antenna and receiver, a LiDAR, a humidity and temperature sensor and two microcantilevers. The IMU unit can be integrated into the Lisa/MX. The GNSS antenna is mounted on top of the UAV, so that it has the best reception of signals. The environmental conditions sensor is also placed outside on top of the UAV. This sensor needs to be outside the UAV such that it is not obstructed by the skin of the body and it can measure the environmental conditions well. It is located behind the antenna because in this way it interferes least with the airflow around the body, as the dimensions of this sensor are significantly smaller than that of the antenna. The two microcantilevers are mounted on the bottom side of the main body, as close as possible to the leading edge to measure the least disturbed airflow. The LiDAR module is mounted inside the nose of the main body in the direction of flight of the tailsitter and the flying wing configuration such that it senses obstacles on its path. In the quadcopter configuration, the LiDAR is still mounted on the same location, but it is tilted perpendicular to the body to point it in the direction of flight. The frontal area through which the LiDAR senses is made of perspex, which is further elaborated on in Section 8.7.4. Since the LiDAR and the GNSS module are separated by the skin, they do not interfere with each other. The GNSS antenna is connected to the GNSS receiver which is inside the body and is connected to the autopilot. The humidity and temperature sensor, microcantilevers and the LiDAR are connected directly to the autopilot. The electrical interface of the GNC module can be seen in Section 8.9.

The autopilot needs sensors data in order to process the data needed to estimate the UAV's full state vector. This vector is needed to determine the location, heading, and movement of the UAV. The vector contains: three position coordinates, three velocity vector components and three to nine parameters to describe the UAV's attitude, airspeed, sideslip angle, angle of attack and rotation rates. The first three items of the state vector are called navigation states and can be measured by an IMU and a GNSS receiver. Using software, the data from the IMU and the GPS is fused to provide position, velocity, and attitude of the UAV. This is further elaborated upon in Section 8.4.2. The rotational rates can also be measured by the IMU. The angle of attack, sideslip angle and the airspeed are also called airdata quantities which are measured by microcantilevers.

The autopilot and the inertial measurement unit (IMU)

In order to determine the vehicle's attitude, the IMU is installed on the UAV. The data collected by these sensors are sent to the mission computer, which then tracks the UAV's position using dead reckoning based on velocity and time. The autopilot unit in the UAV is the Lisa/MX (see Figure 8.4a), in which the Aspirin v2.1 (see Figure 8.4b) is integrated. The Aspirin v2.1 is the IMU containing three accelerometers, three gyroscopes and three magnetometers and a barometric pressure sensor which measures the altitude of the UAV [15]. The accelerometers detect the current rate of acceleration and the gyroscopes detect the changes in rotational attribute such as pitch, roll, and yaw. The magnetometers are used as compass and to calibrate the gyroscopes such that no error in the output of the gyroscopes occurs. The Lisa/MX and the Aspirin v2.1 weigh 10.8 g together, have a dimension of 60 x 33.7 x 8 mm and have a power consumption of 2.5 W. However, to prevent interference between the magnetometers and the batteries, which are positioned on both sides of the autopilot, the Aspirin v2.1 cannot be integrated to the Lisa/MX. Therefore the IMU must be positioned more aft in the body, as far away as the body thickness allows, away from the batteries. The IMU is not allowed to be subject to vibration, which can cause erroneous measurements. In order to damp the vibrations, the IMU is attached to a washer [16]. This has a diameter of solely 8 mm and a thickness of just 1.5 mm, such that the IMU can be placed as aft as necessary in the body.

Microcantilevers

In order to measure the dynamic pressure, an aircraft usually uses a pitot tube. However, downscaling a pitot tube to the size of this UAV leads to erroneous measurements. The angle of attack and the sideslip angle are generally determined using wind vanes, yet these scale down poorly from the use in larger aircraft as well. Therefore, a novel measurement technique is used by implementing microcantilevers (see Figure G.1 in Appendix G) to gather airflow information[17]. The sensor of this system has a mass of 3 g, and the micro cantilever

[15] URL:`http://1bitsquared.com/products/lisa-mx-autopilot` [cited 19 May 2016]

[16] URL:`http://mikrokopter.altigator.com/rubber-neoprene-antivibration-washer-m3-p-41494.html`[cited 15 June 2016]

[17] URL:`http://innovation.kaust.edu.sa/technologies/miniaturized-sensors-improve-uav-maneuverability` [cited 18 May 2016]

beam has a mass of 4 g. Using two units, the angle of attack and the angle of sideslip as well as the wind speed can be measured accurately. In Appendix G the principle of these microcantilevers is explained.

GNSS antenna and receiver

The GNSS receiver module is used since it can receive a broad range of signals (GPS, GLONASS, BEIDOU) which are necessary for operation in remote areas. Using this module, there is a higher certainty of the determined position coordinates of the vehicle. The GNSS receiver receives a single frequency signal (L1), with which a sufficient accurate position can be determined (10 cm). Even though the accuracy of a dual frequency (L1/L2) is higher, the data rate is significantly lower (20 min) compared to a single frequency (within seconds), thus a dual frequency receiver is not chosen. The accuracy of the single frequency is sufficient for navigation purposes. The GNSS receiver installed on the UAV is the Trimble BD910 (see Figure 8.4c), which receives a single L1 signal and has a mass of 19 g. The power consumed by this receiver is 1.1 W and it is 41 x 41 x 7 mm[18]. The GNSS antenna is 45 x 35 x 15 mm and weighs 34 g (see Figure 8.4d)[19]. It is connected to the receiver, which is directly connected to the autopilot.

LiDAR Lite V2

In order to support the autopilot to fly autonomously, the UAV is able to recognise obstacles on its path. For this purpose a sensing device is positioned in the nose of the vehicle. The purpose of this device is to solely detect obstacles which need to be avoided. The device is able to detect obstructions both in visible light as well as in the absence of sunlight, since the UAV should be operable these conditions as well. A device suited for this is the LiDAR lite v2 (see Figure 8.4e), which has a mass of 22 g, and a power consumption of 0.6 W[20]. The LiDAR is always pointed in the direction of flight. This means that it requires an one-axis servo that points the LiDAR in the right direction, which is different for the quadcopter or flying wing configuration. The Blue Arrow BA-TS-2.5 is chosen to do the job, which weighs only 2.8 g, a power consumption of 0.5 W in nominal condition and has a dimension of of 19.6 x 16.3 x 7.9 mm[21]. Whenever an obstacle is detected by the LiDAR, the data is sent to the autopilot, which determines the further steps in the process of avoiding the obstacle.

Humidity and temperature sensor

The DHT22 humidity and temperature sensor is connected directly to the autopilot unit[22]. This sensor (see Figure 8.4f) has dimensions of 27 x 59 x 13.5 mm, a negligibly low power consumption of 7.5 μW, and a mass of 2.4 g. This sensor is chosen because of its large operating temperature range (-40 °C to 80 °C) and its accurate humidity measurements (2 to 5%). This sensor together with the barometer, which is integrated in the Aspirin v2.1, and the microcantilevers measuring the wind speed, track the environmental conditions in which the UAV operates. For example if the pressure drops, humidity increases, and temperature increases, this means that the UAV should be controlled differently and must take caution for more dynamic environmental conditions. Furthermore, there is a weatherstation at the basecamp which measures more accurate humidity, temperature, and wind speed values. This information is mainly used to calibrate the sensors installed on the UAV, but also to forecast the weather, such that they can anticipate on whether to proceed or to stall the investigation. This weatherstation is the MetPak with Integrated WindSonic (see Section 8.3) [23].

[18]URL:`http://www.trimble.com/gnss-inertial/bd910.aspx?dtID=specs` [cited 18 May 2016]

[19]URL:`http://alliantuav.com/product/gpsgnss-antenna-mcx/` [cited 9 June 2016]

[20]URL:`http://www.robotshop.com/en/lidar-lite-2-laser-rangefinder-pulsedlight.html` [cited 19 May 2016]

[21]URL:`http://www.servodatabase.com/servo/blue-arrow/ba-ts-2-5` [cited 16 June 2016]

[22]URL:`https://www.adafruit.com/product/385`[cited 9 June 2016]

[23]URL:`http://www.parallax.bg/en/products/metpak-with-integrated-windsonic/`[cited 13 June 2016]

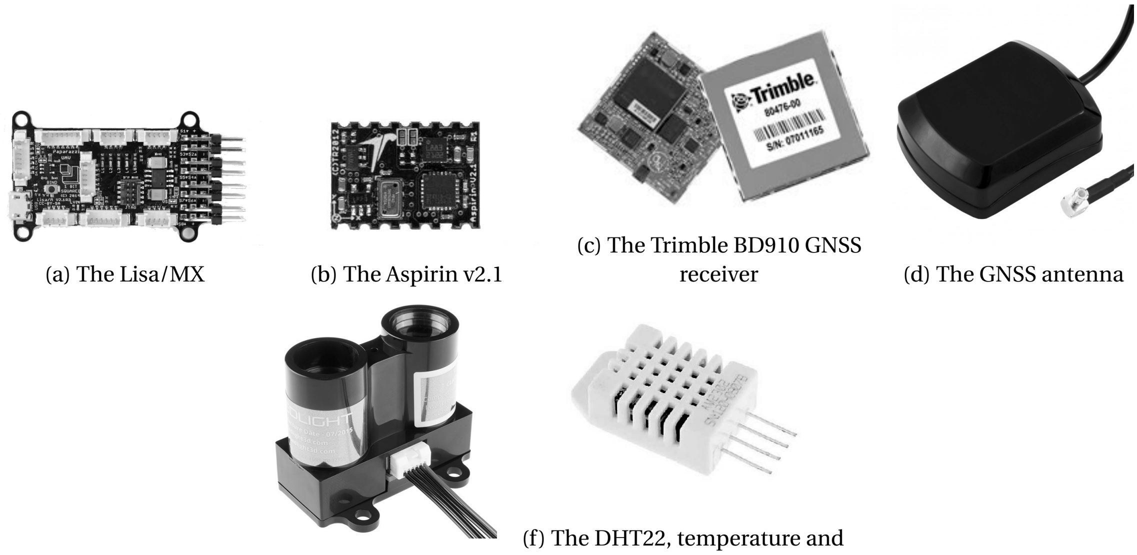

(a) The Lisa/MX (b) The Aspirin v2.1 (c) The Trimble BD910 GNSS receiver (d) The GNSS antenna

(e) The LiDAR Lite v2 (f) The DHT22, temperature and humidity sensor

Figure 8.4: The hardware components of the GNC system

8.4.2. GNC software: Paparazzi and Integrated Navigation System

The hardware components of the autopilot need software to assure a smooth and well working system that navigates, guides, and controls the UAV. This software guides the information through the system, to make sure that the correct information is sent to the correct hardware. To do so, the open source software Paparazzi is used [24]. This software incorporates several files that are specific for the UAV. The files used by this software are the airframe, flight plan, settings and telemetry file. The airframe file is the most important and the most variable configuration file that the UAV delivers, since MIRU operates in three different configurations (see Section 4.1). This file contains all the algorithms and definitions of the actuators and servos to control the vehicle. The flight plan file describes the path to be followed by the vehicle, it contains the waypoints and blocks (units of a mission, such as a landing or an avoidance manoeuvre). In this file the optimum paths, including the waypoints and blocks, from a location to another location are stored. In the settings file the user has specified a list of variables for which the values can be changed in-flight, such as maximum deflection angles for the control surfaces or the step changes. The telemetry file defines the data that is sent from the UAV to the groundstation. For example, the payload data is sent to the autopilot, which the autopilot sends encrypted to the groundstation. The telemetry file defines these files.
Furthermore, because the error of the measurements of the IMU drift over time, the data from the GPS and the IMU are fused for more accurate velocity and position estimates. For this MIRU incorporates the Integrated Navigation System (INS) to fuse these data. This software uses a Kalman filter. This filter filters the difference between the GPS and IMU measurements. The difference is subtracted from the data measured by the IMU for a correct output.

Concluding the GNC unit

In order for the UAV to be able to fly and operate autonomously, hardware and software is needed inside the UAV. This is integrated with the autopilot, the Lisa/MX. The inertial measurement unit is the Aspirin v2.1 and is positioned aft in the body, attached to a damping washer. All the hardware, except for the GNSS antenna is connected directly to the autopilot. This antenna is first connected to the GNSS receiver, which is inside the body and then connected to the autopilot. The other hardware are the GNSS antenna and environmental sensors, attached to the top outside of the body, but covered with a protective fairing, and the microcantilevers (2x) on the bottom outside the body near the leading edge. Lastly the LiDAR is installed in the nose of the UAV for object detection and avoidance. The software used to fuse this data in the autopilot is the open source Paparazzi software and the INS.

[24] URL:`http://wiki.paparazziuav.org/wiki/Software` [cited 22 June 2016]

8.5. Aerodynamic characteristics

To obtain the most efficient design in terms of the range and endurance, the shape of the planform was designed to obtain the necessary and desired aerodynamic characteristics. This was obtained by first conducting a basic sizing of the wing, after which the planform was investigated and designed in more detail, most of all based on stability and controllability. The aerodynamic properties of the UAV serve as a basis for proper calculations in stability, controllability and performance. This is solely done for the flying wing and tailsitter as for the quadcopter those characteristics are solely dependent on the propulsion. The optimal flight condition was determined, as seen in Table 8.7, for flying at maximum range, which led to a flight speed of 15.4 and 16.1 ms^{-1} at sea level for the flying wing and tailsitter respectively. Special attention was taken on the aerodynamic analysis method used (see Section 8.5.4), as this had a large impact on the results.

8.5.1. Basic sizing of the wing

Before any aerodynamic analysis was done, first, basic sizing methods were used to obtain the complete outline of the planform. This served as a basis for the further aerodynamic analysis in which the wing was investigated and designed in more detail.

The area and span of the wing are 0.25 m^2 and 1.3 m respectively. These values came out of a basic sizing method, where the main connecting factor is the wing loading, WS^{-1} (Nm^{-2}), expressing the effectiveness of the wing. The optimum wing loading was found by taking into account the requirements for the flying characteristics, derived from the mission definition. The range and endurance requirements were obtained by specific methods for battery powered aircraft [47].
Furthermore, the aspect ratio (A) was optimized simultaneously with the span and area, by investigating the flying requirements (such as stall speed and climb rate). From this, an optimal aspect ratio was found at 7. From the common wing geometry relations [41], the average chord was then calculated to be 0.19 m.

For the wing loading, a value of 100 Nm^{-2} was chosen as the UAV should still fit in a backpack, thus have a small surface area. Using the overall geometries and wing loading obtained with the basic sizing methods, the optimum was found between an as low as possible stall speed and the ease of fitting the UAV in a backpack, high cruise speed and low friction drag. A low stall speed is beneficial for mapping, transition and hand launch, however, a larger wing is needed to reduce the stall speed. This is in contrast with the operating requirement of being able to fit the wing in a backpack, which requires a small wing, and thus a high wing loading. Also, a high wing loading provides for high cruise speeds and low friction drag.
When the MTOW was filled in to determine the area and span from the wing loading, the values are slightly smaller than the ones stated above, due to the fact that the body gives a reduced lift in reality, caused by the payload fairing. The design was sized for a mass of 2.55 kg to allow for a contingency of 5%, and account for future design changes. The smallest span was used for further aerodynamic analysis to account for the reduction in lift from an early stage on. The extra drag of the payload fairing is taken into account as well, as is explained in Section 8.5.2.
The combination of low stall speed and a backpack sized wing has led to the final size of the wing, with the influence of the payload fairing -decreased lift, increased drag- taken into account.

8.5.2. Optimal flight conditions

To make efficient use of the UAV planform in its forward flying regime, it is important to investigate the optimal flight conditions for the flying wing and tailsitter configuration. The optimal flight condition for maximum range is obtained by combining the optimal flight speed from the performance calculations and the optimal aerodynamic conditions from analysing the geometry, as written out in detail in this section. The final values for these optimal aerodynamic conditions are found in Table 8.7. The aerodynamic analysis also served as a verification for the performance analysis as described in Appendix H, where values as C_{D_0} and airfoil profile were needed as input for the procedure).

The chosen flight condition is slightly below the maximum lift to drag ratio, such that longitudinal stability is guaranteed. The derivative of the moment coefficient (C_{m_α}) is very close to zero at the point of maximum $\frac{L}{D}$. There is the possibility to fly a little slower and to obtain a better endurance, but then in the event of a perturbation the UAV becomes unstable, so constant correction of control surfaces would be required. In the chosen flight condition, the UAV is marginally stable, as can be seen in Figure I.10 in Appendix I. The main reason for this is because the moment coefficient C_m is smaller than for normal more stable aircraft, as seen in Figure 8.6. Since the UAV is designed to fly autonomously, a slightly unstable aircraft is beneficial for manoeuvrability, while the control algorithms keep the instabilities of the UAV to a minimum. The resulting flight condition combines maximum range with minor corrections needed in control surfaces, for good manoeuvrability.

Table 8.7: Overview of aerodynamic characteristics, per configuration at sea level

	Flying Wing	**Tailsitter**
C_{L_R}	0.45	0.50
V_R (ms^{-1})	15.4	16.1
$(\frac{L}{D})_R$	11	11
α_R (°)	5.0	6.0
$C_{L_{max}}$	1.18	1.14
α_{stall} (°)	14.0	13.5
V_{stall} (ms^{-1})	9.8	11.7
C_{D_0}	0.031	0.033
C_{m_α} (1/°)	-0.0010	-0.0024
e	0.77	0.82

The characteristics shown in Table 8.7 are mainly dependent on the flight configuration. The $C_{L_{max}}$ values presented in the table differ slightly per configuration, as these maxima resulted from the used simulation method. The discrepancy here is mainly a result of the non-linearity during stall, which is not modelled accurately with the used analysis method, as the Vortex Lattice Method VLM is linear and works best under the approximation of small angles of attack [11]. This is explained in more detail in Section 8.5.4. The same argumentation holds for the stall angle and stall speed (α_{stall} and V_{stall}), which were normalised to sea level standard conditions. Better investigation of the stall behaviour is needed to determine the accuracy of the current approximations during stall. Using the C_m-α (Figure 8.6), it can also be seen that the chosen condition has the option to take up any perturbations in angle of attack from the nominal flight condition, without the consequence of ending up in a more unstable flight condition or too close to stall.
Clearly, the zero lift drag coefficient (C_{D_0}) for the tailsitter is higher than for the flying wing. This is in concordance to what was expected as the tailsitter has much larger vertical stabilizers. The impact is however rather low compared to the total value of C_{D_0}, as the main sources of the drag are coming from the wing itself (induced drag) and the payload fairing. The drag created by the payload fairing was modelled by approximating the fairing as a sphere, and adding this as artificial drag. By ensuring the accuracy of the approximations for the drag, the simulation in XFLR5 [12] became more reliable and accurate values were obtained for the $\frac{L}{D}$ and thus the corresponding maximum range flight condition.

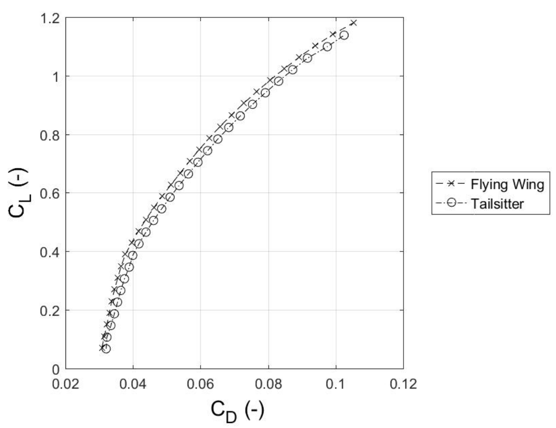

Figure 8.5: C_L-C_D polar, for the flying wing and tailsitter configuration

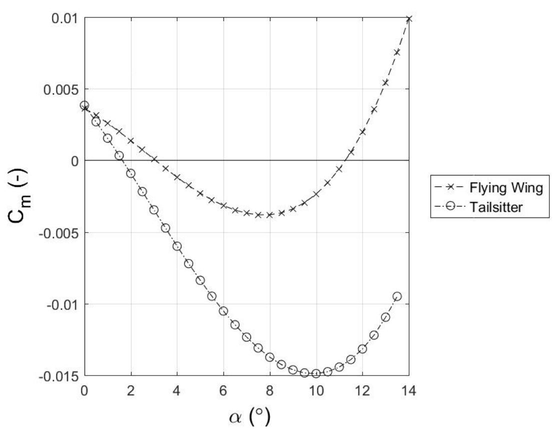

Figure 8.6: C_m-α polar, for the flying wing and tailsitter configuration

The two configurations were investigated not only for their stall behaviour and other flight independent char-

acteristics, but more importantly to define the maximum range flight condition. The characteristics for this optimal flight condition can be found in the last part of Table 8.7. The characteristics at this flight condition were deduced from the polar curves shown in Figures 8.5 and 8.6.
The current C_m-α polar is based upon the worst case center of gravity location for each configuration. When no control surfaces are deflected, the C_m and α are related according to Figure 8.6. As can be seen, the point of no net moment without deflections already provides a feasible flying condition. Only slight trimming is needed using control surfaces to obtain the optimal flight condition for maximum range, which is at a slightly higher angle of attack.

8.5.3. Wing shape and aerofoil profile

The wing shape and therefore the choice of aerofoil is important for the stability of the complete UAV. At the same time, the aerofoil should also accommodate the payload and structure inside the wing and body, which poses some extra limitations. The aerofoil profiles chosen are the Clark-YS (reflexed) and Clark-Y (normal cambered) respectively for the wing and body.

In order to obtain the most feasible solution in terms of wing shape and aerofoil profile, investigations were made with a single aerofoil along the whole span as well. However, trim conditions without control deflections were outside the normal flight regime for both the completely reflexed wing, with Clark-YS profile, and for the normal cambered aerofoil wing, with Clark-Y profile, so in the end a combination of both was found to be optimal. This resulted in the final choice of aerofoils as seen in Figure 8.7.

With this configuration of aerofoil profiles, the moment and lift-drag curves were obtained that can be seen in Figures 8.5 and 8.6. Most importantly one can see from Figure 8.6 that the current trim positions without control deflections are obtained at a beneficial point in the flight regime, at an angle of attack (α) of 2.0 to 2.5°. Only slight trimming (of +2°in α) is required to obtain the maximum range flight condition. Additional polar curves are found in Appendix I.

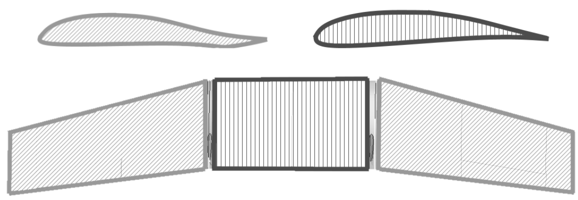

Figure 8.7: Wing and body planform with corresponding aerofoil profiles, Clark-YS (reflexed) and Clark-Y

Using a separate aerofoil for both the wing and body does not cause any issues with manufacturing, as the body and wings need to be separated in order to fit in a backpack. The resulting fact is that the body and wings are manufactured separately as well. A smooth transition between the two aerofoil profiles was designed by allowing a transition zone of 5 mm, which is part of the body.

Secondly, the choice for using a normal cambered aerofoil in the body is to accommodate better placement of the subsystems inside the body. The reflexed wing profile was analysed for its storage capabilities in the trailing edge and compared with the normal cambered profile, and it was found that the Clark-Y, the normal cambered airfoil, fitted the storage needs in the body the best.
To tweak the stability of the complete UAV even further, some other wing sizing parameters were varied in a more detailed stability analysis. The parameters that were used to tweak stability further are sweep, tip twist, taper ratio and dihedral, see Section 8.6.

8.5.4. Aerodynamic analysis methods

XFLR5 [12] has many analysis methods and options to use for an aerodynamic analysis, and even a stability analysis. An investigation was made to obtain what analysis method suits the geometry and operating conditions of the wing, including fins best. The importance of this choice is directly related to the validity of the aerodynamic results. This section mainly focuses on the limitations of the analysis methods, for the complete verification and validation of XFLR5, see Appendix H.

Comparing the results of different methods revealed that LLT has a major limitation, being the fact that this method neglects viscous drag, which is unacceptable given the Reynolds numbers at which the UAV operates. The other limitation of LLT is the fact that the wing is represented as a lifting line, and therefore the results of LLT are most accurate for simple geometries. The most efficient method was the VLM, as it produces reliable results within a satisfactory computation time. The other method, 3D panels, is only capable of analysing the wing by itself, excluding the fins. A 3D panel method could however provide more accurate results for the wing itself, however this method was not used as it does not allow computations for the complete geometry and the computation time for the 3D panel method was much higher than for the VLM, therefore making it more difficult to make quick changes in the design and investigating the results. The downside of VLM on the other hand is that the results only show linear behaviours, and therefore stall cannot be modelled accurately. This way, any aerodynamic behaviours that would be of importance for the transition phase cannot be predicted, making the transition more difficult to model.
All in all, the VLM method was best to use for the design parameters under consideration and given the complexity of the wing geometry. The discarded analysis methods were LLT and 3D panels.

Concluding the aerodynamic characteristics
Using implementations of the final wing geometry in XFLR5, the aerodynamic properties were obtained. The analysis method used for this was the VLM method, as this allowed the analysis of more complex geometries and therefore accounts best for sweep, twist and taper. Moreover, VLM allowed the fins to be included fins in the analysis. Investigations near stall were limited with VLM as it did not account for the non-linearities in stall. The optimal flight conditions for the final geometry were found using VLM, resulting in a cruise speed of 15.4 and 16.1 ms^{-1} for the flying wing and tailsitter configuration respectively.

8.6. Stability and controllability

In order to keep the UAV in the air, it is of great importance that there is sufficient stability and control which is provided by the control surfaces, fins and planform shape. Using XFLR5 [12], the stability and control derivatives were obtained and compared for different planforms shapes. From this, the stability and controllability of the design was analysed and changes were made in order to make the planform stable.

8.6.1. Stability

The stability of the UAV was just like the aerodynamics analysed using XFLR5 [12] for both the flying wing and the tailsitter configuration. The stability for the quadcopter is solely determined by the autopilot, as the quadcopter stability is only dependent on the motor settings and the reaction to gusts. The obtained data showed that the static stability is satisfied, however, the dynamic stability is not satisfied for two modes. The graphs, stability and control derivatives and the eigenvalues generated by XFLR5 are presented in Appendix I.
In order to determine how the longitudinal, lateral and directional stability are achieved for the UAV, the stability characteristics are determined and their influence is explored. MIRU uses mainly six planform characteristics to determine stability, namely sweep, taper, tip twist, dihedral, vertical fins and its aerofoil, which are presented in Table 8.8.

Table 8.8: Planform characteristics

Sweep (°)	**Tip twist (°)**	**Taper ratio (-)**	**Dihedral (°)**	**Aerofoil**
16	-1.5	0.67	2.0	Clark-YS

Sweep
Sweep could generate problems. The reasons to limit sweep are that it causes, among others, a more complex (thus heavier) structure, more drag and tip stall. However, sweep is a must for a flying wing as it has high influence on the directional and longitudinal stability. With a swept back wing, the aerodynamic center moves backward, which means the center of gravity can also travel more to the back. Furthermore, wings with sweep (and washout) can handle gusts better than wings without sweep.

The sweep was set to 16° for the wing only. It was kept as low as possible, but still secures that the aerodynamic center is sufficiently shifted to the back. Moreover, it resulted in a better trim point on the C_{m_α} graph, as explained in Section 8.5.2.

Twist
The tip stall caused by the swept wing was solved by twisting the tip of the wing, called washout. By twisting the wing tip down, the wing tips stalls later than the root. Therefore the elevons are not affected, hence still controllable. However, there are some downsides. Twist create a more complex structure and more drag. Taking all the reasoning into account, UAV was given a tip twist of -1.5°(hence twisting the tip downwards).

Taper ratio
The taper ratio (λ) of the wing is the ratio between the root chord and the tip chord. For stability reasons a high taper ratio is preferred, as tip stall increases with lowering the taper ratio. However, for structures an increase in taper ratio means a increase in the bending moment at the root, which results in a heavier UAV as more structure is required, thus structurally a lower taper ratio is desired. Moreover, induced drag is less with a strongly tapered wing because it approximates the elliptical lift distribution. As also wing twist has been taken into account to make up for the tip stall, some taper was introduced, resulting in a taper ratio of 0.67.

Dihedral
The dihedral angle is the angle the wing makes with respect to the ground, looking from the front view of the UAV and defining positive upwards. It is used regarding the lateral stability, more specifically for the spiral motion. For the directional stability, it makes sure that a sideslip is decreased. The disadvantages are that it makes the UAV less manoeuvrable and controllable and structurally more difficult, which is why it was set to only 2.0°.

Stabilizing fins
The UAV has two different sets of vertical fins. For the tailsitter, they are mainly used to provide attachment for the motors, while for the flying wing they provide weathercock stability. They are sized so that a square in the positioning of the motors is created. For the flying wing smaller fins were used. It purely has a stabilizing function as there is no need for any attachment. The vertical fins are yaw stabilizing as they generate a force to oppose sideslip.

Aerofoil
The choice of the aerofoil influences a lot of the other parameters. For example, if the aerofoil has a reflex camber it usually only needs dihedral in order to achieve longitudinal and lateral stability [21]. If a more regular aerofoil is chosen, other wing characteristics as described before have to be taken into account. For the UAV a reflex cambered aerofoil, Clarky YS, was been chosen. From the XFLR5 data it was clear that it did not have sufficient stability when combined with dihedral, which is why the other characteristics were also taken into account. The aerofoils were already presented in Section 8.5.3.

The UAV's longitudinal static stability is obtained when the C_{m_α} is negative, which means that the UAV creates a counter moment when an external moment is brought into play. In order to obtain this behavior, the position of the center of gravity should be smaller than the position of the aerodynamic center, $\bar{x}_{cg} < \bar{x}_{ac}$, as can be derived from Equation 8.1.

$$C_{m_\alpha} = C_{N_\alpha} \frac{x_{cg} - x_{ac}}{\bar{c}} \tag{8.1}$$

By making use of the reflexed Clark YS aerofoil and the 16 degrees of sweep, the longitudinal static stability was achieved. The neutral point is located at 85 mm from the leading edge, so for the whole range of center of gravities, which is 71 to 82 mm depending on the configuration and payload, the center of gravity stays in front of the neutral point. Regarding the dynamical stability, the short period motion is presented in Figure I.9. Those figures, in combination with the eigenvalues from Figures I.7 and I.8, show clearly that those motions are converging and are therefore stable. The phugoid, however, is diverging as shown on Figure I.10. That means that if the UAV is subjected to imbalance, the UAV starts to oscillate with increasing amplitude. This is not putting the UAV in danger as the autopilot can easily correct for this slowly increasing oscillation.

Static and dynamic stability
The lateral stability is mostly obtained by means of dihedral, of which C_{l_β} is the control derivative. Just like C_{m_α}, it has to be negative to counteract the created moment. The directional static stability, also called the weathercock stability, makes sure the UAV is stable for the yaw motion. This is the case when C_{n_β} is positive, which is positively influenced by the swept wing and the vertical fin and negatively influenced by the fuselage, which is the payload fairing for this UAV. The lateral dynamic stability depends both on roll and yaw and has three important modes: the aperiodic roll, the Dutch roll and the aperiodic spiral. As can be seen in Figures I.11, I.12 and I.13 in Appendix I, it is the spiral that is diverging, which means this is the only dynamical instability for the lateral motions. It is common for aircraft to be unstable in spiral and also for the UAV it is not dangerous, as it is only diverging slowly. Furthermore, just like for the phugoid, the instability can be corrected with control by using the autopilot.

Centre of gravity
The centre of gravity in longitudinal direction differs for every configuration. For the purpose of stability, it is required that the centre of gravity of the UAV is always in front of the neutral point. The neutral point is located at 85 mm from the leading edge. When looking at the centre of gravity in z-direction which is the longitudinal direction, the centre of gravity for all configurations is in front of the neutral point. There exists a range, which is explained by the different payloads used. For Table 8.9, the x-direction is the lateral direction, this is 0, because the UAV is symmetric and lastly the y-direction is the centre of gravity in vertical direction which is mainly determined by the payload bay.

Table 8.9: Centre of gravity locations for each configuration

	X-direction (mm)	**Y-direction** (mm)	**Z-direction** (mm)
Hover configuration	0	-28	55 - 57
Flying wing configuration	0	-20	80 - 83
Hybrid configuration	0	-28	71 - 72

8.6.2. Control surfaces
In order to have three-axis control, an aircraft makes use of primary control surfaces which are the ailerons, rudder and elevators. Because the UAV does not have a horizontal tail, elevons are used which are a combination of ailerons and elevators which provide the necessary control for all configurations.
The sizing of the control surfaces was performed with the use of Aircraft Design [42]. From this, different parameters with respect to aileron sizing were used to determine the size of the elevons. Because the elevons are a combination of ailerons and elevators, the largest parameters were used. In Figure 8.8, the elevon planform can be seen from which $\frac{b_a}{b}$ is equal to 0.3, which results in a span of one elevon of 0.2 m. The $\frac{C_a}{C}$ is equal to 0.25 and $\frac{b_{ai}}{b}$ was estimated at 0.6, which results in starting the inner section of the elevon at 0.4 m measured from the centerline. This value was chosen in this way, so that an unlikely wingtip stall does not influence the effectiveness of the elevons. The maximum deflection of the elevons was set at 25 °, both up and down.

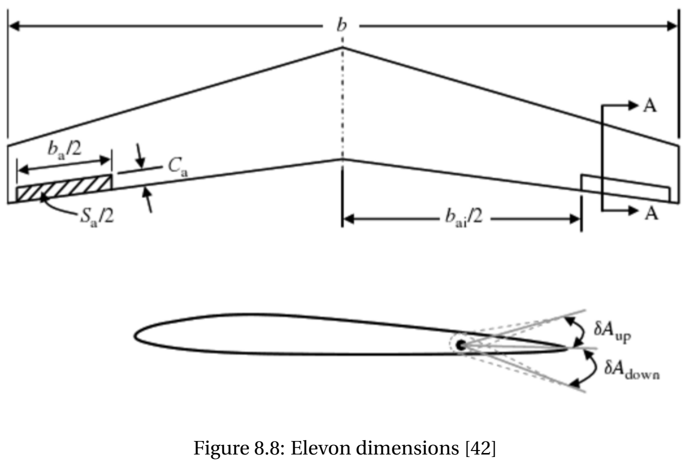

Figure 8.8: Elevon dimensions [42]

The sizing of these elevons was validated with reference UAVs as the Skywalker X8[25], RVJET[26] and some home-built flying wings. From this it resulted that the only parameter which was significantly lower, was $\frac{b_a}{b}$. The method from Aicraft Design gave a maximum of 0.3 for this parameter, where the reference UAVs all had a value of around 0.5. However the moment arm which is determined by $\frac{b_{ai}}{b}$ is larger for this design compared to the reference UAVs, which compensates for the lower $\frac{b_a}{b}$ value.

In Figure 8.9, a cross section of the wing is shown to indicate the layout of the elevon and servo placement. The elevons are deflected with the help of a servo which is triggered by the autopilot. The servo generates a torque which has to be transferred to the elevons. This is done through a push-rod which connects the horns from both the elevon and the servo. The elevon is attached to the wing with three nylon hinges. Using two hinges is sufficient, but one is added as a redundancy measure.

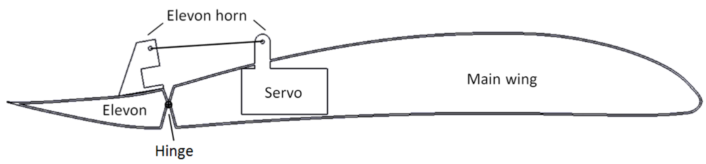

Figure 8.9: Cross section of the wing showing the elevon layout

Because simulating controls in XFLR5 was not precise and no correct parameters were obtained, it is not fully known whether the UAV suffers from adverse yaw. Therefore it is recommended to further investigate this, from which it might be necessary to design a adverse yaw system, which is further explained in the recommendations in Chapter 14.
Comparing the method used by Aircraft Design and reference UAVs, resulted in a lower $\frac{b_a}{b}$ value in the design. For further development it can be investigated if obtaining a larger value for the $\frac{b_a}{b}$ parameter would be more efficient for controlling the UAV.

8.6.3. Controllability

Because the UAV does not have a horizontal tail, the controllability equation for a conventional aircraft with tail therefore reduces to a simplified form, which can be seen in Equation 8.2 [24].

$$\overline{X}_{cg} = \overline{X}_{ac} - \frac{C_{mac}}{C_L} \tag{8.2}$$

From the stability discussed in Section 8.6.1, the static stability margin should be larger than zero. Because for a tailless UAV, the neutral point and aerodynamic centre of the wing coincide, Equation 8.2 can be rewritten as:

$$C_{mac} = C_L \left(\frac{\overline{X}_{ac} - \overline{X}_{cg}}{\bar{c}} \right) \tag{8.3}$$

From this it resulted that the moment about the aerodynamic centre should be positive, also called 'pitch up'. In order to trim the UAV with a positive lift coefficient and a positive C_{mac} would result in a negative cambered aerofoil or an aerofoil with reflexed camber line, from which the last option is used on the UAV as discussed in Section 8.5.3. Furthermore is the control done by the autopilot and control surfaces, which make the UAV fully controllable in all three configurations

Concluding stability and control

The static stability was achieved by taking six platform characteristics into account: sweep, tip twist, taper, dihedral, vertical fins and the Clark YS aerofoil. The UAV is also dynamically stable, except for the phugoid and the spiral motion. Those instabilities are however mild and can be made up for by the controls. The control surfaces of the UAV consist of elevons which are a combination of ailerons and elevators. These are triggered by the autopilot through a servo. Through analysis, the UAV is said to be controllable in all configurations

[25] URL:https://pixhawk.org/platforms/planes/skywalker_x8 [cited 22 June 2016]
[26] URL:http://www.rangevideo.com/18-rvjet- [cited 22 June 2016]

8.7. Structural characteristics

The structure of a UAV must be lightweight, strong and durable. The structure is not there to solely carry loads, but also to add connections to the payload, elevons and electronics. The structure therefore becomes a multipurpose subsystem. The layout of the framework and layout of the system were thus mainly sized based on the location and volume of the batteries, payload and electrical components. The sizing of the actual load carrying components was based on the loads during the different operational modes. To optimise the mass and durability specifically, much attention was spent on the material selection. The durability influences the lifetime and maintenance of the complete UAV, which are important to deliver a competitive design to the market. The outcome of this process was a structural framework composed of a carbon and foam sandwich structure for the wings and fins and a carbon spar structure for the body. All subsystem components fit inside the body and are optimised to move the c.g. most forward for flight stability. The specifics of each framework for the UAV and payload bays are given below after the material selection and load carrying analysis.

8.7.1. Structural layout

A top view of the structure is given in Figure 8.10. The wings and fins were designed as a foam core coated with a thin carbon layer. The foam in such a structure carries almost all shear loads, while the carbon takes care of the bending stresses [49]. The sandwich theory approximation was used to analyse all the stresses [49]. The body was on the other hand based on a structure of two carbon fiber spars carrying all loads. Two spars easily carried the load, while also efficiently dealing with the moments induced by the lift. Still foam with a carbon skin was added to the body to give the body the necessary aerofoil profile and transfer the loads to the spars. The framework of the body therefore left room for the subsystem integration. At the joints reinforcements were added to secure the structural integrity. The spars were analysed using beam theory for tubes [32].

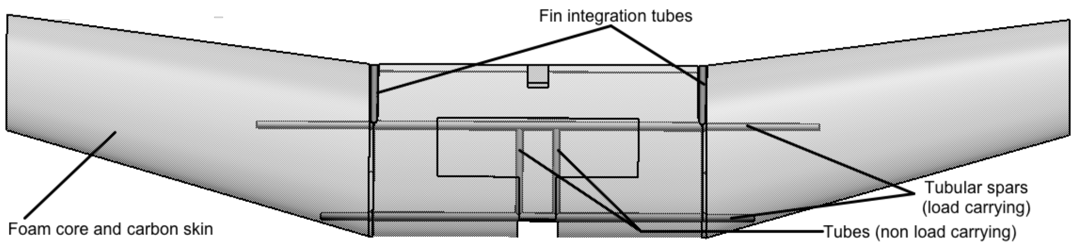

Figure 8.10: A top view of the structure for the wings and body, where the key components are highlighted

The complete structure has a mass of only 0.39 kg. The lightweight structure is very stiff, as the wing tip can only deflect 1.5 mm during the worst load case scenario including a safety factor of 2. The wings therefore maintain the most efficient shape during all flight conditions. More properties of the selected materials are given in the next section. This worst case scenario consists of the tailsitter configuration in horizontal flight enduring a 2.5g loading on the wing, and a 2.8g loading on the motors with all 5 motors running at maximum throttle. The safety factor of 2 on top of this scenario was chosen to create a margin between the idealised and real structure. This case was used throughout all structural calculations.

Materials

Rohacell 31 IG/IG-F is used as the foam core throughout the entire structure. This aerospace quality foam is the lightest of the IG/IG-F series and has the structural properties to sustain the wing loading. The closed cell structure reduces the risk of fluids entering the foam, which improves the lifetime of the structure. The Rohacell 31 foam also has a very small cell size compared to similar foams. In the end this reduces the mass of the final structure with respect to the adhesive as less resin is absorbed at the outer cells, which are cut open during manufacturing. The most important performance specifications are given in Table 8.10. Especially the entries for shear strength and shear modulus should be taken into account, as these determine the performance of the material in the current loading case.

Table 8.10: Specifications of the materials used [19] [8]

	Density (kgm^{-3})	Compressive strength (MPa)	Tensile strength (MPa)	Shear strength (MPa)	Elastic modulus (MPa)	Shear modulus (MPa)
Rohacell 31 IG/IG-F	32	0.4	1.0	0.4	36	13
M56/40%/193PW/AS4-3K	1500	848	924	128	65.9	61.5
CG10.0/08.0	1600	600	570	-	70	70
Redux 870 A/B at 23°C	-	98	-	43	-	-

The composite layer is a combination of HexPly M56 resin and 193PW-AS4-3K woven carbon in a one to one volume ratio [8]. This combination has the lowest combined density for the M56 resin and is tested and developed for UAVs [5]. The technical properties of the selected material are given in Table 8.10.
The adopted carbon-adhesive layered skin has an impressive chemical resistance. The structure is therefore protected from chemical damage during gas detection missions [6].
The carbon fiber fabric has a plain weave (Figure 8.11). This is the least pliable interlaced carbon. However this suits the design, because sandwich theory calculations showed that the structure is stiff with a maximum tip deflection of 1.5 mm.

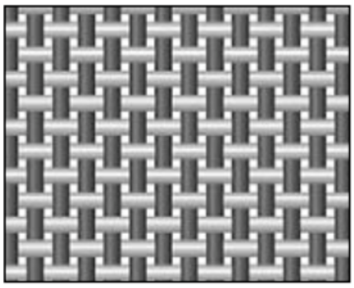

Figure 8.11: Carbon fabric plain weave by Hexcel Corporations [7]

The spars in the wing and body are made from CG10.0/08.0 circular tubes, which are based on a carbon fiber fabric with a resin [27]. The material properties are given in Table 8.10 [28]. The tubes for the body have an outer diameter of 10.0 mm and wall thickness of 1.0 mm. These dimensions still allow for a simple payload integration and fit within the aerofoil. For the wings a tube with an outer diameter of 8.0 mm was adopted with a wall thickness of 1.0 mm. The wing tubes need to fit inside the body spars to transfer the wing loads to the body. This joint is further elaborated on during the explanation of the joints at the end of this section.
The Redux 870 A/B adhesive was chosen to be used to connect the skin and tubes to the foam [29]. This lightweight adhesive does not need a film, has high temperature performance up to and beyond 100 $°C$ and is easy to use during manufacturing with room temperature curing. The adhesive is also specifically able to bond the selected foam and carbon. The specifications can be found in Table 8.10.

8.7.2. Stress analysis and part design

A stress analysis was performed to size the structural components and show that the the structure could cope with all forces and moments. This section simply documents the results, while the next three sections discuss the impact on the structural framework. The applied loads can be seen in Figure 8.12 for the wings, in Figure 8.14 and 8.15 for the leading and trailing edge spar of the body and in Figure 8.13 for the fins. Next, the results of the sandwich structure analysis of the wings are showed, followed by the results of the analysis of the fins and body. Once all stresses are showed, their impact on the design is discussed.

[27] URL:`http://www.carbonfibretubes.co.uk/standard-tubes/` [cited 15 June 2016]
[28] URL:`http://www.carbonfibretubes.co.uk/technology/` [cited 15 June 2016]
[29] URL:`http://www.hexcel.com/Resources/DataSheets/Adhesives-Data-Sheets/870AB_eu.pdf` [cited 15 June 2016]

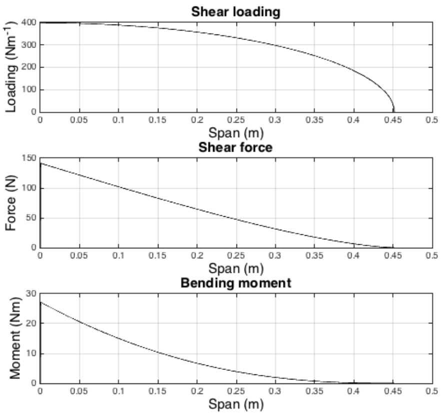

Figure 8.12: Wing loading with an idealised elliptical lift distribution

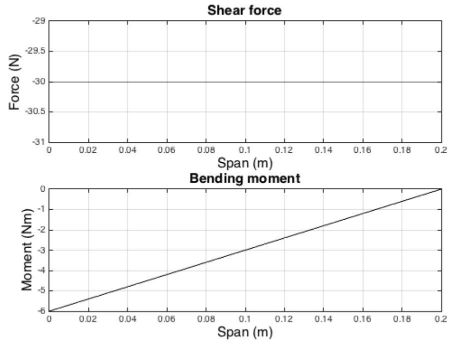

Figure 8.13: Loading of fins with a constant thrust of the hover motors

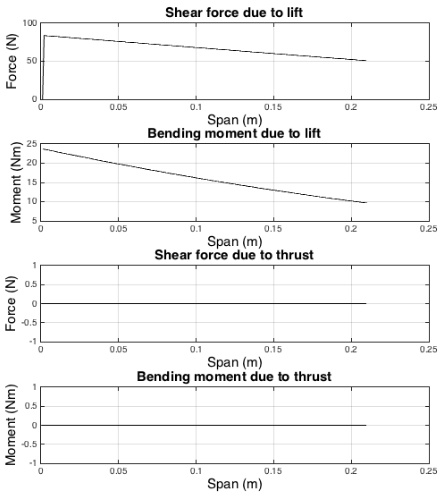

Figure 8.14: Loading of leading edge spar incorporating both the lift and motor loads

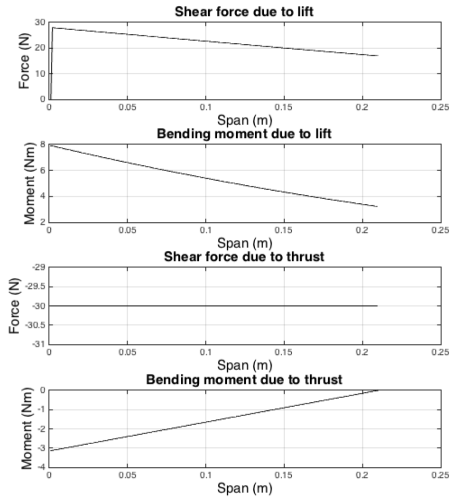

Figure 8.15: Loading of trailing edge spar incorporating both the lift and motor loads

Figure 8.16 shows the stresses in the carbon skin of the wings. Both the stresses for the bottom and top skin were calculated for the maximum wing root thickness along the entire span.

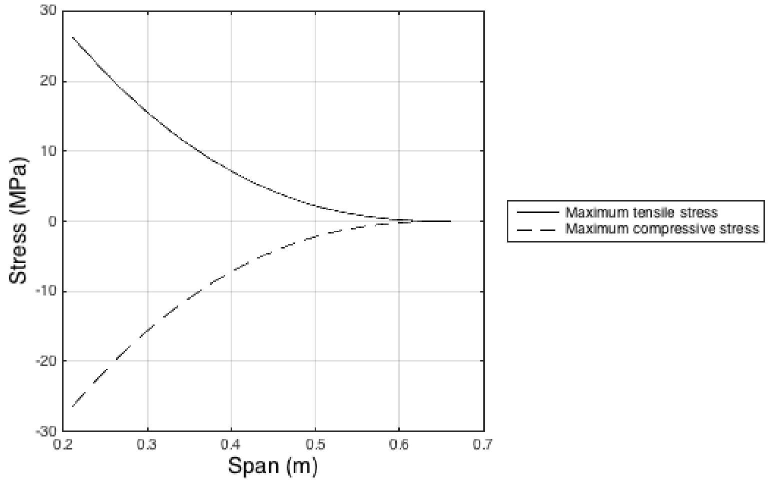

Figure 8.16: Stress distribution for worst case loading of the wings

However for the shear stress calculation, the tip dimensions were used for the idealisation. Thus the structure was again idealised for the worst performing cross section during this loading. The foam has to endure a maximum shear stress of 0.014 MPa. The deformation and rotation of the wing are shown in Figure 8.17.

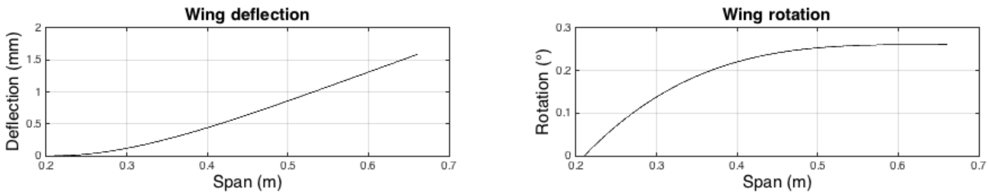

Figure 8.17: Deformation and rotation of the wings

For the analysis of the body only the spars were evaluated, because they are designed to take all the loads. Thus a stress analysis was done incorporating both the aerodynamic and the motor loads. The maximum stress for both spars can be seen in Figure 8.18.

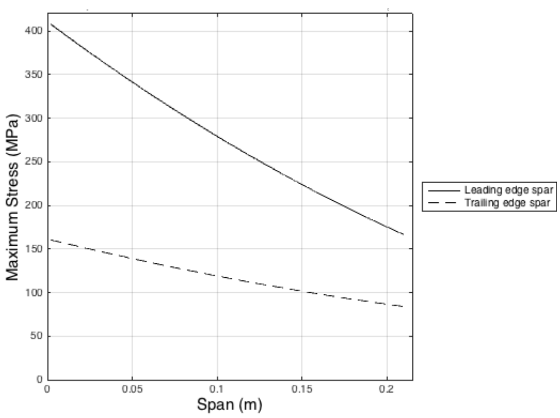

Figure 8.18: Maximum stress along the span for each cross section

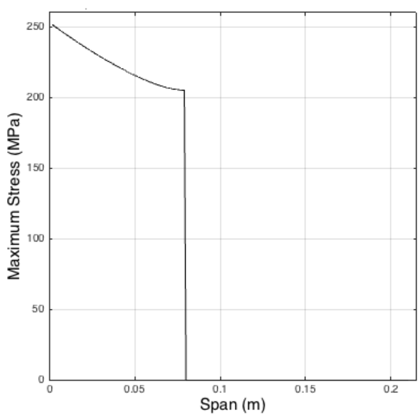

Figure 8.19: Maximum stress along the span of the body for a bungee rope launch

The second high stress loading case for the body is during a bungee rope launch for the flying wing. Figure 8.19 shows the resulting maximum stress in the leading edge spar for this launch including again a safety factor of 2. The attachment hooks of the bungee rope are symmetrically placed 8.0 mm away from the center line of the body. The bungee rope as well as the hooks, therefore do not interfere with any payload bay.
The fins were not analysed using a sandwich structure idealisation, but it was decided to let the skin also carry shear loads. The sandwich structure idealised skin would be placed in line with the hover force and thus carry loads. The fin loads are minimal compared to the wings. It was therefore safely assumed that the stress in the foam does not limit the structural performance. However the skin could restrict the operational capabilities. A single cell carbon structure was evaluated with only the skin properties. The maximum stress for a single fin is shown in Figure 8.20. The span starts at the intersection with the body and ends near the tip of the fin, where the hover motors are located.

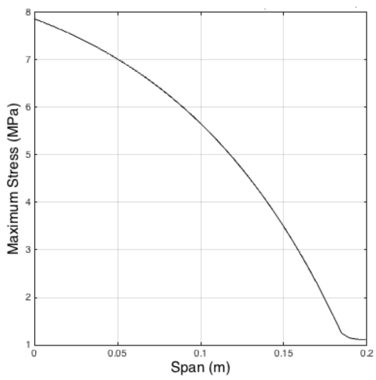

Figure 8.20: Stress distribution for worst case loading of the fin

Wings
The wings have a foam core with a carbon skin of 0.2 mm thick. The calculated bending loads are a factor 30 below their maximum and for the foam the calculations showed a factor greater than 25. Therefore the wings can cope with all the loading cases. The foam makes the wing strong during flight and transport, the carbon skin creates a durable system for example with respect to dents and the complete structure is lightweight.
Near the root the wings are reinforced as two spars for the joint are embedded there. The leading edge spar in the wing has a length of 60 mm, while the rear spar has a length of 140 mm. Both spars have a thickness of 8 mm. The control surfaces of the wing are not taken into account as they cannot take any loads. However the cutout of the elevator must be laminated with a layer of carbon fiber to protect the foam core. The frontal surface of the root chord is laminated for the same reason.

Body
The spars are the main structure of the wing and can take a maximum stress of 570 MPa. The stress analysis showed that the maximum stress in the structure reaches 410 MPa for the maximum loading case in flight. The front spar takes most of the loads. However both spars have the same dimensions to simplify the manufacturing and add redundancy. The trailing edge spar is therefore over-designed compared to the front spar. The structure is therefore able to cope with all loads. However reinforcements should be added to allow a smooth integration with the fins and loads of the hover motors. This integration is shown in Section 8.7.2. Also two tubes are added in the center to ensure structural integrity of the framework. The spars can therefore not shear out of plane and the thrust from the cruise motor is introduced to both spars. The foam is always at least 3.0 mm thick near the skin to make sure the aerofoil keeps its shape. The room left behind in the wing allows for the subsystem integration. Also for the body the cutouts for the motors, fins and LiDAR are covered with a single layer of carbon to protect the inside of the body. The same is true for the tips where the sides are covered with carbon to secure the inner parts and structural integrity.

Fins
The fins have the same structure as the wings with a foam core and a 0.2 mm carbon fiber skin. Although the skin can carry the hover motor loads, which are transferred to the fins by carbon fibre rods, the structure is

still filled with foam. The foam has a broader purpose, because it also helps to distribute the loads, improve the impact resistance and strengthen the load transfer from fin to body. The carbon fiber rods are also used in order to stand firmly on the ground in tailsitter or quadcopter configuration.

Small fins

The stresses of the small fins were not calculated, because the loads are much lower compared to the fins, while the structural outline is the same. The small fins therefore also consist of a foam core with a 0.2 mm thick layer of carbon fiber. Their main purpose is to add lateral stability instead of structural rigidity.

Joints

The first two joints are located between either side of the body and the attaching wing. Here the spars from either side create a male-female connection. Both the male spars come from the wing and slide into the body spars, where they are locked into place with small bolts.
The second set of joints is located at the fin-body integration. The fins slide over a tube which is connected to the rear body spar. A sketch of the t-connector is shown in Figure 8.21 [30]. The fins are also shaped to fit around the rear spar of the body to properly introduce the loads to the framework of the body. The fins are locked into place at the trailing edge of the fins. This type of joint likewise does not hinder the female port of the trailing edge spar joint with the wings and body.
The t-connectors of Figure 8.22 are used to create the last set of joints at the center of the body [31]. As can be seen in the top view of Figure 8.10, two perpendicular spars are connected to the main spars of the body. This joint is permanent, because it does not need to be disassembled during the operations or missions.

Figure 8.21: Example of a t-connection for the fin and spar integration

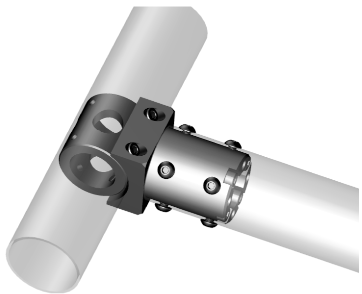

Figure 8.22: Example of a t-connection for the spar integration at the center of the body

8.7.3. Failure Modes

The structure can cope with all the loads. However certain precautions were taken into account, when the failure modes came to mind. The most characteristic failure mechanisms known to a carbon and sandwich panel structure are: section, bearing, shear out and delamination failure [23]. These structural breakdowns can specifically or combined apply to either the face sheet, adhesive, foam core or spars.
As long as no manufacturing errors are present, the sheets and foam of the sandwich structure can withstand the loads. Also the spars are safe from sectional failure.
The bearings are more concerning and thus reinforcements were added. The spars are filled with a carbon piece to secure the bearing. This can also be seen in Figure 8.22.
The stress at the skin for both the wings and fins is still more than 40% under the maximum shear loading, therefore the adhesive should not fail under operating conditions.
The very thin top panel of the wings is loaded in compression and could potentially buckle. The buckling can eventually cause shear out or wrinkling of the top sheet. The loads carried by the top panel are more than a factor 15 below the strength of the carbon fiber skin. Thus the likelihood of buckling is very low.
Delamination is always a risk when layered sheets of carbon are used. On the other hand no carbon structures are simple layups, but consist of a fabric. Fabrics improve the delamination performance, however if real laminate splitting occurs, the part must be replaced immediately. The maintenance program in Section 6.2 defines the steps taken to notice the delamination before failure happens.

[30] URL:`https://www.rockwestcomposites.com/1302` [cited 19 June 2016]

[31] URL:`https://www.rockwestcomposites.com/accessories/carbon-erector/fixed-connector/ce-cl-group` [cited 19 June 2016]

Furthermore impact damage, dents, puncture and heat damage should directly be addressed with repairs [32]. The performance of the structure decreases dramatically and the environment (i.e. gases, water etc.) and fatigue can easily cause more destruction.

8.7.4. Payload mounting and aerodynamic fairings

The payload is mounted on the UAV through a vibrationally isolated aerodynamic fairing. In order to mitigate the influence of the main vibrational disturbance source (i.e. the motor), special ball dampers are used to isolate the payload fairing from the main structure. In order to achieve sufficient amplitude damping, the ratio of the main body (driving) frequency and the natural frequency of the payload fairing should at least be higher than the square root of two [33]. Since the motors rotate at a rate of 14000 rpm, the driving frequency is 233.3 Hz. Therefore the natural frequency of the payload bay system should be lower than 165 Hz. To ensure the low transmissibility between the driving amplitude and the payload bay's amplitude, four damping mounts rated for 50 - 125 g each are needed [34].

The fairing itself was designed in such a way that the space inside is used as efficiently as possible, therefore reducing the induced drag by decreasing the frontal area and making sure the flow is attached and laminar for as long as possible. With the above requirements, a specific payload mount was designed for each configuration. This was combined with the design objective to keep the contribution to the overall centre of gravity the same per configuration, such that consistent stability characteristics are obtained for each configuration. Furthermore, it was designed as such that the centre of gravity shifts forward due to the payload, also aiding in increasing the stability. The configurations can be found below in Figures 8.23 to 8.25. Since these fairings are made of plastic, a scratch-resistant perspex window is inserted to ensure the cameras field of view is not obstructed. For the protection of this perspex during a belly landing, a protective film is applied to the flying wing's payload window. This can then be replaced easily when it is scratched to ensure that not the whole fairing needs to be replaced. Furthermore, since the impact of the belly landing introduces high loads to the flying wing's fairing, it is reinforced with a rib in the circumferential direction. All payload fairings can easily be formed with injection molding. The cameras are mounted using screws through the mounting holes already present on all cameras. The fairing itself has threaded standoffs in the bottom plate on which the payload is screwed in.

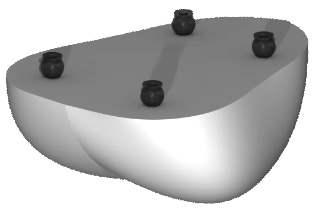

Figure 8.23: Payload fairing for the tailsitter configuration

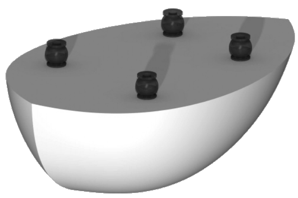

Figure 8.24: Payload fairing for the flying wing configuration

Figure 8.25: Payload fairing for the quadcopter configuration

In a similar fashion to the design of the payload fairing, other fairings for parts that are protruding the body were designed. This includes the antennas, as they must have a clear and minimal unobstructed line of communication, and the LiDAR module, since this needs to be fitted in the nose, and will have to tilt ninety degrees to ensure object range information in both the hovering and forward flight condition. These fairings are shown in Figures 8.26 and 8.27.

[32] URL:`http://www.hexcel.com/Resources/DataSheets/Brochure-Data-Sheets/Composite_Repair.pdf` [cited 20 June 2016]
[33] URL:`http://www.earsc.com/HOME/engineering/TechnicalWhitePapers/Vibration/index.asp?SID=61` [cited 6 June 2016]
[34] URL:`http://mikrokopter.altigator.com/silicone-ball-damper-high-flexibility-p-40764.html` [cited 6 June 2016]

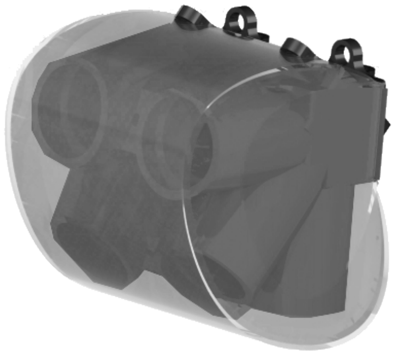

Figure 8.26: Fairing for the LiDAR module, the LiDAR module is shown in three possible positions to indicate the tilt-range

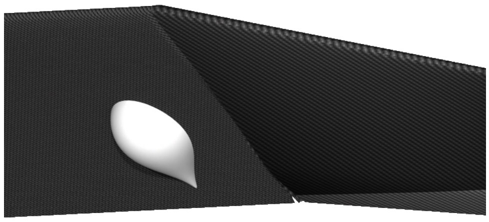

Figure 8.27: Fairing for the antennas in white, the UAV can be seen from the bottom at the body-wing connection

Concluding structures

The mass of the entire structure is only 0.39 kg and 17% of the mass fraction, which is lightweight. The skin is made from HexPly M56 resin and 193PW-AS4-3K woven carbon, the foam core from Rohacell 31 IG/IG-F and then carbon spars from CG10.0/08.0 circular tubes. Furthermore the system is durable, as the skin protects the body, wings and fins from dents, gasses and chemicals. Finally the structure is strong due to the foam in the wings and fins and the two carbon tubes in the body of the UAV. The carbon tubes are naturally stiff, while the low loading of the foam in the wing makes the wings very rigid. All body parts are glued together using an adhesive with a large temperature range to aid the operational conditions of the UAV. Furthermore joints are realised to integrate the wings and fins with the body. The joints allow the UAV to be stored in a backpack and once connected, they transfer the loads between the joined parts.

8.8. Performance and propulsion

To be able to move forward and take-off, the UAV has a propulsion system. The propulsion system is split into two parts as the forward flight needs thrust in another direction than the vertical flight. Also, the amount of thrust needed differs a lot as in forward flight the wing provides lift to carry the weight, so only drag needs to be counteracted by the propulsion. For the vertical flight however, the propulsion system needs to carry the entire weight and counteract drag.

For the vertical flight propulsion system three propeller sets are needed that differed in pitch, not in diameter, to still fit in the backpack and provide a good performance for altitudes from 0 to 4500 m. For forward flight this was not needed, as one propeller suited all altitudes.

As for the flying wing a different take-off method was needed as it does not have vertical take-off, a bungee launch was picked as it needed a small take-off area and simple tools. The flying wing performs a belly landing with reverse thrust to still be able to land on a small area.

Especially Section 8.8.1 is important as this sets the basis for the performance calculations further explained in this section. The section is then structured according to steps 1 through 8 from the mission profile of the tailsitter as shown in Figure 8.35 (Section 8.8.2), as the tailsitter is the basis. From there on, the changes for the flying wing and quadcopter are explained. The verification and validation of the tools used for performance and propulsion is described in Appendix H.

8.8.1. Propulsion system design

As explained before, the propulsion system was split in horizontal and vertical flight. Therefore the design was also split that way. The propeller was chosen first and then the motor was chosen as a correct propeller-motor can greatly improve the efficiency of the propulsion subsystem.

Propeller selection horizontal flight
The propeller used by the UAV for horizontal flight is the CAMcarbon Light Prop[35], as seen in Figure 8.28[36] propeller with dimensions of 28 cm (11 $in.$) in diameter, and 22 cm (9 $in.$) pitch. The high pitch of the propeller can be explained by the fact that the airflow through the propeller disc is higher than in quadcopter configuration. The air has to be sped up from stationary to the induced speed, instead of already having a relative velocity with the UAV, as is the case in horizontal flight.

Although somewhat different propellers give slightly better performance depending on the altitude, it was decided to use only a single 28 cm diameter by 22 cm pitch propellers. One propeller size is chosen in order to keep the setup of the UAV simple and compact, but at the expense of a 2% shorter endurance.

Figure 8.28: CAMcarbon Light Prop propeller used for horizontal flight

Motor selection horizontal flight
The motor was selected based on several parameters. These include mass, motor temperature, no-load current, internal resistance and Kv value.
The mass should be as low as possible since extra mass influences the performance negatively. The temperature determined, was the temperature at maximum power of the motor. This temperature was also kept as low as possible. Motors that produce temperatures above the 80 °C were discarded, since higher temperatures will damage the motor [37].
The no-load current and internal resistance give an indication of the efficiency of the motor. These parameters should be as low as possible, since they account for some of the losses in a brushless motor [38]. These losses cause a difference between the input and output power. Thus for the best efficiency, the losses need to be minimised.
The final parameter is the Kv value. This value is a motor constant that determines the rotational speed and torque produced by a certain voltage and current. This value had to be as such, that the current in the motor stays under the maximum current for the rotational speeds and torque required by the propeller.

A motor performance graph was produced by xcopterCalc [33] giving the efficiency for current. The overall form of these graphs is shown in Figure 8.29. Here it can be seen that from a certain current till the maximum current, the motor performs with an efficiency close to the maximum efficiency. The efficiency range is shown in Figure 8.29 by the two vertical lines.

[35] URL:http://www.fpv24.com/de/aero-naut/aero-naut-camcarbon-power-prop-luftschraube-12x6-8241 [cited June 18, 2016]
[36] URL:http://www.fpv24.com/de/aero-naut/aero-naut-camcarbon-power-prop-luftschraube-12x6-8241 [cited June 18, 2016]
[37] URL:http://www.rccaraction.com/blog/2013/07/05/how-to-get-the-most-out-of-your-brushless-motor/ [cited June 26, 2016]
[38] URL:http://www.radiocontrolinfo.com/brushless-motor-efficiency/ [cited 26 June 2016]

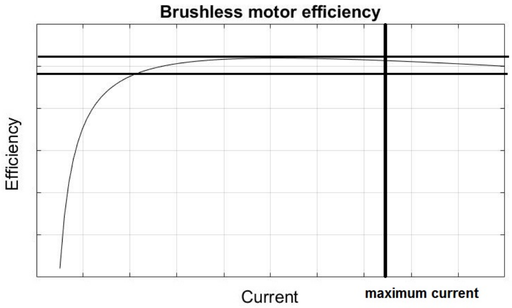

Figure 8.29: A generic performance graph for brushless motors

It was chosen to use the Turnigy 2632-1500[39] brushless outrunner motor, together with the MPI ACC347 Speed 400 Gear box[31] running on a gear ratio of 2.5:1. This gear ratio ensured that the motor can run at a sufficiently high rotational speed, while the propeller can rotate slower at a more efficient rotational speed. The Turnigy 2632-1500 has a mass of 52 g, and a Kv of 1500. Using a Kv of 1500 and a 2.5:1 gearbox instead of a 600 Kv motor is more efficient, as motors with a Kv value of 600 are designed for higher power, and become less efficient if only a faction of this power is used. So, using a smaller motor at a higher rotational speed has a higher efficiency -up to 78.1% during horizontal flight-, because of which the operational temperature of the motor for horizontal flight can be kept below 70 $°C$ for an ambient operating temperature of 45 $°C$. The motor and gearbox used for forward flight can be seen in Figures 8.30 [40] and 8.31 [41], respectively.

Figure 8.30: Turnigy 2632-1500 brushless outrunner motor used for horizontal flight

Figure 8.31: MPI ACC347 Speed 400 Gear box used for horizontal flight, attached to a generic brushed motor

Propeller selection vertical flight

Three sets of propellers were needed for the UAV. These sets were needed to provide a thrust-to-weight ratio of at least 1.5 for different altitudes. The larger the propeller diameter, the more efficient the UAV can hover [42], so it would be ideal to have the largest propellers possible. However larger propellers lead to a design that was less easy to transport in a backpack, because large propellers require a large vertical stabiliser. It was found that a vertical stabiliser with a span of 40 cm would be the largest that easily fits a backpack. A vertical stabiliser of this size is enough for propellers of 28 cm diameter, while still leaving enough space for the body. Thus the maximum propeller diameter of 28 cm (11 $in.$) was determined as diameter for all three sets. One propeller can be seen in Figure 8.33.

The propeller sets vary in pitch, which indicates the amount of twist given to the propeller, as can be seen in Figure 8.32. The first set has a pitch of 5.0 cm (2 $in.$). These propellers provide enough thrust for both configurations up to an altitude of 2500 m. At altitudes between 2500 and 3500 m another set is used, which has a pitch of 7.6 cm (3 $in.$). And between 3500 and 4500 m the third set is used, with a pitch of 12.7 cm (5 $in.$).

[39] URL:`http://rcsearch.info/hobbyking/i8503/` [cited 18 June 2016]
[40] URL:`http://www.hobbyking.com/hobbyking/store/__8503__Turnigy_2632_Brushless_Motor_1500kv.html` [cited 26 June 2016]
[41] URL:`http://truerc.com/index.php?main_page=product_info&cPath=33&products_id=449&zenid=iappgvva94rrm0uclug8lak614` [cited 26 June 2016]
[42] URL:`http://www.krossblade.com/different-rotors-for-different-purposes/` [cited 26 June 2016]

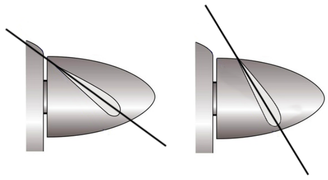

Figure 8.32: Propeller pitch with high pitch on the left and low pitch on the right

The pitch was chosen to give the UAV a thrust-to-weight ratio of at least 1.5 and to maximise endurance. Increasing pitch increases the angle of attack seen by the propeller airfoil. This increases the lift produced by the propeller, which is the thrust. However, the propeller drag also increases, which increases the torque and the power needed from the motor. It was found that at the maximum altitude of 4500 m a pitch of at least 12.7 cm was needed. But at lower altitudes it was found that a lower pitch would increase flight time. It was also found that at lower altitudes with a higher density the torque required was too high, leading to a current that exceeds the maximum current of the motor. Thus the pitch was decreased for lower altitudes resulting in 2, 3 and 5 in. propellers for increasing altitude ranges.

Figure 8.33: Foldable propeller used for vertical flight

Figure 8.34: Turnigy 2836-1000[2] brushless outrunner motor used for vertical flight

Motor selection vertical flight
The motor that is used for hovering is the Turningy 2836-1000[2] brushless outrunner motor. This motor has a mass of 78 g [43], which can be seen in Figure 8.34[44].

The motor was selected with the same method as for horizontal flight, based on the mass, motor temperature, no-load current, internal resistance and Kv value. The maximum temperature of the Turingy 2836-1000[2] is 62°C at an operating ambient temperature of 45 $°C$. It was also determined that a Kv value of 1000 $rpmV^{-1}$ was the most optimal for the design. The lower Kv value of the motors for vertical flight compared to the motor for horizontal flight is explained by the higher power delivered to the motors for vertical flight. This resulted in the Turnigy 2836-1000[2], which operates close to the maximum efficiency, while never exceeding the maximum current for all operating conditions and configuration weights. At most the efficiency is 3% lower than the maximum efficiency of 84.3%.

8.8.2. Tailsitter performance
The performance of the tailsitter is structured according to the mission profile of the tailsitter as shown in Figure 8.35 and Table 8.11.

[43] URL:`http://www.hobbyking.com/hobbyking/store/__8139__Turnigy2836_Brushless_Outrunner_1000kv.html` [cited 26 June 2016]
[44] URL:`http://www.jokerhobby.com/turnigy-2836-1000kv-brushless-outrunner.htm`

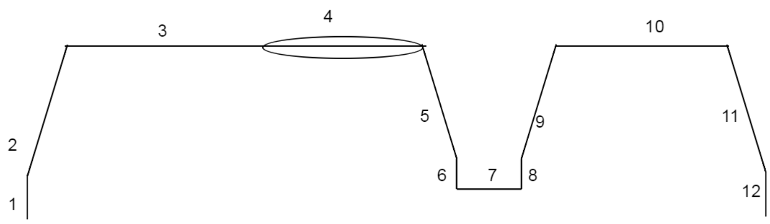

Figure 8.35: Remote mapping and toxin detection mission profile in tailsitter configuration

Table 8.11: Remote mapping mission profile ID's in tailsitter configuration

ID in profile	Flight mode
1	Vertical take-off/climb
2	Climb with wings
3	Forward flight to accident site
4	Forward flight at accident site (mapping)
5	Descend with wings
6	Vertical descend
7	Hover
8	Vertical climb
9	Climb with wings
10	Forward flight from accident site
11	Descend with wings
12	Vertical landing/descend

Vertical take-off and climb

Vertical climb is used for the UAV to reach the desired height and to perform vertical take-off. For the payload the maximum height for detailed mapping was determined to be 15 m, as specified in Section 8.1. Thus the calculations were made for a climb of 15 m. The climb velocity is 3 ms^{-1}. This resulted in a energy usage for different altitudes, which can be seen in Figure 8.36. The energy usage for climb to 15 m is between the 0.7% and 1.2% of the energy available for propulsion.

The velocity of 3 ms^{-1} was chosen since this gives the performance needed, because the UAV can climb to the required height of 15 m in a relatively short time of 5 s, without taking acceleration and deceleration into account. At this climb velocity also little of the electrical energy is used. The performance for this velocity was determined accurately, as for climb velocities above 7 ms^{-1} the propeller characteristics become harder to predict with the models used. In Figure 8.37 it can be seen that the energy needed to climb 30 m decreases with increasing velocity. This means it would be most efficient to climb at the highest possible velocity. However, 3 ms^{-1} was chosen to account for possible gusts. It was calculated that the UAV can climb with at least 7 ms^{-1}, so when climbing the UAV can at least withstand vertical wind of at least 4 ms^{-1}. Thus it was also assumed that the UAV can withstand gusts. Furthermore, no maximum climb speed was determined, since at these low velocities the thrust needed is always under the maximum thrust.

Thrust calculations for vertical climb

The calculation of the vertical climb performance is based on the helicopter vertical climb performance method from *Helicopter Performance, Stability, and Control*[39]. However the induced velocity in climb that is needed for the calculations could not be determined, since the exact propeller geometry was not found. Thus it was decided to simplify the method. The thrust was calculated by the sum of weight and drag. This simplified method neglects the influence of the induced velocity in the wake. The induced velocity was neglected, because it was found that the drag force is much smaller than the weight for the velocity range the UAV is operating in, thus the influence of this assumption would have a negligible effect on the required thrust. The drag coefficient (C_D) is determined using XFLR5, as described in Section 8.5.2.

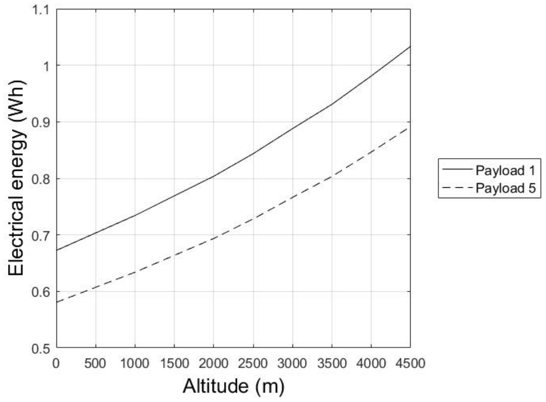

Figure 8.36: The energy needed to climb at 3 ms^{-1} to 15 m for different altitudes for the tailsitter

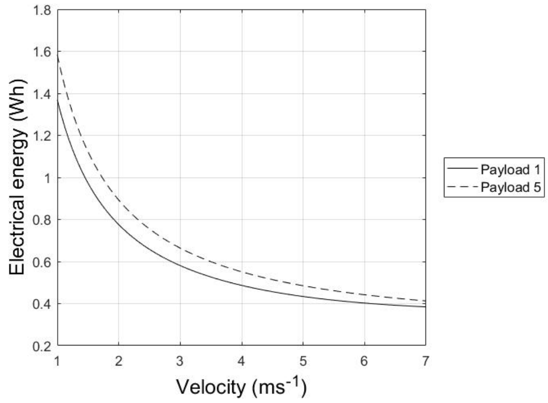

Figure 8.37: The energy needed to climb 15 m for different climb velocities at sea level for the tailsitter

Power calculations for vertical climb

The power consists of the power needed to provide the thrust, and an extra term ΔP is needed to account for the climbing motion. The power to provide the required thrust was calculated using the thrust and power coefficients of the propeller. These coefficients were calculated for static conditions from the hovering performance results using Equations 8.4 and 8.5. Note that the rotational speed Ω is in rps. However, if the propeller experiences an inflow velocity, the coefficients change. The effect of this was examined by analysing data from the UIUC Propeller Database [45]. This database provides experimental data on a number of propellers, the data of an APC Free Flight 4.2x4 propeller is used in this section as an example. The data is presented using the velocity coefficient (J), which is calculated using Equation 8.6.

$$C_T = \frac{T}{\rho \Omega^2 d^4} \tag{8.4}$$

$$C_P = \frac{P}{\rho \Omega^3 d^5} \tag{8.5}$$

$$J = \frac{V_c}{\Omega d} \tag{8.6}$$

Data for an APC Free Flight 4.2x4 propeller at 3000 rpm is presented in Figure 8.38. It can be seen that the thrust and power coefficients are almost equal to the static coefficients for low velocity coefficients. A similar behavior was found from analysis of other propellers.

With the data from the UIUC Propeller Database the influence of the rotational speed was also investigated. In Figure 8.39 data can again be found for an APC Free Flight 4.2x4 propeller for static conditions. It can be seen that the thrust and power coefficients are almost constant for different rotational speeds. Only at lower rotational speeds this does not seem to be the case. A similar behavior was found from analysis of other propellers. Thus the thrust and power coefficient were assumed to be independent from the rotational speed. It was determined that for the operating climb speeds of UAV, the velocity coefficient does not exceed 0.2, which corresponds with a velocity of 7 ms^{-1}. Thus the static thrust and power coefficients can be used. To account for the uncertainty with higher velocities the thrust coefficient used for vertical climb was decreased linearly with the velocity coefficient and the power coefficient was increased linearly. The static thrust coefficient was decreased linearly with 0% to 15% for $J = 0$ to $J = 0.2$. While the static power coefficient was linearly increased from 0% for 15%. These values give a very conservative estimate for the coefficients, based on the behaviour of C_T and C_P observed in the data from the UIUC Propeller Database.

Finally the extra power ΔP for vertical climb had been calculated. The calculation was based on equations from the helicopter vertical climb performance method from *Helicopter Performance, Stability, and Control*[39]. It was again assumed that the induced velocity is negligible. These resulted in Equation 8.7.

[45]URL:`http://m-selig.ae.illinois.edu/props/propDB.html` [cited 26 June 2016]

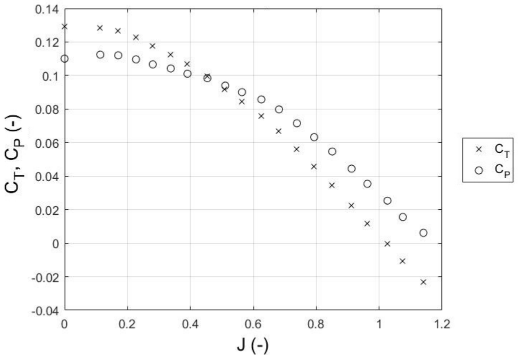

Figure 8.38: Change of C_T and C_P with velocity coefficient

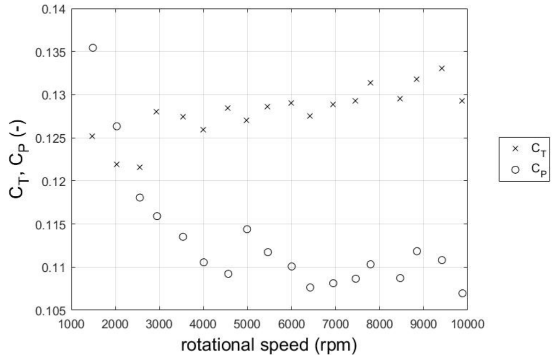

Figure 8.39: Change of C_T and C_P with rotational speed

$$\Delta P = WV_c + DV_c \tag{8.7}$$

The power calculated here is the mechanical power needed for the propeller. The electrical power is higher, since the motor also has a certain efficiency. This efficiency was assumed to be the same as the efficiency in hover, which was a result from the hovering performance calculation, described in Section 8.8.2.

Transition to horizontal flight

To calculate whether the transition is possible, a tool was created, in which the UAV performs an arc shaped movement by means of simple flight mechanics. It is supposed that, before the manoeuvre starts, the UAV is hovering perfectly meaning that it is not moving in any direction. In order to turn to the right, the push motor provides full thrust, the left motors provide full thrust and the right motors provide 0.1 N less thrust than the left motors. This gives the UAV a moment, which causes it to turn 90° in approximately 4 s. This manoeuvre is shown in Figure 8.40 [22] as 'optimal path'.

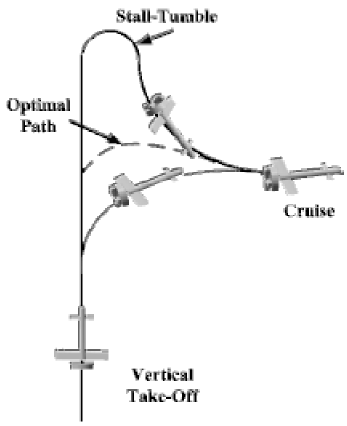

Figure 8.40: Transition according to the optimal path method

By computing the acceleration in both x- and z-direction, the speed and position follow by time integration. The acceleration comes first of all from the propellers using, but is also dependent on the drag and is for the z-direction also dependent on gravitational acceleration.

Figures 8.41, 8.42 and 8.43 show the output of the speed against time in x- and y-direction and the path during its manoeuvre respectively. It is clear that the UAV, after it has performed the complete manoeuvre, has established a speed of 16.2 ms^{-1}, which is higher than the stall speed of 12 ms^{-1}. This means it is able to fly horizontally after the transition, so the transition is successful.

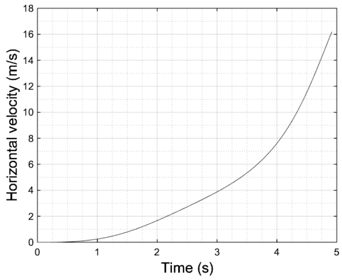

Figure 8.41: Horizontal v-t diagram transition

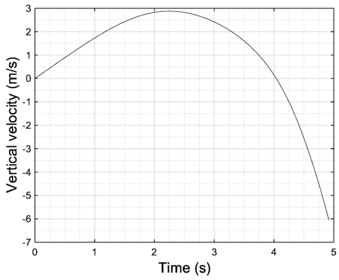

Figure 8.42: Vertical v-t diagram transition

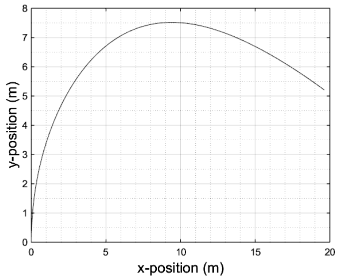

Figure 8.43: Position diagram transition

The reason for the drop in the speed in y-direction is because of the propellers that do not provide sufficient lift to accelerate the UAV at angles larger than 27.6°. The drag in y-direction is increasing with increasing angle, as the frontal area in that direction increases. For the x-direction it is vice versa, which is why the plot has an exponential nature. The drop in speed in y-direction is the reason that also the path encounters a drop in y-direction.
Although the method comes with some promising results, there are some limitations. Due to the lack of resources about the behavior of the the lift and drag during the manoeuvre, those were not fully taken into account. Only the drag due to the frontal area has been considered. Furthermore, in order to check whether the transition works out, it was only taken into account that final speed in horizontal direction should be higher than the stall speed. However, the UAV can already fly at higher angle of attack by the created lift.

Climb with wings
As it is less energy efficient for the tailsitter configuration to climb till the cruise altitude on vertical climb, it is possible to transition and then climb to the cruise altitude on the horizontal flight propeller. At 0 m altitude, the UAV has a maximum climb rate of 3.3 ms^{-1} in tailsitter configuration and a maximum climbing rate of 4.8 ms^{-1} in the flying wing configuration, as seen in Figure 8.44. From the figure, it can be seen that at an altitude of 4500 m, the UAV has a maximum climb rate of 2.4 ms^{-1} in tailsitter configuration, and a maximum climb rate of 3.3 ms^{-1} in flying wing configuration.

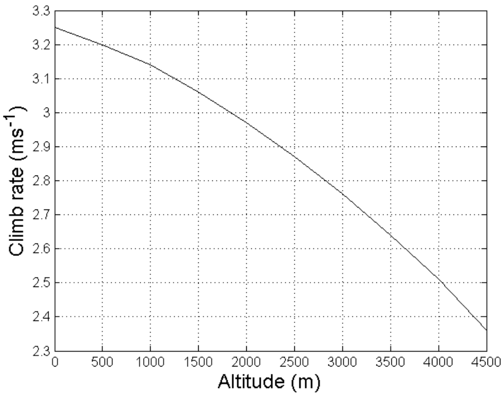

Figure 8.44: Rate of climb of both the tailsitter and flying wing for different altitudes

These results were obtained with MotoCalc 8 [2] which is explained in the following section, Forward flight, using the propeller and motor sized for forward flight. By analysing the climb performance for different climb rates at different heights, it was concluded that a climb rate close to 3 ms^{-1} was the most energy efficient climb rate to gain height. This means that the height per unit energy was maximised. When a climb speed of 3 ms^{-1} cannot be reached, the maximum climb rate was the most efficient.

Forward flight
After transitioning, the tailsitter is capable of flying like a flying wing. For this configuration it only needs the

pusher propeller at the back and the four propellers for hovering are folded in such a way that they cause the least amount of drag. The propeller tips are folded towards the fins which is done by diminishing thrust and by the drag the propeller blades experience when they are open. With the propellers folded, the UAV experiences a lot less drag, which extends the endurance of the UAV. The endurance and range of the UAV for the tailsitter with payload configuration 5 can be seen in Figure 8.45 and 8.46.
It can be seen that the endurance decreases from 77.2 min at 0 m altitude to 62.6 min at 4500 m altitude. This is due to the air becoming thinner, and thus, the UAV needs to deliver more power to remain airborne, draining the battery more quickly. On the other hand, the range increases only a little bit from 74.6 km at 0 m altitude to 75.9 km at 4500 m altitude. This is because the optimal velocity increases -due to the thinner air, the UAV needs to fly faster to deliver enough lift- faster than endurance decreases with increasing altitude.

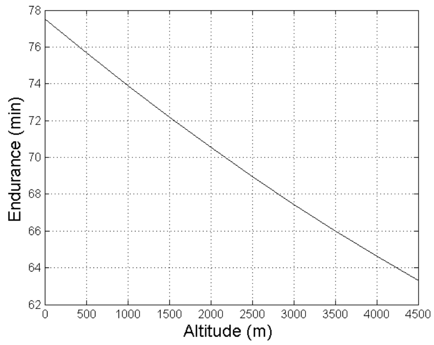

Figure 8.45: Endurance of the tailsitter for different altitudes

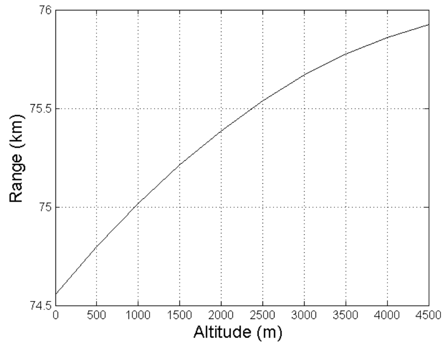

Figure 8.46: Range of the tailsitter for different altitudes

The results were found with MotoCalc [2]. With this tool, the horizontal flying performance of a UAV can be estimated, with motor, drive system -including propeller, gears and ducted fans-, ESC and battery as input. By using general UAV characteristics and parameters such as empty weight, wing area, desired characteristics -from sailplane to aerobatic 3D aeroplane- and general aerofoil shape, the tool suggests a propulsion setup, which is used as baseline for further optimisation.
The optimisation itself is done by letting the tool analyse combinations of ranges of batteries and/or propellers and gears. From these analyses, the most promising combinations with the largest range are verified further, after which the best combination was chosen as propulsion setup for horizontal flight.

Descent with wings
When starting the descend in order to land, it is more efficient to have a certain glide slope towards the landing or hovering spot before the transition is done. This is due to the fact that gliding takes less energy and a longer distance can be bridged. Using MotoCalc, it was found that the zero throttle rate of descent increases from 1.39 to 1.74 ms^{-1} with altitude for the tailsitter configuration as seen in Table 8.47.

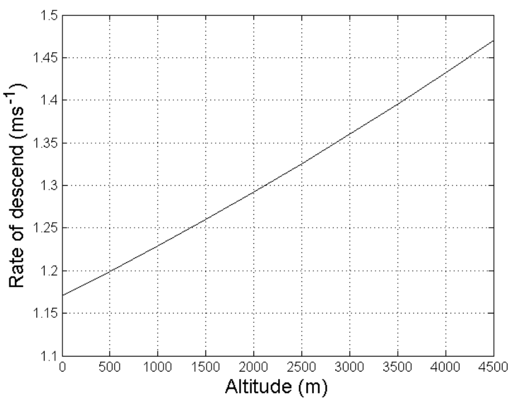

Figure 8.47: Zero throttle rate of descent of the tailsitter configuration

Transition to vertical flight
The transition from forward flight back to vertical flight to make sure that the UAV is able to land, is very important when the tailsitter configuration is used. The transition back is done with a strong pull up 'pull-up to vertical' after which the UAV ends in an upright position as can be seen in Figure 8.48 and can land as explained in Vertical descent performance.

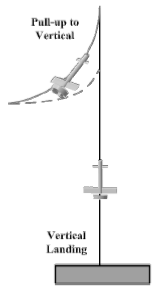

Figure 8.48: Pull-up to vertical maneouver [22]

Vertical descent and landing
When transition to vertical flight is performed and the UAV needs to descend, this can be done by reducing throttle through which the thrust-to-weight ratio drops below 1.0 and the thrust thus no longer can support the weight. The UAV then accelerates downwards until the height at which it needs to hover, where the throttle is increased again. When it needs to land, it is descending until it is just above the ground at the same throttle setting. Then, to reduce the landing forces, the throttle is increased slightly so that the acceleration becomes less and the touch down on the landing rods is softer.

Hovering
Hovering is necessary for the UAV in order to do toxin detection and to map places that are hard to reach. Hovering also is a good indication of the overall performance for the tailsitter configuration. The hovering performance is calculated using the tool xcopterCalc. The UAV has a maximum hovering endurance of 16.1 min in the tailsitter configuration. This is with the lowest payload mass, which gave a total mass of 2.21 kg. This is for payload configuration 1. However the performance decreases with increasing altitude. This can be seen in Figure 8.49. As can be seen, the endurance is always at least 8.5 min for the tailsitter.

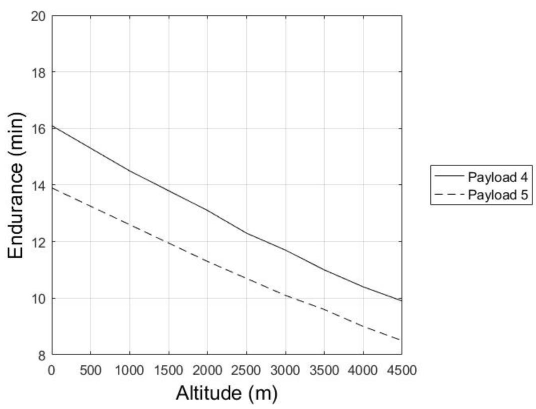

Figure 8.49: The hovering flight endurance for different altitudes for the tailsitter

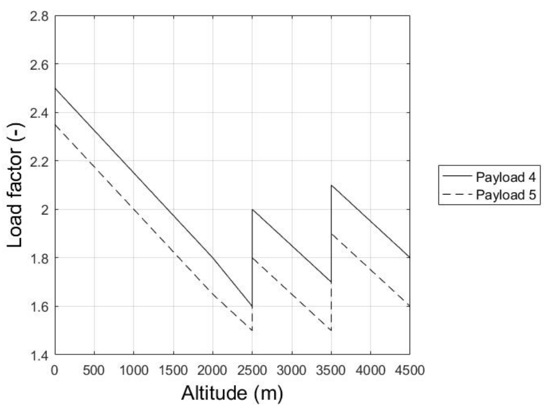

Figure 8.50: The load factor for different altitudes for the tailstitter

Also the load factor was determined, which was assumed to be equal to the thrust-to-weight ratio. The thrust-to-weight was based on the maximum thrust the propulsion system can provide. The heaviest option is used which gives the lowest load factors. The results can be seen in Figure 8.50. Here it can be seen that the maximum load factor is always above 1.5, which is important for manoeuvring and stability[46]. The highest load factor possible is 2.5, this maximum load factor was used for structural design.

The hovering performance of the UAV was calculated using the tool xcopterCalc from eCalc. This tool consists of a database of electric motors. The performance analysis is based on a 8000 mAh battery, as explained in Section 8.9.3, of which 7000 mAh can be used for propulsion with a maximum depth of discharge of 80%.

The tool xcopterCalc calculates several parameters, including the current at maximum power, thrust-to-weight ratio, electrical power during hover, mechanical power during hover, total efficiency during hover, rotational speed during hover and motor temperature at maximum throttle. These parameters were used for further calculations and analysis.

8.8.3. Flying wing performance

The tailsitter configuration will not always be used as explained in Chapter 4 and especially for long endurance the flying wing can be used. The main difference between the tailsitter and the flying wing is the take-off and landing as the flying wing cannot perform VTOL. The flying wing mission profile can be found in Section 5.2. The performance values for flight modes 3, 4 and 5 from the tailsitter are updated as the values differ due to the change in weight.

Launch of flying wing

For the flying wing, there is no vertical take-off possible as the fins with motors are detached in this configuration and replaced by small fins on the top side of the body. The UAV is launched with a bungee cord construction to reach a speed of 15% above the stall speed when it lifts off. From this point, the flying wing can continue flight with its own power and lift.
For this launch system a tent peg is needed, to which the bungee cord can be attached. The bungee cord used is the 8 mm Silicon Rubber Bungee Hi-Start Cord which is 10 m in length[47]. The cord has to be stretched 8.6 m. With this length, the cord provides enough energy and force to pull the flying wing and accelerate it to at least 1.15 times the stall speed, which is 10 ms^{-1}, so that it can fly by itself [36]. With an average Young's modulus of 1.0 MPa [48], a cord area of 30.6 mm^2 and an initial length of 10 m, the spring constant is 3.1 Nm^{-1}. As the initial velocity of the UAV is zero and the elongation when the UAV lets loose is zero, a simple energy balance results in an elongation of 8.6 m needed for take-off. However, it is preferred to accelerate the flying wing even more, thus it is recommended to stretch the cord with 11.3 m so that it achieves 1.5 times the stall speed.

Climb with wings

The rate of climb for the flying wing is calculated in a similar way as for the tailsitter, however due to the lower weight, the climb rate ranges from 4.8 to 4 ms^{-1} with increasing altitude as is shown in Figure 8.51.

[46] URL:https://www.kdedirect.com/blogs/news/90453763-upgrading-quadcopter-motors-for-aerial-photography [cited 26 June 2016]
[47] URL:http://www.hobbyking.com/hobbyking/store/__10609__HobbyKing_174_8mm_Silicon_Rubber_Bungee_Hi_Start_Cord.html [cited 15 June 2016]
[48] URL:http://www.azom.com/properties.aspx?ArticleID=920 [cited 15 June 2016]

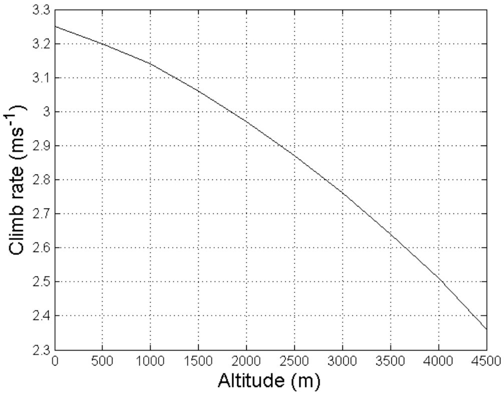

Figure 8.51: Rate of climb of the flying wing for different altitudes

Forward flight
The forward flight performance is determined in the same way for the flying wing as for the tailsitter configuration. However, the flying wing has a lower weight due to the change from fins to small fins and dropping the hovering motors and propellers. The flying wing is analysed with payload configuration 2 and the endurance and range results are showed in Figure 8.52 and 8.53. Like with the tailsitter configuration, the endurance decreases with altitude. For the flying wing, this decrease is from 122 min at 0 m altitude to 105 min at 4500 m altitude. The endurance decreases less than the endurance of the tailsitter, which is due to the lower weight of the flying wing. The range increases from 115 km at sea level to 123 km at 4500 m altitude. As explained before, this is because the optimal velocity increases faster than endurance decreases with increasing altitude.

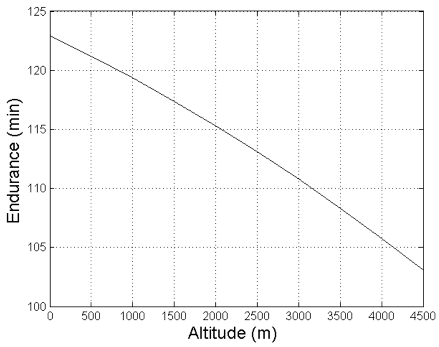

Figure 8.52: Endurance of the flying wing for different altitudes

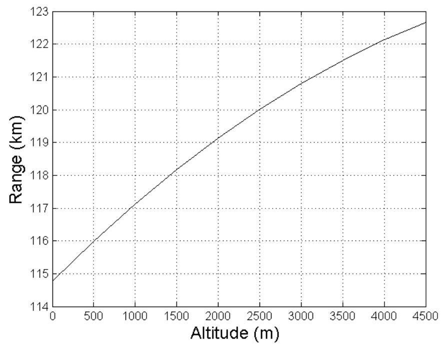

Figure 8.53: Range of the flying wing for different altitudes

Descent with wings
The rate of descent for the flying wing is calculated in the same manner as for the tailsitter, however due to its lower weight, the descent rate ranges from 1.2 to 1.5 ms^{-1} as is shown in Figure 8.54.

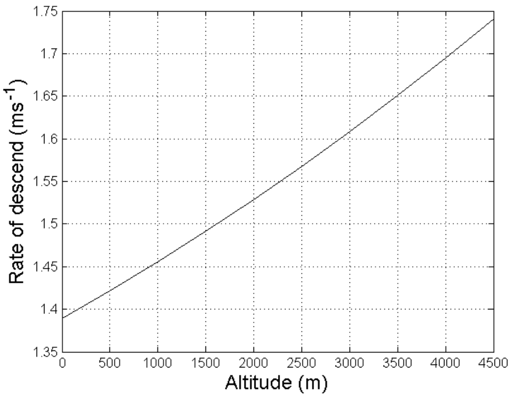

Figure 8.54: Zero throttle rate of descent of the flying wing configuration

Landing in flying wing configuration

As the flying wing has no option to land vertically, another landing method is applied, namely reverse thrust landing. The advantage is that the area needed for this landing is small and can be planned accurately, within a 10 m radius.[49] During this maneuver, the LiDAR measures the distance above the ground which gets smaller as long as the flying wing keeps descending. Then at a height of 5 m, the thrust is reversed so that the UAV slows down very quickly. From here it is safe to start a steep descend as it is low enough to not generate high loads during descent or to hit an investigator when it would further descent at a shallow rate. The lift cannot support the weight then anymore, through which the flying wing starts to descend. The concern for the propellers getting damaged during touch down is not needed as the forward velocity of the UAV is low enough for the propeller not to get caught in the ground[50].

The payload fairing is a weak point as the flying wing lands on top of that, however, it is a plastic casing reinforced with a rib which is a strong structure and it thus survives the impact and does not have problems with scratches as is described in Section 8.7.4.

However, if the longer endurance of the flying wing is not needed, the tailsitter with the payload fairing from the flying wing can be deployed and used as well.

8.8.4. Quadcopter performance

As with the flying wing, the tailsitter sometimes is not the most optimal configuration and therefore it can also be changed to a quadcopter for detailed mapping. In this case, the wings are taken off, so flight modes 1, 7 and 8 are disregarded and a new mode is added as the quadcopter needs to perform forward hovering flight. The flight modes that were included for the tailsitter already, are updated with new values. The quadcopter mission profile can be found in Section 5.5.

Vertical take-off and climb

The quadcopter configuration uses a climb velocity of 3 ms^{-1}. As can be seen in Figures 8.55 and 8.56 in the quadcopter configuration the energy needed to climb 15 m decreases with velocity. Using the same considerations as for the tailsitter, described in Section 8.8.2, a climb velocity of 3 ms^{-1} was determined, since it also leaves room for wind resistance. With 3 ms^{-1} the energy needed to climb 15 m is between the 0.7 and 1.2% of the energy available for propulsion.

Hovering

The minimum and maximum endurance at different altitudes can be found in Figure 8.57. The maximum endurance in hovering for the quadcopter configuration is different due to the fact that the weight is lower than for the tailsitter configuration. The minimum endurance is 11 min for the heaviest payload option resulting in a weight of 2.04 kg and its maximum endurance is 18.7 min for its lowest weight of 1.99 kg. Furthermore the load factors for different altitudes can be seen in Figure 8.58. As can be seen the load factor, and thus

[49] URL: `https://www.sensefly.com/support/faq.html` [cited 15 June 2016]
[50] URL:`https://www.youtube.com/watch?v=UyzuUYA2vHg` [cited 15 June 2016]

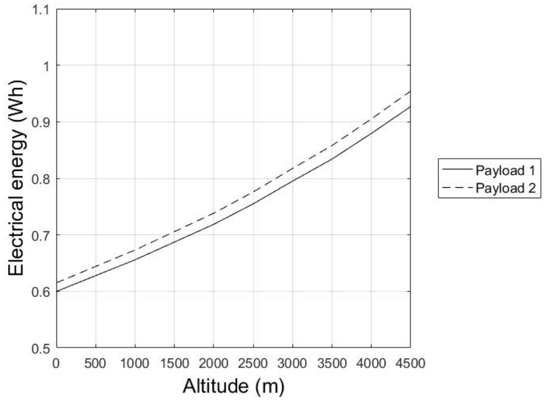

Figure 8.55: The energy needed to climb at 3 ms^{-1} to 15 m for different altitudes for the quadcopter

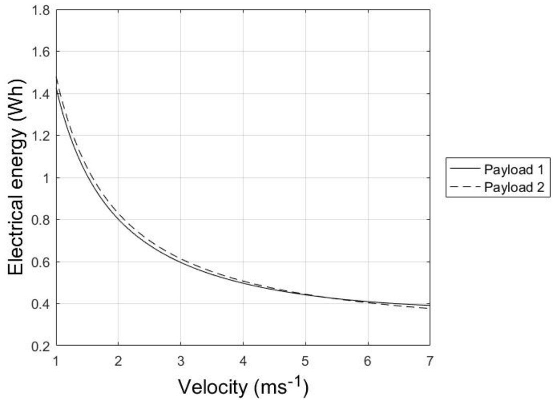

Figure 8.56: The energy needed to climb 15 m for different climb velocities at sea level for the quadcopter

the thrust-to-weight ratio, for the quadcopter is also always higher than 1.5. The maximum load factor is 2.8, which is important for structural design, as explained in Section 8.7.1.

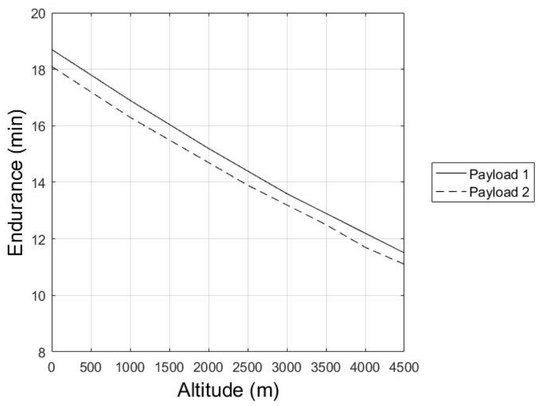

Figure 8.57: The hovering flight endurance for different altitudes for the quadcopter

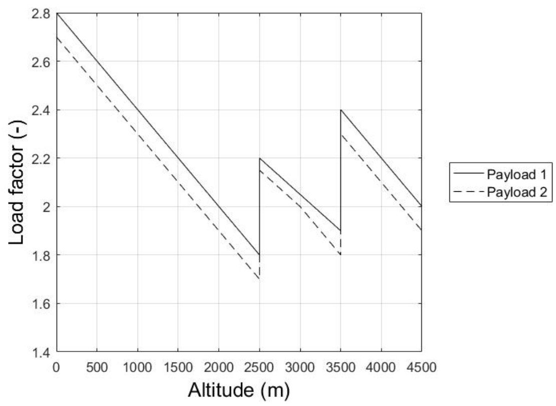

Figure 8.58: The load factor for different altitudes for the quadcopter

Forward hovering flight

In order to map a certain area, the UAV in the quadcopter configuration has to be able to perform forward hovering flight. Forward hovering flight can also be performed in the tailsitter configuration, but this is not needed to perform its mission. Thus the performance was only calculated for the quadcopter configuration. The UAV flies forward with the surface of the wing facing the velocity direction, which can be seen in Figure 8.59.

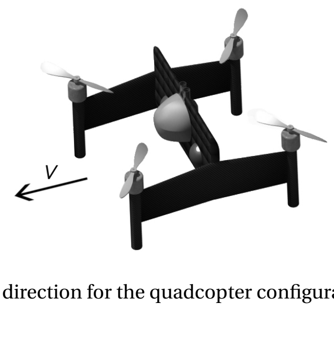

Figure 8.59: The flying direction for the quadcopter configuration in forward flight

In Figure 8.60 the range in forward hovering flight for different altitudes can be seen. These calculations are based on the battery specifications as explained in Section 8.9.3. In Figure 8.60 it can be seen that there is a maximum range for each altitude. The maximum range at 0 m altitude is 7.8 km at a velocity of 12 ms^{-1}. It can be seen that the maximum range at higher altitudes is achieved with higher velocities.

However, these velocities are too high for all payload cameras, as described in Section 8.1, so the range during a mission is reduced. For payload configuration 1 the range is 3.7 km at 3.7 ms^{-1}. In Figure 8.61 it can be seen that the corresponding tilt angle is 2.6°, which is still acceptable for this payload. The range for payload configuration 2 is 1.1 km at a velocity of 1.0 ms^{-1}. The corresponding tilt angle is 0.2°, which is also acceptable for the payload.

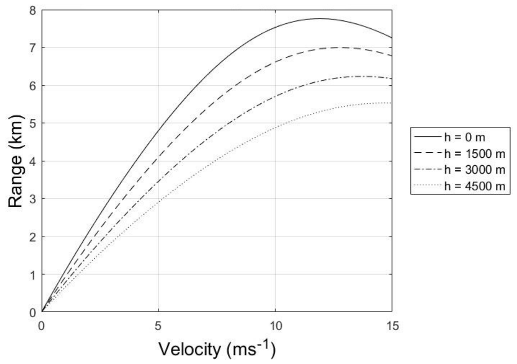

Figure 8.60: Range for forward hovering flight for different velocities and altitudes

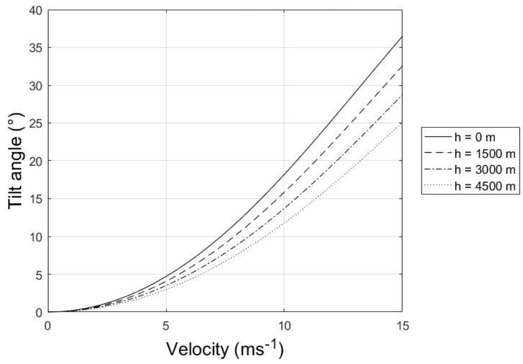

Figure 8.61: Tilt angle for forward hovering flight for different velocities and altitudes

Thrust calculation for forward hovering flight

The thrust required for forward hovering is calculated using a force equilibrium. This is shown in Figure 8.62. For forward flight the UAV has to tilt with a certain tilt angle γ. This leads to a force equilibrium where for a certain forward velocity V_f the thrust has to be equal to the weight and drag. Since the aerodynamic shape of the UAV in forward flight is basically a flat plate, the drag coefficient (C_D) thus is 1.2 [17].

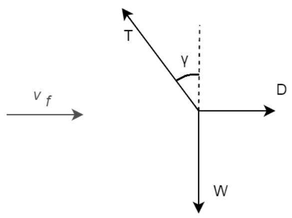

Figure 8.62: Forces acting on the UAV in forward hovering flight

Power calculation for forward hovering flight

The power calculated in a similar way as the power for vertical climb, described in Section 8.8.2. For forward hovering the power also consists of the power to provide the thrust and an extra term ΔP [39]. The same assumptions and corrections were applied to this calculation as for vertical climb. This results in Equation 8.8. The power was also corrected with the motor efficiency. For forward hovering flight the efficiency was assumed to be the same as for hovering flight.

$$\Delta P = DV_f \tag{8.8}$$

Vertical descent and landing

Vertical descend and landing for the quadcopter is the same as for the tailsitter, where thrust is decreased, so the thrust cannot support the weight of the UAV anymore.

Wind resistance
Using the same calculations as used for forward hovering flight the wind resistance of the UAV was analysed. To do this, the thrust-to-weight needed was calculated for a forward velocity of 15 ms^{-1}, because it is the maximum velocity where the propeller coefficients could be determined with certainty. The results of these calculations can be seen in Figure 8.63. It can be seen that the thrust-to-weight needed for a forward velocity of 15 ms^{-1} is always lower than 1.25. This is much lower than the 1.5 minimum thrust-to-weight provided by the propulsion system. Thus the UAV can resist a headwind of 15 ms^{-1} when hovering. And with the thrust-to-weight lower than the maximum, the UAV can also still manoeuvre and resist some gusts.

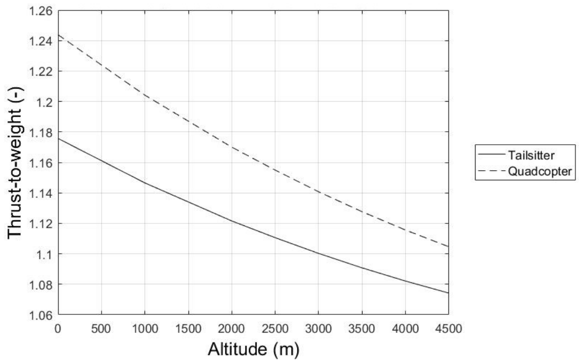

Figure 8.63: The thrust-to-weight ratio at a forward velocity of 15 ms^{-1} for different altitudes

Concluding performance and propulsion
The propulsion subsystem consists of one 28 cm diameter, 22 cm pitch, pusher propeller that provides the thrust in forward flight, which is connected to a gear box with a gear ratio of 2.5:1 and a motor with an efficiency of 78%.
For vertical flight, 3 propellers were chosen with a diameter of 28 cm and a pitch of 5, 7.6 and 12.7 cm to be able to provide sufficient thrust for the 0 to 2500 m, 2500 to 3500 m and 3500 to 4500 m range altitudes respectively. The most important performance for the tailsitter is that it is able to hover for 16.1 min and fly forward 77 min, it can also perform a vertical take-off and landing. For the flying wing this is different, this configuration is launched with a bungee cord and lands with applying reverse thrust and a steep descent belly landing for which it needs an area of 10 m radius at least. It has a forward flight performance of 122 min. Lastly, the quadcopter was presented which has the vertical take-off and landing, but not the forward flight performance. The endurance in hovering however is better than that from the tailsitter, it is 18.7 min with a forward hovering endurance of 16.7 min in which a distance of 3.7 km can be mapped.

8.9. Electrical system
In every vehicle, all the electrical components need to have an electrical connection, either being a power cable or signal wire, in order to communicate with or power each other. As not every component can be connected directly to each other, there is need for other electrical components such as power converters in order to regulate the three power circuits and digital converters. All these components are connected to the autopilot, the Lisa/MX, by means of wires. Next to that, all the electric components have to be powered, which calls for an energy source, which is elaborated on in Section 8.9.3. Taking care of this all is the responsibility of the electrical subsystem.

First of all, one of the main tasks of the electrical subsystem is to distribute power to all the subsystems and electrical components. This distribution of power can be divided into two categories: high voltage wiring, which runs at the same voltage as the battery, which is 14.8 V, and low voltage wiring, which runs at 5 V. This latter voltage was chosen as most of the electrical components run on 5 V, and the few components that run on 3.3 V can be powered by the autopilot itself. The high voltage wiring only runs from the battery to the propulsion system, as these need the most power. The low voltage wiring is distributed from a 5 V regulator able to deliver at least 1.98 A of current, which is the peak current draw for all missions[45].
Next to that, the wiring also takes care of the data communication and signals in between different electrical components. This is done by dividing all the communication of the electrical components as efficiently as

possible among all the different busses available on the Lisa/MX, as documented on the Paparazzi website[51], which is further elaborated on in Section 8.9.1. A general layout of all the connections can be seen in the hardware and software block diagram in Figure 8.64, in this figure, the kind of data going from one subsystem to another is labelled next to the dotted lines.

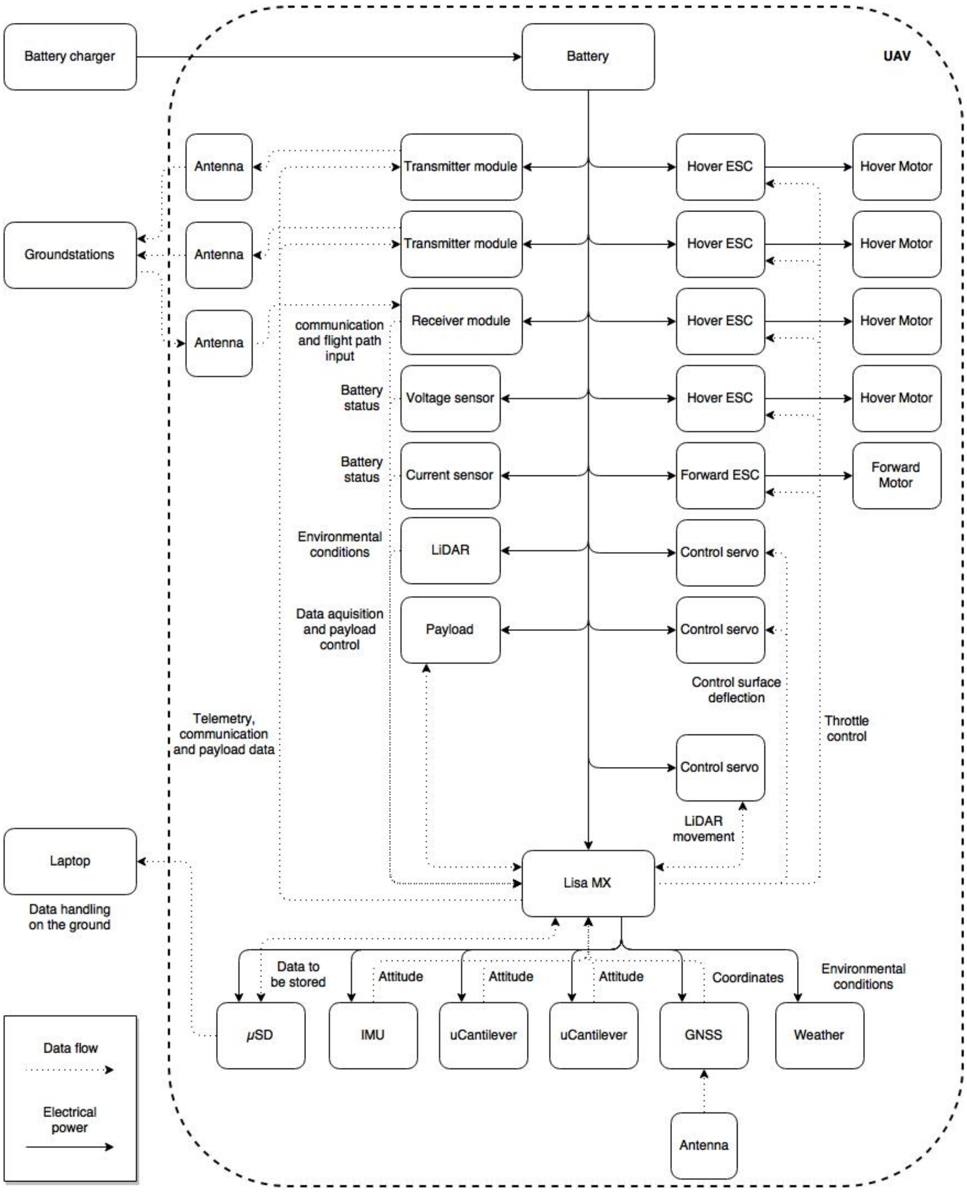

Figure 8.64: Hardware and software block diagram

8.9.1. Layout of electrical system

In order to minimise the amount of wiring in the UAV, great care is taken in placing the electrical components as efficiently as possible. Next to this, special care was taken to minimise the parallel routing of wiring, in order to make the wiring lighter. A complete layout can be seen in Appendix C in the electrical block diagram in Figure C.1. In this figure, the division of all the components of all the ports can be seen. The ports of the Lisa/MX were also used as efficiently as possible, by assigning the electrical components to a specific PWM, I2C, UART, SPI or analog port.

First of all, the three servos used for actuating the control surfaces and for moving the LiDAR are connected to three of the PWM ports, as PWM is the most simple way to control a servo. Next to that, the ESC used for the

[51]URL:`http://wiki.paparazziuav.org/wiki/Lisa/M_v2.0` [cited 16 June 2016]

horizontal flight motor is also connected to the PWM bus, as this ESC needs to be controlled separately from the other four ESCs.
The other four ESCs are connected to one of the I2C busses available on the Lisa/MX, in order to establish a fast and secure communication with the ESCs needed for hover. The other I2C bus is connected to the LiDAR module, being the default communication protocol used for this module.
Next to that, three out of the five UART busses available on the Lisa/MX are taken by the electrical subsystem. The first one is taken by the ADC which reads the signal coming from an ammeter and voltmeter, which reads the current and flowing from the battery, and the voltage of the battery, respectively. The second UART port is taken by the communication modules, while the third one is reserved for only the GNSS receiver, being the default communication protocol for all the modules.
Next to the I2C and UART, also the SPI bus is taken, being used by the payload bay, external IMU and microSD card. By grouping these two components, writing data from the payload bay to the microSD card can happen simultaneously with writing data to the autopilot.
Lastly, the three analog pins available on the Lisa/MX are used by the micro cantilevers and weather sensor.

Not all connections can be wired directly from one component to another. Because of this, several electronic components were needed. These components add up to a mass of 36 g. The detailed table of the electronic components can be found in Appendix C in Table C.1.
Included in the list of components are a current and voltage sensor, which monitors the battery usage and health. Next to that, two fuses are included for safety reasons. When there is a malfunction in the propulsion system, the high current fuse will blow, preventing short-circuit damage to the battery.
When the high current fuse is blown, the subsystems other than propulsion are still powered, enabling a controlled crash landing. When there is a short circuit in the electrical subsystem, the low current fuse will blow, ensuring overheated wiring cannot start a fire on-board.
When the low current fuse is blown, the UAV is not able to make a controlled landing anymore, and will crash. This, however, it is preferred that the UAV can be recovered with most of the on-board components still intact, rather than there is a chance that the UAV catches fire, and that most of the on-board components are lost, and having a chance of starting a fire on the ground.

8.9.2. Wire selection & budgeting

When the layout of all the electrical components was made, the type of wires could be selected. This was done by estimating the maximum current going through the wires for three different kind of wires. These wires and the maximum current encountered in them can be seen in following list:

- High voltage-high current wiring: maximum 114 A
- High voltage-low current wiring: maximum 28 A
- Low voltage wiring: maximum 2 A
- Sensor wiring: no current

The maximum current trough the high voltage-high current wiring was estimated to be equal to the worst case current for the four hover motors, which is 28 A per engine[52], and the current for the electrical system, which totals to a maximum current of 114 A. For this type of wiring, Radox KDJ-11 wire was chosen with a size of 10 mm^2[18].
For the high voltage-low current wiring, the maximum current through the wiring was estimated to be equal to the highest current drawn by any motor, which is 28 A. Because of the lower current, a lighter wire was chosen, being Radox KDJ-11 wire with a size of 1.5 mm^2[18].

Next, for the low voltage wiring, a maximum current of 1.88 A was calculated in Section 4.5.2, which is low in terms of electrical wiring. Because of this, a very light wire can be chosen. However, as wires smaller than 0.13 mm^2 are difficult to handle as they are fragile, a limit was put on 0.13 mm^2 size wires. In this case, Raychem 55PC0211 was chosen[40]. For the same reason, this type of wire is also used for sensor wiring.

All the wiring combined reaches a length of 20 m, but due to light, aerospace grade wires, it has a total mass of 179 g. This, together with the specifications of the chosen wires, can be seen in Table C.3 in Appendix

[52]URL:http://www.hobbyking.com/hobbyking/store/__8139__Turnigy2836_Brushless_Outrunner_1000kv.html [cited 26 June 2016]

C. Using aerospace grade wires ensures robustness of the wiring, while still being lightweight. Next to the wiring, also connectors, solder and shrink tube used during assembly need to be taken into account, as well as PCBs on which the electronic components should be mounted. Due to limited resources, the number and placement of these connectors and weight of solder, shrink tube and PCBs are not yet designed. Because of this, an contingency of 20% was taken into account for the mass of the wiring, resulting in a total mass of 212 g including contingency factor.

8.9.3. Battery selection

Batteries were chosen as the energy source of the UAV, as batteries have a higher power density than fuel cells or solar cells, and batteries can be lighter than an internal combustion motor module. It can also be replaced more easily than refuelling a fuel cell or internal combustion motor. When selecting a battery, there were many variables to decide on, such as the chemistry, which influences the energy and power density, the life span and the safety. Next to that, the number of cells and the capacity influence the power contained by a battery pack. It was decided to use Lithium Cobalt (LiCo) batteries enhanced with graphene. These batteries have a high specific power, long life span and are among the safer options of LiPo chemistries[53,54]. Enhancing the batteries with graphene also enhances the energy density, and reduces the internal impedance, which induces a higher depth of discharge and higher discharge rates.

The number of cells also has a great impact on the efficiency of the propulsion system, with a higher voltage being more efficient. This, however, is limited by the space in the body, and by the maximum voltage most brushless motors can handle. As the battery had to be split in two smaller packs, an even number of cells was desired. The highest even number of cells which fit in the body, and can be handled by most motors, is four, which means the battery consists of 2 battery packs of 2 cells each.

Next to these variables, the capacity of the battery was determined. For the propulsion system, a charge capacity of 7000 mAh was chosen, as this was the maximum charge capacity which fits in the body. This maximum was needed to get reasonable vertical flight endurance. For the electrical subsystem, the energy capacity needed is about 10.61 Wh, which, at 14.8 V nominal, equals 0.72 mAh for a nominal mission, as determined in 4.5.2. With a depth of discharge of 80% and a power conversion efficiency of 91%, the extra charge capacity needed equals about 0.98 Ah[45]. This all adds up to a battery of 7980 mAh. Using Turnigy Graphene[55] and Turnigy nano-tech Ultimate[56] batteries as references, the parameters of the battery are listed in Table 8.12. The battery charge capacity was rounded to 8000 mAh, as LiPos are generally produced with capacities rounded to the closest hundred.

Lastly, it has to be checked that the battery can provide the peak current needed by all the electric components. This is done by choosing a battery with appropriate C-rating, which is related to the peak current. As the battery has to deliver a peak current of 114 A and has a charge capacity of 8000 mAh, the required C-rating for the battery needs to be 14.25 C. As graphene batteries easily have C-ratings higher than 20C[57], the C-rating is not a limiting factor of the battery.

[53]URL:http://batteryuniversity.com/learn/article/the_li_polymer_battery_substance_or_hype [cited 13 June 2016]
[54]URL:http://www.graphene-info.com/graphene-batteries [cited 13 June 2016]
[55]URL:http://www.hobbyking.com/hobbyking/store/uh_viewitem.asp?idproduct=91213 [cited 13 June 2016]
[56]URL:http://www.hobbyking.com/hobbyking/store/uh_viewitem.asp?idproduct=49509 [cited 13 June 2016]
[57]URL:http://www.hobbyking.com/hobbyking/store/__91385__Turnigy_Graphene_5000mAh_4S_Hardcase_Lipo_Pack_ROAR_APPROVED_EU_Warehouse_.html [cited 21 June 2016]

Table 8.12: Battery parameters

Parameter	Value	Unit
Nominal voltage	14.8	V
Charge capacity	8000	mAh
Energy capacity	118	Wh
C-rating	20	C
Mass	700	g
Length	180	mm
Width	50	mm
Thickness	20	mm

Concluding the electrical system

So, to conclude this section, it can be seen that the electrical system consists of 2 electric circuits with several parts which are all connected to each other by means of lightweight, aerospace grade wiring, having a mass of 211.61 g. One circuit is for the propulsion system only, running at the battery voltage of 14.8 V, while the other circuit is for all other subsystems inside the UAV, running at 5 V or 3.3 V when the power is delivered by the autopilot itself. All these components also need an energy source, which will be done by a a 4 cell Lithium Cobalt, graphene enhanced LiPo battery of 8000 mAh, with a mass of 700 g.

9 Design feasibility analysis

The feasibility of the design was analysed to know if the design is able to meet all the requirements. For this a sensitivity analysis and feasibility analysis were performed. From the sensitivity analysis the robustness of the design was determined. This sensitivity analysis is used to check the feasibility further with a compliance matrix, to determine whether all requirements were met. From the ones the design did not meet, a reasoning was made why the design did not meet the requirement and which modifications were made in order to meet the preset requirement.

9.1. Sensitivity analysis

For the sensitivity analysis, the changes in the design solution were evaluated for different design parameters. After that, the conclusion was drawn to determine the robustness of the design solution.

Take-off weight and the available battery capacity are the major system parameters of which the effect was investigated. For all three configurations a study was performed to determine their influence on the flight range, flight endurance, hovering endurance, hovering power and wing area. The results of this sensitivity analysis can be found in Table 9.1.

Table 9.1: Sensitivity analysis on the effect of the take-off weight and battery capacity on all configurations

	Nominal	**10% increase in take-off weight**	**10% decrease in battery capacity**
Tailsitter			
Flight range (km)	93.2	84.7 (-9.1%)	83.8 (-10%)
Flight endurance (min)	96.5	82.6 (-14.4%)	86.8 (-10%)
Hovering endurance (min)	16.1	14 (-13%)	14.5 (-10%)
Hovering power (W)	309	355 (+13%)	309 (-)
Wing area (m^2)	0.25	0.27 (+8%)	0.25 (-)
Flying wing			
Flight range (km)	143.2	140.5 (-1.9%)	128.9 (-10%)
Flight endurance (min)	153	142.8 (-7.1%)	137.7 (-10%)
Wing area (m^2)	0.25	0.27 (+8%)	0.25 (-)
Quadcopter			
Hovering endurance (min)	18.7	16.3 (-13%)	16.8 (-10%)
Hovering power (W)	265	305 (+13%)	265 (-)

An increase in weight can be caused by the need for heavier subsystems. In general an increase in weight leads to a decrease in performance. From Table 9.1, it can be seen that an increase in weight has an impact on all configurations, but more on the tailsitter and quadcopter configuration since these have the ability to hover. The wing area increases, as the weight increases in order to keep the wing loading at the same level.

A decrease in battery capacity is due to the depth of discharge which is decreased by 10% after 250 complete discharge cycles. From Table 9.1, the influence on the range, endurance, power and wing area can be seen if the battery capacity is decreased by this 10%. It can be concluded that the wing area does not depend on the battery capacity. Also it can be easily seen that the range and endurance in flight decrease with the same percentage as the decrease in battery capacity. From this it can be calculated at what times the batteries need to be changed in order to still be able to perform its required missions. Therefore the feasibility of the design is increased.

9.2. Feasibility analysis

For the feasibility analysis, the complete compliance matrix can be found in Appendix J. From the 107 requirements set, only 11 were not met or 90% of the requirements were met. When looking at the driving requirements, it can be concluded that all these requirements are met, which lead to the conclusion that the design is qualitatively feasible.
A feasibility analysis was performed for the requirements which were not met to show why the design does not meet the requirement and what modifications need to be made in order to meet the preset requirement. This reasoning can be seen below.

- **SYS-SUR-1.1.6** This requirement is not met because of the increase in camera weight when a zoom-function is present. In order to obtain the required zoom, the UAV can fly at a lower altitude.
- **SYS-COM-1.1.2 (a,b and c)** Because the UAV is flying at a maximum altitude of 4500 m, depending on the classification of the airspace, communication with ATC might be necessary. Because in event of an air crash the ATC will mostly redirect air traffic from the crash site. No communication with ATC is obtained by the UAV, but as a recommendation it is included as for other markets this might be necessary. Therefore the requirement is not met [14].
- **SYS-COM-1.4** A selectable frequency is not obtained for the communication, but the frequency can be tuned. This indirectly gives a selectable frequency.
- **SYS-COM-1.6** This requirement was not well defined. If the line of sight is interpreted as still visible, then this requirement is met. But if the line of sight is interpreted as without any obstacles in between the groundstation and the UAV, this requirement is not met. In this case the UAVperforms its mission autonomously and has communication once in line-of-sight again.
- **SYS-CTR-1.1.2** The requirement to control the UAV remotely is not met, because from a further discussion with the stakeholders, this was not needed anymore. However the investigators can operate the system by choosing points of interest once the UAV is on site.
- **SYS-STR-1.1.2** This requirement is neglected since the mapping payload does not function within volcanic ashes. Therefore the structure does not have to withstand volcanic ashes.
- **SYS-STR-1.1.3** This is a killer requirement and is not feasible. A lightning strike destroys the electrical components in the UAV and other components will melt away, leaving the UAV non-operational.
- **SYS-SFY-1.4** In the design of the UAV, no certifications were taken into account for the operations since the nature of the UAV's mission is essential and supported by governments. Therefore this requirement is not met, however, this is recommended in 14 for the use in future markets.

Concluding design feasibility analysis
From this analysis, it can be concluded that the design is feasible. The requirements set by the stakeholders and design team were met, which leads to a crucial factor in the design phase which is achieved. From the feasible design, further investigation and evaluation have to be performed which lead to an even better design, which can be implemented on the market. This is all done in the next chapters.

10
Risk and reliability

From the previous chapter, it resulted that the design is feasible, when looking solely at the requirements. Fulfilling most of the requirements and performing the desired missions on the other hand do not generally generate a valuable product. An actual valuable product is obtained, if it is reliable, available, maintainable and safe. The impact of the use should furthermore not limit the operational application. This is only obtainable if all risks are mitigated to a low occurrence or a minimised impact. As value is a key component of MIRU, a RAMS and risk assessment were performed. The RAMS analysis resulted in the application of safety critical functions and a redundancy philosophy. For the risk assessment the most likely risk was the fact that the UAV could get out the line-of-sight of the groundstation. The most catastrophic risk is the failure of a hover motor, which would unavoidably result in a crash or crash landing. Both these risks have a low impact or likelihood respectively.

10.1. RAMS

The RAMS characteristics make the design safer, more productive and more sustainable. All four fields of RAMS engineering were taken into account for the design of MIRU. If MIRU is being operated, the associated risks and accompanying reliability determine the potential market value. The RAMS analysis and design application thus generate value for the final design. Each specific RAMS area of interest is now explained and the application to the design is shown.

Reliability

The reliability of a system is the probability that the system performs adequately, for a given period of time, and under specific operating conditions. The system could only be reliable, if each component of the system had a stable performance. Safety factors and overall redundancy make the system reliable. However a few parameters are not controlled by the design, while still disrupting the reliability. First of all the system can be stable, but the investigators can make MIRU malfunction. A manual, training and software improves the reliability of the investigator for both the groundstation and the UAV. Secondly the environment can disrupt the operational certainty. The autopilot, multiple UAV configurations and a large range of feasible operational conditions (Chapter 6) counteract the environmental hazards. Furthermore, the design uses multiple off-the-shelf products which already were subjected to multiple tests, so these products add a lot of reliability of the design.

Availability

All parts of MIRU are in theory always available. However, before the system is operable, the batteries must be charged, the UAV assembled, the payload selected and the groundstation set up. It is immediately clear that the system consists of a lot of components, which individually cannot be helpful for a successful mission. The disassembly of the system is an asset to the transportation, but a limitation to any urgent availability. Frankly a prompt availability is no necessity, as an investigation generally has a slower pace compared to for example the search and rescue operations at the crash site. The time in chichthe system needs to become ready for use perfectly fits within the investigation rhythm of a crash site.
The lifetime of LiPo batteries is on the other hand a real concern, when it comes to the availability of the UAV. Research has shown that the charge capacity decreases with 10% after 250 complete discharge cycles [1]. The

[1] URL:http://batteryuniversity.com/learn/article/how_to_prolong_lithium_based_batteries [cited 17 June 2016]

maintenance program for the batteries solved this problem as described in Section 6.2.
When components break during transport or flight, the system becomes unavailable. Therefore a set of spare parts was included in the transportation box. The design philosophy of the layout and subsystem integration allows the end user to simply replace the components.
The safety critical functions also describe the measures taken to comply with the availability of the system.

Maintainability
All maintenance operations can be performed by the operators of the system and do not need a high level of training. This lengthens the lifetime and durability of the system. The maintenance operations were already discussed in Section 6.2. The fact that the UAV can be taken apart, complements the maintenance procedures, because more parts are accessible. The ease of performing maintenance is in the end also economically beneficial as it does not require much time or specialized people.

Safety
Three parties have the highest stakes when it comes to safety: the operators on the ground, the UAV and the environment. All three parties influence each other and it is the task of MIRU to improve the safety on an individual basis. Each stakeholder is now discussed.
The safety of the operators on the ground can be strengthened by the UAV or the environment. The UAV is safe as long as some precautions are taken into account. When the motors are turned on during take-off or when the UAV lands, the operator should for example stand back. If the relation between the operators and the environment is discussed, MIRU increases the safety of the investigators. MIRU reduces the risk investigators have to take to access remote sites. The site is also mapped beforehand, which gives the investigators a tactical advantage and does not leave them in the dark.
Crashing is the main safety hazard of the UAV. In the same manner as for the reliability the safety impact is minimized for the influence of external sources like the operators and environment. During transport, the UAV is carried in a safe casing, so no damaging can occur to the UAV during this phase. Furthermore multiple precautions were taken into account for the design, which are discussed in the safety critical functions.
When MIRU is used to investigate an accident scene, the environment is less disturbed compared to conventional investigations. This accounts for more remote missions, where normally the impact of human civilization is negligible. Using the coarse map the investigation site can become more compact, as the debris field is known exactly. Also the accessibility for the investigators can be planned better. Therefore the nature is less damaged and the marks of the crash impact are preserved better. The overall quality of the investigations thus becomes better.

10.1.1. Safety critical functions
Three parts of the investigation can be involved in accidents: the UAV, the groundstation and the operator. All can lead to failure of the system. Therefore preventive measures were incorporated in the design to prevent and stop the development of accidents. For all three elements safety critical functions were developed.
An accident of the UAV would cause a crash or crash landing. The following list contains the taken measures to minimise the occurrence and impact of accidents.

- The entire wetted area of the UAV is covered with a layer of carbon and foam to protect the internal structure from external impacts.
- If the UAV loses motor power in forward flight, the planform is still stable and can therefore safely land.
- All other subsystems than the propulsion system have a separate electrical circuit, which, in case of propulsion system failure still makes the UAV operable.
- The GNC module, together with sensors (i.e. LiDAR, micro cantilevers etc.) makes the UAV fly autonomous and avoid obstacles.
- When the signal of the groundstation is lost, the UAV can still fly autonomously and finish the mission.
- Skids on the payload bay prevent damage during a belly landing.
- All payload has a fairing to ensure impact protection.
- Both the structure and electronics were designed with redundancy and safety factors to minimise the occurrence of failures.
- An emergency button is incorporated in the groundstation interface to create a feedback link between the machine and operator.
- Landing struts were installed on the fins to provide safe landings.

- The autopilot is isolated from vibrations for optimal performance.
- A preflight check of all systems is performed using software and a visual inspection.
- The UAV has a protecting transportation case.

A failure of the groundstation happens if hardware or software components break or the station fails to bring the UAV safely back home. The following adjustments prevent this from happening.

- The tablets have a shockproof casing to improve the robustness.
- The groundstation software has a clear interface with warnings for lost signal, battery status etc.
- A manual is included with instructions for normal to calamitous occasions.
- The software always traces the UAV and saves the last point of contact to make UAV retrieval easier.
- A preflight check is performed at the groundstation to check the connection and initialise the software. Also, it is determined whether the interface flight mode equals the real payload and planform configuration.

To prevent accidents which could cause physical harm to the investigation or to prevent actions which could contaminate the accident site, precautions have been taken.

- The tailsitter and quadcopter configuration allow for safe take-off and landing in harsh environments.
- The gas detections payload ensures no gaseous damage occurs to the on-site investigators.
- Difficult natural environments can be mapped, which reduces the risk that investigators have to search the site of interest.
- If a ranged mission has taken place to create a coarse map, the investigator can take measure to ensure safety before accessing the site.
- The communication relay reduces the amount of occupational accidents.
- Less investigations information is lost, as an detailed overview of the debris field is generated.
- The payload is vibrationally isolated to optimise the imagining quality.

10.1.2. Redundancy

The design and redundancy philosophy are intertwined. With respect to the design, MIRU should be a tool to simplify and not to complicate operations. As soon as setbacks occur, the investigator must switch focus from the investigation to the technical system. The investigator becomes an asset to the tool instead of the other way around. Redundancy was therefore a top priority, as it empowers the system with all RAMS characteristics and creates a safety boundary between the operation, investigator and failure.

The critical systems of MIRU were designed to be fail safe. This accounts for critical functions as well as technical components. Because the investigator is most important to the design, the critical systems were selected from a user point of view. First the functions and later the components are discussed.

A demanding function of the system is the take-off and landing of the UAV. The redundant solution was to have vertical and horizontal take-off and landing configurations. If one fails to adapt to the mission specifications, the other configuration can save the day. Furthermore the different flying configuration also reduce the amount of limiting operational scenarios. Lastly the emergency command function on the groundstation creates a feedback loop between the autopilot and the operator. If the GNC module makes a misjudgment, the operator can make the UAV safely return to the ground.

When it comes to the critical technical components, a list of measures was taken into account. This list is given below:

- Both the payload and autopilot are connected to the framework with four connections, where at least one is redundant.
- Both the ailerons have three hinges instead of only two.
- A safety factor of 2 has been applied to the entire structure to make sure that a small fracture does not immediately result in failure.
- A separate circuit for the propulsion system and all other electronics was established. Thus failure of the motors does not directly cause the other electronic subsystems to fail.
- Multiple tablets could function as the master link. If connection to the master tablet is lost, tablets within line of sight of the UAV could obtain master status.
- The UAV still has stable gliding performance, when the cruise motor would lose power.
- The wings are secured twice to the body to secure these essential devices for forward flight.

- The weatherstation on the ground is used to calibrate the on board sensors . If the sensors fail, the software can adjust their readings correctly.

These redundancy principles show that the risk of system failure is massively decreased. The taken measures enable the investigators to solely investigate and work along side MIRU.

10.2. Risk assessment

A series of events could make the system loose its functionality. The reliability of MIRU is thus important, because it directly reduces the occasion of failure. A customer simply expects the system to keep its functionality over time. Risk analyses have been performed to define and mitigate the impact and occurrence of the hazards. Three risk analyses have been performed: one each for the operational risk, environmental risk and organisational risk. The operational risk map is presented in Figure 10.1.

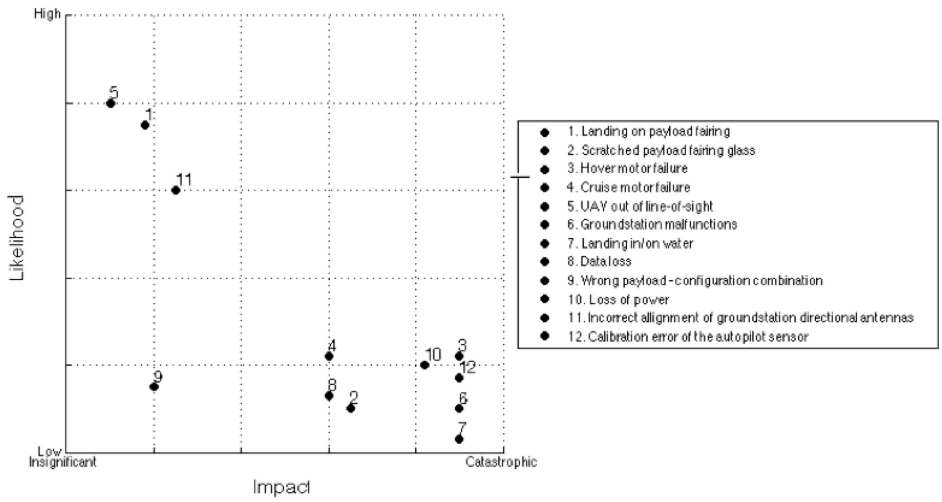

Figure 10.1: Risk analysis for the operations of MIRU

The likelihood of a belly landing is high as the UAV in flying wing configuration always lands on its belly or payload fairing. As this is known, the payload fairing is designed to withstand the forces introduced by landing and thus the impact is low. As a consequence of a belly landing, the fairing perspex can be scratched. The impact of scratched perspex is that the payload inside the fairing does not function properly. The consequence is that the mission has to be redone. The likelihood is limited by using a protecting foil as described in Section 8.7.4.

When a hover motor fails, the UAV in quadcopter and in tailsitter configuration becomes difficult to control. Both have to make a controlled crash landing. As the UAV is equipped with PID-controllers, it should autonomously anticipate on the loss of thrust to minimise the damage caused due to the sudden loss of thrust. If the cruise motor fails the UAV can glide in both the flying wing and tailsitter configuration. While gliding, the UAV tries to return to the basecamp. If that is not possible, it identifies possible locations to make a controlled landing. The elevons are used to keep control of the UAV. In the tailsitter configuration, the UAV can transition back to the quadcopter configuration to try to reach the basecamp or make a controlled landing. The likelihood of a motor failure is decreased by using reliable electrical components. Also proper pre-flight inspection and periodic maintenance should reveal defects before the UAV is used.

When the UAV is out the line-of-sight, there is no communication possible with the UAV. But as the UAV can operate autonomously after its mission and the areas of interest are defined, this does not cause any problems. The scenario of the UAV being out the line-of-sight has been anticipated and thus designed for, limiting the impact of the risk.

Without groundstation, the UAV cannot operate. As the groundstation consists of all items necessary for operation of the UAV, the impact of malfunction is large. To lower the likelihood of happening, back-up systems are made available to the user.

The UAV can operate over water in the flying wing configuration, but it is not designed to operate over salty water. Also the UAV is not designed to land on water. As the operation limitations have been set, the user can

be properly informed about the limitations, and the likelihood of occurrence has been decreased.
Data loss can be any action where data is lost where it should not have been lost. This can be due to the user formatting the SD card with the data gathered by the UAV, the SD card being full or the SD card is not correctly in place. Other loss of data can happen when the payload is not correctly attached or when the field of view is blocked. To prevent this of happening, the UAV performs an automated pre-flight check using software to check whether all connections are attached properly. Also, the user is led through a step-by-step pre-flight inspection on the tablet user interface to check whether the UAV is ready for flight.
When a non-optimal combination of configuration and payload is chosen, the user receives a warning asking whether they are sure they want to perform the mission in the current configuration. This warning shows up when for example the quadcopter and communication relay are selected. When the user still sends the UAV away on its mission, the results are not optimal, but it has no big consequence.
A total loss of power is experienced when the batteries die due to a short circuit of the wires. As the UAV make use of aerospace grade wiring, the chances are small that a short circuit actually happens. When all power is lost, the UAV is a glider without control surfaces and is uncontrollable.
The UAV can also experience loss of propulsive power when there is a short circuit at one of the motors. However, this does not harm the power distributed to the subsystems due to a high current fuse which blows when it experience high current. In this state, the UAV can glide in a controlled manner.
When the directional antennas on the groundstation are not correctly aligned with the groundstation due to the movement of the UAV, there is no communication link. To reestablish connection, the user has to point the antennas towards the UAV. The direction of the UAV is indicated on the tablet so pointing towards the UAV is not difficult.
When the autopilot sensors are faulty calibrated, the autopilot receives and processes faulty commands. This will make the UAV inoperable. As calibration of several sensor is necessary before flight and periodic maintenance is scheduled to calibrate other sensors. Thus the likelihood is minimised.

The environmental and organisational risk map is presented in Figure 10.2. The likelihood of most of the environmental risks are reduced by the operational limitations set. If the user abide the limitations set, the risks are greatly reduced.

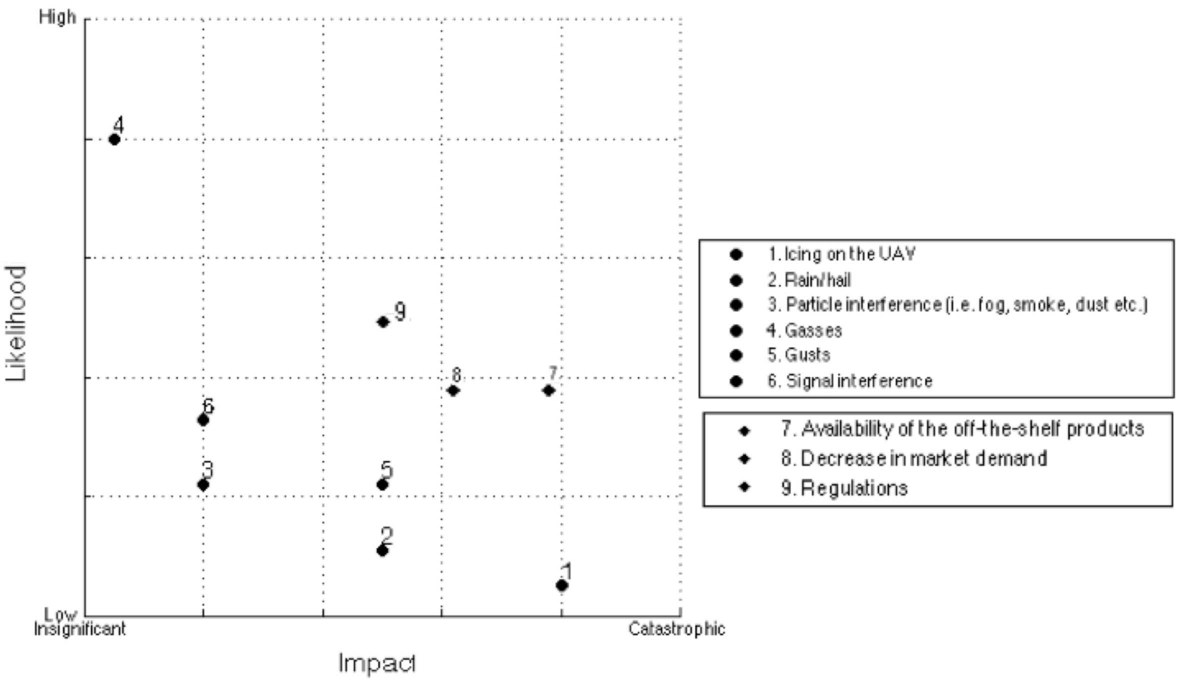

Figure 10.2: Risk analysis for the environment and organisation of MIRU

As the UAV can operate at a maximum altitude of 4500 m, icing on the UAV is expected due to the low temperature. While the UAV is not to be operated in humid, low temperatures, the skin of the UAV can be lubricated with an anti-ice lubricant to prevent the skin from becoming brittle, limiting the impact of the risk. However

the effective duration of the lubricant is limited and thus the impact is still large.
The UAV is splash water resistant. However, the UAV is not designed to be operated in rain- and hailstorms as this damages the carbon skin and foam inner wing as well as the electronic components.
When there are small particles in between the ground and the UAVsuch as fog, smoke and dust, the payload cannot 'see' the ground and thus the UAV cannot properly perform its mission. So the deployment of the UAV is delayed, however no damage is sustained and thus, the impact is small.
As the UAV performs toxin detection, it is highly likely that the UAV comes in contact with toxins in the sense of gasses. The UAV is designed for this as a carbon skin has been chosen with a resin which is chemical resistant. Together with proper inspection and maintenance, the likelihood is reduced.
Gusts will always be experienced in-flight. Thus operational limits have been set. As a sudden gust can cause performance limitations, the impact is average.
When the UAV is transmitting at an area with many devices sending out signals with similar frequency, signal interference is experienced. If the signal is interfered, the user cannot send a new input command of the area of interest to the UAV and the UAV cannot send data to the groundstation. As communication is not required once the software of the UAV has been initialised and the areas of interest have been indicated, this does not harm the operations of the UAV.

The organisational risks are closely related to actions which are not controlled by MIRU, these risks are availability of the off-the-shelf products, decrease in market demand and regulations.
First of all, the availability of the off-the-shelf products depends on the production rate of the producer. As MIRU is dependent on the manufacturers, if several components are not produced any more, it has consequences for MIRU. To ensure that the dependency does not cause any problems, MIRU makes sure that it keeps regular contact with the manufacturers through scheduled reviews such that it is made sure that contracts are signed for the expected number of sales over a certain time span.
Secondly, as the absolute number of air accidents is expected to increase, a decrease in market demand is not expected. However, the goal of investigators is to minimise accidents so if the demand decreases, MIRU can easily be used on other markets as well such as tracking in the event of disasters, as the modularity and interchangeable configuration opens a lot of new markets.
Lastly, special care needs to be taken as each country has its own regulations. Currently MIRU has been designed for the use of the government and not all regulations have been taken into account, thus making MIRU not ready for the commercial market yet. To deploy MIRU in all countries, an analysis on regulations has to be conducted. Also, the fact that the regulations can change over time, makes the impact and likelihood of this risk average.

Concluding the risk and reliability
The risks were mitigated and MIRU obtained all necessary RAMS characteristics. The design therefore made a transitions from only feasible to also valuable. The safety critical functions, redundancy and maintenance program make sure the product stays valuable during the entire lifetime.

11 Market analysis

Although MIRU is designed especially to aid air safety investigators on request of the air safety sector, the market is analysed to confirm that a large enough offset is possible to make the system feasible in economic sense. This step is also important for the development phase, so that if the development can commence, the correct focus and marketing in the further development is applied. The market analysis showed that the design is economically feasible as the current market is growing and several possibilities are present for new markets that can be easily entered without making major design changes.

11.1. Current market

To analyse the current market, various aspects were analysed from which the needs analysis, target audience analysis and SWOT analysis are particularly interesting. These give insight in how valuable MIRU can be and for whom it would be of main use which is necessary to determine if it is worthwhile to actually continue the design process. The outcome is that there is a high demand as MIRU can reduce the time for investigations by at least half for documenting the area while remaining the high detail needed for the investigator to determine the cause. It is also multipurpose in the sense that it can do toxin detection and locating of the site as well. The investigators will not need multiple UAVs to perform the different missions MIRU can perform, and the investigators do not require the use of low quality satellite images of the accident site. Thus the target audience mainly focussed on are the air safety boards.

11.1.1. Needs analysis

Nowadays, air crash investigators encounter difficulties in locating accident sites in remote area, which takes up valuable time. After the accident site has been located, the investigators need a few days to document the complete accident site. However, in this time span, critical evidence such as traces on the ground could already have disappeared. So it would be very convenient if this could be done faster. The use of an aircraft or helicopter to locate the accident site as well as taking aerial photographs is too expensive and the operation is often limited by daylight. Also the images are compromised due to humans taking the images and due to the vibrations from the helicopter Therefore, investigators would like another locating and mapping device such as a UAV that fills the gap between the investigator and the aircraft or helicopter.
MIRU reduces the amount of resources necessary during investigations and helps in locating and mapping the crash site. It is also operable when there is no sunlight available, so that the investigation can be performed anytime. It should however be noted that the UAV is a tool to assist investigators performing the investigation, not to replace the investigators. MIRU makes it possible for the investigation team to work more efficiently.

11.1.2. Target audience analysis

The target market for which this design is intended, is the air accident investigation sector, meaning the air safety boards for which the investigators work. Although each country must have its own investigation agency, some countries do not have a separate air safety board but have it included in other safety boards that for example investigate chemical accidents as well. In total there are 205 accident investigation boards [1]. The expectation that every safety board needs a UAV however is not true. Some boards are more developed than others and some are also larger than others. For instance, the United States of America has one of the largest aircraft manufacturers, Boeing, and thus has to be included in all investigations concerning a Boeing aircraft

[1] URL:`http://www.icao.int/safety/AIA/Pages/default.aspx` [cited 16 June 2016]

[20]. Besides having one of the largest aircraft manufacturers, America is a very large country with a lot of incoming and departing flights. Combining the two factors, the wish for multiple MIRUs has been identified. While a country with a very low number of incoming, departing or overflying flights might not see the use of having one. Lastly, countries as the United States of America or the Netherlands are more likely to invest in new technologies as they are going through a technological growth. But upcoming countries in especially South-East Asia are very likely to soon catch up as they are experiencing fast technological growth and interest. Other markets in which MIRU can operate, implying a new target audience, are explained in Section 11.2.

11.1.3. Competitive analysis

The main competitors of MIRU are satellites, existing mapping UAVs and the current method of performing an investigation. The advantages and disadvantages are all explained here.
When MIRU is compared with other mapping devices, ranging from UAVs to satellites, the main advantage is that it is employable in different missions, while still having a good performance, especially considering its size and mass.
The other existing options, ranging from flying wings to quadcopters can be used as well, however, MIRU has a better performance in flying wing and tailsitter configuration, 122 and 77 km respectively compared to 60 km of existing UAVs with a MTOW of around 2.5 kg, which is similar to the mass of MIRU in its heaviest configuration [2,3]. For the quadcopter configuration, the endurance of MIRU is 18.7 min. Compared to the other systems [4,5,6], in which the endurance range from 8 to 25 min, MIRU performs well but is not the best. Nonetheless, the disadvantage of the other systems is that multiple UAVs are needed to perform all the missions MIRU can perform and thus increasing the difficulties in operations and logistics. Also, these UAVs are not capable of providing communication relay or toxin detection and thus, MIRU fills a gap for the investigator.
Another possibility is to use imaging satellites instead of a UAV. Their advantage is that they can easily map vast areas. However, satellites can only present the desired images when their orbit crosses the accident site. Thus it is not always possible for the investigators to receive images taken by imaging satellites. Also clouds could possibly block the line-of-sight of the imaging sensor. Furthermore, these satellites cannot achieve the accurate resolution of at least 80 pxm^{-1} that is needed for ground slopes higher than 20 $^\circ$[7]. So all-in-all, satellites cannot out value MIRU as the latter is more versatile and can perform the same as well as other operations.
Another option is to continue to use the current method, which is renting helicopters to make an aerial overview. As this does not provide a lot of detail, it is not considered as a good option or alternative. Also, the cost of hiring a helicopter is relatively high, as it costs €3000 per hour [8] and the helicopter has to be rented for a full day.

11.1.4. Environmental and sustainable analysis

The environmental analysis includes both the external and internal environment. The most detailed method to analyse this is to use the PESTLE method which includes Political, Economic, Social, Technological, Legal and Environmental factors [9]. However, this method is considered to be too extensive for the scope of this project. Also, as MIRU is not yet in production or made into a real company, several factors such as credit accessibility cannot be analysed and therefore only the technological and environmental aspect are analysed.
The technological aspect includes new discoveries, rate of technological obsolescence, rate of technological advances and innovative technological platforms. At this point, MIRU contains state of the art and yet to be produced technologies such as microcantilevers and a multispectral camera and therefore the rate of technological obsolescence will be very small. Furthermore, innovation in this area is not expected to harm the market share of MIRU as it has swappable payload and components, making MIRU easy to adapt to innovations.
For the environmental aspect, MIRU has a sustainable design on a few items. MIRU replaces the helicopter or aircraft normally necessary for air accident investigations and as MIRU is battery-powered and lighter, it reduces carbon emission significantly. Also the use of rechargeable Lithium Cobalt Graphene Enhanced bat-

[2] URL:http://uas.trimble.com/specifications [cited 18 June 2016]
[3] URL:https://wingtra.com/technology/ [cited 18 June 2016]
[4] URL:http://agribotix.com/enduro/ [cited 18 June 2016]
[5] URL:http://www.cartum.org/en/cartum/drones-cartum/ [cited 18 June 2016]
[6] URL:https://www.sensefly.com/drones/albris.html [cited 18 June 2016]
[7] URL:http://www.satimagingcorp.com/satellite-sensors/worldview-3/ [cited 15 June 2016]
[8] URL:http://www.aircharterguide.com/AircraftSearch.aspx?AircraftCategory=Helicopter&pageNum=1 [cited 20 June 2016]
[9] URL:http://pestleanalysis.com/what-is-environmental-analysis/ [cited 16 June 2016]

teries is a more sustainable choice than any other battery type as graphene makes the batteries more durable and less polluting to the environment [10]. But sustainability covers much more than just the power source, f.i. sustainable materials, re-usability and sustainable production. The material itself is not recyclable however it has a long lifetime and the materials are not from a depleting source. Furthermore, the UAV is re-usable as it can perform a controlled landing after every operation so that it can be relaunched again. Besides this MIRU can resist various weather conditions and/or large impacts such as gravel on lift-off and impact with objects and it is possible to change only components, making sure it does not have to be replaced completely. Additionally, as MIRU is employable in very different missions with just small adjustments to the design, there is no need of producing various different UAVs. Therefore, less production methods, that all introduce their own waste, are needed for the design. Also the emphasis was put on using parts who share similarities as much as possible, to even more decrease the production methods. Unfortunately, the groundstation and its generator are less sustainable as the fuel needed for the generator is unleaded petrol. However, a generator is only necessary when the basecamp is situated in a remote area. Also, the batteries of use for each groundstation and UAV component have been selected to last long to minimise the necessity of the generator.

11.1.5. SWOT analysis

The SWOT analysis gave the insight that the UAV still needs to improve on endurance for detailed mapping, but that the modularity is a strength and opportunity. However, regulations are a potential threat when the UAV is brought out on the commercial market. The analysis can be seen in Figure 11.1.

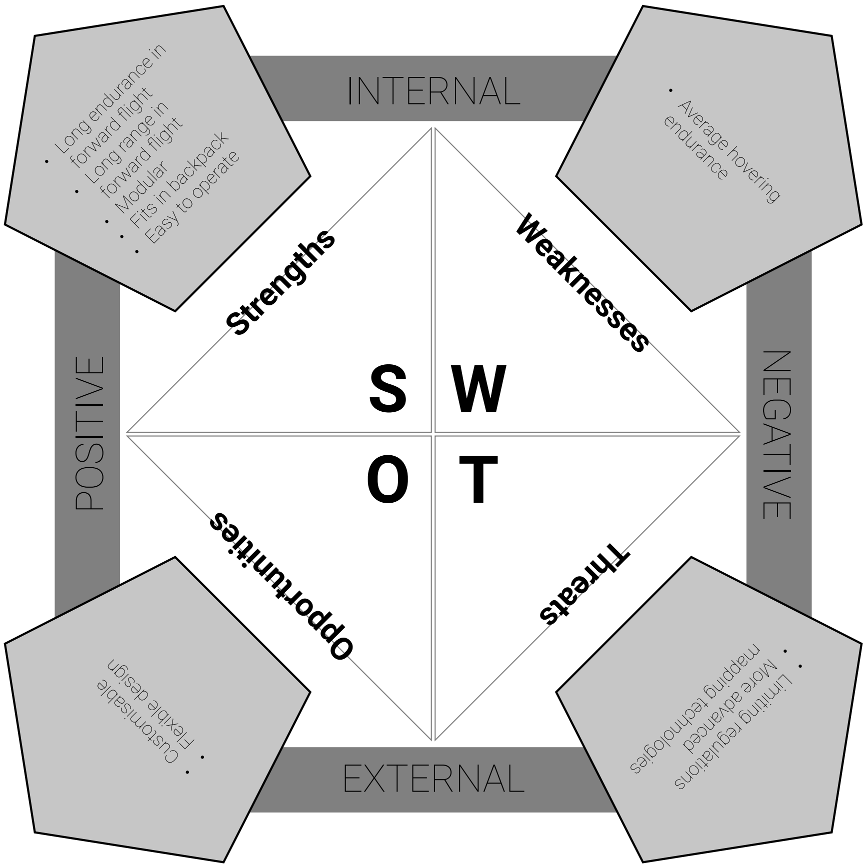

Figure 11.1: SWOT analysis outcomes

The analysis was done by answering questions concerning the subjects of SWOT [11]. For the strengths it was found that the key strength of the design is the long endurance and range in forward flight which is better than the competitors as defined in Section 11.1.3. Also the modularity of the UAV, its size and the ease of operation are highly valued. However, the main weakness that the system has to improve upon is the power required for

[10]URL:`http://www.graphene-info.com/graphene-batteries` [cited 16 June 2016]
[11]URL:`https://www.mindtools.com/pages/article/newTMC_05.htm` [cited 17 June 2016]

hovering. At this point, the hovering endurance is average compared to other systems, but MIRU aims to be the market leader. Also, with improved hovering endurance, less often the batteries have to be changes and thus reducing the weight of the groundstation as the batteries have to be carried to the groundstation. This is an aspect that really needs to be improved, without reducing the quality of the rest of the system, to be able to keep competitors at a distance.
The opportunities that MIRU has, mainly come from the fact that it is customisable. The customer can decide to buy another type of payload or to use the payload for a different mission than an air safety investigation. The flexible design thus opens up new markets rather easily. The threat with this is unfortunately that the UAV needs to be limited to certain heights and distances to be certified for regulations. MIRU can apply for a special operations certificate, depending on the intended use of the UAV, but this still imposes constraints on the performance. Another threat is the changing quality standards such as the wish for a higher detailed map or the need of a video stream during flight. The modularity in this case is the solution to the threat of coming out-dated as it is easy to replace the out-dated with new payload.

11.1.6. Global market segmentation

The market is split up into several segments as it depends on the user what he finds more interesting. The market segments that are defined are:

- Isolation of area of investigation
- Number of air traffic movements
- Cost budget

Especially the latter one is of importance for the market analysis as the UAV is partially designed for remote areas and one can imagine that in countries as the Netherlands, locating of the aircraft can be done without a UAV. However, for countries as Canada with long stretched forests or mountainous areas this is a very interesting function.

Another reason in which the market differs is the dependency on air traffic. If a country has a lot of incoming and outgoing flights, or a large amount of flights passing through their airspace, they are more likely to be involved in an investigation. This also accounts for countries that have an aircraft manufacturer. For these countries MIRU is a good investment as the UAV is anticipated to be in use a lot of the times. However, when a country is (almost) never involved in an investigation, the UAV might be a too large investment for the air safety board. This immediately links to the second segment, the cost budget. As some countries are richer than others, the offset will differ per country. Norway could buy multiple, so that they can be deployed not only for their air safety board, but also for other safety boards. While on the other hand, Haiti could prefer to stick to the old fashion due to the acquisition cost.

All markets can be served when slight changes are made to MIRU. For example, if the costs are too high, the customer can go with lower cost payload that still provide sufficient results. Also, as MIRU can be used for various different investigations apart from the air safety investigations, a customer can buy one and use it wherever needed. The fact that some countries have less remote areas than others, does not mean that there is no added value for these countries. In fact, all the functions the UAV can fulfil are still very useful for them. So all in all, the three market segments as defined above can all be addressed.

11.1.7. Expected offset

There are 205 air safety boards worldwide[12], some of which operate independently of any organisation and others are still belonging to larger investigation boards.
As explained before, the countries that are involved in the investigation are the country of the airframe manufacturer, the country of the motor manufacturer, the country of origin of the airline and the country of the crash site [20] Thus countries with a large aircraft manufacturer are more likely to be involved in investigations rather than others and thus those countries have larger safety boards.

Although MIRU does not have competitors, it is expected that MIRU is not sold in large numbers to air safety boards as there are only 205 of them and a good estimation would be 100 units sold within the first 5 years. It will take time to prove that the UAV is really aiding the investigation, which will be a trigger to other safety

[12]URL:`http://www.icao.int/safety/AIA/Pages/default.aspx` [cited 18 June 2016]

boards to buy one. There are only few countries which need multiple for air accident investigation, which is also accounted for in the 100 units. Over a longer period of time, MIRU could be introduced in other markets for which MIRU is an asset to the current technologies with its wide range of possible operations as explained in Section 11.2.

11.2. New markets

As MIRU is a UAV which is employable in many different conditions, is modular and has very good performance, it can be implemented in other markets. Possible new markets are [38]:

- Tracking in the event of agriculture/forest/marine pollution
- Mapping of land registry
- Geological and mining researches
- Gas and oil leaking research
- Vegetation and archaeological monitoring
- Plant and forest species investigation
- Border control
- Providing communication relay in disaster struck areas
- Industrial accident investigation

Out of these markets, the first market will have the most potential as quick and flexible response is necessary in such situations. The design can be deployed in case of emergency tracking and monitoring in seismic active areas, water hazard prone areas, wildfire prone area, (tropical) cyclone prone area and other disaster prone areas such as near nuclear facilities and oil rigs. The customers are the safety boards and the governments as they lead the operations and investigations after a disaster has occurred. Larger and smaller governments are both interested in the design as they have to facilitate the investigation.
There are already UAVs available which are used to aid in disasters but they are smaller or have lower endurance. One example is the senseFly[13], which offers UAVs designed for mapping of areas and first response in case of a disaster. But senseFly has an endurance of only 50 min. Also large UAVs are already available to perform first response operations, but they are restricted in take-off and landing locations and are often far more expensive. Thus in this market segment, the design will still fill up a niche.

The changing climate will very likely cause future catastrophes and influence existing nature phenomena [14]. Also, due to the increasing number and the growing wealth of the people, the severeness of a disastrous event is increased. Thus the market size has an increasing trend, especially due to the very flexible payload features of MIRU. MIRU helps in observing and tracking in the early moments after the disaster and helps the aid workers in the initial response. Also, the area can be mapped to identify possible hazardous situations and toxins.

For all markets, it accounts that the customers are mainly governmental organisations, the government itself or large companies such as Shell or a nuclear energy power plant company as the acquisition cost of MIRU are relatively high for individuals and small companies.

11.3. Future aviation market

The future is never one hundred percent certain, but there are some facts in aviation that are certain to happen. First of all, due to the growing population and wealth, the aviation industry will grow exponentially [15]. This means more and more flights will be performed in the future. Although aviation becomes safer with every new technology and with every investigation, the absolute number of accidents might increase as more flights will happen. Next to that, technological advances in navigation and reliability and endurance of aircraft make it possible that flight routes will shift to more uninhabited areas. This is further enhanced by flight routes avoiding busy airspace. When a crash happens in these remote areas, a UAV to assist the investigators find and map the wreckage becomes increasingly more beneficial. Also the developments in space tourism should be taken into account. Due to increasing popularity and decreasing costs of going to space[16], the number of (sub)orbital flights will increase in the future. As these vehicles are not as developed as aircraft nowadays, the number of crashes with spacecraft might increase. Thus, although the investigation boards try to make

[13] URL:https://www.sensefly.com/applications/humanitarian.html?L=0 [cited 15 June 2016]
[14] URL:http://earthobservatory.nasa.gov/Features/RisingCost/rising_cost.php [cited 15 June 2016]
[15] URL:http://www.iata.org/pressroom/pr/Pages/2014-10-16-01.aspx [cited 26 April 2016]
[16] URL:http://motherboard.vice.com/read/how-elon-musk-willed-spacex-into-making-the-cheapest-rockets-ever-created [cited 15 June 2016]

themselves obsolete, due to the possibility of an absolute increase in air accidents, this is not likely to happen and therefore, there will be a market for MIRU in the future.

Concluding market analysis

Concluding, there is a market for a purpose designed air safety investigation UAV, but the market is small with an estimated offset of 100 units. However, there are other markets where MIRU could be of great help, such as mapping disaster stuck areas or in gas and oil leakages detection, which is one of MIRUs opportunities. A threat however is that it cannot be easily introduced on the market as these markets have other flight regulations. The main weakness, its endurance in vertical flight, could potentially limit the introduction to other markets as well, as an existing UAV could do better there. The likelihood of these threats is reduced by the strength of MIRU which is its modularity and therefore easy adaption to other markets. Lastly, it is forecast that the demand from air safety boards will not decrease as more and more aircraft will be flying and space accidents have to be taken into account with the increasing amount of space tourism. Thus it is feasible to develop MIRU and put it out on the market.

12

Post-DSE design and development logic

Now that it is confirmed that the design is feasible in sense of design risk and economics, the further course of the design can be determined. Therefore a plan was made that analyses the recommendations and provides a new design loop until the design converges enough and gives optimised results, as then a product is made that can be put on the market. This chapter also includes the production plan in Section 12.2 which is very important as it states all the steps needed to be able to manufacture MIRU. All these steps bring certain cost along and they also determine the customer acquisition cost which relates back again to market analysis, which is touched upon last.

12.1. Post design and development logic

When the DSE is finished, the product will go past the preliminary design phase. However, before production starts, still a lot of steps need to be taken. These steps are put in logical order and can be found in Figure 12.1.

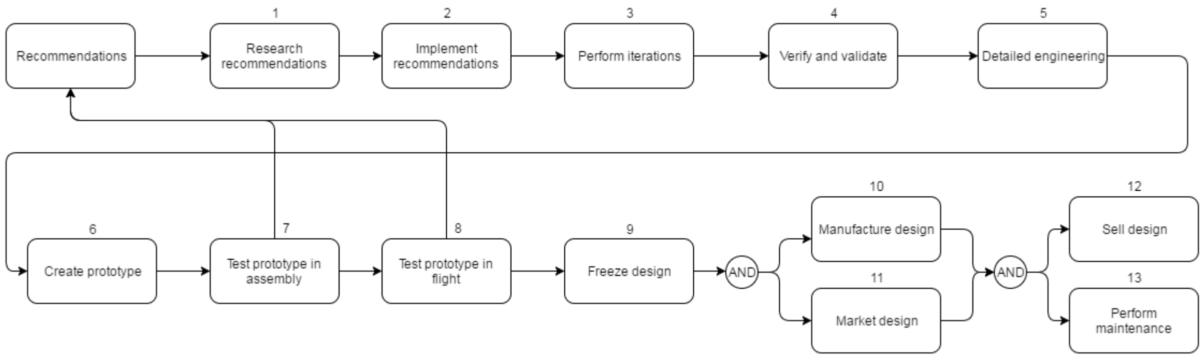

Figure 12.1: PD&D logic which outlines the main activities to be performed in the phase after the DSE is finished

First, the recommendations as proposed by the DSE project group to improve the design need to be examined. The question is if these recommendations provide the improvement needed and if they can be properly implemented. If so, these must be worked out and implemented, from there on new iterations can take place as the mass, span or any other characteristic may change. When these iterations converge, the values can be verified and validated, although the individual programs must already have been verified and validated before.
When the main parts have been designed, the detailed design can commence, in this phase all bolts and small attachments are designed. After these steps, the first prototype can be made as explained in Section 12.2.
As the design consists of various sub parts to make it a modular design, testing if the design is quick and easy to assemble is an important step. After assembling, the UAV can be tested in flight. New recommendations can come out of these tests which make the process go back to step 1 again. Eventually, no new (major) changes will come out anymore and this is when the design is finished and all the design parameters can be frozen. From there on, the manufacturing and marketing can take place, with the plan as described in Section 12.2.
When the first UAVs are finished and sold, the UAVs will start to come back for updates and maintenance, which is the last step in the plan.
The Gantt chart of the post design and development logic can be found in Appendix K, where also a phase 're-assess design' is included which is the iteration from 7 and 8 in Figure 12.1.

12.2. Production plan

The production plan is set up in three phases: manufacturing, assembly and integration. In order to produce MIRU, some base parts of the UAV need to be manufactured, and some need to be ordered. Since different materials are used and different shapes have to be produced, different manufacturing techniques need to be applied. After the constituent parts have been manufactured, the structure can be assembled and the subsystems can be integrated into the platform. These phases are subdivided in stages which are set in a time ordered outline. The manufacturing phase is given in the flow chart in Figure 12.2. The fabrication of the moulds for the composite layers and the moulds for the plastic components can be done simultaneously. Hot wire cutting the foam components and ordering the off-the-shelf parts can also be done at the same time. The off-the-shelf parts in this case are the tubes, spars and rods. Of course these need to be adapted to an optimum form for this UAV's design. These parts are delivered in standard sizes and need to be cut or adapted to the sizes needed for this UAV. With this, stage 1.2 is reached where composite layers and plastic components are formed. The perspex windows for the LiDAR and the payload bay are also formed here. Lastly also the cutouts in the foam components (which are already formed in stage 1.1) are made. In this stage the cutouts where the fins will be attached are cut out of the foam and the part where the LiDAR is placed is cut out as well. Small cutouts such as holes for cabling are made in stage 1.3. In stage 1.3 the constituent parts are made ready for assembly and integration of the systems. In this stage the holes for the wires that go through the structure are made.

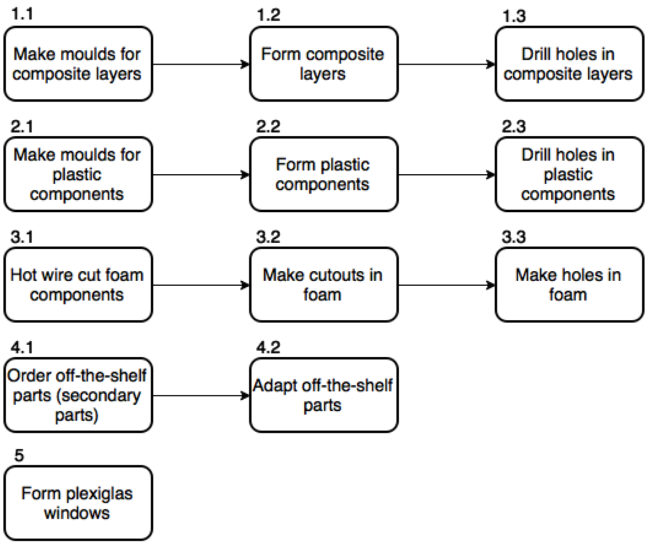

Figure 12.2: Manufacturing plan flow chart

After the manufacturing phase is finished, the assembly of the constituent parts can commence (see Figure 12.3. First the secondary parts such as the spars and tubes are attached to the foam body and wings. When this is done, the composite layer has to be attached to the foam body and the wings. The foam fins also have to be joined to the composite layer now. Parallel to this the perspex window can be attached to the payload bay. After this is done, the perspex window in front of the LiDAR is positioned from the inside (attached to the bottom part of the body), and the payload bay mounting has to be attached to the bottom of the body. Now the constituent parts have been assembled leaving two wings, one bottom body part, one top body lid, two large fins and two small fins.

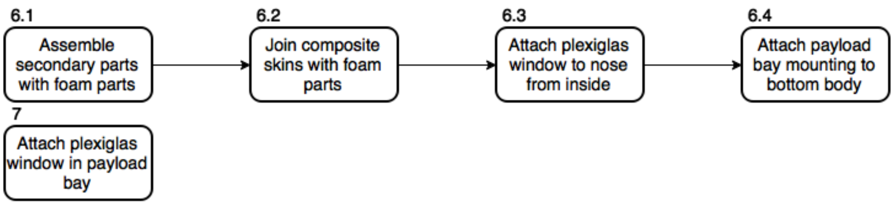

Figure 12.3: Flow chart of the assembly of constituent parts

When the assembly phase is finished, one can start with integrating the subsystems (see Figure 12.4). The LiDAR is positioned first together with the wire rope isolators, which are mounted on the bottom (with adhesive to the foam). Parallel to this also the servos in the wings can be integrated, together with its wires, and the communication antennas, transmitters and receiver can be attached. The GNSS antenna and weather sensor can also be placed on the top lid parallel to these processes. After this is done the Lisa/MX can be mounted together with the Aspirin, on the isolators. Furthermore the remaining GNC sensors are mounted in the body, and the antenna fairing can be attached to the bottom of the body. If this all has been done, the wiring can be laid out and all systems can be connected to the autopilot.

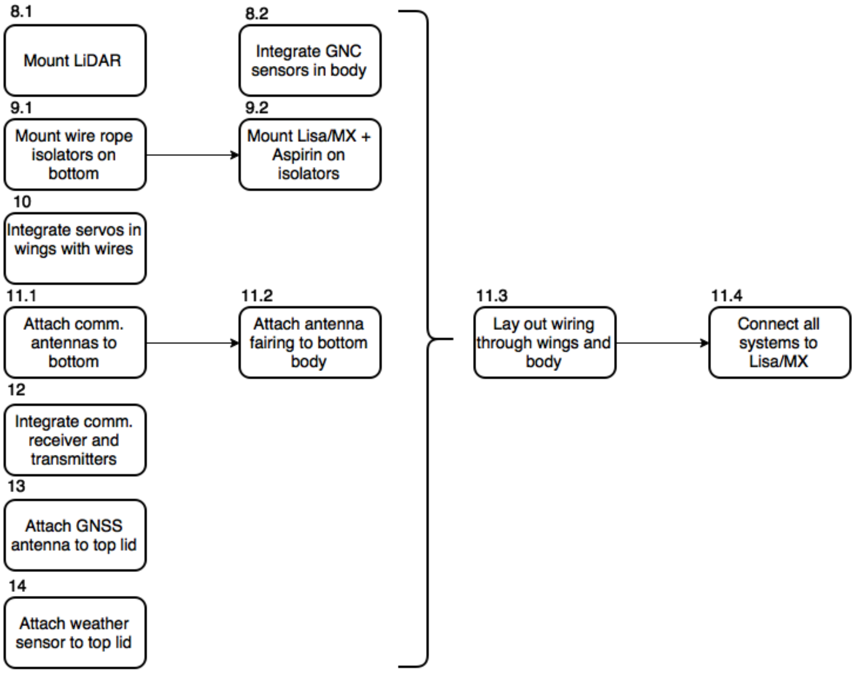

Figure 12.4: Flow chart of integration of subsystems until full end product

12.3. Cost breakdown

As all steps were defined for the further design and development phase, a cost estimation for this phase was made from which the acquisition cost are determined. The cost of all phases is split up into different topics as shown in Figure 12.5.

The total system cost were determined by the Eastlake model [15]. However, the Eastlake model applies to general aviation aircraft and is based on a statistical analysis taking into account, amongst others, structural weight. This gives a distorted view as the mass of MIRU is far lower than that of an aircraft. Thus for the cost assessment instead of the calculation for engineering hours needed, an estimation was made that next to the Design Synthesis Exercise, a team of 10 persons would continue for 0.6 business year full-time. This is supported by the idea that a student team works full-time for one year with 15 to 20 persons, however their products are larger [1]. For the tooling and manufacturing hours also estimations were made instead of calculating it and these came out to be 1000 h each, meaning that the production of one UAV takes 10 h with a production of 100 systems as explained in Section 11.1. This includes the learning curve, thus in the beginning the production will be very slow, but towards the end the engineers are more skilled and the process goes faster. The tooling needs 1000 h to produce all moulds and test the production methods as hot wire cutting as well as testing the most efficient assembly line. Also the cost for development support and flight tests needed to be altered, and for this 30% of the engineering cost and 20% of the development cost were taken respectively. As the cost for the material and propulsion are already known, these are put in instead of estimated. The results, rounded and corrected for FY2017 when the first unit will be put on the market, are shown in Table 12.1.

In the table, also the cost per flight hour is shown which are based on the replacement time of the batteries, storage, inspection and insurance.

[1] URL:`http://www.ecorunner.nl/the-team.html` [cited 26 June 2016]

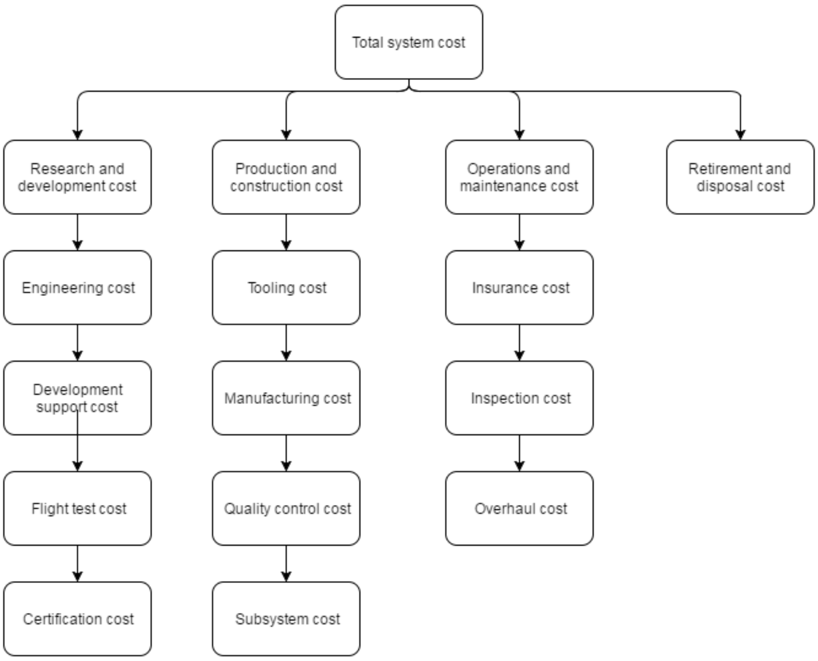

Figure 12.5: Cost breakdown structure of the full design project

Table 12.1: Product cost of MIRU

Name	**Cost** (€)
Minimum acquisition cost	34,500
Maximum acquisition cost	45,600
Cost per flight hour	59

The cost estimation is also confirmed with the performance based acquisition methodology for military UAVs [37]. The payload, weight and ground system estimation are not taken into account as the military generally has larger and heavier UAVs that are not specifically designed for mapping and expensive payload as a multispectral camera. Moreover they need ground equipment and systems that are more complex and introduce higher cost, which is the reason this is also not comparable.

Concluding design and development logic
After analysis of a full design process, the iterative loop between recommendations, design and testing is seen as the most time consuming period before the design can be taken into production. This phase will be done with 10 persons full-time for 0.6 business year. The production is then started in the three phases manufacturing, assembly and integration from which a final product can be delivered with a minimal acquisition cost of €34,500 and a maximum of €45,600.

13
Conclusion

Cost and time are two very valuable resources when an air accident investigation has to be performed. As these resources are needed even more when an aircraft has crashed in a remote area, there was a need for a solution that bridges the gap between the detailed, but incomplete information that can be gathered from the investigators on the ground, and the less detailed information gathered by satellites or aircraft. MIRU is designed to aid air safety investigators by facilitating a faster and lower cost investigation, while maintaining the completeness of the information gathered by aerial vehicles, but with the level of detail that can be obtained from the ground.

The UAV fills this gap with its modularity and compactness. It is lightweight (2.44 kg) and fits inside a backpack, such that investigators can carry it easily to an accident site. MIRU has two main missions in which it operates: the remote mission, where it locates the wreckage, coarse maps it and incidentally performs toxins detection, and the on site mission, where it detail maps the accident site. In order to map in a broad range of environmental conditions, MIRU carries a swappable payload which contains specific mapping devices for specific missions. These devices are a visible light camera to map during daylight, an IR camera to map in the absence of sunlight, and a multispectral camera, to locate the wreckage when it is camouflaged in its surroundings. It can also carry a toxin detection sensor, which is deployed when it is needed to know whether toxic or explosive gases are present before the investigators enter the crash site.

Furthermore, to be applicable in this wide range of environments, MIRU stands out because of its modularity. It can be operated in tailsitter configuration, where it can perform both horizontal flight, with a maximum endurance of 77 min, and vertical flight, where the maximum endurance is 16 min. This configuration is deployed when it has to be operated in a remote area and there is no take-off space, thus VTOL has to be performed. This configuration is also deployed when the UAV needs the ability to hover to perform toxin detection. When it is desired to increase the vertical flight endurance, for example to detail map during the on-site mission, MIRU can be transformed to a quadcopter by taking off the wings of the tailsitter and replacing these with caps. In this configuration the maximum endurance is 19 min. It can also be desired to increase the horizontal flight performance when the UAV is used as a communication relay or for remote mapping, when vertical flight is unnecessary. In this case, when no toxin detection or a VTOL is needed, MIRU can be deployed as a flying wing. In this configuration the maximum endurance is 122 min.

In order for MIRU to obtain this compactness and low weight, the UAV's structure is made out of foam and a carbon fibre layer on the outside. Furthermore, to enhance the strength of the structure, the internal structure consists out of two spars and two tubes. Using joints the UAV can be assembled in the different configurations. To ensure the endurance for each configuration, two battery packs are installed in the body, which are easily switchable. To assure the investigators with a smooth investigation process, the groundstation and UAV incorporate long range and short range antennas such that the UAV is always optimally connected to the investigators. By making use of the application on the groundstation tablets, the investigators can input targeted locations and track the route of the UAV. While mapping, the investigators receive images every two seconds, assuring an interactive and reliable mapping process. The investigators can also make use of the instant messages or speech communication on the tablets which goes over the communication relay of the UAV.

MIRU offers the solution to the time and cost problem that comes with remote air accident site investigations, and fills the niche between the ground observation and air observation. This market is rather small with an estimated offset of 100 units. However, other markets could use MIRU as a solution as well, such as in disaster struck areas or in gas detection applications. The demand on this problem solution in the air safety industry will not decrease due to the increasing number of aircraft and the increasing space accidents that may follow from the increasing amount of space tourism. Thus it is very feasible to develop MIRU and put it on the market. After it has been established that the design is feasible and ready for the market, the design goes into the detailed phase, where the more detailed features such as the joints and connections are designed. After this is done, the design will go into production. The final product that will be delivered has a minimal acquisition cost of €34,500 and maximum of €45,600.

14 Recommendations

When designing a system in limited time, there are always parts left which can be improved or added to the system. In this chapter recommended actions are discussed which can be added to the design later, which will improve the the safety, feasibility and robustness of the design.

Frise elevons
A common problem in making a roll movement is the tendency of the UAV to yaw in the opposite direction of the roll. The down-going elevon creates more lift, hence also more drag, which results in a yawing motion called 'adverse yaw'. A possibility to control this adverse yaw is by using Frise elevons. The Frise elevon is attached at an offset from the rotation point, so when deflecting the elevon upwards, the leading edge of the elevon is now pushed into the airstream creating more drag which should be enough to compensate for the adverse yaw [1]. In further development, these elevons could be necessary to reduce the adverse yaw effect if it occurs.

Elevon sizing
The validation of the sizing of the elevons was done through comparing the method used by Aircraft Design and reference UAVs. This resulted in a lower $b_a b^{-1}$ value as discussed in Section 8.6.2. For further development it can be investigated if obtaining a larger value for the $b_a b^{-1}$ parameter would be more efficient for controlling the UAV and parameters such as roll rate and turn radius can be evaluated.

Watertight design
Trade-offs made in the design phase of MIRU were not done with emphasizing on keeping the design watertight and weatherproof. For example the electrical components like the motors and servos are splash water proof, but not watertight. As recommendation, the design has to be made resistant to water. This adjustment will add weight to the UAV, reducing the performance. Therefore a whole new iteration process has to take place, but will definitely be advantageous for the use of the UAV, since new markets will open, for example the search and rescue in flooded areas and during heavy rainfall.

Better suited performance tools
When optimising the propulsion subsystem of the UAV, it was found that MotoCalc is a tool that is made by and for model aircraft enthusiasts. This can be motivated by the fact that the tool is based on test data rather than equations, and has simplified 2D aerodynamics instead of more accurate 3D aerodynamics. Due to outliers in the test data, the tool is also not designed to optimise a propulsion system.
It is recommended that for future design, a tool should be made based on equations of aircraft and rotorcraft performance, in combination with equations to calculate the performance of ESCs, electric motors and propellers, for which there were no resources available in the previous research. This tool can then be verified with MotoCalc as a guide line.

[1] URL: `http://www.boldmethod.com/learn-to-fly/aerodynamics/adverse-yaw-what-is-it-and-how-do-you-prevent-it/` [cited 13 June 2016]

Quick release lock pins
The connections between wing-main body and fins-main body are now secured with the use of bolts which are screwed into both tubes, as discussed in Section 8.7. Using quick release lock pins, the process of assembling the UAV can be made faster and easier[2].

Anti-icing tool
MIRU is designed to perform up until altitudes of 4500 m, but no anti-icing system is present. As with these altitudes, low temperatures are expected, the common problem is the formation of ice on the frontal surfaces of the wings. Therefore it is recommended to use anti-icing tools which remove the ice and leave the UAV operable in cold weather.

Receiver for ELT signals
In order to make searching a wreckage even more efficient, it might be wise to equip MIRU with a receiver for Emergency Locator Transmitter (ELT) and Personal Locator Beacon (PLB) signals. These signals are currently used by satellites to track the location of an accident [35], however the satellites do not always provide an accurate location. Receiving an ELT signal from a closer distance might greatly increase the accuracy of knowing the accident location, and a UAV even has the possibility to track the signal to its exact location. The signal is not always present, as it is dependent on whether the aircraft is equipped with a transmitter for such a signal.

Detailed ICE-operations
Currently, there are no detailed procedures set for in case of emergency operations. Also, it is not defined what exactly an emergency is. Emergency could be when the cruise motor fails in tailsitter configuration, and the UAV has to continue forward flight using the four hover motors. While analysing all these conditions, design flaws should be identified which have to be implemented in the design.

Transition
The transition method as proposed with an optimal climb and pull-up was realized with a simple tool which did not fully represent the real life dynamic behavior of the air around the aerofoil. Therefore, a more extensive tool is required or real test data should be acquired. One of the tools that can be used is X-plane[3], in which the whole design has to be implemented before the checks can be done. Although this is a tool that can confirm whether transition is possible, it will not output specific data of the manoeuvre.

Another method considered is the inverted pendulum method with external forces applied to it. This method was tried, however, the dynamic forces cannot be modeled in a sufficient accurate way as turbulence, stall and lift when would be taken up again were hard to determine. The initial results are however promising and therefore some more time could be invested to analyse this.

Perform detailed gust analysis
Only some basic calculations regarding gusts were made, due to limitations of the tools used and limited resources. To get a better view of the operational limits of the UAV detailed gusts analysis needs to be performed, so it is known at what weather conditions the UAV can operate.

Regulations
The last recommendation is to look more into regulations. As the design is now, only the government was taken into consideration. This will increase the market for MIRU, and make the UAV more safe to operate. One of the items could be to improve the visibility of the UAV and thereby increasing the compliance with regulations. Navigation lights should be added such that other airspace users, or ground teams can spot the UAV which will make the UAV safer to operate at night.

[2]URL:`https://www.rockwestcomposites.com/accessories/locking-mechanisms/quick-release-ball-lock-pins` [cited 24 June 2016]
[3]URL:`http://www.x-plane.com/desktop/home/` [cited 27 June 2016]

Bibliography

[1] Allegro MicroSystems, LLC. "Thermally Enhanced, Fully Integrated, Hall Effect-Based Linear Current Sensor IC with 100 $\mu\Omega$ Current Conductor", 2015. ACS758xCB Datasheet.

[2] Capable Computing Inc. MotoCalc, Software Package, Ver 8.09, 2015.

[3] Chitode, J.S. *Principles of digital communications.* Technical Publications Pune, 1st edition, 2008.

[4] Cobham plc. "Real-time surveillance just got lighter". Aviator UAV 200 Brochure.

[5] Hexcel Corporation. "Aerospace Selector Guide", Jan 2001.

[6] Hexcel Corporation. "Technical Fabrics Handbook", Dec 2010.

[7] Hexcel Corporation. "Reinforcements for Composites", Dec 2010.

[8] Hexcel Corporation. "HexPly M56", Feb 2014. FTA283c.

[9] Cypress Semiconductor Corporation. "USB-Serial Dual Channel (UART/I2C/SPI) Bridge with CapSense and BCD", 2015. Dual Channel (UART/I2C/SPI) Bridge Datasheet.

[10] Dassault Systemes. CATIA, Software Package, Ver 5.21.6, Oct 2013.

[11] Deperrois, A. "XFLR5 v6.02 Guidelines", Feb 2013.

[12] Deperrois, A., Scherrer M., Drela M. and Youngren H. XFLR5, Software Package, Ver 6.13, May 2016.

[13] Dräger Safety AG & Co. K. DrägerSensor & Portable Instruments Handbook, 2015.

[14] Federal Aviation Administration. Pilot's Handbook of Aeronautical Knowledge, 2008.

[15] Gudmundsson, S. *General Aviation Aircraft Design.* Elsevier Inc., 1st edition, 2014.

[16] Hewlett Packard. "HP Elitebook 8570w Mobile Workstation", June 2012. Specifications.

[17] Hoerner, S. F. *Fluid-Dynamic Drag.* Published by the author, 1st edition, 1965.

[18] Huber+Suhner AG. "Wires and cables for industrial applications", Sep 2015. Raychem 55PC0211 wire Specification Control Drawing.

[19] Evonik Industries. "ROHACELL IG/IG-F", Jan 2014.

[20] International Civil Aviation Organization. *Aircraft Accident and Incident Investigation.* International Standards And Recommended Practices, 1944.

[21] Jones, R.T. "Notes on the stability and control of tailless airplanes". Technical Report 837, National Advisory Committee For Aeronautics, Dec 1941.

[22] Jung, Y., Hyunchul-Shimy, D. and Ananthkrishnanz, N. "Controller Synthesis and Application to Hover-to-Cruise Transition Flight of a Tail Sitter UAV", Aug 2015.

[23] Kassapoglou, C. *Design and Analysis of Composite Structures.* Wiley, 2nd edition, 2013.

[24] La Rocca, G. Requirement Analysis and Design principles for A/C stability & control (Part 1) [Powerpoint slides], 2015.

[25] Littlefuse, Inc. "MEGA® Fuse Rated 32V", 2012. MEGA® Fuse Datasheet.

[26] Littlefuse, Inc. "473 Series, PICO® II, Slo-Blo Fuse", 2015. 473 Series, PICO® II, Slo-Blo® Fuse Datasheet.

[27] Lockheed Martin Corporation. "Design of UAV systems". online presentation, 2003. Week 6, communications.

[28] Lyon, C.A., Broeren, A.P., Giguere, P., Gopalarathnam, A., and Selig, M.S. *Summary of Low-Speed Airfoil Data*, volume 3. SoarTech Publications, Virginia, Dec 1997.

[29] MathWorks. MATLAB, Software Package, Ver R2015a-R2016b, 2015-2016.

[30] Maxtor. "M3 Portable External Hard Drive", Dec 2015. Specifications.

[31] Maxx Products International Inc. "MPI ACC347 Speed 400 Gear Box". MPI ACC347 Speed 400 Gear Box Datasheet.

[32] Megson, T. *Aircraft Structures for Engineering Students*. Butterworth-Heinemann, 5th edition, 2012.

[33] Müller, M. XcopterCalc, Software Package, Ver X6.70, 07.04.16, 2016.

[34] National Transport Safety Board. "Aviation Investigation Manual", Nov 2002. Appendix A, pages A-2 to A-6.

[35] National Transportation Safety Board. *Crash After Encounter with Instrument Meteorological Conditions During Takeoff from Remote Landing Site*. National Technical Information Service, Springfield, Virginia, 2011. NTSB/AAR-11/04 PB2011-910404.

[36] Novaković, Z. and Medar, N. "Analysis of a UAV Bungee Cord Launching Device", 2013.

[37] ODASA-CE Technomics. "Unmanned Aerial Vehicle System - Acquisition Cost Estimating Methodology", 2004. Cleared for open publication - March 22nd 2004.

[38] Ozdemir U., Aktas Y.O. and Vuruskan A. *Design of a Commerical Hybrid VTOL UAV System*. Springer, Oct 2013.

[39] Prouty, R. W. *Helicopter Performance, Stability, and Control*. Robert E. Krieger Publishing Company, 2nd edition, 1990.

[40] Raychem Wire & Cable. "Wire, radiation-crosslinked, modified, EFTE-insulated, general purpose, light airframe". Raychem 55PC0211 wire Specification Control Drawing.

[41] Ruijgrok, G.J.J. *Elements of airplane performance*. VSSD, Delft, the Netherlands, 2nd edition, 2009.

[42] Sadraey, M. H. "Aircraft Design, A Systems Engineering Approach", 2012.

[43] Skyview. "MetPak RG Weatherstation". 7 Reference Quality Parameters, Datasheet.

[44] Texas Instruments. "LSF0108-Q1 Automotive 8-Channel Multi-Voltage Level Translator (Rev. A)". 8-Channel Multi-Voltage Level Translator Datasheet.

[45] Texas Instruments. "LMZ22008 8-A Simple Switcher® Power Module With 20-V Maximum Input Voltage and Current Sharing", 2015. LMZ22008 Power converter Datasheet.

[46] Times Microwave Systems. "LMR lite-400 Flexible Low Loss Communications Coax", 2014. LMR lite-400 brochure.

[47] Traub, L.W. "Range and Endurance Estimates for Battery-Powered Aircraft", 2011.

[48] Yamaha. "EF2000iS", Feb 2011. Owner's Manual.

[49] Zenkert, D. *The Handbook of Sandwich Constructions*. Engineering Materials Advisory Services Ltd, 1st edition, 1997.

A
Technical drawings

The following figures contain the technical drawings of the UAV. In these drawings, the precise dimensions of the most important characteristics can be found. Figure A.1 the drawing of the flying wing configuration, Figure A.2 contains the drawing of the tailsitter configuration and finally, Figure A.3 details the quadcopter.

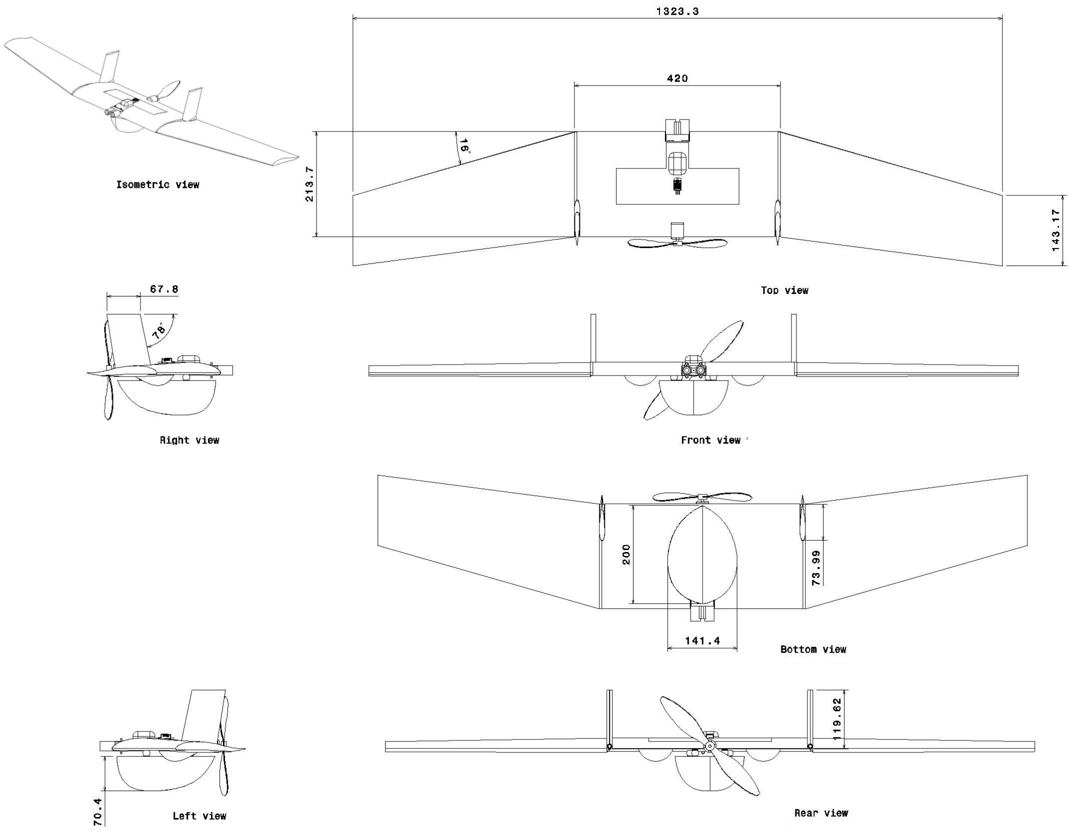

Figure A.1: Technical drawing of the flying wing configuration

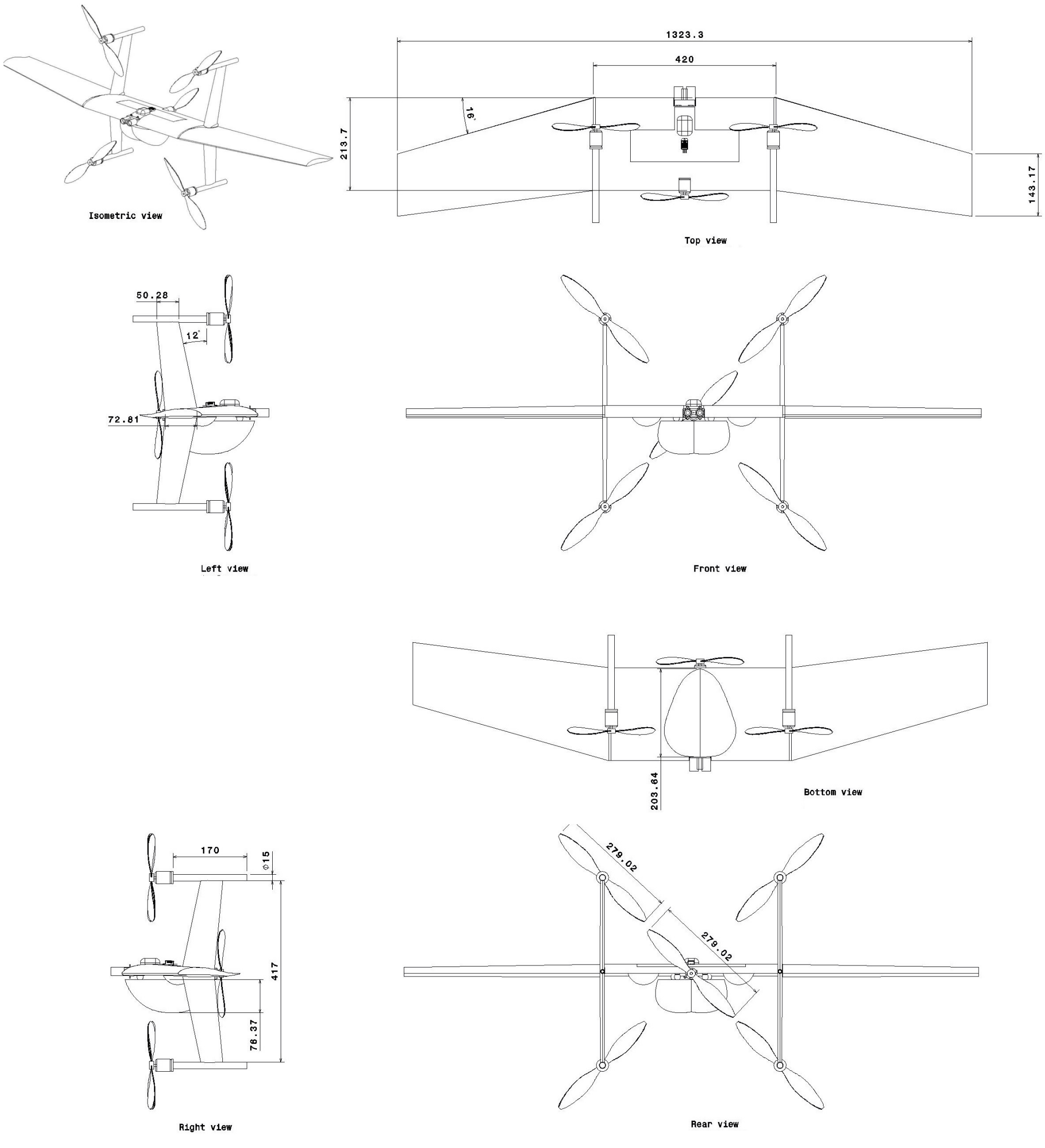

Figure A.2: Technical drawing of the tailsitter configuration

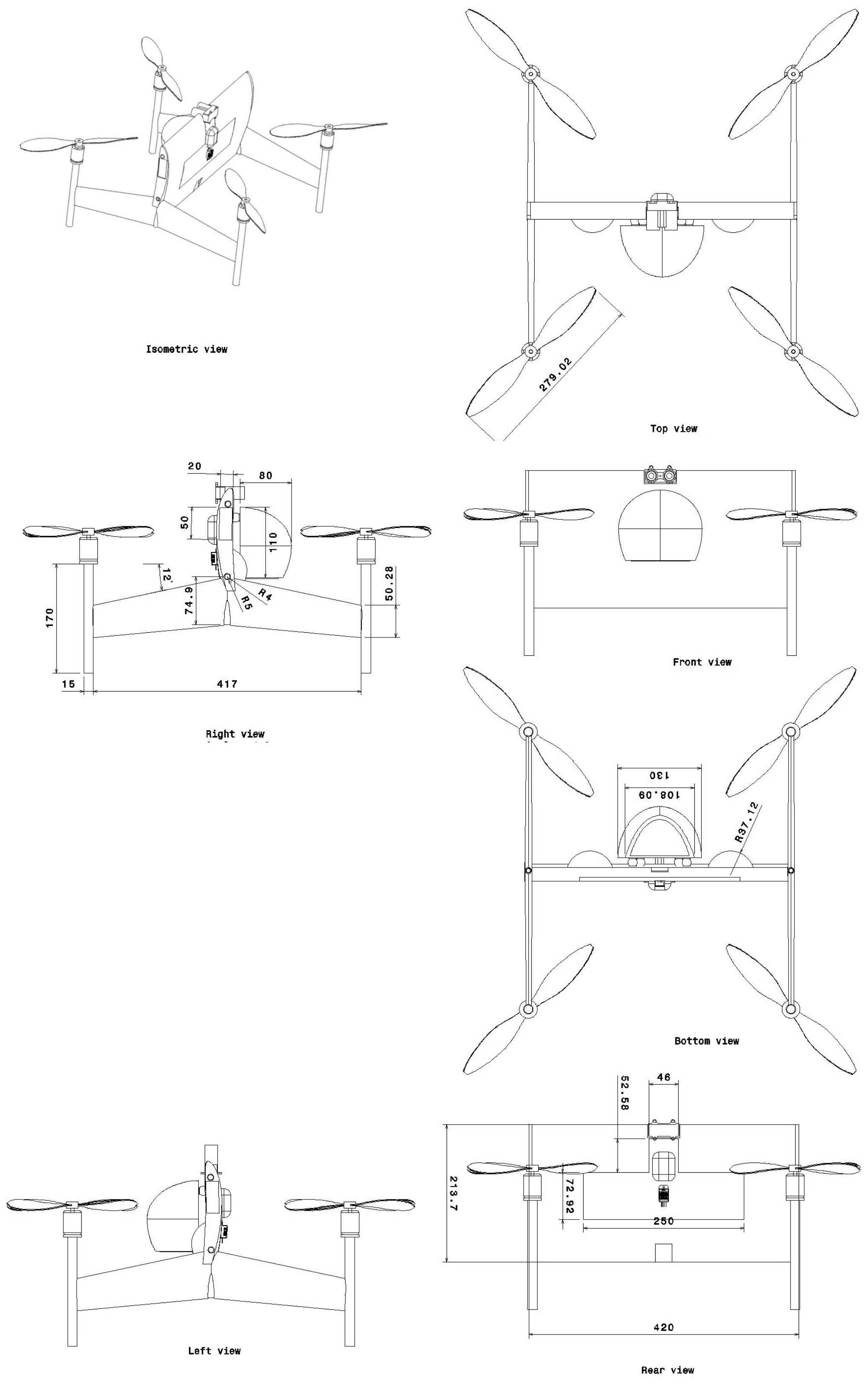

Figure A.3: Technical drawing of the quadcopter configuration

B
System functions

This appendix shows an in-depth breakdown and flow for the system functions as presented in Section 4.3. From the three configurations, the FFDs can be made. The tailsitter configuration covers almost all functions and is therefore considered first, see Figure B.1.

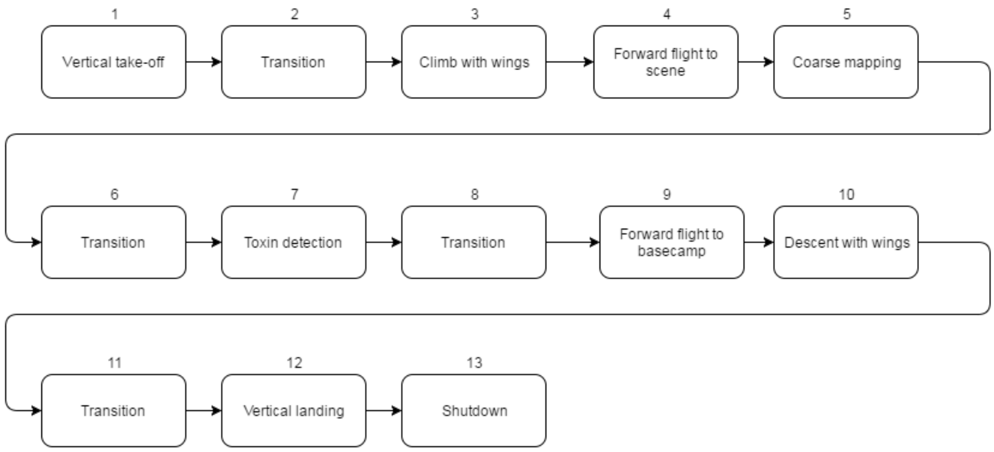

Figure B.1: FFD of the tailsitter configuration

When the tailsitter is transformed to the flying wing configuration, the transition function drops out as it is no longer needed to fly vertically. However, the take-off and landing methods have to be changed now as it can no longer do this vertically. Thus a bungee cord launch and a belly landing are added as can be seen in Figure B.2.

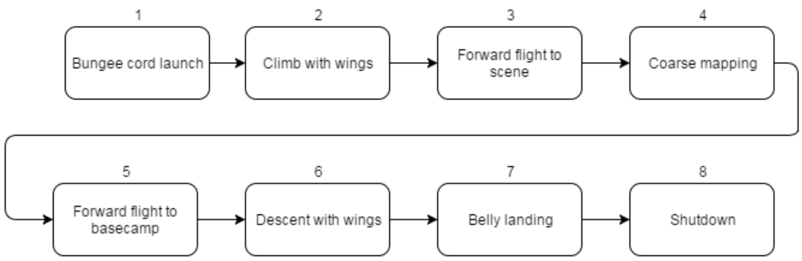

Figure B.2: FFD of the flying wing configuration

For the quadcopter all elements involved with horizontal flight are left out, so that the elements in Figure B.3 are left.

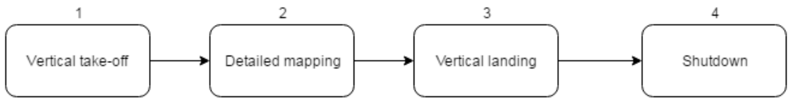

Figure B.3: FFD of the quadcopter configuration

Figure B.4 shows the functions necessary for forward flight. The flow presented in the figure is for the tailsitter, but for the flying wing, only the number would change ranging from REF 3 to REF 4, seen in Figures B.1 and B.2.

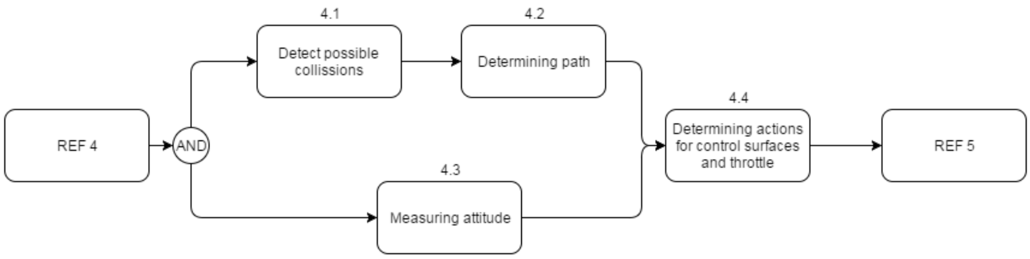

Figure B.4: Forward flight to scene for tailsitter configuration

Figure B.5 presents the coarse mapping of the tailsitter. Again, the flow presented in the figure is for the tailsitter, but for the flying wing, only the number would change ranging from REF 4 to REF 5. For the quadcopter this would differ a bit more. Now block 5.1.1 will drop out, as the quadcopter does not locate the accident site as it is already on the site. The locating of the accident site is done by either the tailsitter or flying wing, the quadcopter only maps the site. So block 5.1.2 changes from coarse mapping into detailed mapping. Other than that, the numbers change so that it ranges from REF 2 to REF 3.

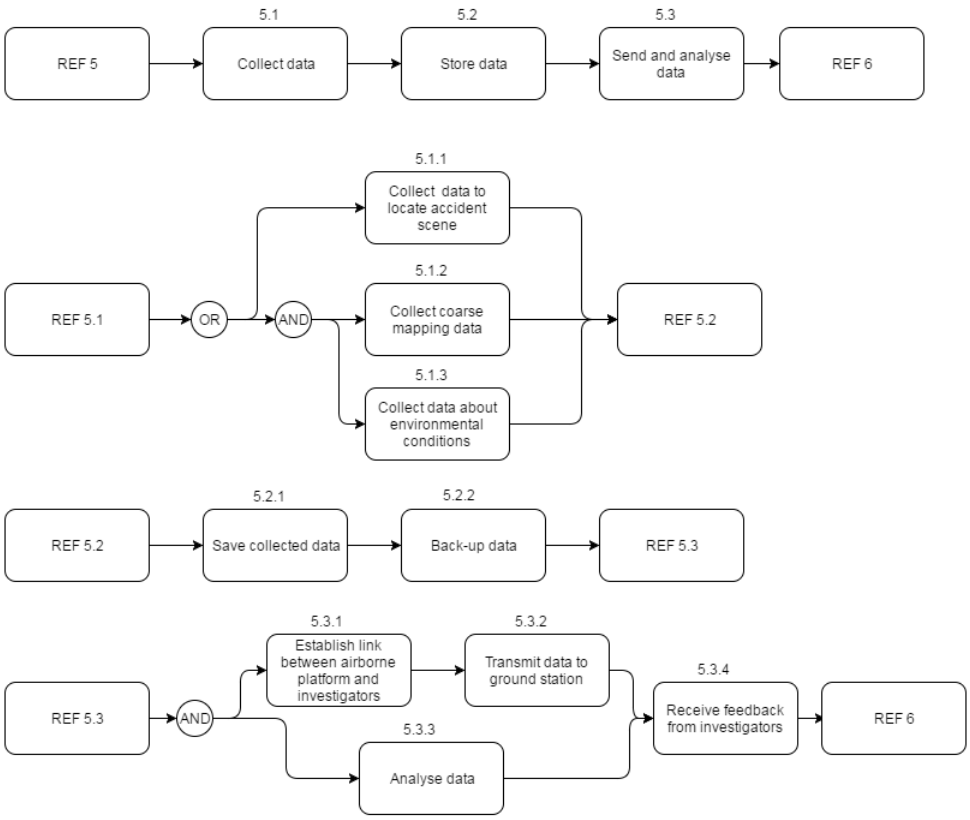

Figure B.5: FFD for mapping for the tailsitter

Figure B.6 presents the safe mode initialisation of the tailsitter. The flow for the flying wing and quadcopter would be exactly the same, only the numbers change to REF 9 and REF 5 respectively.

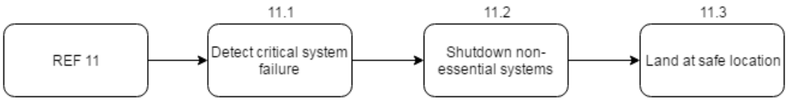

Figure B.6: Safe mode initialisation for tailsitter

Figures B.7, B.8 and B.9 present the FBS. The FBS include the same functions as in the FFD, but they are now grouped together for each specific function.

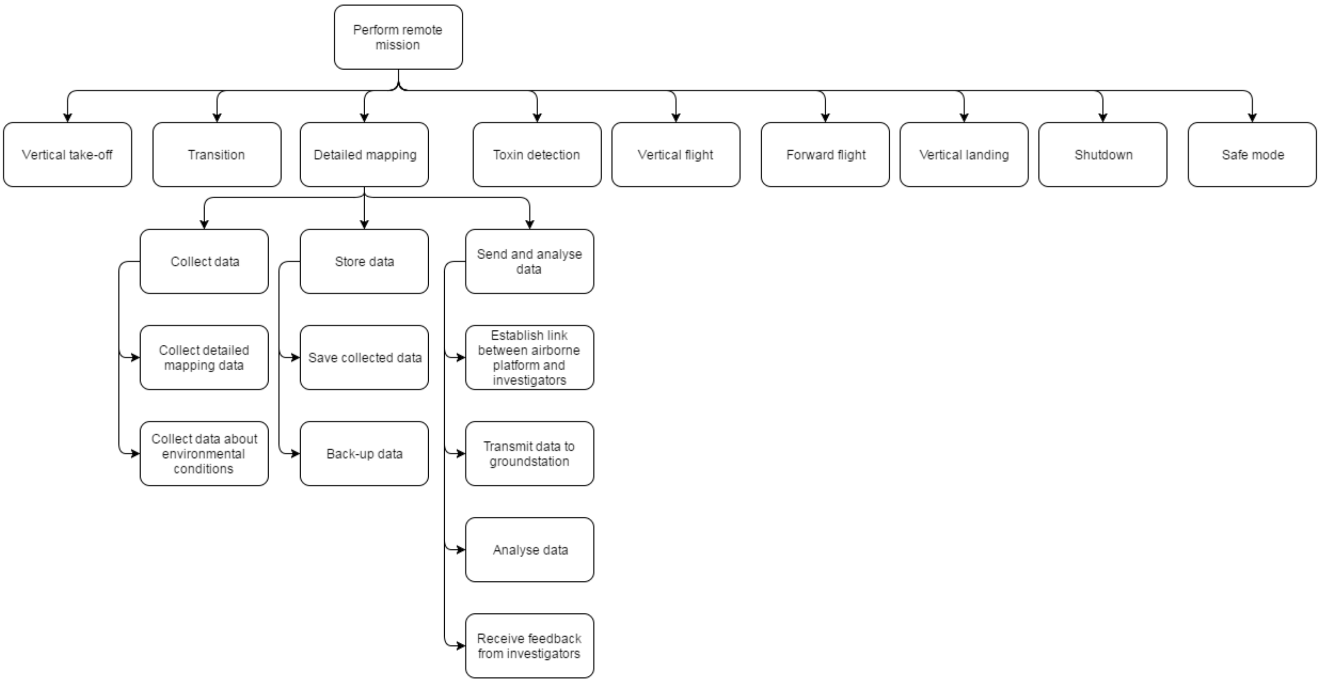

Figure B.7: FBS of tailsitter configuration

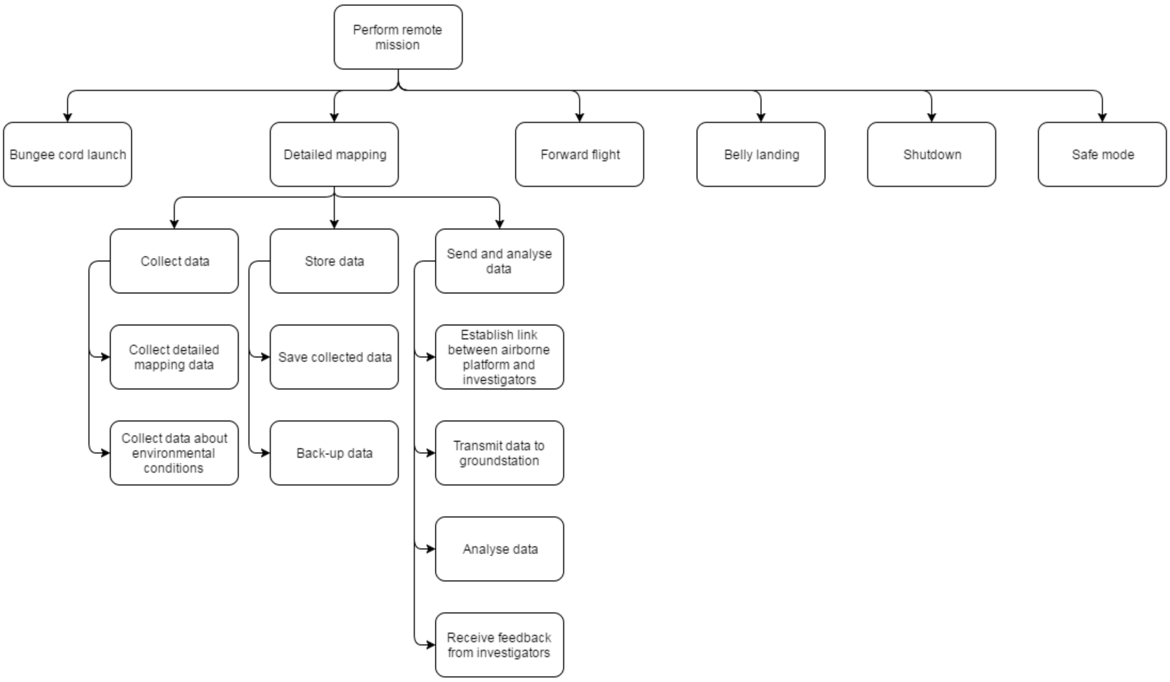

Figure B.8: FBS of flying wing configuration

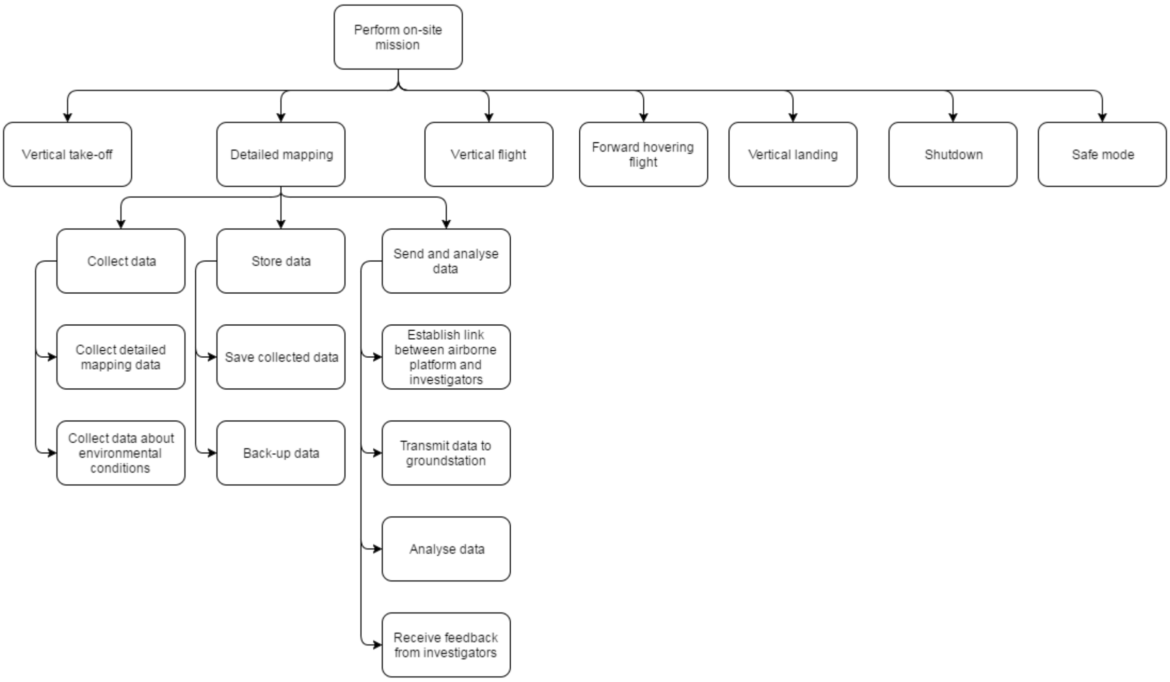

Figure B.9: FBS of quadcopter configuration

C
Electrical subsystem components and layout

The electrical subsystem is responsible for providing a solid communication and power connection between electrical components. Due to a different voltage level or communication protocol, some electronic components were added, which again causes more connections to be taken care of. An overview of these components can be seen in Table C.1. Next to the location of all the electrical components, the current flowing from and to them, as well as their power usage needs to be monitored. An overview of the power consumption of all the active -power consuming- electrical components can be seen in Table C.2.

Table C.1: Overview of electronic components used

Component	Model	Power consumption (mW)	Mass (g)
5 V regulator[45]	LMZ22008	0	10
Level shifter (x2) [44]	SN74LVC245A	0	2 (x2)
Digital converter bridge[9]	CY7C65215 Dual Channel Bridge	0	5
Analog to digital converter	FrSky SP2UART	100	3
Current sensor[1]	ACS758KCB-150U	25	5
Voltage sensor	E96 Voltage divider	0.20	2
Low current fuse[26]	Littlefuse 473 Series	0	2
High current fuse[25]	Littlefuse MEGA	0	5
	Total	125.20	36

Table C.2: Detailed component power budget

Subsystem	Component	Peak power (W)	Time on during mission	Average power (W)
Control	Servo 1	1.00	50% of mission time	0.50
	Servo 2	1.00	50% of mission time	0.50
	Subsystem total	2.00	-	1.00
G&N	Lisa Mx	0.50	Continuously	0.50
	GNSS Receiver	1.16	Continuously	1.16
	LiDAR	0.75	Continuously	0.75
	LiDAR servo	0.50	5 s	0.00069
	microcantilever (x2)	0.05	Continuously	0.05
	IMU	0.021	Continuously	0.021
	Subsystem total	3.03	-	2.53
Communication	Receiver	0.55	Continuously	0.55
	Transmitter	0.30	Continuously	0.30
	Subsystem total	1.15	-	1.15
Payload	Camera	2.50	45 min	0.63
	Toxin detection	0.66	15 s	0.0017
	microSD	0.33	Continuously	0.33
	Weather sensor	0.01	Continuously	0.01
	Subsystem total	3.50	-	0.97
Electronics	Current sensor	0.03	Continuously	0.03
	Digital converter	0.10	Continuously	0.10
	ADC	0.10	Continuously	0.10
	Subsystem total	0.23	-	0.23
	Overall total	9.90	-	6.37

It should be noted that the factor of 50% operation in Table C.2 is chosen because the peak power, 1 W per servo, is the stall power of the servo, or the power at which the servo delivers its maximum torque[1]. In reality, servos are operated as efficiently and as far from this stall power as possible, and thus, a factor of 50% was used. When the power required for all the electrical components has been added, the power the wiring needs to withstand was calculated. With that, the wires listed in Table C.3 were chosen.

Table C.3: Types of aerospace grade wiring used

Type	Wire density (gm^{-1})	Maximum Current (I)	Total length (m)	Total mass (g)
Radox KDJ-11 10 mm^2 [18]	111	132	0.30	33.30
Radox KDJ-11 1.5 mm^2 [18]	20	29	5.85	117.00
Raychem 55PC0211 AWG 26 [40]	2.05	3	13.88	28.50
		Total	20.03	178.80

Keeping an overview of all the connections requires neat bookkeeping, and figures and tables help a lot with this compared to lists or text. Because of that, Figure C.1 was made where all the connections between components can be seen in a qualitative way.

With this figure, the quantitative Table C.4 was made which includes all the connections between the electrical components and the length, the number of wires and the type of wiring used per connector. This helps in budgeting the wiring mass, and identifying problems with the location of components from an electronics point of view.

[1] URL:`http://www.servodatabase.com/servo/towerpro/mg92b` [cited 16 June 2016]

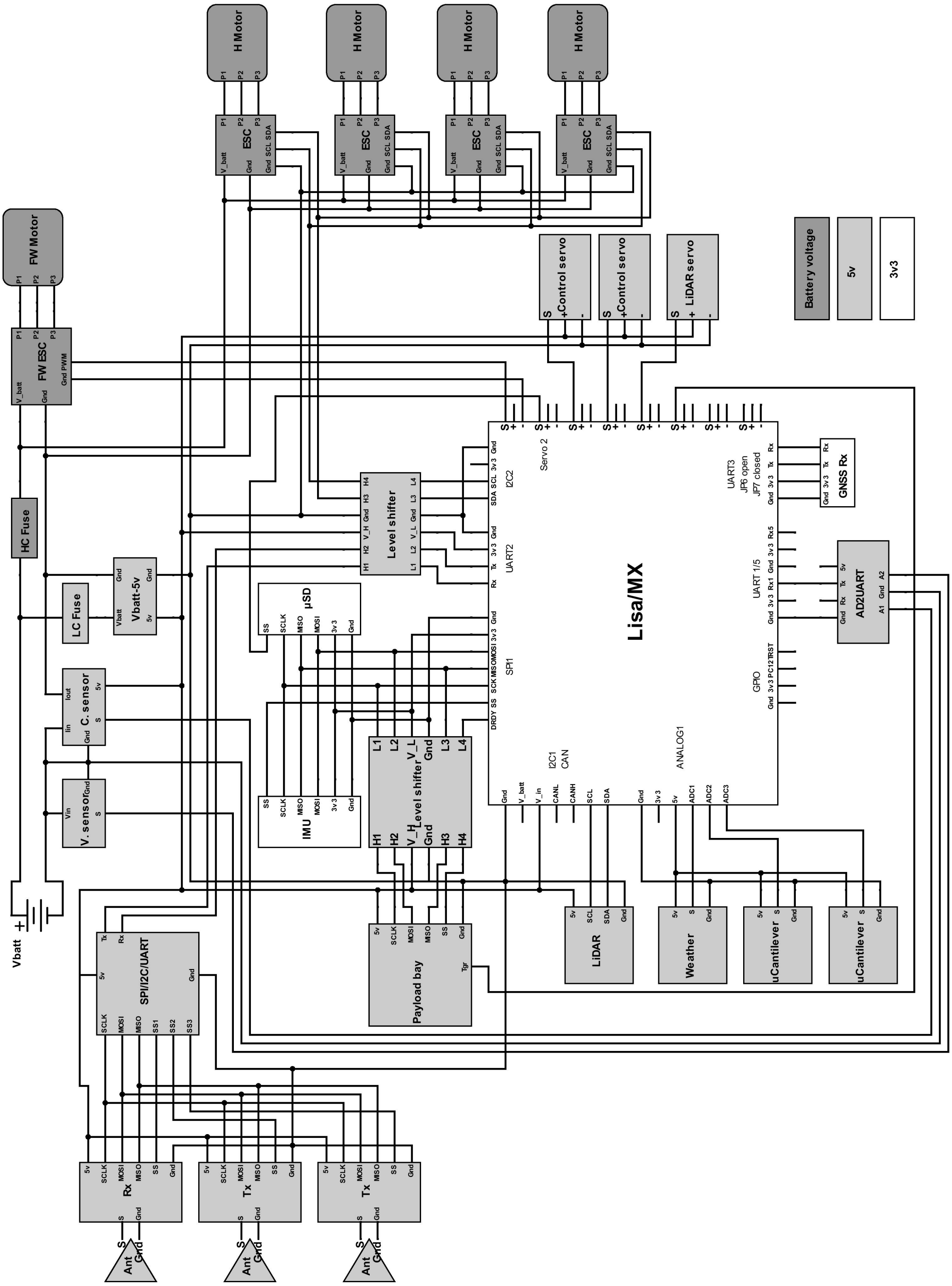

Figure C.1: Detail of electrical connections

Table C.4: Quantitative overview of all electrical connections

	From	To	Type	Length (m)	# wires	Mass (g)
Power & Propulsion	battery	splice	power	0.15	2	33.30
	splice	ESC FW	power	0.05	2	2.00
		ESC H (x4)	power	0.25	2	10.00
	battery	5 V regulator	power	0.02	2	0.12
	ESC FW	Motor FW	power	0.05	3	3.00
	ESC H	Motor H (x4)	power	0.30	3	18.00
	5 V regulator	Level shifter 1	power	0.02	2	0.12
	Lisa MX	Level shifter 1	power	0.05	2	0.29
		Level shifter 1	signal	0.05	4	0.41
	Level shifter 1	ESC H 1	I2C2	0.25	3	1.54
	ESC H 1	ESC H 2	I2C2	0.05	3	0.31
	ESC H 2	ESC H 3	I2C2	0.55	3	3.39
	ESC H 3	ESC H 4	I2C2	0.05	3	0.31
GNC	Lisa MX	GNSS Rx	power	0.10	2	0.59
		GNSS Rx	UART3	0.10	2	0.41
		uCantilever (x2)	power	0.10	2	0.59
	Lisa MX	uCantilever (x2)	analog	0.10	1	0.21
	Lisa MX	weather sensor	power	0.15	2	0.88
		weather sensor	analog	0.15	1	0.31
	5 V regulator	LiDAR	power	0.10	2	0.59
	Lisa MX	LiDAR	I2C1	0.05	2	0.21
	5 V regulator	Servo (x2)	power	0.5	1	1.47
	Lisa MX	Servo (x2)	PWM	0.50	2	2.05
Communication	5 V regulator	Tx (x2)	power	0.10	2	0.59
		Rx	power	0.03	2	0.18
		Digital converter	power	0.03	2	0.18
	Tx	Digital converter (x2)	SPI	0.05	4	0.41
	Rx	Digital converter	SPI	0.05	4	0.41
	Level shifter 1	Digital converter	UART2	0.05	2	0.21
Mapping	Lisa MX	Payload	PWM	0.05	1	0.10
	Level shifter 2	Payload	SPI	0.10	4	0.82
	5 V regulator	Payload	power	0.10	2	0.59
	Lisa MX	Level shifter 2	power	0.05	2	0.29
	5 V regulator	Level shifter 2	power	0.03	2	0.18
	Lisa MX	Level shifter 2	signal	0.05	4	0.41
	microSD	Level shifter 2	signal	0.2	4	1.64
Electrical	Battery	Current sensor	power	0	0	0
		Voltage sensor	power	0	0	0
	ADC	Current sensor	analog	0.05	2	0.21
		Voltage sensor	analog	0.05	2	0.21
	Lisa MX	ADC	analog	0.05	2	0.21
	5 V regulator	ADC	power	0.03	2	0.189
		Current sensor	power	0.03	2	0.18
					Total	176.34

D
Detailed budgets

This appendix shows a summary of the mass, cost and power budgets for the UAS. This includes the UAV, its payload and the groundstation. All values can be found in Table D.1. For the power of the propulsion and power subsystem and the payload subsystem, a range is given as it really is dependent on the mission and configuration.

Table D.1: Detailed mass, cost and power budgets

Part	Function	Amount	Total weight (kg)	Total cost (€)	Total power (Wh)
UAV			**2.02**	**2362.82**	**10.6**
GNC			**0.115**	**1673.98**	**4.2**
Lisa/MX	Autopilot	1	0.0232	202.20	0.83
Aspirin	IMU	1	0.0009	8.70	0.83
Microcantilver	Airspeed sensor	2	0.014	100.00	0.0833
GNSS receiver	Position determination	1	0.019	1200.00	1.925
GNSS antenna	Position determination	1	0.034	21.98	0
LiDar	Object detection	1	0.022	141.10	1.25
Control surfaces			**0.038**	**16.00**	**1.67**
Servo	Elevon deflection	2	0.038	16.00	1.67
Electrical system			**0.951**	**141.83**	**0.55**
Wires	connect components	1	0.21	40.00	-
Battery	Energy source	1	0.7	58.00	-
Connectors	-	-	0.041	43.83	-
128 GB SD	Data storage	1	0.001	94.00	0.55
Communication			**0.056**	**126.22**	**1.9**
Antenna (SR)	-	2	0.030	41.00	-
Antenna (LR)	-	1	0.02	18.00	-
Transmitter	-	2	0.0005	43.00	0.5
Receiver	-	1	0.0005	23.00	0.9167
Coax cables	-	-	0.005	1.22	-
Propulsion and power			**0.593**	**321.40**	**18 - 400**
Motor	-	5	0.363	85.40	18 - 400
Propeller	-	5	0.075	129.20	-
Controller	-	5	0.1	99.60	-
Spinner	-	4	0.032	9.60	-
Gearbox	-	1	0.023	19.60	-

Part	Function	Amount	Total weight (kg)	Total cost (€)	Total power (Wh)
UAV			**2.02**	**2362.82**	**10.6**
Airframe			0.492	**160.44**	-
Wing	Provide lift	2	0.177	33.82	-
Large vertical fin	Provide stability	2	0.040	4.52	-
Small vertical fin	Provide stability	2	0.007	0.71	-
Main body	Carry payload	1	0.17	70.39	-
Payload fairing	Protect payload	1	0.06	5.00	-
Antenna fairing	Protect antennas	2	0.02	10.00	-
Engine tubes	Carry engines	4	0.018	36	-
Others					
Groundstation			**51.40**	**8861.61**	**205.27**
Battery	Energy source	12	8.4	696..00	-
Battery charger	Charge batteries	1	1.5	185.00	-
Battery board	Parallel charging	4	0.08	36.00	-
Tablet	Communication	4	1.56	1026.88	19.7
LR communication	-	1	2.15	414.32	5.1
Weatherstation	Weather update	1	4.1	3750.00	0.2
HP Elitebook	Data processing	1	3.1	1250.00	179.12
128 GB SD card	Storage	4	0.005	376.00	0.55
4 TB hard drive	Storage	1	0.2	140.00	0.6
Generator	Energy generation	1	20.0	882.00	-
Unleaded fuel	Fuel for generator	-	1.0	2.10	-
Bungee rope	Launch device	1	0.100	8.74	-
Table and chairs	Comfort	1	5.2	94.57	-
Payload			**0.417**	**8185.21**	**1.875 - 2.44**
Mapir Survey 2	Mapping camera	1	0.047	400.00	1.875
Micro Rae	Toxin detection	1	0.18	791.21	1.875
FLIR Vue Pro R	Thermal imaging	1	0.10	3499.00	1.875
Tetracam ADC Snap	Multispectral camera	1	0.09	3495.00	1.875

E
Transportation casing dimensions

All components of MIRU are transported to the basecamp in a truck. To design the casing, the dimensions of the components and their weight were tabulated. This is presented in Table E.1. In total, MIRU is transported in three boxes. The horizontal lines in the table indicate the components in each box. From the basecamp, all components necessary for the on-site mission are carried in a backpack. Check marks in the table represent these components. Two battery packs are brought, as indicated by a double check mark.

Table E.1: Transportation case dimensions and mass

Component	Size ($lxwxh$ in mm)	Mass (kg)	Brought in backpack
Backpack	590 x 360 x 250	1.8	✓
Wings including small fins	545 x 240 x 70	2.00	✓
Fins including engine mounts	300 x 70 x 40	0.49	✓
Body	430 x 225 x 70	0.90	✓
Flying wing payload fairing and multispectral camera	230 x 160 x 125	0.66	-
Tailsitter payload fairing and toxin detector	210 x 155 x 105	0.74	-
Quadcopter payload fairing, IR camera and visible light camera	125 x 120 x 110	0.56	✓
UAV battery (packed per eight batteries, three necessary)	190 x 110 x 90	3.19	✓✓
Laptop	390 x 265 x 45	4.07	-
Tablet (one, four necessary)	220 x 150 x 25	0.92	-
UAV battery charger	285 x 180 x 70	2.10	-
Long range communication	315 x 240 x 150	2.23	-
Long range communication tripod	500 x 100 x 100	2.00	-
Weatherstation	360 x 300 x 150	2.91	-
Weatherstation tripod	660 x 100 x 100	2.66	-
Foldable table with chairs	945 x 430 x 165	6.57	-
Electricity generator	500 x 465 x 290	21.2	-
Generator propellant	285 x 135 x 75	2.00	-

F

Payload component characteristics

F.1. Camera characteristics

In this table the camera characteristics and the ground resolution at a height of 100 m are given.

Table F.1: Camera characteristics and ground resolutions of the Mapir Survey 2, FLIR Vue Pro R and the Tetracam ADC Snap

	Mapir Survey 2	**FLIR Vue Pro R**	**Tetracam ADC Snap**
Sensor width (mm)	6.174	-	6.59
Sensor height (mm)	4.631	-	4.9
Focal length (mm)	2.8	19	8.43
Pixels width (n)	4608	640	1280
Pixels height (n)	3456	512	1024
Survey altitude (m)	100	100	100
HAOV (rad)	1.668	0.559	0.32
VAOV (rad)	1.382	0.419	0.25
Width of field (m)	220.5	57.35	66.5
Height of field (m)	165.4	42.63	51.3
Pixels per meter width (n)	21	11	20
Pixels per meter height (n)	21	12	20

F.2. Ground resolution analysis research

With this research it was analysed which ground resolution was necessary for recognition in the remote mission, and for identification in the on-site mission. The research was done using the Samsung NX500 camera, which has adaptable pixel formats, so that different resolutions could be compared and a good analysis could be performed for the desired resolution of the payload for this UAV [1]. The camera specifics are given in Table F.2 in Appendix F. The photos from this research were analysed and using the camera specifics a resolution in pixels per meter was calculated for each pixel format setting. From this research, it resulted that for coarse mapping a ground resolution of 15 pxm^{-1} up to 50 pxm^{-1} is needed from an altitude of 100 m, in order to recognise the wreckage. For detailed mapping a ground resolution of 250 pxm^{-1} up to 520 pxm^{-1} was desired from an altitude of 10 m. Note that these tests have been performed during daylight in urban areas. The obtainable ground resolution with this camera at an altitude of 100 m, 50 m and 10 m were analysed, and the results for an altitude of 100 m are given in Table F.2. In this table the camera characteristics can be seen, and for reference also the ground resolutions obtained at an altitude of 100 m are given. Note that the tests have been performed during daylight. Furthermore, in Figure F.1 two pictures are depicted which were taken during this research. Here the difference can be seen between identification and recognition.

[1] URL:`http://www.samsung.com/us/photography/digital-cameras/EV-NX500ZBMIUS` [cited 9 June 2016]

Table F.2: Camera characteristics of the Samsung NX500

Samsung NX500			
Sensor width (mm)	23.5		
Sensor height (mm)	15.7		
Focal length (mm)	16		
Pixel formats	6480 x 4320	Ground resolution at 100 m (pxm^{-1})	51.87
	4320 x 4320		34.50
	4560 x 3040		36.50
	3264 x 2176		26.13
	2160 x 1408		17.29
	2112 x 1408		16.90
	2048 x 1152		16.40

(a) Example of identification: 100 pxm^{-1}

(b) Example of recognition: 25 pxm^{-1}

Figure F.1: Ground resolution examples for identification and recognition

F.3. Toxins sensors principles

There are four possible types of gas detection suited for this UAV, namely: electrochemical sensors, catalytic bead sensors, IR sensors, and PID sensors [13].

An electrochemical sensor can be seen as a micro-reactor, which produces a current as a certain gas passes through it. This method, however, is susceptible to cross sensitivity which means that it might produce a signal, if a gas of the same type passes through it which reacts more easily than the desired measured gas.

A catalytic bead sensor works on the principle that flammable gases and vapours can be oxidised, which releases reaction heat. This is achieved with a suitably heated catalyst material, where the reaction heat increases the resistance, which in turn can be measured. This yields an accurate reading of the quantity of the gas present.

IR sensors are used to detect the presence of hydrocarbons in the air. Since these hydrocarbons have a specific absorption wavelength (3.3-3.5 μm), when hydrocarbons are present some of the IR light is absorbed. The degree of absorption then determines the abundance of hydrocarbons.

Lastly, PID sensors are used to either detect entire groups of gases or, if it is calibrated accordingly, it can be used to detect an individual substance. The PID sensor works by drawing in air through a porous membrane into the measurement chamber, where an UV-lamp generates photons which ionise certain molecules in the gas flow. This ionisation degree can be measured with electrodes.

G

Microcantilever working principle

Microcantilevers measure its vibrations and air deflections to gather information about the surrounding airflow. The output is transmitted to the autopilot. In the case of MIRU, two microcantilevers are used, one to measure the angle of sideslip and angle of attack which is positioned in line with the airflow, and one to measure the air pressure, so it is positioned perpendicular to the airflow.
The working principle can be explained by the use of Figure G.1 [1]. The micro cantilevered beam is coated with a piezoresistor layer, and in its original position it is deflected upwards. When the wind flows around the beam, it is deflected downward due to the force. This deflection downward causes a change in cross-sectional area, and hence a change of the resistor. This change in resistance is measured and communicated to the autopilot. In this way changes of resistance are continuously communicated to the autopilot.

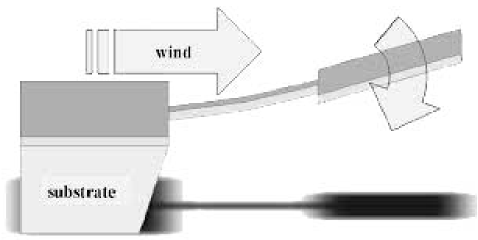

Figure G.1: Working principle of microcantilevers

[1] URL: `www.mdpi.com` [cited 30 May 2016]

H

Verification and Validation procedures

Multiple tools were developed to design the MIRU, which were all verified and validated. This ensures that the obtained results of the tools are correct and credible. This chapter shows the used procedures for the different types of tools. The verification procedure was similar for all tools and is discussed first. Later some specific verification techniques are given per tool. Next, the individual validation methods are discussed for the Matlab [29] based tools followed by the different Excel and off-the-shelf tools.

H.1. Verification

First of all, it was determined that all model assumptions adhered to the real system specifications. The simplifications did not cause any implications which limit the model appliance. The simulations always simplified reality, but that is the nature of simulations and why they were used in the first place. Evidence was provided to ensure the model did reflect the real world as accurately as necessary.
Once the models did represent the purpose, the model was turned inside out with respect to the content. General variable checks, unit tests and bug checkups were imposed. In the code separate sections were defined, where the sub-results were checked.
The calculation to obtain the results were based on reference sources. Thus the equations and methods were verified on their own. However the application and integration of the calculations in the model had to comply to the results. Thus the behaviour of the results was analysed next.
The manner of the results was checked with respect to a scenario, where the input variable were zero. The output was verified to also equal zero. Furthermore the mechanics of the model and the real system are known, therefore their interaction was evaluated from a specialists view. The behaviour of the results was justified, when the input variables were increased or decreased.
Now some specific verification techniques will be discussed, which were used on top of the previously described techniques.

H.1.1. Matlab code

For all structure tools multiple force checks were performed. Therefore it was continuously made sure that no loads were lost or amplified during the calculations. Furthermore each calculation was checked before it was added to the main loop of the model. All sub-calculations and stress distributions were plotted individually to understand and verify the results.

The transition tool was verified by starting with ballistic trajectories. The acceleration, velocity and position for these trajectories are well known thus easy to check. The next step is to add -per direction- the drag. Therefore, the drag coefficients have been checked for all angles and were investigated separately from the ballistic trajectories. Finally, the addition forces and accelerations were added one by one to check their influence on the result.

The tools for hovering climb and forward flight were checked by calculating the output variables by hand and checking these with the output of the tool.

Furthermore all code was checked by a separate team member other than the developer of the code to verify the code.

H.1.2. Excel

For several subsystems, Excel was used for simple calculations and bookkeeping of all the different values. The advantage of Excel is that simple calculations can be extrapolated, and the matrix-like sheets give a better overview compared to the line-based Matlab.
In order to keep the Excel sheets free from mistakes, the calculations were thoroughly checked before implementation and double checked by a team member other than the creator of the sheet. Next to that, as the equations used in the Excel sheets are very simple and have few variables, a one-factor-at-a-time approach is used to check if the impact of changing a variable is according to expectation. Also manual calculations were done to ensure the equations are correct and the right input variables are selected.

H.1.3. Off-the-shelf tools

MotoCalc [2], XcopterCalc [33] and XFLR5 [12] were used and thus must be verified. The tools themselves are already verified by the tool developers, but the user should also understand the outcome of the program. Therefore this verification process is also a verification of the user of the team instead of solely the tool.

MotoCalc

For the performance of the UAV in horizontal flight, first a Matlab program was made in order to model the performance of brushless permanent magnet motors. Due to limited resources, this tool could not be verified to a usable extend. Because of this, MotoCalc was used. This empirical tool bases its results on a large database of propeller, gearbox, ESC, motor and battery combinations, which are analysed independently. These combinations are analysed together with a simplified model of the UAV with span, wing area, mass and airfoil data as input.

During the optimisation process of choosing the best propeller-gearbox-motor-ESC combination, the filled in variables were constantly checked by the main user, and a team member other than the main user. After becoming familiar with the characteristics, the one-factor-at-a-time approach was used at regular intervals to check if the impact of a change in a variable was according to expectation. This could only be done by the main user, as it required some experience with the tool to estimate the impact of a change in one of the variables, which made the tool hard to verify.

xctoperCalc

This tool was verified by changing certain input and checking if the output showed the behaviour as it was expected. This expected behaviour was based on literature or general knowledge.

The parameters that were used for verification were the UAV mass, battery capacity, motor no-load current, motor internal resistance, motor Kv-value, propeller diameter and propeller pitch. For an increase in mass an increase in electrical and mechanical power was expected. This was also observed using the tool.
With an increase in battery capacity the same electrical and mechanical power was expected. A constant mechanical power was discovered. However a slight increase in power needed was detected. This discrepancy was ignored, because for a capacity increase of 100% the change in power needed stayed below 1%.
The next parameters are the motor parameters for an increase in the no-load current and internal resistance for which it was expected that the mechanical power stays the same but electrical power increases, because these parameters are a measure for the losses of the motor. This was also witnessed.
The final parameters are the propeller parameters. For an increase in diameter an increase in propeller efficiency was expected. This means a decrease in both electrical and mechanical power. This was also observed. For an increase in propeller pitch it was expected that the rotational velocity decreased, but the electrical and mechanical power increased. This was also noted.
The final verification was done for the endurance calculation. The endurance is equal to the total energy available divided by the electrical power for hover. This was also marked during use of the tool.

XFLR5

The verification of XFLR5 was done by investigating the analysis methods used in XFLR5 and checking the documentation [11]. From the documentation, the implemented methods for the 3D analysis are the LLT, VLM and 3D-panel method. All three methods were used in a wing analysis of reasonable complexity, meaning this geometry included sweep, dihedral and tip twist and fins. Comparing the results of the different methods

revealed that LLT has a major limitation, being the fact that this method neglects viscous drag. The most efficient method was the VLM, as the 3D panel method had a much longer computation time and therefore was difficult to use in the design process. Also, the 3D panel method could only be used on a wing without vertical fins, so only the wing itself could be analysed. Complete verification procedures were performed many times with this open source software [11], showing that the methods are consistently implemented in the program.
The program was further verified by using the one-factor-at-a-time approach, where for instance an increase in span or camber, should show an increase in lift. This verification was done for all parameters used in the design, either in the phase of fully understanding the program or later during the design phase.
The prediction of the moments of inertia was verified using the predictions made in CATIA [10]. The moments of inertia were used to perform the stability analysis in XFLR5. Deviations in the moment of inertia predictions were in the order of a factor 2. Because the mass centers of the subsystems are taken into account in CATIA, this prediction is very likely more accurate. Also, the prediction of the moments of inertia is a known issue with XFLR5 [11] and it was therefore advised to use better estimates for the moments of inertia when available.

H.2. Validation

The validation procedures are discussed for the Matlab, Excel and off-the-shelf tools separately as the procedures are not always comparable.

H.2.1. Matlab code

The Matlab based tools include the structures and volume-mass calculation tools. All tools were validated using a numerical solution for a simplified structural planform.
For the structural applications two different tools were developed: a sandwich theory tool and closed cell approximation tool. In the case of the sandwich panel approximation the numerical solution for the deflection of a cantilever beam with a point load was evaluated [49]. The final results matched with only a difference of -0.050 %. For the closed cell also a cantilever beam with a point load was analysed for a square cross section with a constant wall thickness. The final load equilibrium resulted in a difference of only +0.051 % with respect to the numerical solution. The mass and volume tool was only validated for the volume, because the mass is simply the product of a constant density and the calculated volume. CATIA was used as the reference for the volume verification. The solutions matched with a error of only +1.95 %.

Table H.1: Validation of Matlab tools

Structural	**Validation reference**	**Error margin**
Sandwich theory	Numerical solution	+0.050 %
Closed cell approximation	Numerical solution	-0.051 %
Volume-mass tool	Catia	+1.95%

The transition tool has been validated by the optimal path of Figure 8.40 [22]. The shapes of both lines come very close which makes the tool reliable. A validation with numbers is impossible due to lack of (numerical) information about transitions.
The tools for hovering climb and forward flight were validated by comparing the climb and forward velocities to those of existing UAVs. Since no aerodynamic and motor properties were found for existing UAVs, the tools could not be validated by concrete examples. Thus for the forward flight velocity the order of magnitude of the forward flight velocity for maximum range calculated was compared that of similar UAVs. This was found to be in the same order of magnitude. Since no maximum climb velocity was calculated, this could not be compared. However, the climb capabilities of our UAV seem to be in the same order of magnitude as those of similar UAVs.

H.2.2. Excel

The Excel tools that were developed for the performance of off-the-shelf products were validated by comparing the output values of the sheets to values given by the manufacturer of the designated system. For instance,

example input values were inputted into the tool, which should give the same results as the manufacturer gave. After this was done and the same values resulted, the tools were validated. Some minor errors occurred, which were mainly caused by different rounding in between calculation steps.
The Excel tools that were developed for the calculation of planform characteristics were validated by confirming these values to values of similar planforms and their characteristics. After the input values from similar existing planforms resulted in values that lie in the same range, the tool was validated.
The communication tool was validated by implementing example values given by Lockheed Martin Corporation lecture slides [27]. There was a small difference between the final outcome (data rate), but this was mainly caused due to a different signal-to-noise ratio and rounding of the final outcome.
The payload tool was validated by comparing the ground resolution outcomes with the ground resolutions as given by the manufacturer. These corresponded to the values of all the cameras. Furthermore the mapping speed was also calculated using an Excel sheet, which was validated by comparing the resulting mapping speeds to the speeds as given by the manufacturers, which also corresponded. Thus this tool was validated.

H.2.3. Off-the-Shelf Tools

MotoCalc

When results were obtained and the optimisation process was completed, the results from MotoCalc were compared with the results obtained from XFLR5. More specifically, the stall and optimal flight velocities and aerodynamic coefficients were compared to see if they were equal to each other. It was found that there is a difference in results from MotoCalc and XFLR5, due to the fact that MotoCalc assumes 2D aerodynamics, while XFLR5 is able to simulate 3D aerodynamics.
Next to that, when plotting graphs of different variables versus the altitude with MotoCalc, the graphs were not smooth, but had discontinuities. This is explained by the fact that MotoCalc is a tool based on a database of test data, and is thus not solely based on equations. The tool is also aiming for simulating the performance of model aircraft, which generally do not have a large flight envelope.
As the tool is also based on a database of test data from different people conducting the tests, the test data might vary from test to test, making the results of MotoCalc somewhat less accurate. The creators of MotoCalc also warn for this in their online manual[1]. However, being aware of the limitations of the tool is one of the most important ways to get around these limitations, as one can take them into account and anticipate on possible inaccuracies when analysing the results of this tool by checking whether the above mentioned caveats are present or by applying a safety factor, and with that, get reliable data from the tool.

xcopterCalc

xcopterCalc claims that its tool provides an accurate prediction of performance within 15%, which was considered to be accurate enough for the performance analysis. This accuracy was tested by giving the input of a known propulsion system of a UAV. This was done for the Agribotix Enduro [2]. For this UAV all input parameters were known, except the propeller profile. However this has a relatively small influence on the endurance, not bigger than 0.5 min. With xcopterCalc an endurance of 24 min was calculated, while the endurance given by the manufacturer of the Enduro an endurance of 25 min was calculated. This is a difference of 4%, which was within the required 15%.

XFLR5

Validation of XFLR5 was difficult to implement as the available resources to fully validate the program are limited, however some use was made of test data from other sources. 2D experimental tests for low Reynolds numbers were compared with the results of similar Reynolds numbers in XFLR5 [28]. The test data and simulation were compared on zero-lift angle of attack, $C_{L_{max}}$, and α_{stall}. The results matched very closely the simulation data on these parameters. The total polar graphs showed errors in the order of less than 5%. The 3D wing analysis was difficult to validate by itself, as less experimental data is readily available on generic 3D wings. However the 3D analysis was validated as various validations have already been applied to XFLR5 and documented [11].

[1] URL:`http://www.motocalc.com/motocalc.htm#topic_6` [cited 20 June 2016]
[2] URL:`http://agribotix.com/enduro/` [cited 21 June 2016]

I

XFLR5 results

In this appendix, a complete overview is given of the aerodynamic results. In Figures I.1 to I.4, the polar plots are presented for the final planform, of which the justification and parameters are found in Sections 8.5 and 8.6. In Figures I.5 and I.6, the elevon trim curves are found. For investigating the stability of the UAV, the eigenvalues are found in Figure I.7 for the flying wing configuration, and in Figure I.8 for the tailsitter. The response curves for the eigenmodes are found in Figures I.9 to I.13, in the following order: short period, phugoid, roll damping, dutch roll and spiral.

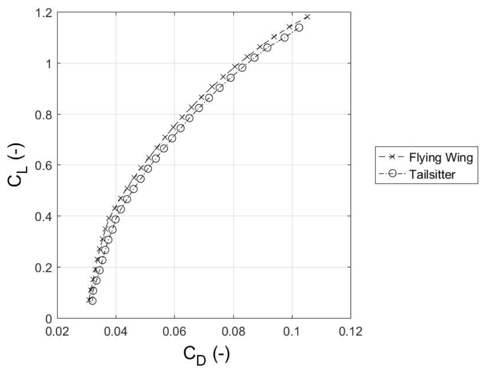

Figure I.1: C_L-C_D polar, for the flying wing and tailsitter configuration

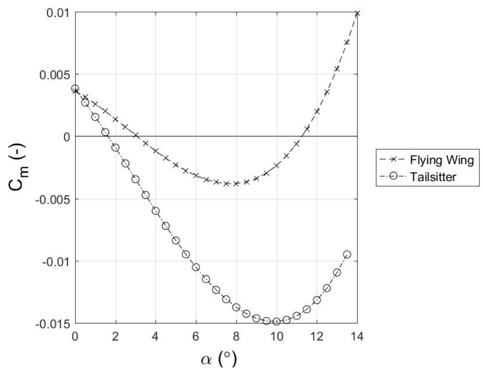

Figure I.2: C_m-α polar, for the flying wing and tailsitter configuration

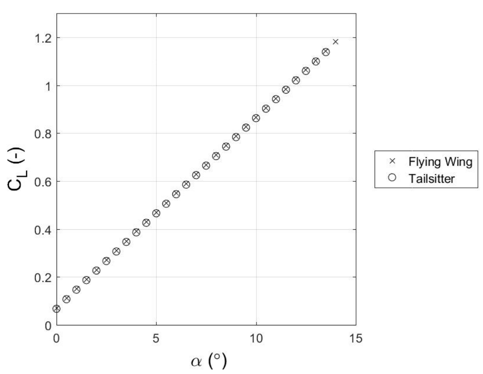

Figure I.3: C_L-α polar, for the flying wing and tailsitter configuration

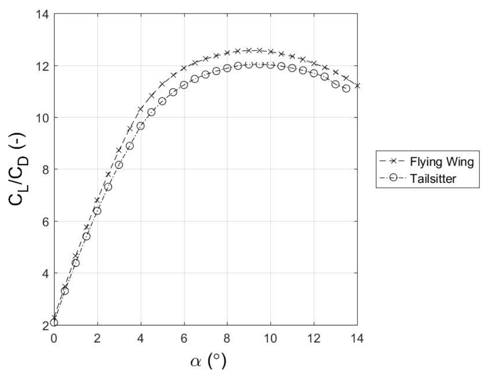

Figure I.4: C_L/C_D-α polar, for the flying wing and tailsitter configuration

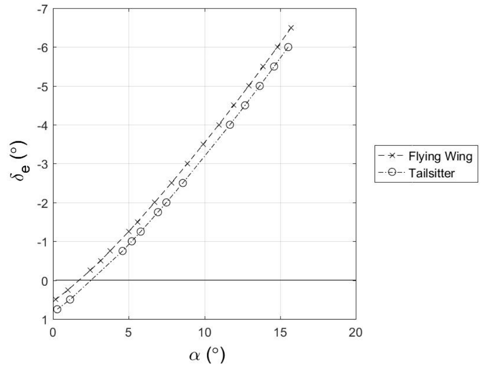

Figure I.5: δ_e-α trim curve, for the flying wing and tailsitter configuration

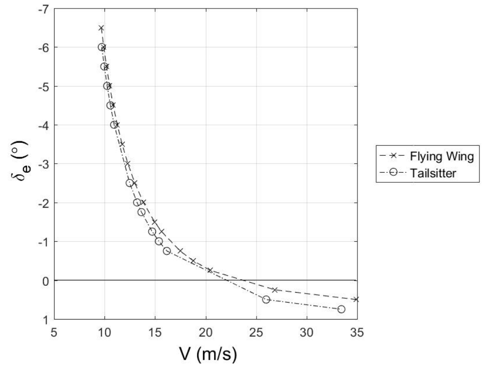

Figure I.6: δ_e-V trim curve, for the flying wing and tailsitter configuration

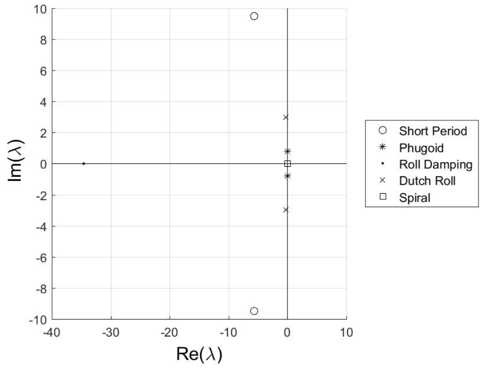

Figure I.7: Eigenvalues of the flying wing configuration, for the longitudinal and lateral modes

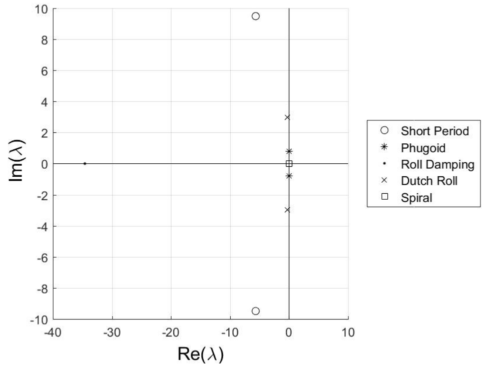

Figure I.8: Eigenvalues of the tailsitter configuration, for the longitudinal and lateral modes

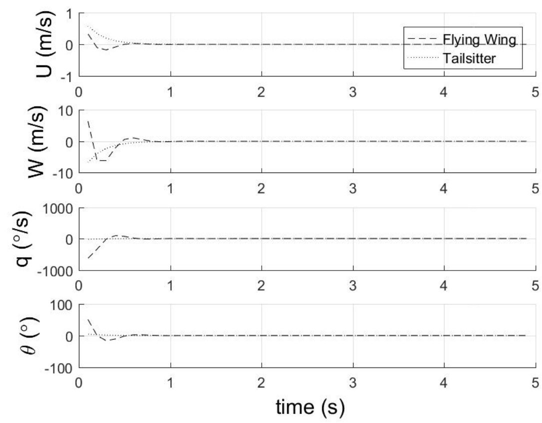

Figure I.9: Short period response of the flying wing and tailsitter configuration

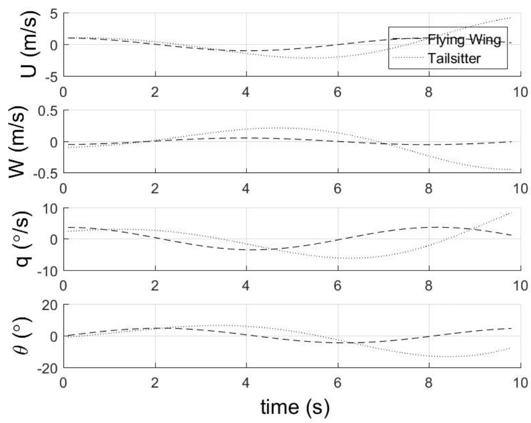

Figure I.10: Phugoid response of the flying wing and tailsitter configuration

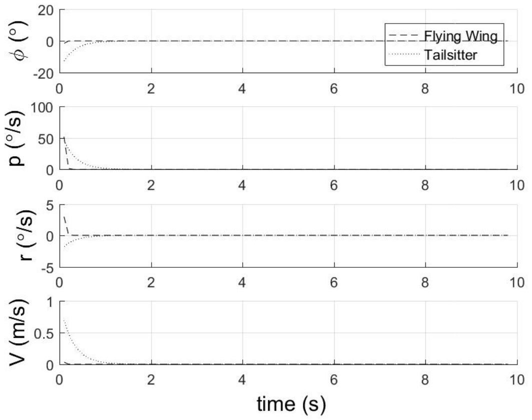

Figure I.11: The roll damping of the flying wing and tailsitter configuration

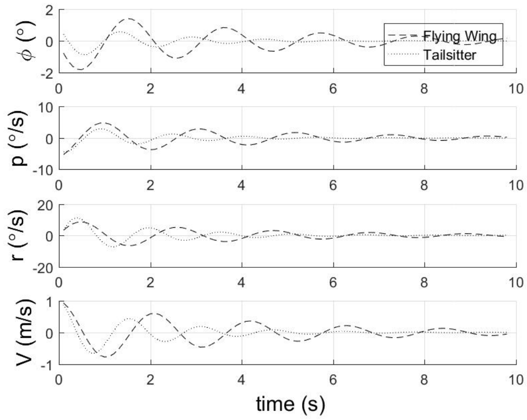

Figure I.12: Dutch roll response for the flying wing and tailsitter configuration

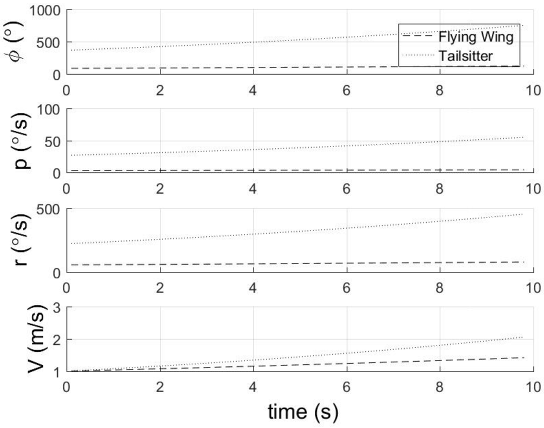

Figure I.13: Spiral response of the flying wing and tailsitter configuration

J Compliance Matrix

The compliance matrix shows which requirements were and were not met. Chapter 9 discusses in detail the cause and effect of the failed requirements.

SYS-SUR-1	The design shall be able to survey the area of interest.	✓
SYS-SUR-1.1	The survey design shall survey the area of interest.	✓
SYS-SUR-1.1.1	The ground surveying design shall be able to survey the ground during all daily light conditions.	✓
SYS-SUR-1.1.2	The ground surveying design shall be able to survey the ground with a location accuracy of at least 0.5 m.	✓
SYS-SUR-1.1.3	The resolution of the design shall allow for severe damage detection.	✓
SYS-SUR-1.1.4	The resolution of the design shall be sufficient to distinguish wreckage pieces from the ground surface.	✓
SYS-SUR-1.1.5	The ground surveying design shall be stable around its three rotational axes.	✓
SYS-SUR-1.1.6	The ground surveying design shall be able to zoom.	✗
SYS-SUR-1.1.7.a	The 3D imaging design shall have an accuracy of at least 25 $cm^2 per pixel$.	✓
SYS-SUR-1.1.7.b	The 3D imaging design shall be stable around its three rotational axes.	✓
SYS-SUR-1.2	The design shall survey an area of 1 x 1 km.	✓
SYS-SUR-1.3	The design shall be able to survey its aerial environment.	✓
SYS-SUR-1.3.1	The aerial surveying design shall measure meteorological conditions.	✓
SYS-NAV-1	The design shall have a navigation system.	✓
SYS-NAV-1.1	The navigation system shall allow the use of an auto-pilot.	✓
SYS-NAV-1.2	The navigation system shall be able to determine its geographical location.	✓
SYS-NAV-1.2.1	The geographical location of the design shall be determined with an accuracy of at least 0.5 m.	✓
SYS-COM-1	The design shall be able to communicate.	✓
SYS-COM-1.1	The communication design shall have an up- and down-link.	✓
SYS-COM-1.1.1	The up- and down-link communication system shall have a connection with teams on the ground.	✓
SYS-COM-1.1.2	The up- and down-link communication system shall have a connection with ATC.	✗
SYS-COM-1.1.2.a	The ATC communication shall comply with the global regulations for UAVs.	✗
SYS-COM-1.1.2.b	The ATC communication shall be able to identify vocal commands given by ATC.	✗
SYS-COM-1.1.2.c	The ATC communication shall be able to communicate data with ATC.	✗
SYS-COM-1.1.3	The Up- and Down-Link communication system shall be able to communicate with the groundstation.	✓
SYS-COM-1.2	The subsystems shall be able to communicate with each other.	✓
SYS-COM-1.3	The communication shall be secured.	✓
SYS-COM-1.4	The communication shall have a selectable frequency.	✗
SYS-COM-1.5	The communication shall be in real time with a maximum delay of 30 seconds.	✓
SYS-COM-1.6	The design shall be able to act as a communication relay beyond the line of sight.	✗

SYS-DAT-1	The design shall have a data handling system.	✓
SYS-DAT-1.1	The data handling system shall be able to process the received data.	✓
SYS-DAT-1.1.1	The data handling system shall be able to detect wreckage from the surveying payload of at least 0.5 m in cross section.	✓
SYS-DAT-1.1.1.a	The wreckage detection system shall save the location of wreckage.	✓
SYS-DAT-1.1.1.b	The wreckage detection system shall label the detected wreckage pieces.	✓
SYS-DAT-1.2	The data handling system shall be able to store all data.	✓
SYS-DAT-1.2.1	The data storage shall have enough memory to store all data.	✓
SYS-DAT-1.2.2	The data storage shall be redundant.	✓
SYS-TRS-1	The system shall be transportable.	✓
SYS-TRS-1.1	The system shall not leak any fluids during transport.	✓
SYS-TRS-1.2	The system shall not fail under the load factors experienced during transport.	✓
SYS-TRS-1.2.1	The system shall not fail under load factors experienced during aerial transport.	✓
SYS-TRS-1.2.1.a	The transportable system shall not fail under a maximum longitudinal load factor of 3.0 [35].	✓
SYS-TRS-1.2.1.b	The transportable system shall not fail under a maximum lateral load factor of 1.5 [35].	✓
SYS-TRS-1.2.1.c	The transportable system shall not fail under a maximum vertical load factor of 3.0 [35].	✓
SYS-TRS-1.2.2	The system shall not fail under load factors during ground transport.	✓
SYS-TRS-1.2.2.a	The transportable system shall not fail under a maximum longitudinal load factor of 3.5 [35].	✓
SYS-TRS-1.2.2.b	The transportable system shall not fail under a maximum lateral load factor of 2.0 [35].	✓
SYS-TRS-1.2.2.c	The transportable system shall not fail under a maximum vertical load factor of 6.0 [35].	✓
SYS-TRS-1.3	The system shall be stored during transport.	✓
SYS-TRS-1.4	The size of the system shall be changeable for transport.	✓
SYS-TRS-1.4.1	The transportable system shall fit in a 60 l backpack.	✗
SYS-TRS-1.4.2	The transportable system shall weight less than 15 kg.	✗
SYS-CTR-1	The design shall be controllable.	✓
SYS-CTR-1.1	The design shall have different flight modes.	✓
SYS-CTR-1.1.1	The design shall be able to fly autonomously.	✓
SYS-CTR-1.1.2	The design shall be able to be controlled remotely.	✗
SYS-CTR-1.2	The design shall allow for different operating modes.	✓
SYS-WGT-1	The weight of the design shall not hinder the designs capability to fly.	✓
SYS-WGT-2	The weight of the design shall be manageable for the designs users.	✓

SYS-WGT-1	The weight of the design shall not hinder the designs capability to fly.	✓
SYS-WGT-2	The weight of the design shall be manageable for the designs users.	✓

SYS-STR-1	The structure of the design shall remain intact during the designs lifetime.	✓
SYS-STR-1.1	The structure of the design shall not fail due to environmental impacts.	✓
SYS-STR-1.1.1	The structure of the design shall not fail due to runway debris.	✓
SYS-STR-1.1.2	The structure of the design shall not fail due to volcanic ashes.	✗
SYS-STR-1.1.3	The structure of the design shall not fail due to lightning strikes.	✗
SYS-STR-1.1.4	The structure of the design shall not fail due to bird strikes.	✓
SYS-STR-1.1.5	The structure of the design shall not fail due to precipitation.	✓
SYS-STR-1.2	The structure of the design shall be rigid enough so that the design shall not fail due to all the design loads encountered.	✓
SYS-PWR-1	The design shall possess enough power to perform the missions for which it is designed.	✓
SYS-PWR-1.1	The design shall possess enough power to power the payload.	✓
SYS-PWR-1.2	The design shall possess enough power to take off.	✓
SYS-SZE-1	The designs size shall be manageable for the designs users.	✓
SYS-SCH-1	The conceptual phase of the design shall be finished by June 23rd 2016 (23-06-2016) .	✓
SYS-SFY-1	The design shall not harm its environment.	✓
SYS-SFY-1.1	The design shall not contaminate its environment.	✓
SYS-SFY-1.2	The design shall have a manual.	✓

SYS-SFY-1.3	The design shall not harm humans.	✓
SYS-SFY-1.4	The design shall be certified according to the special flight operations certificate.	✗
SYS-SFY-1.5	The design shall have a identifiable appearance.	✓
SYS-SFY-1.6	The design shall not fail due to the environmental conditions during the execution of a mission.	✓
SYS-SFY-1.6.1	The design shall not fail due to the climate it is flying in.	✓
SYS-SFY-1.6.2	The design shall not fail due to the weather it is flying in.	✓
SYS-SFY-1.7	The design shall avoid collisions.	✓
SYS-SFY-1.7.1	The design shall avoid collisions with the ground.	✓
SYS-SFY-1.7.2	The design shall avoid collisions in the air.	✓
SYS-SUS-1	The design shall be sustainable.	✓
SYS-SUS-1.1	The sustainable design shall minimise its economic footprint.	✓
SYS-SUS-1.2	The sustainable design shall minimise its environmental footprint.	✓
SYS-SUS-1.3	The sustainable design shall minimise its social impact.	✓
SYS-ACC-1	The designs measurement equipment shall have an accuracy to guarantee an surveying accuracy of 0.5 m.	✓
SYS-END-1.1	The design shall have a total mission endurance of at least 6 hr on location.	✓
SYS-END-1.2	The design shall be able to loiter for at least 15 min.	✓
SYS-RNG-1.1.1	The design shall be able to get from the storage area to the take-off site.	✓
SYS-RNG-1.1.2	The design shall be able to get from the landing site to the storage area.	✓
SYS-RNG-1.2	The system shall be able to autonomously travel from the take-off site to the area of interest for at least 15 km.	✓
SYS-RNG-1.3	The system shall be able to autonomously travel from the area of interest to the landing site for at least 15 km.	✓
SYS-STB-1.1	The system shall have a stable reaction to aerodynamic disturbances during the mission.	✓
SYS-STB-1.2	The system shall be stable during its ground operations.	✓
SYS-TKO-1.1	The system shall be deployable for take-off within 30 min.	✓
SYS-TKO-1.2	The system shall have a take-off length of at most 75 m.	✓
SYS-TKO-1.3	The system shall be able to take-off on any terrain which is accessible by the transport vehicles.	✓
SYS-LND-1.1	The system shall have a landing distance of at most 75 m.	✓
SYS-LND-1.2	The system shall be able to land on any terrain which is accessible by the transport vehicles.	✓
SYS-MAN-1.1	The system shall be simple to maintain.	✓
SYS-MAN-1.2	The maintenance of the system shall require a training of no more than one day.	✓
SYS-MAN-1.3	The system shall be able to be maintained by universal tools.	✓
SYS-MAN-1.4	The system shall be able to have an interchangeable payload.	✓

K
Post-DSE Gantt chart

After the Design Synthesis Exercise is finished, MIRU can be designed on a deeper level so that it can become a product that can be manufactured and actually sold. The Gantt chart for this process is shown in Figure K.1.

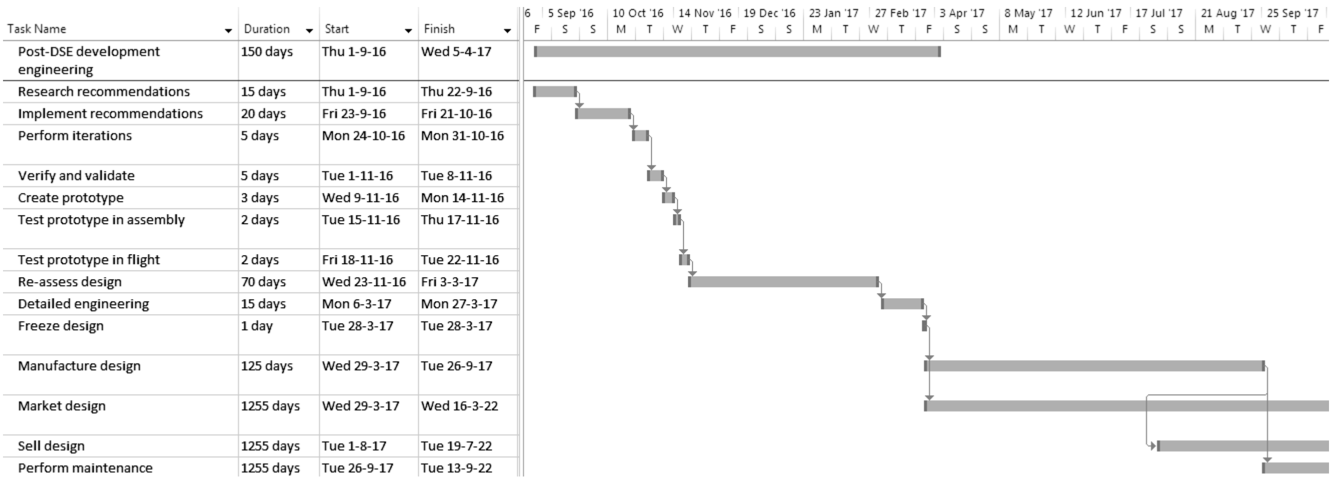

Task Name	Duration	Start	Finish
Post-DSE development engineering	150 days	Thu 1-9-16	Wed 5-4-17
Research recommendations	15 days	Thu 1-9-16	Thu 22-9-16
Implement recommendations	20 days	Fri 23-9-16	Fri 21-10-16
Perform iterations	5 days	Mon 24-10-16	Mon 31-10-16
Verify and validate	5 days	Tue 1-11-16	Tue 8-11-16
Create prototype	3 days	Wed 9-11-16	Mon 14-11-16
Test prototype in assembly	2 days	Tue 15-11-16	Thu 17-11-16
Test prototype in flight	2 days	Fri 18-11-16	Tue 22-11-16
Re-assess design	70 days	Wed 23-11-16	Fri 3-3-17
Detailed engineering	15 days	Mon 6-3-17	Mon 27-3-17
Freeze design	1 day	Tue 28-3-17	Tue 28-3-17
Manufacture design	125 days	Wed 29-3-17	Tue 26-9-17
Market design	1255 days	Wed 29-3-17	Wed 16-3-22
Sell design	1255 days	Tue 1-8-17	Tue 19-7-22
Perform maintenance	1255 days	Tue 26-9-17	Tue 13-9-22

Figure K.1: Post-DSE Gantt chart